Space Programs Summary No. 37-24, Volume III

for the period September 1, 1963 to October 31, 1963

The Deep Space Instrumentation Facility

JET PROPULSION LABORATORY
CALIFORNIA INSTITUTE OF TECHNOLOGY
PASADENA, CALIFORNIA

November 30, 1963

Space Programs Summary No. 37-24, Volume III

for the period September 1, 1963 to October 31, 1963

The Deep Space Instrumentation Facility

JET PROPULSION LABORATORY
CALIFORNIA INSTITUTE OF TECHNOLOGY
PASADENA, CALIFORNIA

November 30, 1963

Preface

The *Space Programs Summary* is a six volume, bimonthly publication designed to report on JPL space exploration programs, and related supporting research and advanced development projects. The subtitles of all volumes of the *Space Programs Summary* are:

Vol. I. The Lunar Program (Confidential)
Vol. II. The Planetary–Interplanetary Program (Confidential)
Vol. III. The Deep Space Instrumentation Facility (Unclassified)
Vol. IV. Supporting Research and Advanced Development (Unclassified)
Vol. V. Supporting Research and Advanced Development (Confidential)
Vol. VI. Space Exploration Programs and Space Sciences (Unclassified)

The *Space Programs Summary,* Volume VI is an unclassified digest of appropriate material from Volumes I through V, plus the space science instrumentation studies of the JPL Space Sciences Division.

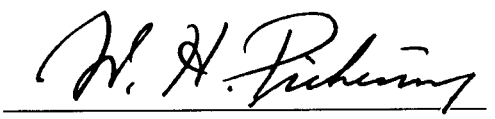

W. H. Pickering, *Director*
Jet Propulsion Laboratory

(NASA CR ---; JPL SPS-37-24, vol. III)

Space Programs Summary No. 37–24, Volume III

Prepared under Contract No. NAS 7-100, National Aeronautics & Space Administration
(NASA)

Contents

I. Résumé 1

II. Goldstone Operations 5

III. Engineering Development 9

A. Mark I Ranging Subsystem 9

B. Systems Engineering 12

C. Antenna Engineering 13

References 23

IV. Research and Development 24

A. Ground Antennas 24

B. Planetary Radar Project 43

C. Lunar Radar Project 51

D. Ranging and Tracking System Development 59

E. S-Band Implementation for DSIF 76

F. Telemetry System Development 81

G. RF Signal Generation and Control 95

H. Mesa Antenna Range 97

References 99

V. Advanced Antenna System 101

A. Synopsis 101

I. Résumé

The DSIF is a precision tracking and data acquisition network which is designed to track, command, and receive data from deep space probes. It utilizes large antennas, low-noise phase-lock receiving systems, and high-power transmitters at stations positioned approximately 120 deg around the Earth. Its policy is to continuously conduct research and development of new components and systems and to engineer them into the DSIF so as to continually maintain a state-of-the-art capability.

Goldstone operations. A 50-w backup transmitter, a command system, and a Beckman decommutator have been installed and tested at the Echo site in preparation for *Ranger 6*. Compatibility tests with the RCA video equipment have also been successfully completed. The hydromechanical building at the Pioneer site has been completed and all equipment has been reinstalled. Road and site construction has begun at the Mars site in preparation for the installation of the 210-ft antenna.

Engineering developments. The Mark I ranging subsystem is designed for use by the DSIF with "turnaround" spacecraft transponders for ranges up to 800,000 km. Its test panel includes an internal readout pulse generator and a variable frequency generator to simulate doppler, and "shift and decision" switches so that the ranging equipment can be tested prior to operation.

Project engineering for the DSIF included test plans and information for the *Surveyor, Ranger* Blocks III and V, *Pioneer, Lunar Orbiter, Mariner C* (Mars mission, 1964), *Mariner B* (*Centaur*-based entry capsule mission) and *Apollo* Projects. The problems of Sun and Moon noise temperature contributions and signal acquisition are also being studied.

Extensive tests indicate that thermal loads on a parabolic antenna materially affect the quadripod and mechanical axes pointing errors. To help prevent this, the antenna is painted with a specially developed white paint with a spectral gloss of the order of 2%. Special hoisting slings and service trailers have been developed to handle the Cassegrain cones at each station. The cones are built of 0.080-in. 7178-T6 aluminum to ensure survival in severe hailstorms, and are drilled from JPL-owned templates to assure interchangeability. The Cassegrain hyperbola is built with a new lamination process which

provides a five-fold increase in tolerances and uses a stronger aluminum alloy (6061-T6) to provide hailstone resistance. The positioning hardware has been designed to be less expensive, less complicated, and more reliable.

Ground antennas. After the new surface on the 85-ft antenna at the Goldstone Venus site had been aligned, accurate gain measurements showed a gain improvement of 0.4 db to a new value of 54.4 ± 0.15 db. Pattern measurements indicate that the quadripod shadow causes a gain loss of 0.7 db and a zenith noise temperature contribution of 5°K.

A radiometer and gas tube noise generator were used at X-band (8448 Mc) to measure the antenna noise temperature of the 30-ft antenna at the Venus site. Preliminary calculations indicate a noise temperature of 18.4 ± 2.7°K.

The astronomical techniques which have been developed to calibrate 85-ft antennas were used to boresight the 85-ft Az-El antenna at the Venus site and its optical tracker. A continuous tracking method was used with corrective angular offsets used to determine the amount of boresight error. Boresight corrections of −0.061 deg in azimuth and +0.021 deg in elevation were made. A systematic elevation error readout was also found.

The mobile antenna test instrumentation system was used to measure wind and thermal loads on the 85-ft Az–El antenna at the Venus site following the installation of the new surface. Wind velocity and direction, temperatures at 24 different antenna locations, and ten deformation measurements were made simultaneously and automatically recorded. The deformations were smaller than expected.

Planetary radar. The recently designed water rotary joint was installed on the Az–El 85-ft antenna at the Venus site and placed in operational use. A few days after installation, the leaks amounted to 1 gal every 2 hr, but are now less than 1 gal/day. This indicates the seals are wearing in.

The 100-kw S-band transmitter has been completely documented and some design improvements to the crowbar circuitry have been completed. The filament of a power klystron was damaged by an arc-over and is being replaced. A silicon rectifier for the power supply unit is being investigated for possible replacement of the tube rectifiers. It will deliver 0 to 33 kv dc at 30 amp and 33 to 55 kv at 1 Mw over a temperature range from −25 to +135°F.

The Mod IV ranging equipment has a wired program special purpose computer with six available programs, five of which are selectable. These programs will:

(1) Provide ephemeris programmed signals.

(2) Make a closed-loop range measurement.

(3) Make a closed-loop range measurement plus a measurement of the signal delay in the range system.

(4) Perform a closed-loop calibration measurement.

(5) Provide transmit–receive keying signals.

(6) Synchronize the ephemeris tape with station time.

The ephemeris programmed signals are used for spectrum analysis, radiometer analysis, and multiple range-gate analysis of radar echoes. The transmit–receive keying signals control the alternate connection of transmitter and receiver to a single antenna.

Using the same techniques used on Venus in 1962, radar measurements were made on Mercury in May 1963. These measurements were:

(1) Total echo power.

(2) Analysis of the radar echo into frequency components.

(3) Analysis of range-gated radar echo into frequency components.

The radar cross-section of Mercury was found to be 5% of its geometric cross-section compared to 10% for Venus and 3% for Mars. The measurement of the speed of rotation of Mercury agreed with its known period, and thus corroborates the measurements made on Venus. It was found that residuals in the doppler and range measurements could be essentially eliminated by correcting the argument of the ephemeris by 6 sec and the astronomical unit (AU) by 10^5 m. This data provides striking confirmation of the accuracy of the radar measurements of Venus made in 1961 and 1962.

Lunar Radar Project. Additional tests on klystron noise power, for 100 kw at 2388 Mc, show that when the tube is tuned broad-band, the noise power per cycle decreases as the bandwidth increases, while for either high efficiency or synchronous tuning, there is little change in the noise power per cycle as the bandwidth is increased.

Because of the short round-trip time for a radar echo to the Moon it has been decided to use the 85-ft reflector for transmitting and a 6-ft diameter dish, with a shielding tunnel 20 in. deep mounted to its periphery, for receiving. The 6-ft antenna will be mounted at the apex of the 85-ft quadripod. System noise temperatures as a function of klystron beam voltage and antenna elevation were measured. A figure of merit was defined as the ratio of the transmitted power to the system noise temperature measured with the same klystron beam voltage but with no excitation. The figure of merit is presented as a function of transmitted power. Noise stability measurements indicate it may be desirable to sacrifice a db or so of figure of merit to improve the accuracy of the power measurements.

Ranging and tracking development. To establish operating parameters for a satellite radar at S-band, a preliminary analysis of expected worst case target dynamics has been made. Using a worst case doppler requirement of $\pm$ 120 kc, it was found that an additional $\times$ 20 in dc loop gain is required to meet the VCO constant of 4330 cps/v. A feedback limited amplifier with sufficient short- and long-term stability has been found to be satisfactory to furnish this gain. For unaided tracking of a satellite at 250-mi altitude, the maximum doppler rate requires a loop bandwidth $2\beta_{L_0} = 100$ cps. Since this is 13 db worse than the goal of 5 cps, either a programmed change in frequency or a variable bandwidth will be required. These constraints require operation, at least temporarily, between 20- and 63-cps bandwidths and have the effect of increasing the keying rates in order to reduce the effects of poor phase integrity and degradation of performance of the anti-sideband system. Typically this would be 300 to 900 cps for satellites.

The monostatic keyed radar is intended to provide a model for a DSIF S-band tracking system for use during initial passes of a spacecraft. The system design has been influenced by the problems which have been encountered and, in its present state, it consists of a ranging system only. Ultimately the capability will be extended to include the tracking of doppler and angles. Using a rubidium vapor standard frequency oscillator and counting RF as well as clock frequencies, a range resolution of 1.25 m is obtained. The ranging code has the interesting property of possessing a two-level auto-correlation function whose value at any displacement is equal to the ratio of the number of agreements minus the number of disagreements to the number of agreements plus the number of disagreements. The transmitter has a second phase modulator for the range-gating subsystem. An additional 3-db improvement in signal-to-noise ratio is obtained by keying the receiver in opposition to the transmitter. An anti-sideband lock system is used. Digital control equipment generates the ranging code and provides a stored program computer to automatically acquire and make range measurements.

A digital system for performing RF acquisition, including anti-sideband lock, has been tested and proved to be successful. It was also made capable of controlling the transmitter to achieve acquisition of the ground-to-spacecraft link. With the addition of a small amount of RF and signal conditioning equipment, the digital computer which controls the pointing of the antenna can be used.

S-band implementation for the DSIF. Traveling wave masers with closed cycle helium refrigerators are planned for operational use at DSIF Stations. The prototype unit, complete with performance measuring equipment, operated successfully at the Venus site for 600 hr before condensation of impurities in the gas supply line forced a shutdown for repairs. This unit has a net gain of 40 db, a bandwidth of 12 Mc, and a noise temperature of 9°K.

The design of the S-band acquisition aid system has been completed. It consists primarily of the basic 85-ft antenna feed horn and a separate receiver system. The use of a separate receiver system allows smooth transition from acquisition aid antenna to the 85-ft antenna. The acquisition aid receiver is also used to control the automatic gain control of the 85-ft antenna receiver system until successful switchover is achieved. This prevents acquisition on a side lobe of the large antenna.

Telemetry development. A large number of trial runs was made on a biorthogonal telemetry system which was described in *SPS 37-18*. Using a 4-kc square wave biphase modulated subcarrier and sampling it at a rate of 8000 samples per second, the bit error rate was measured with various signal-to-noise ratios. The results were within 0.3 db of theoretical even when the noise power was 15 times greater than the signal.

It has been found desirable to design a set of logic modules which can be used in the development of all types of JPL digital systems. As the result of a comprehensive study, including market survey, it was decided to standardize on a printed circuit card 4.75 by 3.18 in. with each card holding four separate identical circuits and with cards that use pin connectors for wiring. There are four basic logic circuits, which use highly reliable

parts such as epitaxial silicon semiconductors. They are connected together using synchronous logic. The basic concept and design are now undergoing tests following the receipt of sample products from two separate manufacturers.

RF signal generation and control. Both the receiver and transmitter systems usually require frequency control over the local oscillator in small steps over a large range. To replace the free running voltage controlled oscillators which are normally used, it has been proposed that a pseudonoise generator be used with a frequency synthesizer and a phase-lock loop circuit to generate a very stable variable frequency. An experimental test showed virtually no degradation in phase noise.

Mesa Antenna Range. In order to improve the capability of the Mesa Antenna Range, two RF anechoic rooms will be built and a ¾-mi range will be added. The building housing the two anechoic chambers is under design and the new range is about 60% complete.

Advanced Antenna System. A master summary schedule for the installation of the 210-ft antenna at Goldstone has been approved and work is generally proceeding on schedule. Site clearing and antenna foundation construction has begun, and the access road is virtually complete. A 200-ton, 180-ft tall, grey derrick mounted on a 135-ft tower has been procured for use in installation work. Design and analysis work is continuing on various component parts of the antenna structure.

II. Goldstone Operations

Ranger 6 preparation is the current primary activity at Goldstone. Of major importance is the successful completion of the compatibility tests between the receiver and the video equipment. Updating of equipment has been completed, and necessary personnel training has been accomplished. Final preparations are being completed, with a full readiness scheduled in November.

1. Equipment

a. Echo site. Beckman decommutator equipment has been installed and validated (Fig. 1). Personnel training is completed. The unit has been tested during preliminary station tests, and all interface problems with associated equipment have been resolved. Beckman decommutators for overseas sites were checked out and shipped during the month of September.

The 50-w back-up transmitter and the 200-w low-power mode of the 10-kw transmitter are operational. The 50-w transmitter has been installed on the antenna (Fig. 2). The antenna contains a manual switch arrangement to permit changing from one transmitter to the other. A safety-interlock arrangement prevents accidental turn-on of the 10-kw transmitter in either mode during the time that the 50-w transmitter is in the antenna feed operation.

The L-band exciter has been installed and operationally tested with associated tracking equipment. All interface problems have been resolved.

The JPL/RCA compatibility tests were conducted through September. All tests were successfully completed. Specifically, they involved determinations of the following data:

(1) JPL/RCA receiver bandwidth.

(2) RCA receiver threshold.

(3) RCA/JPL receiver threshold.

(4) Peak-to-peak video to rms noise.

(5) Cruise mode telemetry (Channel 8).

(6) 225-kc RCA telemetry threshold.

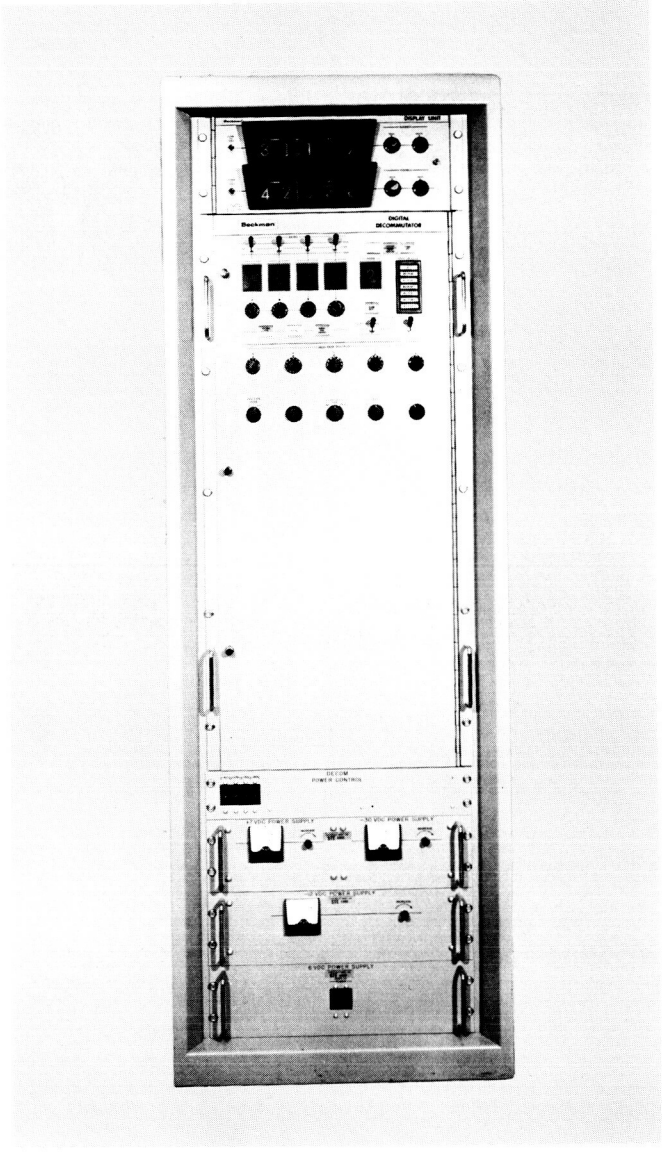

Fig. 1. Beckman decommutator

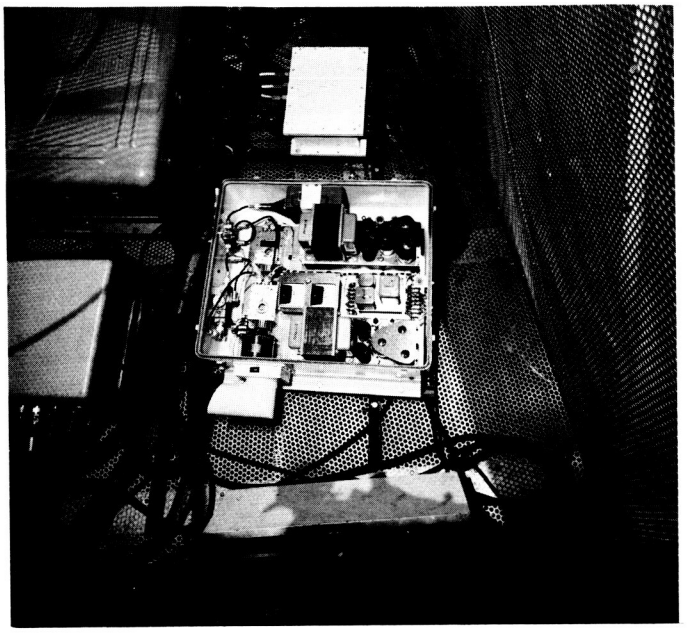

Fig. 2. 50-w transmitter installation

A mission orientated command system has been installed and tested for use during *Ranger 6* and subsequent missions (Fig. 3). This command system authenticates tapes received via teletype from JPL in Pasadena. The command system modulates the transmitter continuous wave (CW) signal, and this command signal is received and demodulated by the spacecraft. It also monitors the actual transmission by the use of an independent receiver. By comparing the transmitted message with the tape presentation, an automatic inhibit can stop transmission when an error is detected. In an emergency, the automatic features of the command system can be manually bypassed.

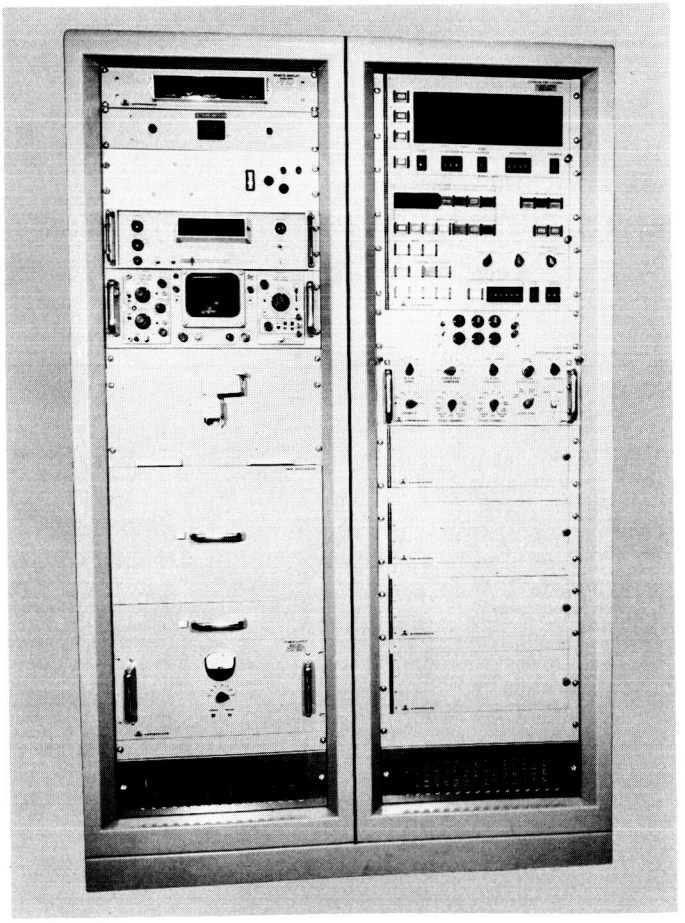

Fig. 3. Astrodata command system

A digital instrumentation system has been installed and program tested. The system is able to sample either analog or digital data at various sampling rates and record the data on magnetic tapes. Simultaneously to the data gathering, an identical standby computer can maintain vigil on the station parameters and detect errors to determine station failure. These errors are read out in typewritten form. In addition, the system may also be used to initiate and prepare periodic station reports.

A multiplex microwave system between Pasadena and Goldstone is still in the process of being installed and tested. Fig. 4 illustrates the equipment room, and Fig. 5 illustrates the antenna tower. The system will initially provide ten 4-wire 3-kc voice/data channels, two 2-wire 3-kc voice/data channels, two 2-wire 6-kc data channels, one two-way 300-cps to 96-kc wideband data channel, and one one-way 30-cps to 6.0-Mc wideband video data channel. Expansion capabilities provide for an additional eight 4-wire 3-kc voice/data channels and one 48-kc wideband data channel; or, expansion of the 96-kc channel to 140 kc, or, twelve 4-wire 3-kc data channels.

b. Pioneer site. The hydromechanical building is completed and equipment is currently being installed. Receiver, data, and instrumentation equipment have been

Fig. 5. Microwave antenna tower

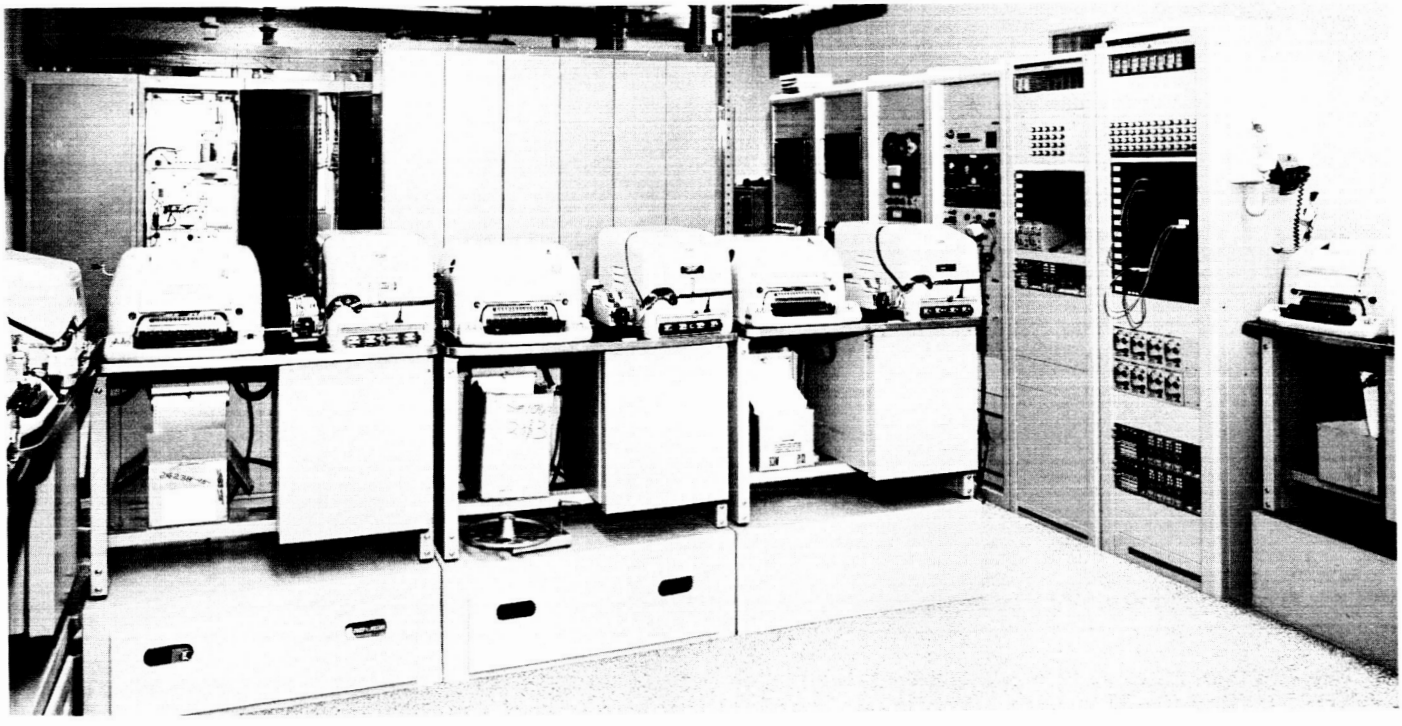

Fig. 4. Microwave equipment room

reinstalled in the control building. The antenna has been modified to include a new quadripod and feed holder. The maser and parametric amplifier have been modified and will be remounted on the apex of the new quadripod.

All equipment removed for building construction has been reinstalled. During this period the receiver T-frames were up-dated and rewired, and data system was completely reracked and rewired to the Goldstone Duplicate Standard (GSDS). Currently, all equipment is being checked out and interface problems are being resolved.

c. Mars site. Preparation of the Mars site has begun. A 600,000-gal reservoir to provide water for road construction was filled by pumping water from a local well and has been completed. Road and site construction contractors arrived on site, October 14, and site clearing began the following day. Fig. 6 illustrates the reservoir, and Fig. 7 shows the beginning of site construction.

2. Construction

The access road to the Venus site (Fig. 8) is now completed.

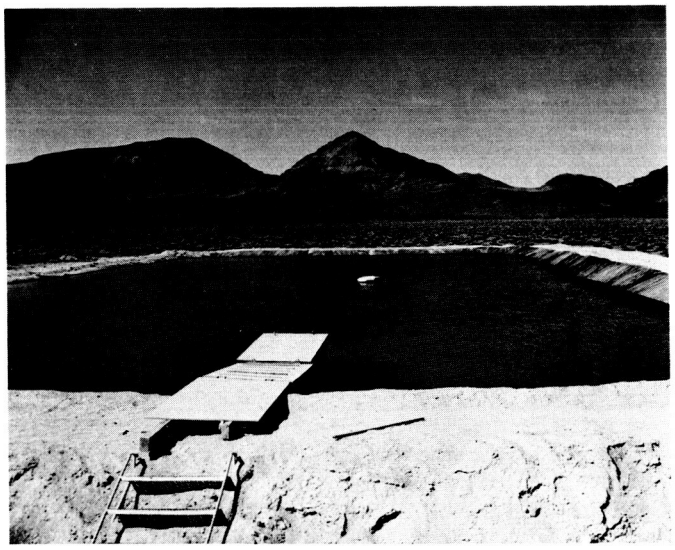

Fig. 6. Mars construction reservoir

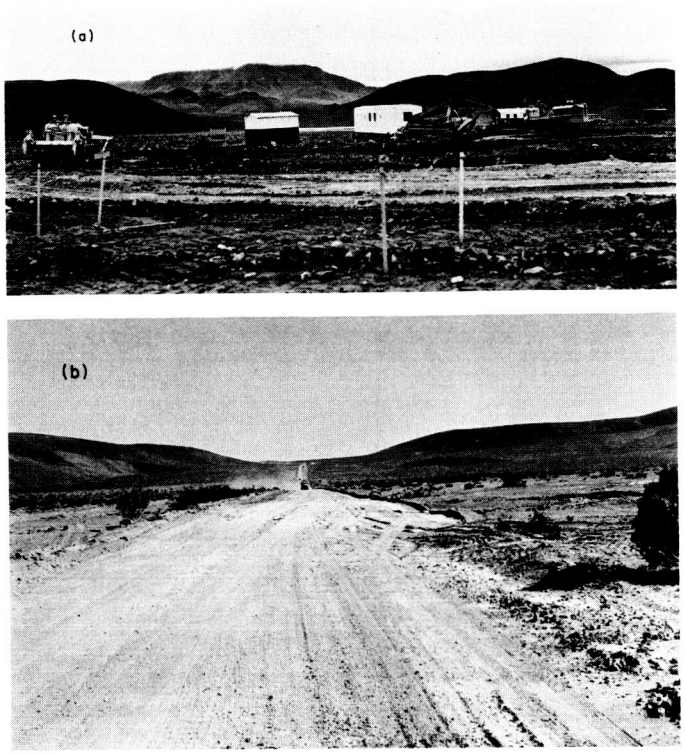

Fig. 7. Mars site construction (a) start; (b) road construction

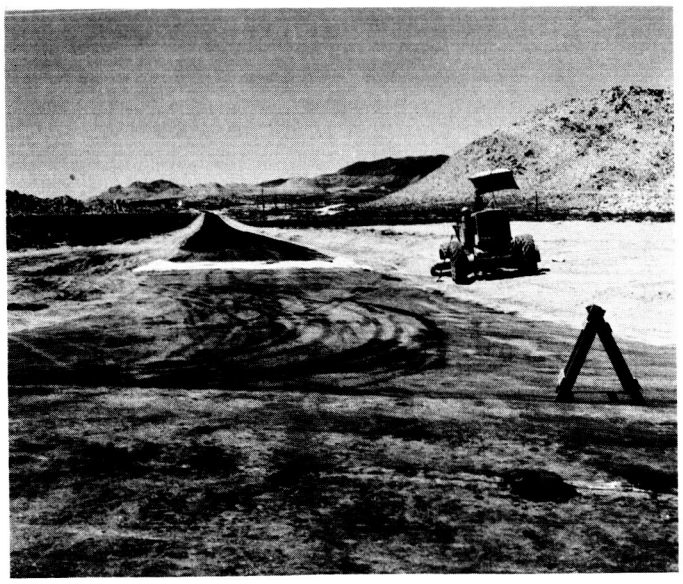

Fig. 8. Venus site access road

The text on Page 7 of *SPS 37-23*, Volume III, relating to Fig. 3 is incorrect. Proper description will be printed in *SPS 37-25*, Volume III.

III. Engineering Development

A. Mark I Ranging Subsystem

The DSIF Mark I ranging subsystem is being designed and built to equip the DSIF with the capability of ranging on spacecraft "turnaround" transponders to distances of 800,000 km. The ability to range on passive satellites is also inherent in this subsystem; however, single-station operation of the DSIF S-band system abrogates this capability. Earlier installments of the description of this subsystem have been given in Volumes III of *Space Programs Summaries Nos. 37-20, 37-21, 37-22,* and *37-23*. In this summary the operational and test control features are described.

1. Manual Controls and Visual Indicators

The manual controls and visual indicators of the Mark I ranging subsystem are located on three panels on the front of the cabinet. These are the power panel, the test panel, and the control panel. The power panel contains the master ac line circuit breaker, a "power on" indicating light, and a running-time meter. In normal use, all other power switches remain permanently on, so that the entire subsystem can be turned on and off by means of this single switch. The test panel controls are used only for certain nonoperational testing and troubleshooting procedures, never as part of an operational procedure. The control panel contains all operational controls and indicators. An indicator light on the control panel serves to inform the operator that all controls on the test panel are in operational position.

2. Control Panel

The layout of the control panel is shown in Fig. 1. The functions and use of its indicators and controls will be explained in the order of their application. (For reference to the operations involved, see *SPS 37-23*, Vol. III, pp. 11–14.)

(a) It is necessary to ensure that all switches on the test panel are in the operational mode, so that all controls originate either from the control panel or, automatically, from the system itself. Suitable interlocks cause the RANGING OPERATIONAL indicator to be lit when this is the case.

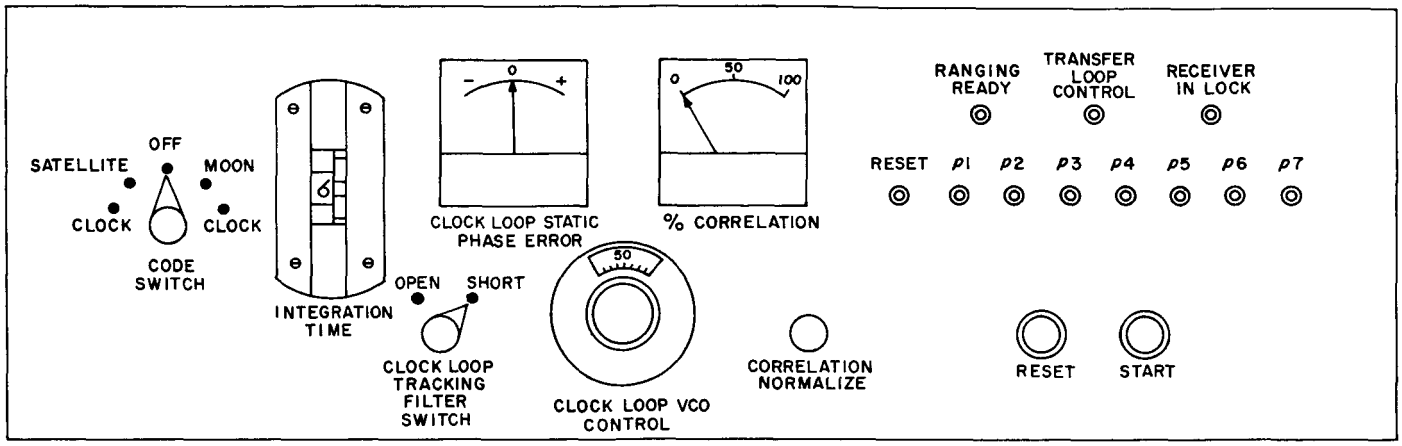

Fig. 1. DSIF Mark I ranging subsystem—control panel layout

(b) The clock-transfer-loop control relay may be actuated either from the RF receiver or from the ranging subsystem. Operationally, it must be controlled from the ranging subsystem. The operator must ensure that the TRANSFER LOOP CONTROL indicator is lit; this indicates that control rests with the ranging subsystem.

(c) A check is made to ensure that the RF receiver is in lock by ascertaining that the RECEIVER IN LOCK indicator is lit.

(d) The operator must select either the "Satellite" or "Moon" code to be modulated on the carrier, by appropriate setting of the CODE switch. The satellite code permits more rapid acquisition; however, it should not be used for estimated ranges exceeding 10,000 km. The Moon code permits a maximum unambiguous range of approximately 800,000 km.

(e) Having obtained, from the receiver operator, a report of the received signal strength (AGC), the ranging operator decides on the required integration time and makes the appropriate setting of the INTEGRATION TIME switch.

(f) The subsystem is put into the "Reset" state by pushing the RESET button, preparatory to acquiring the "clock" code component.

(g) The clock loop tracking filter is shorted by means of the switch so designated, and the clock loop static phase error is observed on the meter.

(h) Unless, or until, the static phase error indication is zero, the clock loop VCO frequency must be varied by means of the VCO control potentiometer which serves to inject a very stable, variable dc voltage.

(i) When the clock loop static phase error has been zeroed, the clock loop tracking filter is unshorted by means of the CLOCK LOOP TRACKING FILTER control.

(j) Since the clock loop is now locked up, the correlation is 50% of maximum and the reading of the % CORRELATION meter is normalized to 50% (midscale) by means of the CORRELATION NORMALIZE control.

(k) The subsystem stands by for acquisition of the four code components and the initiation of range determination. When this is desired, the START button is pushed. The subsystem automatically goes through program states $p1, \cdots, p6$ into $p7$, with a correlation indication of 100%.

(l) Once range tracking is in effect, there is no further need for the code as such, provided that clock lock is maintained. Thus, should it be desired to cut down the sideband spectrum to frequencies of multiples of 498 kc from the carrier, the operator may turn the CODE switch from MOON (or SATELLITE) to CLOCK. In this mode the 498-kc clock waveform only is modulated on the transmitted carrier, and the receiver code is cut off.

(m) Should lock be lost subsequently, the subsystem will automatically revert to the "Reset" state. If the RECEIVER IN LOCK indication reappears, and the CODE switch is in MOON (or SATELLITE) position, the START button may again be pressed to achieve a new ranging acquisition.

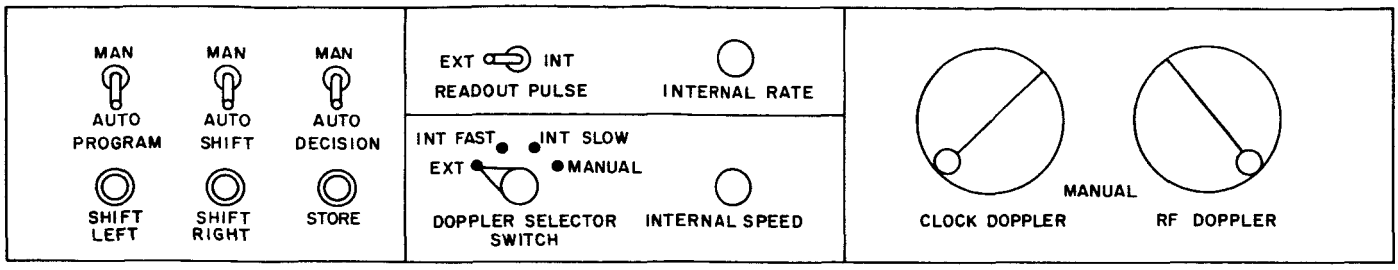

Fig. 2. DSIF Mark I ranging subsystem—test panel layout

3. *Test Panel*

The layout of the test panel is shown in Fig. 2. As previously mentioned, the controls on this panel are used exclusively for testing and troubleshooting. Means are provided, through these controls, to "exercise" the subsystem in the absence of the receiver and data-handling subsystems.

(a) Readout pulses, which normally are received from the data-handling subsystem, can be internally generated by an asynchronous, variable-frequency pulse generator. The READOUT PULSE switch selects between EXT and INT, while the INTERNAL RATE control knob beside it permits variation of the internally generated readout pulse intervals from ½ to 2½ sec.

(b) Operationally, the DOPPLER SELECTOR switch is in the EXT position, in which the clock and RF doppler inputs are obtained from the receiver. In the two INT positions, an asynchronous, variable-frequency generator supplies pulses which serve to run the doppler-simulating flip-flops, located in the digital-logic portion of the subsystem. The rate of this simulated doppler is controlled by the INT FAST or INT SLOW setting of the DOPPLER SELECTOR switch and, more finely, by the INTERNAL SPEED control beside it. When the DOPPLER SELECTOR switch is in the MANUAL position, the doppler signal inputs are derived from sine–cosine potentiometers whose control cranks are at the right of the panel. When turned, the one serves to simulate clock doppler, the other independently simulates RF doppler. Unless the DOPPLER SELECTOR switch is in the MANUAL position, these cranks are ineffective.

(c) The PROGRAM switch is operationally in the AUTO position. When set to this position, the subsystem requires the actuation of the START button to go from the reset state to program state $p1$, whence it proceeds automatically through program states $p2, \cdots, p7$. When the PROGRAM switch is in the MAN position, the actuation of the START button is required to go from any program state into the next in sequence.

(d) The SHIFT switch is operationally to the AUTO position. When in this position, all shifting of code components in the process of code acquisition is done automatically under control of the acquisition subroutine; all shifts are right (i.e., component-delaying) shifts. When the SHIFT switch is in the MAN position, shifting (either right or left) must be done, 1 bit at a time, by actuating the SHIFT RIGHT or SHIFT LEFT pushbutton, respectively.

(e) The DECISION switch is operationally in the AUTO position. When in this position, the finite time integral of the correlation voltage for a particular code-component shift position is automatically compared with the largest time-integrated correlation voltage previously determined, and made to replace it in the high-correlation storage if the new value exceeds the old. When the DECISION switch is in the MAN position, the comparison must be made by inspection of the % CORRELATION meter. The storing of a (new) value in the high-correlation storage, and the simultaneous storing of the corresponding shift position, is accomplished by the manual actuation of the STORE pushbutton.

4. *Project Progress*

The system design has been completed. The laboratory prototype has been constructed and has undergone preliminary tests with the S-band test receiver–transmitter. Helicopter transponder ranging tests are to be flown shortly. Construction of the Serial No. 1 (Pioneer) and Serial No. 2 (Johannesburg) GSDS subsystems is proceeding satisfactorily. Documentation to permit construction of Serial Nos. 3 and 4 off-Laboratory is progressing satisfactorily.

B. Systems Engineering

The systems engineering function within the DSIF is concerned with three types of activity:

(1) DSIF engineering (the definition of the Deep Space Instrumentation Facility and documentation of its capability).

(2) DSIF project engineering (the definition of DSIF requirements and commitments to spacecraft projects such as *Ranger, Surveyor,* and *Mariner*).

(3) DSIF system analysis (the detailed theoretical analysis of circuits, systems, and problems related to DSIF performance).

The status of these activities is as follows:

1. Engineering

Support of the DSIF S-band project was continued during this period. Revised issues of the project status report were prepared showing the details of staffing, funding, procurement, and scheduling.

Coordination meetings were held with the cognizant subsystem development groups. Three individuals were assigned the responsibility of coordinating critical interface areas. These were layout of equipment racks, cabling between subsystems, and signal interface between subsystems. In addition, a systems engineer was made responsible for coordination of equipment installation within the electronics room on the antenna structure.

2. Projects

DSIF support was provided for the following projects:

a. **Surveyor.** A test plan was prepared for compatibility testing of the Hughes Aircraft Company CDC and the feasibility model of the S-band radio equipment (Ref. 1). These compatibility tests will establish the adequacy of the command, telemetry, and television modes used in *Surveyor.*

An additional test plan is under preparation for the purpose of testing the T-21, *Surveyor* spacecraft, with a full GSDS S-band system at Goldstone. Several coordination meetings have been held to establish the type of tests and the facilities required to accomplish them.

The proposals for the *Surveyor* Roving Vehicle Project were reviewed for compatibility with the DSIF.

b. **Ranger III.** The receiving systems at Goldstone Pioneer and Echo sites were modified and adjusted to provide the required 2-Mc bandwidth to accommodate the television signals from the RCA television experiment on the *Ranger* Block III.

c. **Ranger V.** A planning document[1] was prepared for *Ranger* Block V showing the DSIF capability. This document essentially outlines the L-band capability to be retained at several of the DSIF Stations to provide support of this mission during calendar year 1965.

DSIF performance information and capability data have been supplied to the Aeronutronic Division of Philco in support of their capsule study under a contract from Northrop Space Laboratory.

d. **Pioneer.** A support plan was prepared for Ames Research Center showing DSIF commitments for the *Pioneer* Project.

e. **Agena *class lunar orbiter.*** Project personnel from the Langley Research Center were briefed at JPL on the DSIF capability and the S-band project status. DSIF consultation was provided at the proposal evaluation committee meetings held by Langley Research Center in Hampton, Va.

f. **Mariner C *(Mars mission, 1964).*** A plan was prepared for the *Mariner C* project office showing the necessary equipment for simultaneously recording signals from two planetary probes. (Should two probes be successfully injected into planetary orbit, they would be within the beamwidth of a tracking station during the final planetary approach phases. Simultaneous signal reception would be possible.)

g. **Mariner B. (Centaur-*based entry-capsule mission).*** Participation in the *Mariner B* study consisted of a preliminary capability statement, a preliminary commitment of stations, and a review of signal acquisition problems. The study considers the use of the 210-ft antenna installation under construction at the Goldstone Mars site.

[1] "Capability of the Deep Space Instrumentation Facility for the Lunar Missions of *Ranger* Block V," JPL Engineering Planning Document No. 184.

One particular method of signal acquisition currently under detailed study involves the use of predetection recording of signals under adverse signal-to-noise conditions and the subsequent recovery of data.

h. **Apollo.** Specifications prepared by Goddard Space Flight Center for the Manned Space Flight Network (MSFN) were reviewed and commented upon by systems engineering personnel. A meeting was held at JPL with Goddard personnel to further detail JPL technical support of the implementation of the MSFN.

3. Analysis

A study is being performed on the systems temperature contribution from the Sun and the Moon as seen by the DSIF 85-ft antennas at L- and S-band. This data will be made a portion of future DSIF capability documents.

The problem of DSIF acquisition of spacecraft signals is continuing. In particular, the constraints of amplitude change rate and of phase change rate have been established. Project engineering personnel can use this information in establishing receiver performance under varying tracking conditions.

In particular, the ability to track a survival capsule during its final descent phase can be defined under the conditions of known signal-to-noise ratio.

C. Antenna Engineering

1. Antenna Temperature Control Investigations

In the early stages of a space vehicle's flight, angle pointing data from the ground-based antennas tracking the vehicle are very important. Therefore, any factor that might degrade the data warrants investigation.

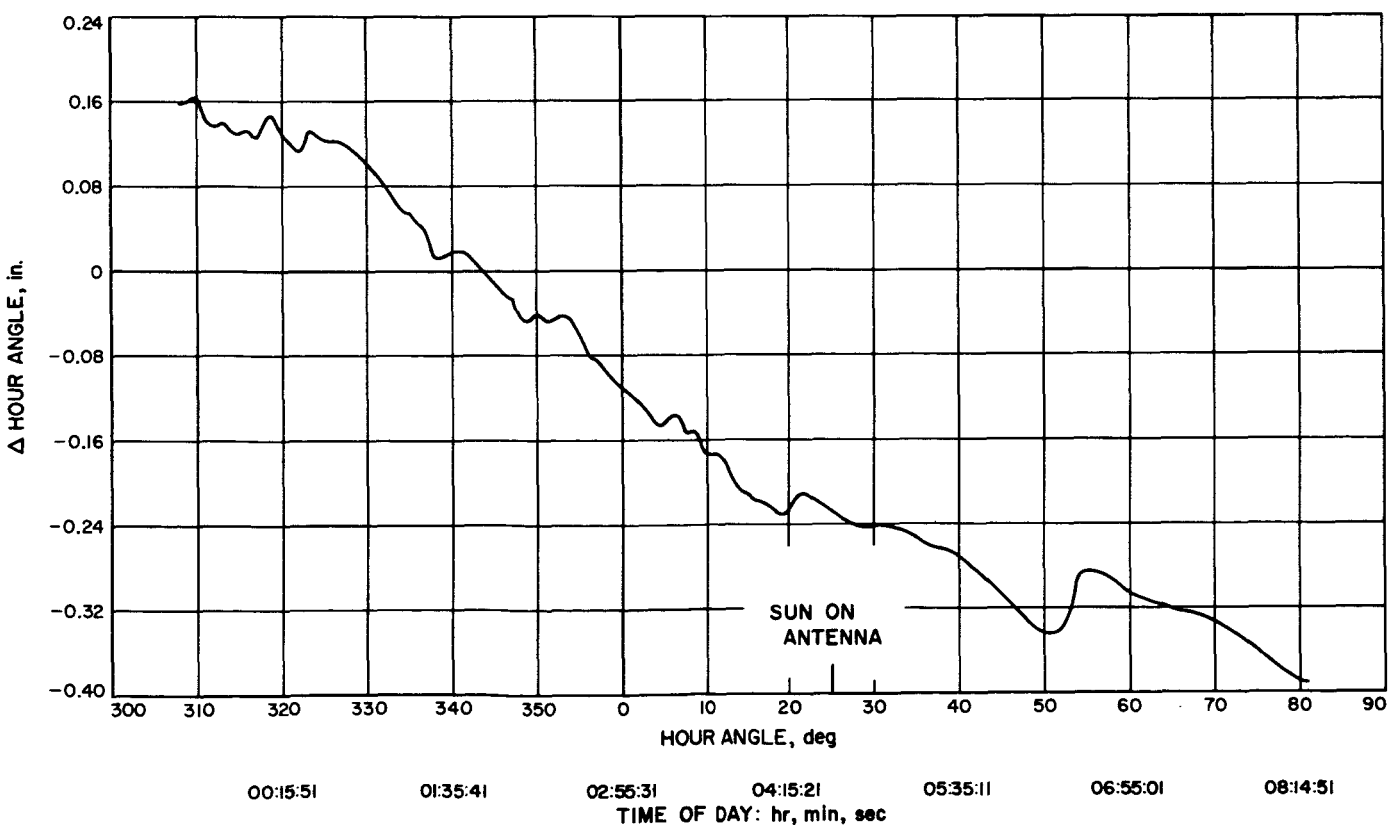

Fig. 3. ΔHA simulated *Ranger 3* Test No. 3, March 17–18, 1962, quadripod deadload and thermal deflections

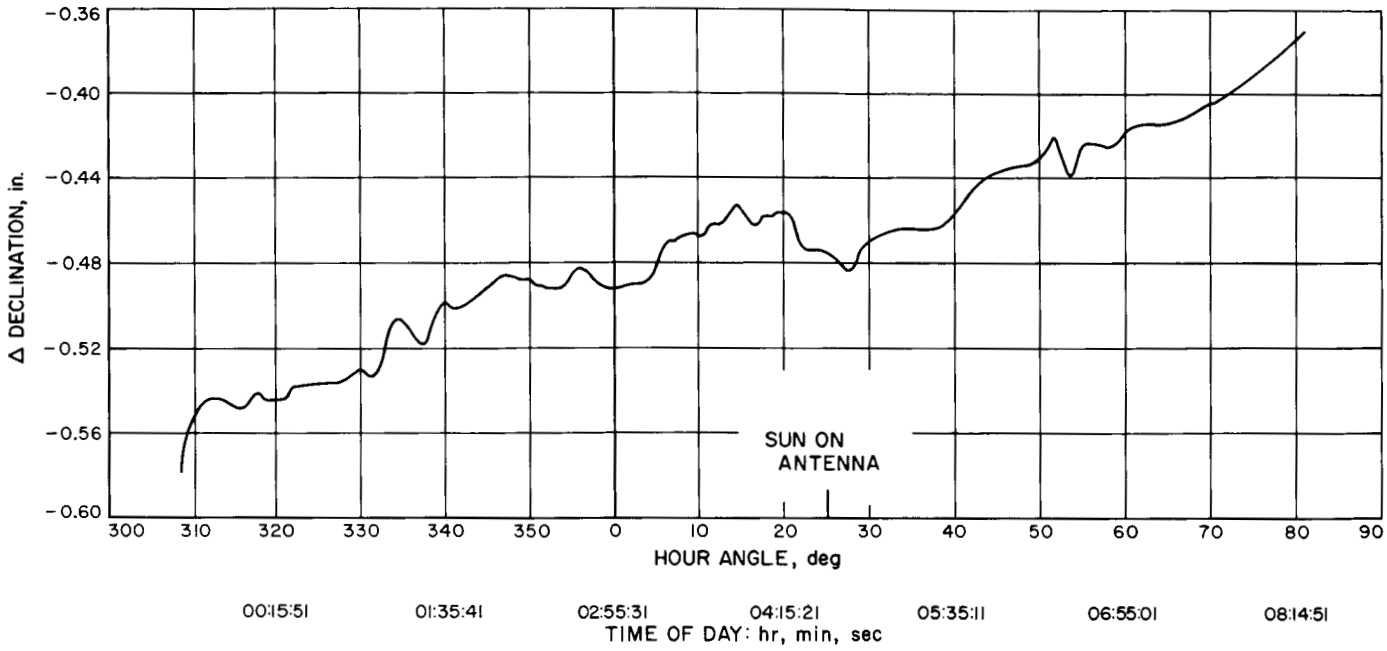

Fig. 4. ΔDec simulated *Ranger* 3 Test No. 3, March 17–18, 1962, quadripod deadload and thermal deflections

The possibility that solar energy or thermal inputs cause distortion of the antenna structures led to an investigation to determine whether or not thermal or solar energy inputs distort antenna structures to a degree that would significantly affect angle pointing data.

The first step in the investigation was to resolve the degree to which solar or thermal inputs affected angle pointing data. This was done by applying the following tests (Ref. 2):

(1) Comparison of nighttime and daytime startrack angle data.

(2) Nighttime into daytime or transition startracks to record any abrupt changes in angle data.

(3) Monitoring of the antenna focal point or quadripod movement relative to the dish structure.

(4) Comparison of collimation tower TV and RF boresight data, as the angle of solar or thermal energy input varied over a 24-hr period.

Typical results of Tests (1) through (4) are shown in Figs. 3 through 9. These tests show RF quadripod pointing errors as large as 0.02 deg, mechanical axes pointing errors as large as 0.05 deg, and significant shifts in collimation tower boresight data.

The next step was to determine what might be done to reduce or eliminate the thermally induced distortion causing the angle pointing errors.

The essential conditions governing temperature control of a body are radiation characteristics, heat capacity, and local wind conditions. Since little can be done about the antenna's heat capacity or local winds, the obvious solution to reducing thermal distortion was to attempt to modify the antenna's radiation characteristics.

The temperature of an isolated body can be expressed as:

$$T = [k_1 (\alpha s/\epsilon)]^{1/4}$$

where

k_1 = a constant.

αs = solar absorptivity.

ϵ = total hemispherical emittance at the body's temperature.

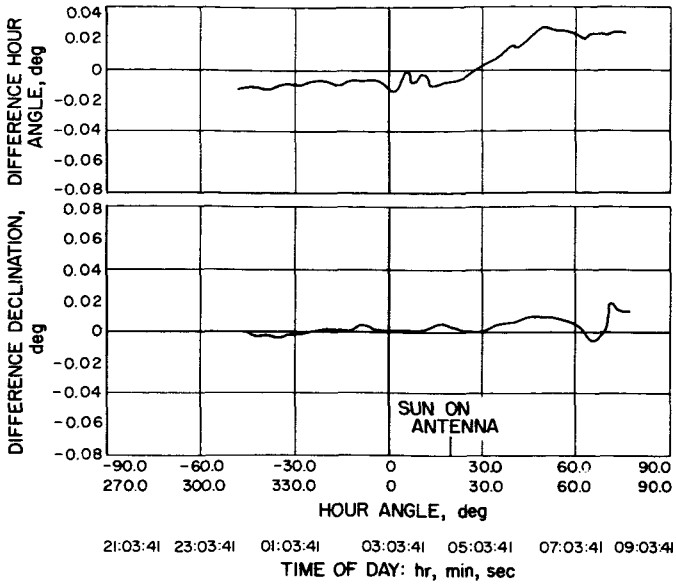

Fig. 5. Transition startrack Test No. 1 compared with nighttime startrack, March 15, 1962 with March 26, 1962

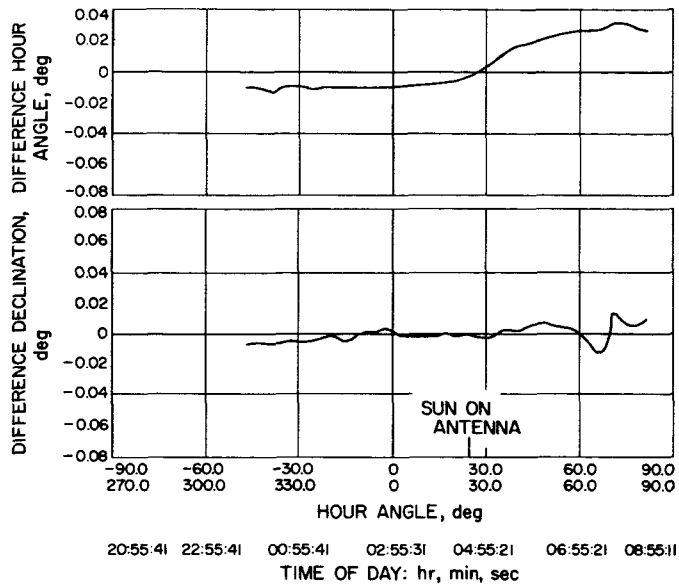

Fig. 6. Transition startrack Test No. 3 compared with nighttime startrack, March 17, 1962 with March 26, 1962

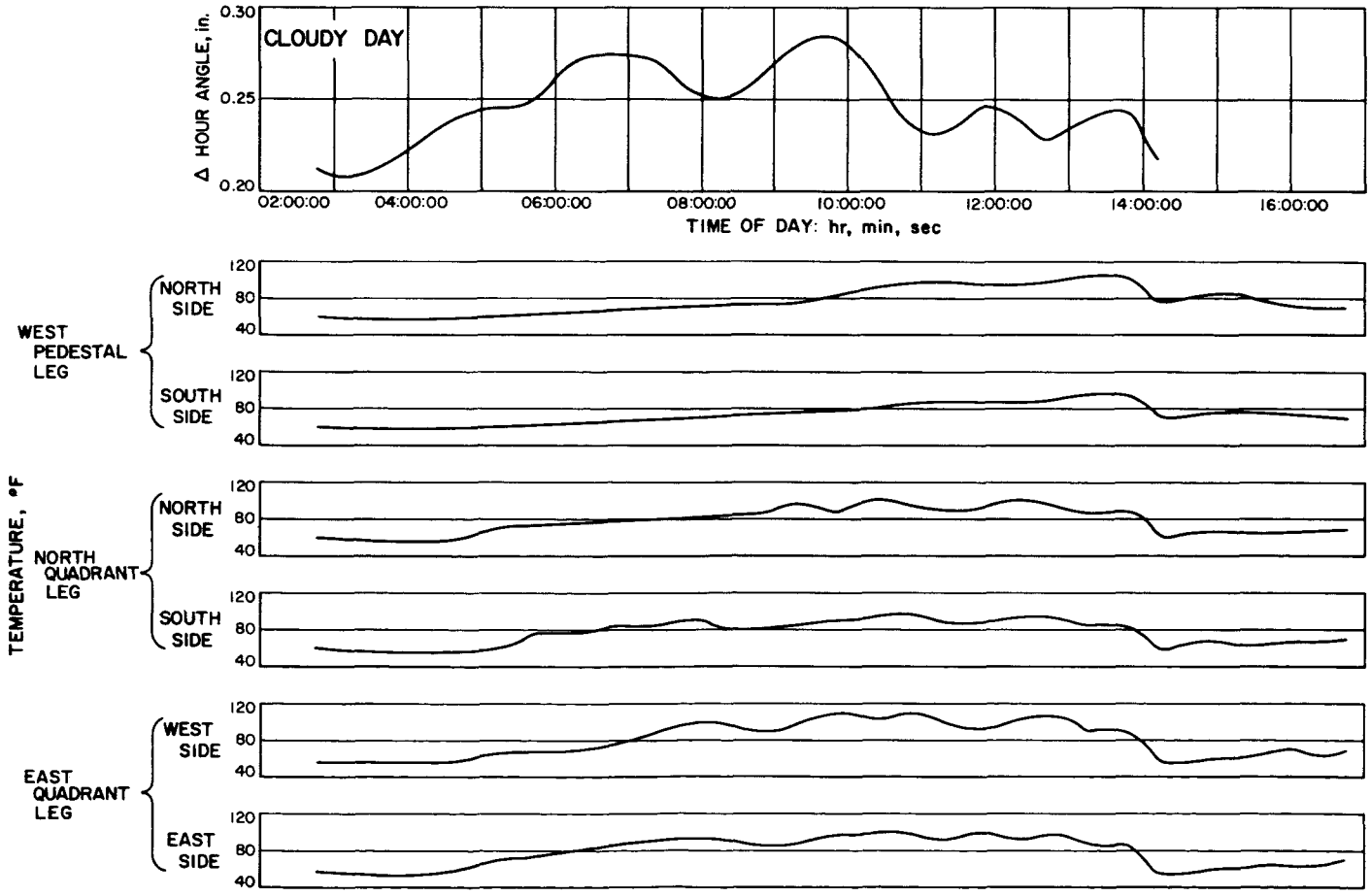

Fig. 7. Collimation-tower ΔHA deflection temperature Test No. 1, March 26, 1962

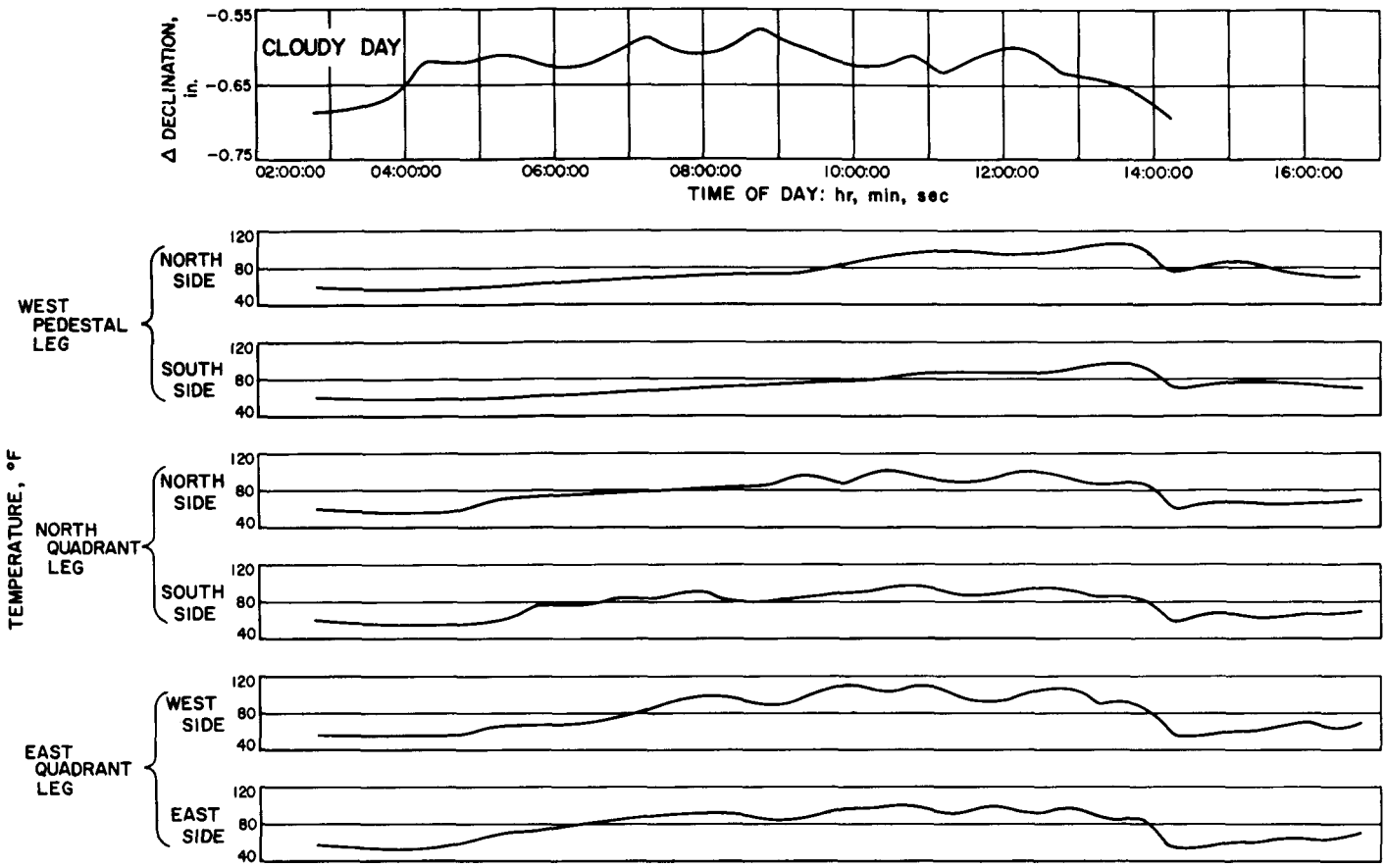

Fig. 8. Collimation-tower ΔDec deflection temperature Test No. 1, March 26, 1962

As αs and ϵ are essentially surface phenomena, the temperature of a body will depend on its surface material and finish. Therefore, it was decided that a change in the antenna's surface material (finish or coating) was required.

Investigation proved that, of the various approaches, paint coatings not only provided better radiation characteristics but lower cost, excellent corrosion protection, and improved appearance. Further investigation of paint coatings supplied the following data:

(1) The paint coatings should have a dry film thickness in excess of 0.004 in. (normally two coats) to assure solar reaction to the radiation characteristics of the paint only; otherwise, solar energy would permeate the coating and bring the radiation characteristics of the material underneath the paint into effect.

(2) The coating should not be too thick, about 0.006 to 0.008 in. or less, so that the difference in expansion and contraction of the antenna materials and paint coating does not cause a failure or deterioration of the coating.

(3) The dish or focusing element of the antenna uses a paint whose optical characteristics are such that they cause diffusion of incident optical energy (low spectral gloss) so that focal zone equipment or structural elements are not overheated.

(4) The rest of the antenna structure, the nonfocusing portion, should have a tight film coating—one highly resistant to such hazards as excessive wetting with hydraulic fluid, steam cleaning solvents, grit, sand, human traffic, etc.

Various paints were tested on materials of equal heat capacity, with similar wind conditions (Figs. 10, 11, and 12) and consultations were carried out with local and national paint manufacturers. Fig. 13 (a) through (f) illustrate typical data indicative of the different temperature

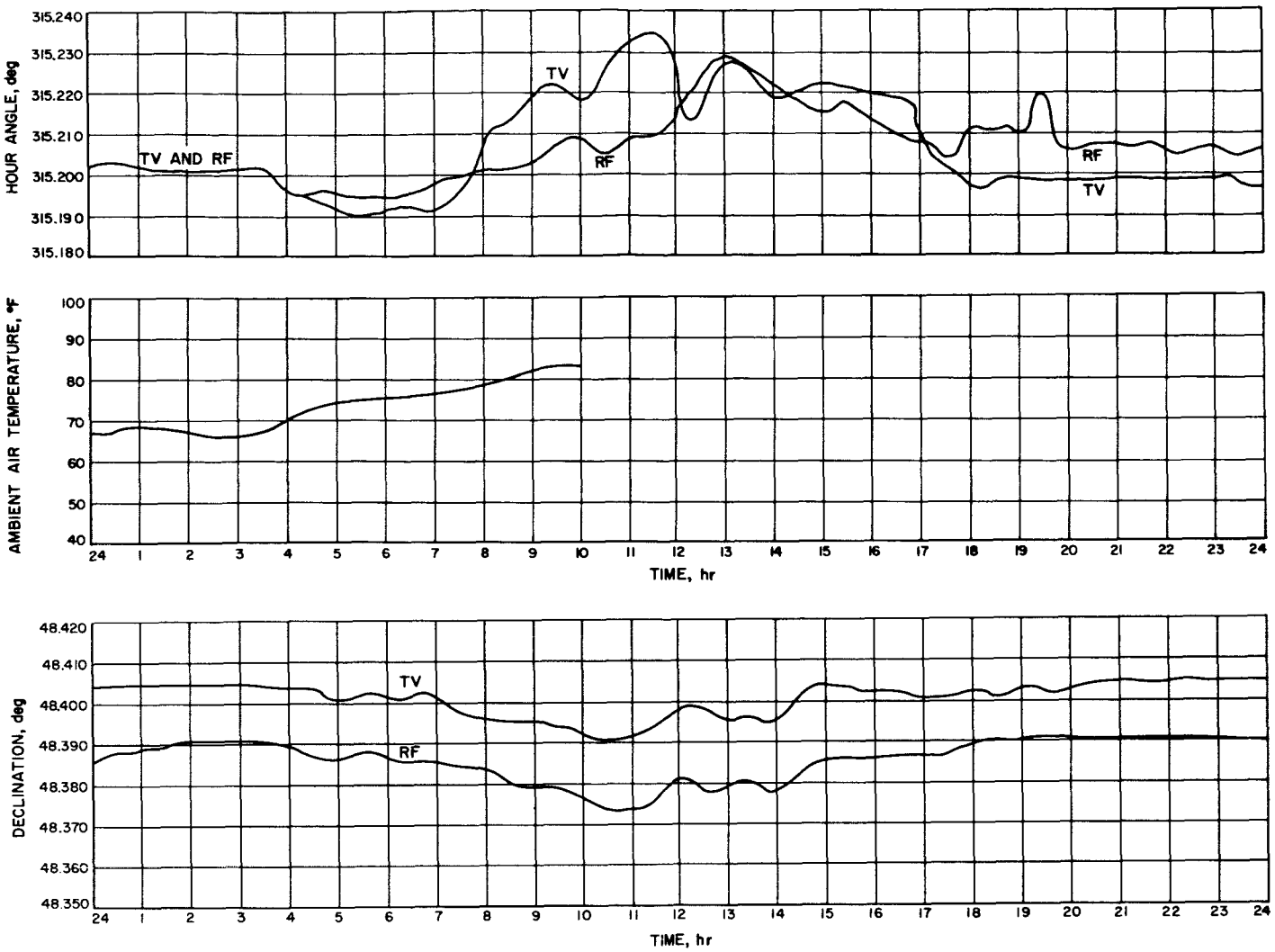

Fig. 9. RF-TV boresight versus temperature, HA and Dec, November 29, 1961

characteristics of bodies of equal heat capacity, subjected to similar solar exposure and local winds, but having different surface finishes or coatings. These tests and consultations indicate the following:

(1) White paints of proper film thickness afford the largest reduction in solar heating, and exhibit the lowest ($\alpha s/\epsilon$) radiation characteristics ratios of the various practical coatings.

(2) Maximum temperature control by any paint coating requires a minimum of two standard top coats.

(3) Depending on the body's heat capacity, local winds, and the ambient temperature, temperatures above ambient can be reduced by a factor as large as five.

(4) Paints having spectral glosses as low as 2% with good life characteristics can be obtained commercially. Spectral glosses of this level can significantly reduce focal point heating; for example, coating of the JPL 30-ft Az-El antenna surface with such a paint actually reduced focal point heating (when the Sun was tracked for approximately 5 min) from 1672 to 88°F (when the Sun was tracked for approximately 2 hr).

(5) Temperature control characteristics of an organic or inorganic coating are a function not only of pigmentation, but other constituents. A coating must be examined not only for its spectral gloss and life characteristics, but for coloring and aging characteristics which may cause it not to appear white to solar energy, or which may change its reflectance coefficient with aging, such as yellowing with age.

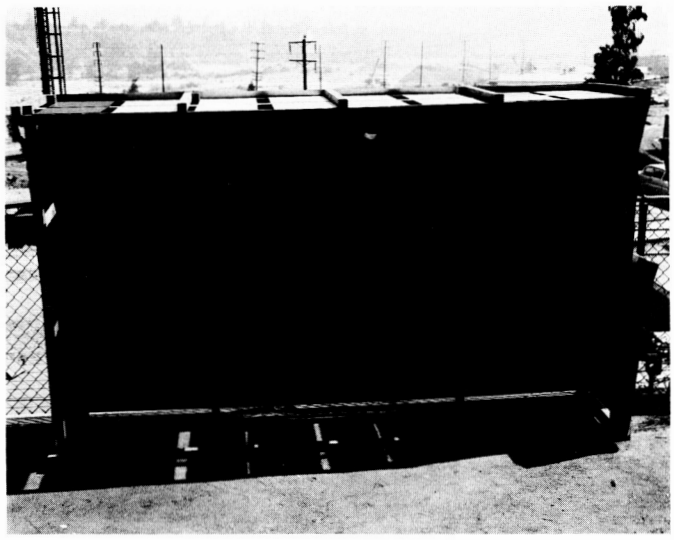

Fig. 10. Paint test samples and test frame

Fig. 11. Paint test samples—top view

As a result of the preceding efforts, three commercial coating systems were found to have the desired characteristics: one for the focusing portions of the antenna

Fig. 12. Paint test samples showing temperature transducers—bottom view

(FSP-1), and two for the nonfocusing portions (NFSP-1 and NFSP-2). Two of these systems, FSP-1 and NFSP-2, are currently being applied to the Johannesburg 85-ft, polar-mounted antenna as a test case. After coating, the Johannesburg antenna will be measured to determine if any reduction of thermally caused angle pointing data errors has been achieved.

2. Cassegrain Cone Handling Equipment

The Cassegrain cones of the Cassegrain system for the 85-ft polar antennas require three pieces of handling equipment for their installation, removal, and servicing: a 35-ton crane with a 100-ft boom and a 30-ft jib, an adjustable sling or cradle for lifting and positioning, and a service trailer. The following is a description of these items and the current status of the various DSIF Stations regarding the equipment.

a. Cranes. The Woomera, Pioneer, and Echo sites have existing units (P&H 35-ton cranes with 100-ft booms and 30-ft jibs). Similar cranes have been purchased for the Johannesburg, Canberra, and Madrid Stations.

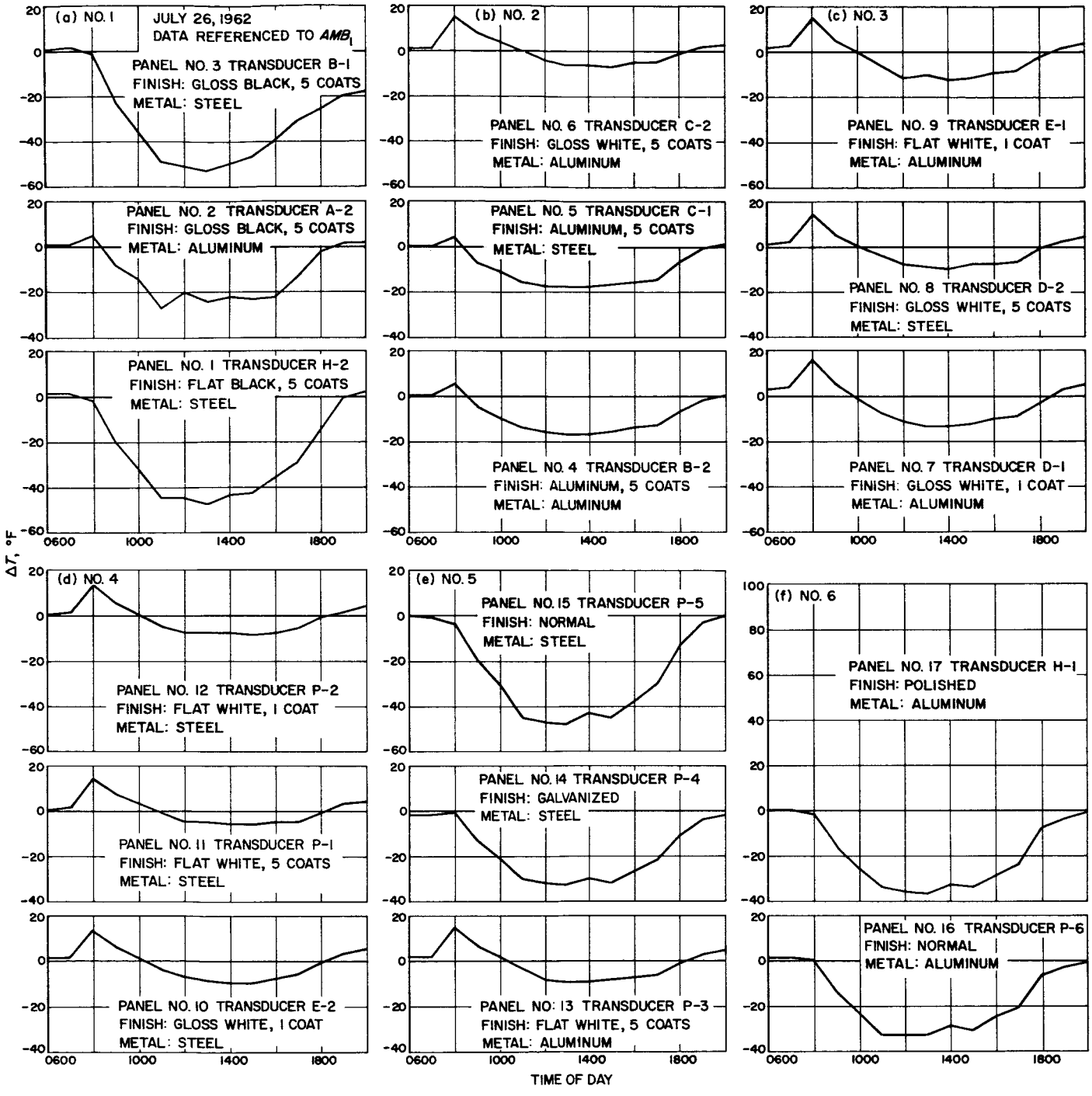

Fig. 13. Temperature spectrum for paint samples

b. Slings. Hoisting slings that provide manual two-axis control (Fig. 14) are currently being fabricated for all stations.

c. Service trailers. Service and storage trailers have been fabricated for all stations (Figs. 15, 16, and 17). These trailers provide either mobility or permanent positioning and levelling, using four hand-operated screw jacks.

3. *Transmitter-Electronics Cage Mock-Up*

A full-scale precision mock-up of the new transmitter-electronics cage, incorporated in the declination wheel

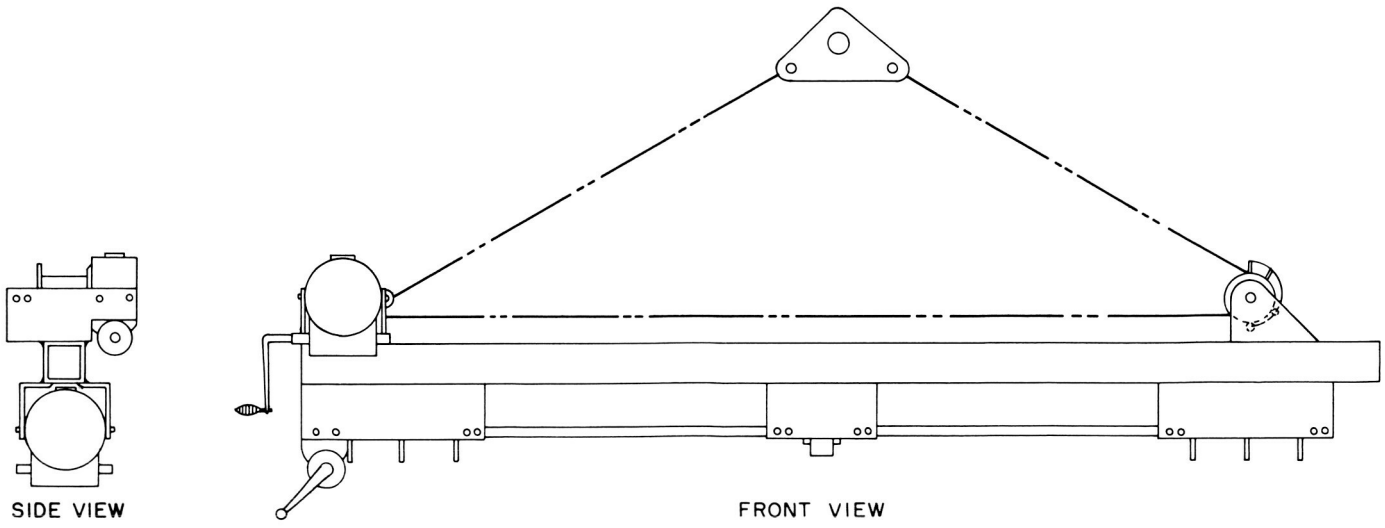

Fig. 14. Artist's sketch of Cassegrain cone handling sling

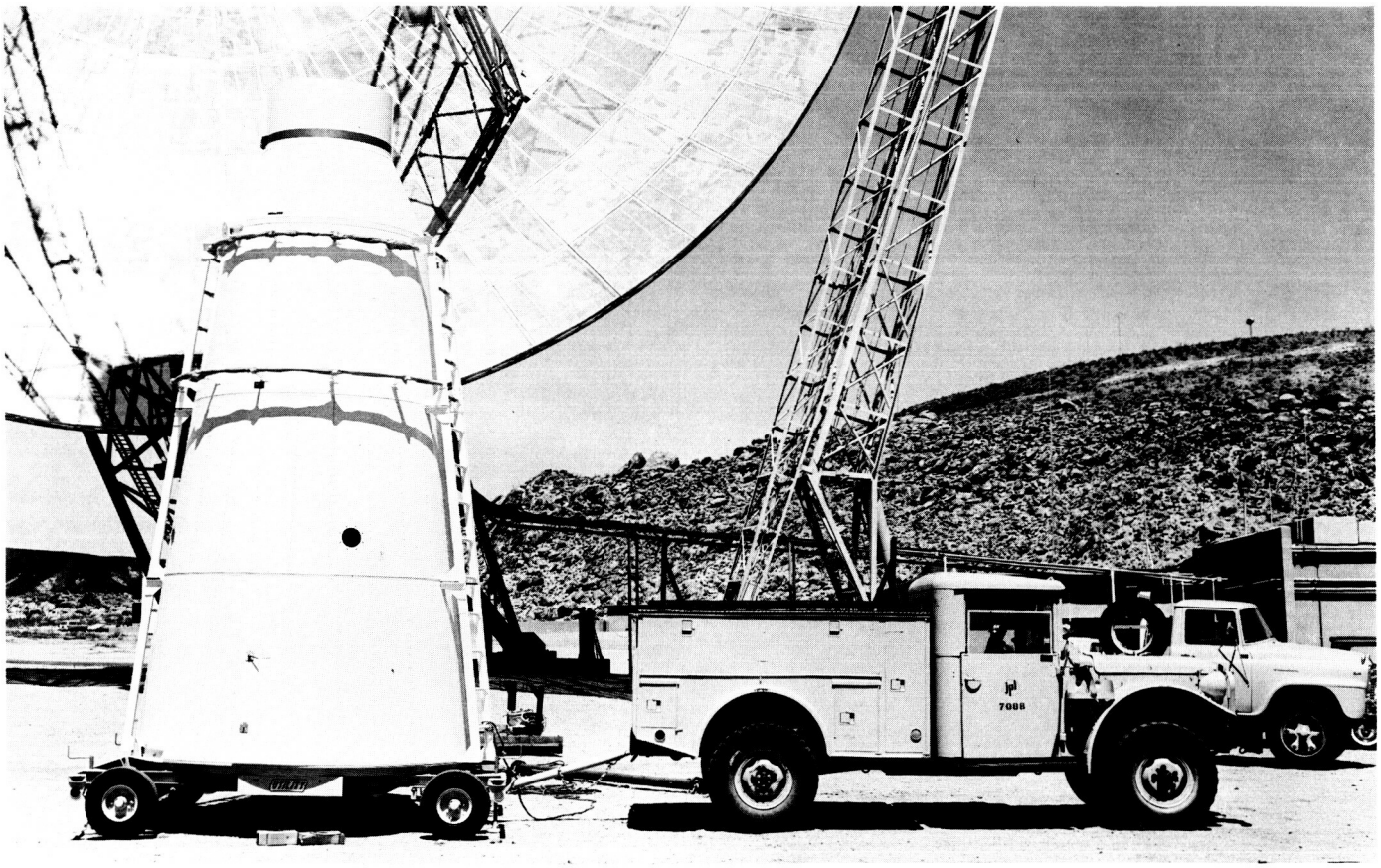

Fig. 15. Cassegrain cone service trailer with cone mounted

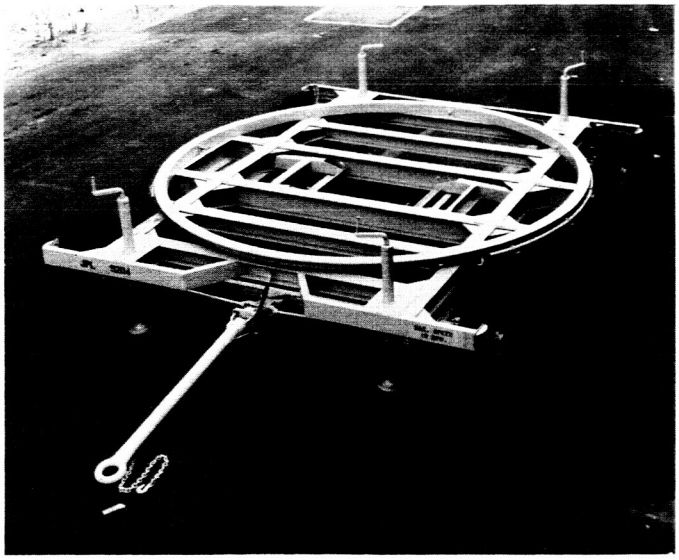

Fig. 16. Cassegrain cone service trailer showing leveling jacks—top view

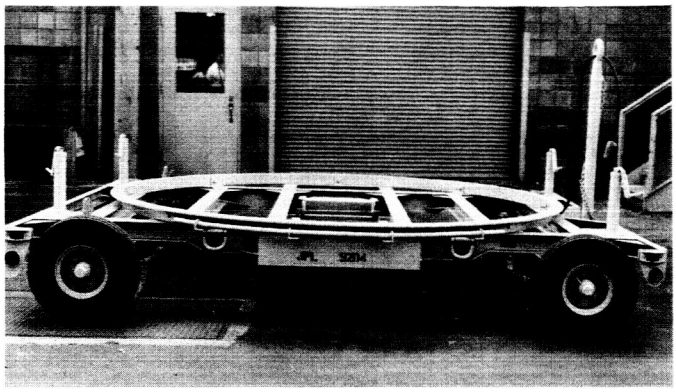

Fig. 17. Cassegrain cone service trailer—side view

of the DSIF 85-ft, polar-mounted antennas, has been erected at Goldstone (Fig. 18).

The mock-up will be used to mechanize the installation and arrangement of the various RF (L-band and S-band) hardware configurations of the DSIF Stations. Use of

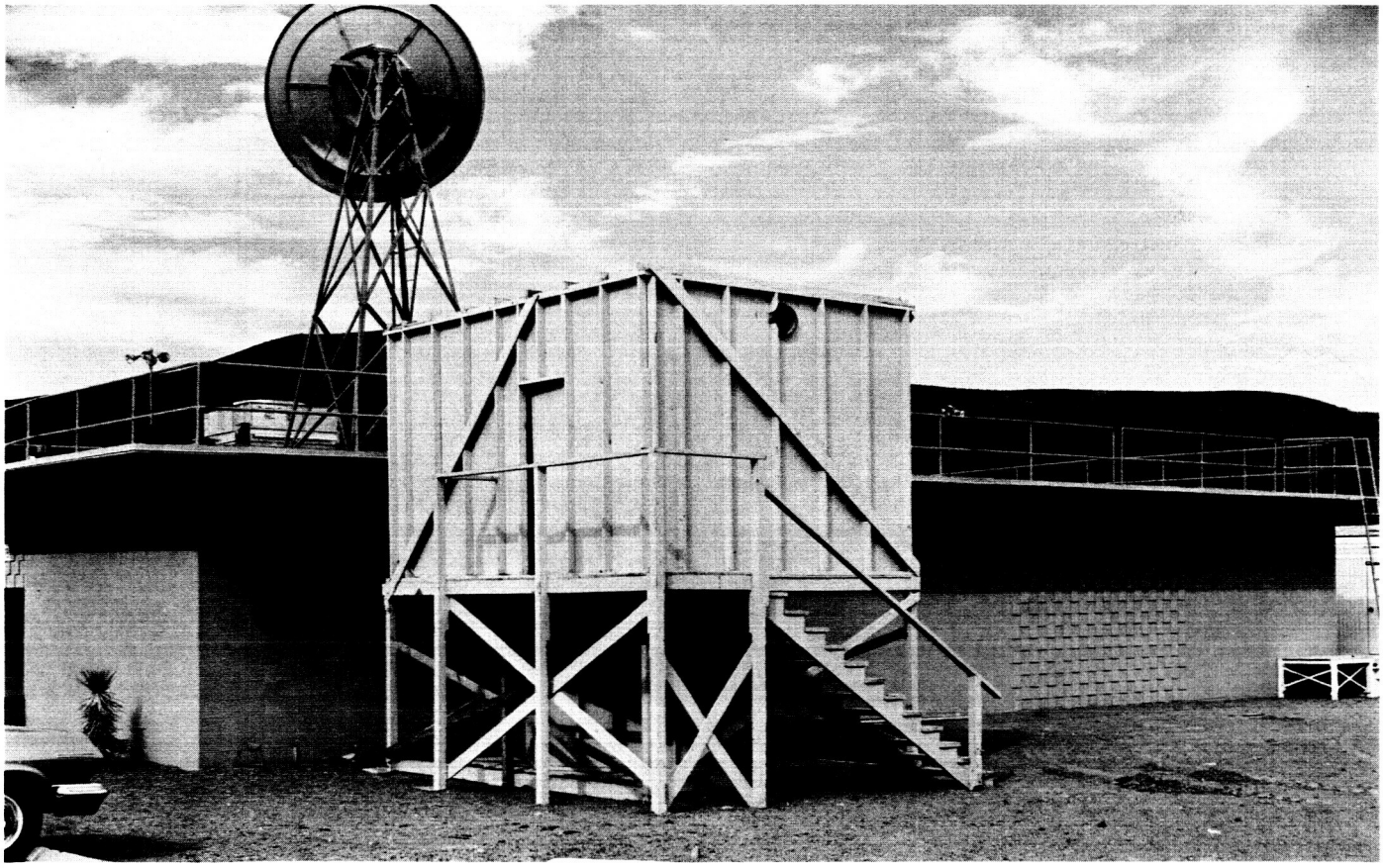

Fig. 18. Transmitter-electronics cage mock-up

the mock-up will reduce expensive overseas field installation work, facilitate complicated waveguide installations, allow the overseas configurations to be laid out at Goldstone, and resolve mechanical interfaces before hardware is shipped overseas.

4. Cassegrain Cones Subsystem

Since the conversion of the DSIF Net to an S-band Cassegrain configuration requires the net to be supplied with Cassegrain cones, such cones have been purchased for all stations. These cones are improved versions of the original prototype (Fig. 15) and are described as follows:

(1) All parts are fabricated from JPL source control drawings to ensure similarity.

(2) All bolt hole patterns for mating units are established from JPL-owned master templates to assure interchangeability of all units.

(3) All sections or units are equipped with integral lifting lugs (Fig. 19) and safety hand rails.

(4) The external skins of the cones are made of 0.080-in. 7178-T6 aluminum to ensure the units' survival capabilities in case they are used at stations subject to severe hailstorms (hailstones up to 3 in. in diameter).

(5) To ensure good temperature control characteristics and minimum solar energy focusing, all units are coated with JPL's new paint system, FSP-1.

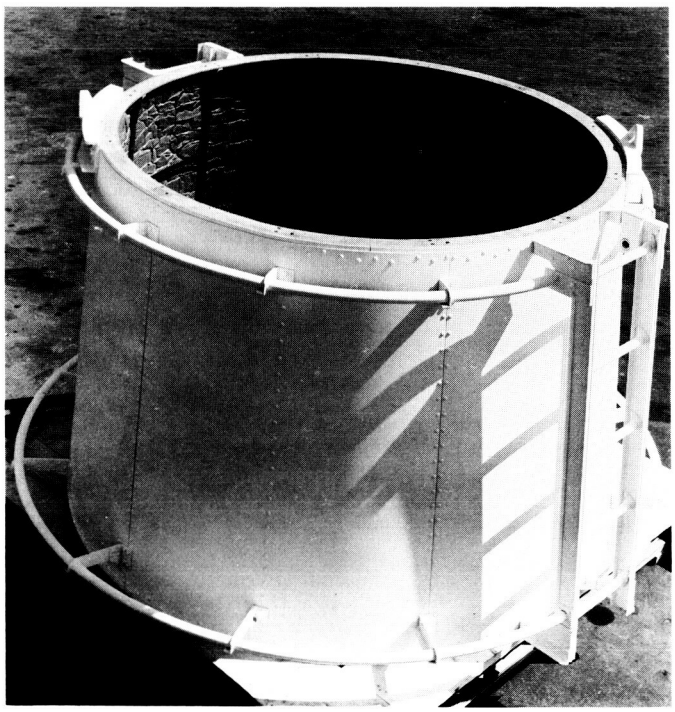

Fig. 19. Cassegrain cone section showing lifting lugs and hand rails

5. Hyperbola Subsystem

The conversion of the DSIF Net to an S-band and Cassegrain configuration requires that the net be supplied with hyperboloidal secondary reflectors having remotely adjustable back-up structures (Fig. 20).

The hyperbola subsystems are improved versions of the prototype systems and are described as follows:

(1) The hyperboloidal surface is manufactured by using a new lamination process which provides an improvement factor of about five in the manufacturing tolerances (rms values of 0.020 to 0.010 in.). Figs. 21 and 22 show a cross-section and top view, respectively, of a sample reflector.

(2) The reflector skin is made of a stronger aluminum alloy (6061-T6 rather than 2024-0 and 3004-0) for increased rigidity and for surface hailstone resistance if they are to be used at stations susceptible to severe hailstorms (hailstones with diameters up to 3 in.).

(3) The hyperboloidal reflector and back-up structure are coated with the new JPL paint system FSP-1

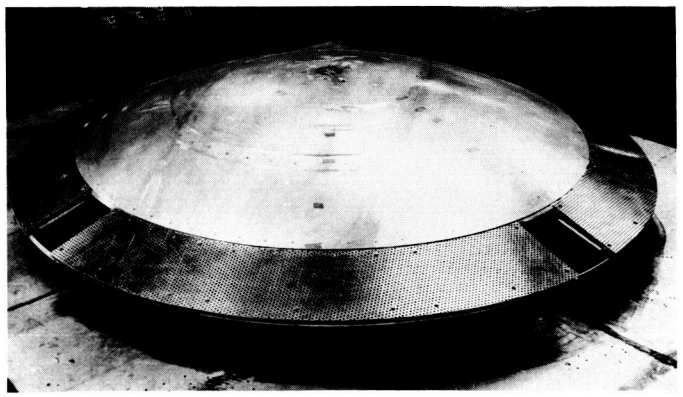

Fig. 20. New laminated hyperboloidal reflector—top view

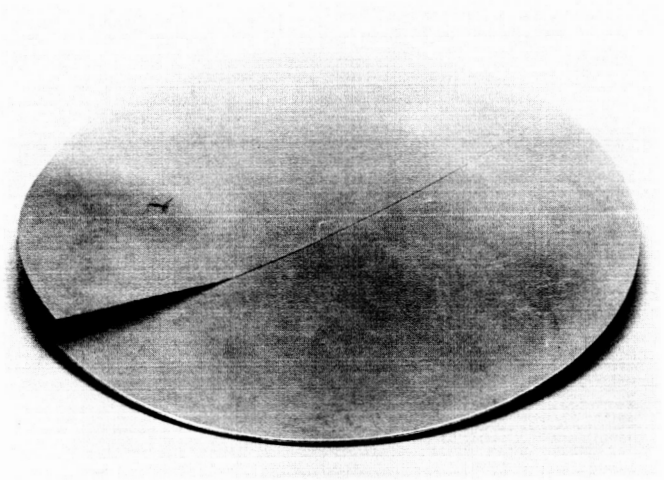

Fig. 21. Sample laminated reflector showing laminated construction—top view

to provide maximum temperature control, reduce thermal distortions, and improve thermal energy reflections and scatter.

(4) The reflector position-indicating hardware has been replaced with less expensive, less complicated, and more reliable equipment. The existing rotary limit switch, synchro transmitter, and chain drive configuration has been replaced with a linear transducer, micro-switch, and rack and pinion drive configuration, with calibrated dc meter readouts.

(5) All subsystem components are fabricated from JPL source control drawings to ensure similarity.

(6) All subsystem and quadripod bolt hole patterns for mating units are established from JPL-owned master templates to ensure interchangeability of all units.

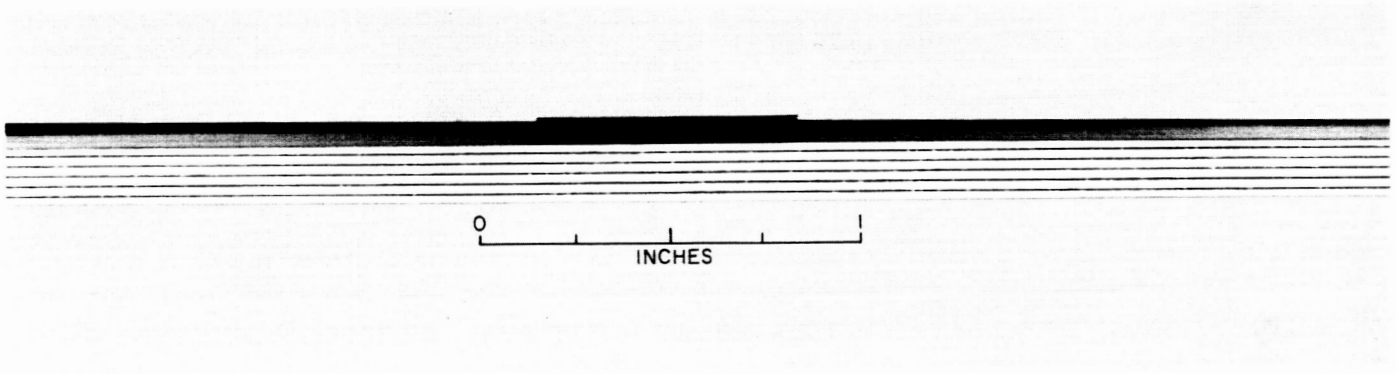

Fig. 22. Sample laminated reflector showing laminated construction—side view

References

1. "CDC/DSIF Compatibility Tests" (Feasibility Model), Surveyor Laboratory, Hughes Aircraft Company, Space Systems Division, Mission Operations Plan No. 5, September 30, 1963.

2. Stoller, F. W., "Investigation of the DSIF 85-Foot Antenna Structural Deflections Caused by Deadload and Thermal Inputs," Technical Memorandum No. 33-94, Jet Propulsion Laboratory, Pasadena, California, August 7, 1962.

IV. Research and Development

A. Ground Antennas

1. S-Band Antenna Gain and Pattern Calibrations

a. Summary. Accurate gain tests have been performed to calibrate the 85-ft Venus site antenna at 2388 Mc. These tests were performed after the antenna surface was resurfaced and realigned. This measurement indicates an improvement of 0.4 db due to resurfacing, thus yielding a new gain of 54.4 ± 0.15-db probability of error (p.e.).

Radiation patterns have been measured in the plane of the antenna quadripod structure and are compared to radiation patterns calculated by machine program. Further tests are necessary to arrive at a quantitative description of the quadripod effect at 2388 Mc; however, both the pattern and the gain tests indicate an opacity factor of 0.6 to 0.8, a gain loss of 0.7 db, and a zenith noise temperature quadripod contribution of 5°K.

b. Recent work.

Gain calibration. As described in *SPS 37-22,* Vol. III, pp. 11–15, an accurate gain calibration was performed at the Venus site 85-ft Az-El antenna, utilizing the Mt. Tiefort remote range. The system utilized, method of data reduction, and estimation of possible errors is described in detail in that report. These gain tests were performed prior to the antenna resurfacing project. After the recent completion of the resurfacing and surface alignment, the gain test was repeated. Great care was taken to use exactly the same technique and the same equipment; this was done to the point of using the same serial number instruments and the same personnel that were used previously. The new measured gain is:

Elevation angle = 0.8 deg

Frequency = 2388 Mc

Venus site 85-ft antenna gain = 54.40 ± 0.15-db p.e. (1)

Venus site 85-ft aperture efficiency = 0.655 ± 0.020 measurement p.e.

The data in Eq. (1) indicates a gain increase of 0.4 db, ascribable to the resurfacing of the antenna.

It is of interest to upgrade the table of predicted and measured feed system performance as published in *SPS 37-16,* Vol. III, p. 52, July 1962. Table 1 indicates

Table 1. Predicted and measured performance

Item	Associated gain, db	Aperture efficiency
Theoretical maximum	56.24	1.000
Illumination factor (includes phase loss)	−1.06	—
Gain for perfect surface and no quadripod	+55.18	0.783
Surface tolerance loss (0.032-in. rms)	−0.05	—
Gain for no quadripod	+55.13	0.775
Gain loss for 100% opaque quadripod (machine computed)	−1.19	—
Gain loss for 63% opaque quadripod	−0.73	—
Predicted gain for 63% opaque quadripod	+54.40	0.655
Measured gain	54.40 ± 0.15 p.e.	0.655±0.020 p.e.

the present status of the predicted and measured feed system performance for the Venus site 85-ft Az–El antenna.

There is no particular significance to the 63% quadripod opacity, other than the fact that it makes the predicted and measured gains agree. It should be noted, however, that if the energy in the 63% opaque region is assumed to be scattered isotropically, a zenith noise temperature contribution of 5°K would result. This contribution is in excellent agreement with the observed noise temperature.

Radiation pattern measurements and computations. In this section computed radiation patterns for the 85-ft Az–El are given and compared with actual measurements. Four computed cases are presented which were programmed using various degrees of quadripod shadow opaqueness for the purpose of determining appropriate constants related to the quadripod. The quadripod is a somewhat open truss structure on the 85-ft Az–El.

Previous computations on the 30-ft Az–El antenna at 8450 Mc have shown the ability of the Radiation Pattern Program to accommodate aperture illumination functions having shadowed regions (*SPS 37-23*, Vol. III, pp. 34–36). Because the structural quadripod members on the 30-ft antenna are solid and of reasonable size with respect to the wavelength at X-band, complete shadows were used in the calculations.

The relatively open truss type structure used on the 85-ft Az–El leads one to qualitatively expect some paraboloid illumination to be derived via ray paths through the quadripod structure. That this phenomenon is an appreciable effect is not apparent until the quadripod and subreflector geometry is considered. As shown in Fig. 1, comparatively close spacing exists between the inner portion of the quadripod structure and the hyperboloid; so close, in fact, that the flange utilized is necessarily notched. The result of this close spacing is a relatively large quadripod outline aperture blockage: 14.4%.

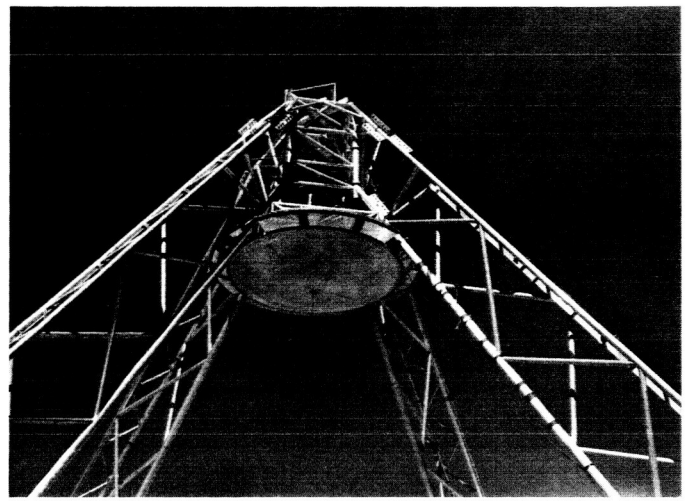

Fig. 1. Truss type quadripod

Figs. 2 through 5 show computed results for various degrees of quadripod opaqueness. Computations were made for $\phi = 45$ deg, i.e., in the plane of the quadripod. In the computations, experimentally determined feed illumination amplitude and phase data were used, from scale model tests in the absence of a quadripod. The optically shadowed regions were assigned intensities corresponding to 0, 50, 75, and 100% opaqueness, on a power basis, relative to the intensities which would exist in the absence of blocking. The reflector surface was assumed perfect ($DZ = 0$) and matrix size was $NR = 27$, $N\beta = 64$.

As might be expected, Figs. 2 and 5 are the most divergent in terms of sidelobe level. Considering the first and second sidelobes, Figs. 2 and 5 show differences of 4.5

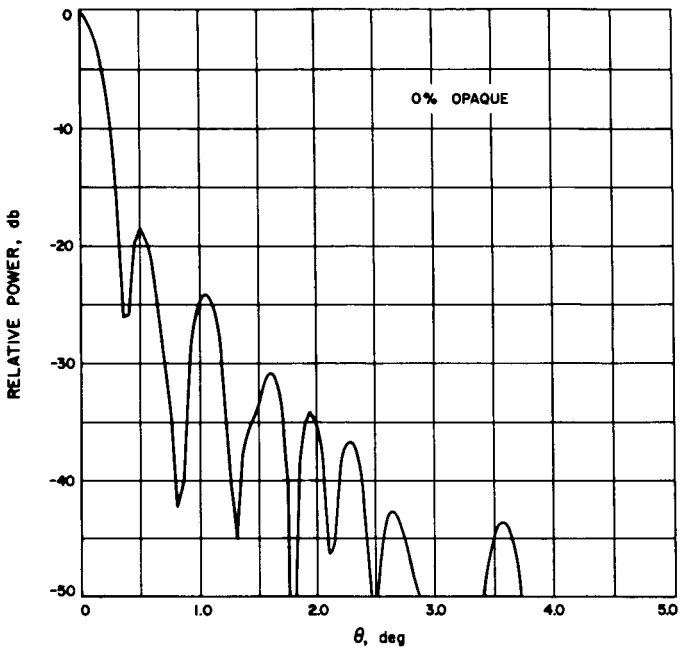

Fig. 2. Computed 45-deg plane pattern, 0% opaque

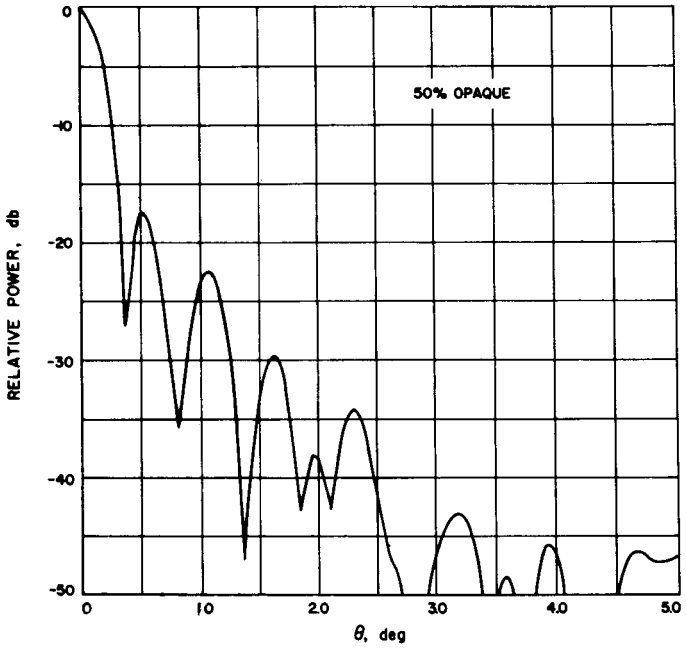

Fig. 3. Computed 45-deg plane pattern, 50% opaque

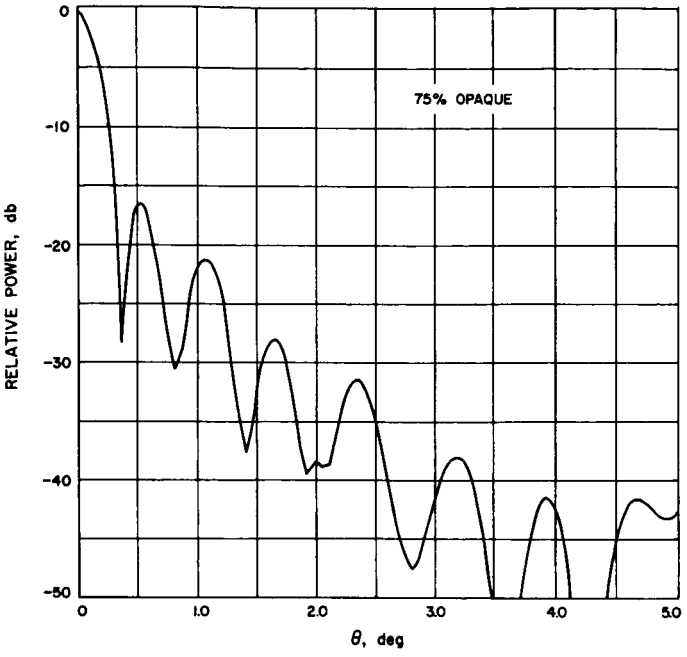

Fig. 4. Computed 45-deg plane pattern, 75% opaque

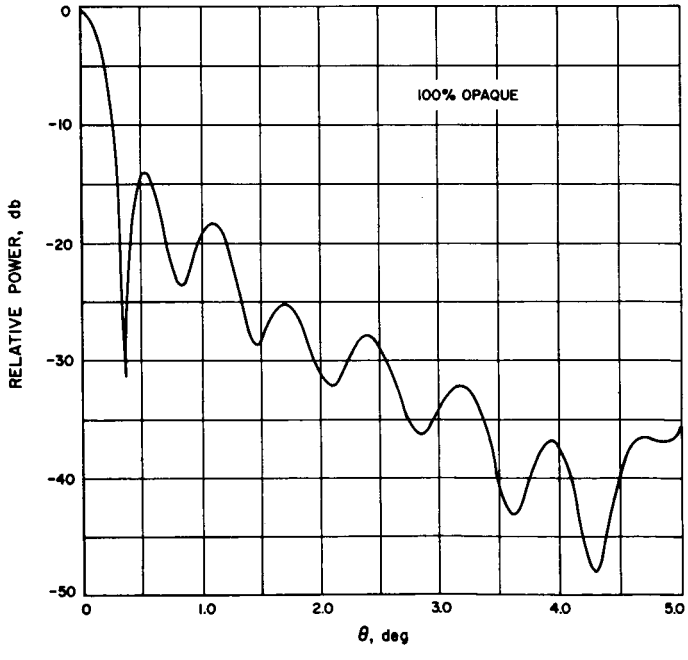

Fig. 5. Computed 45-deg plane pattern, 100% opaque

and 5.5 db, respectively, with the fully shadowed computation showing the highest levels.

Fig. 6 shows experimental 45-deg plane cuts taken with polarization parallel with and perpendicular to the plane of the cut (E-plane and H-plane, respectively). Because wide angle, i.e., $1.0 < \theta < 5.0$ deg, experimental azimuth and elevation patterns are unavailable at this time, the basis for correlation is limited; tentatively, the truss type quadripod appears fairly opaque at S-band ($\approx 75\%$).

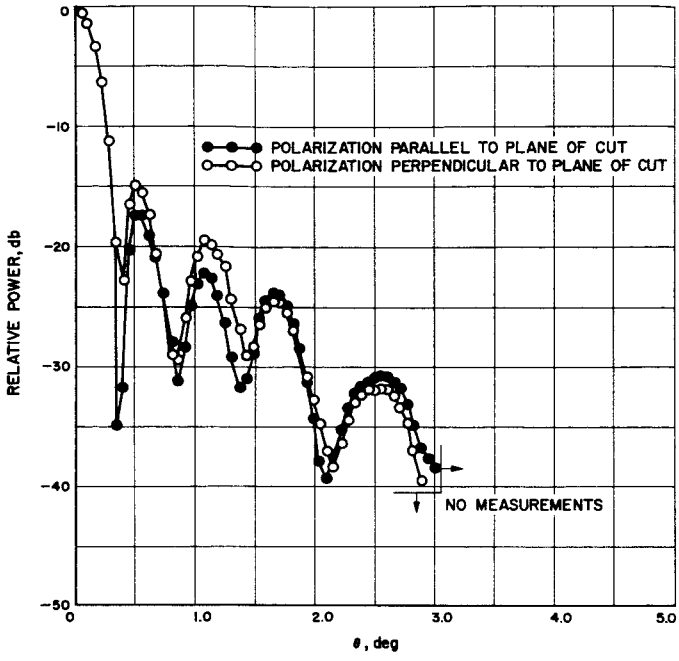

Fig. 6. Experimental 45-deg plane patterns, 2388 Mc

Availability of experimental azimuth and elevation patterns would allow a better evaluation of quadripod opacity. The programming of the above cases neglected a possibly significant factor: that is, the variation of opaqueness as a function of half aperture angle Ψ. One possibility for future improvement is the determination of a suitable taper and the inclusion of this in the computations.

2. *Radio Astronomical Techniques for Ground Antenna Calibrations*

Summary. The program to calibrate the Goldstone 30-ft Az–El antenna using radio astronomical techniques has continued. This work is complementary to measurements of the antenna using the Tiefort Mountain long distance antenna measurement range. The basic objectives of the work are development of improved gain and pointing calibration techniques and improved radio frequency performance versus mechanical accuracy design techniques for DSIF ground antennas.

The X-band radiometer and associated instrumentation (*SPS 37-23*, Vol. III, pp. 30–33) were used to measure the antenna temperature of the 30-ft antenna at 8448 Mc. The preliminary reduction of the measurement gives a minimum antenna temperature of 18.4 ± 2.7°K.

Recent work. During September an X-band antenna temperature calibration was carried out on the Goldstone 30-ft Az–El antenna at the Venus site. A preliminary description of this program is given in *SPS 37-23*, Vol. III. Fig. 7 is reproduced from that report; it is the block diagram of calibration system and radiometer.

Using the equipment (Fig. 7), antenna temperature data were taken throughout the night of September 20 and through the following day. The sky was clear with no clouds and no visible moisture in the air. Humidity readings taken at the Echo site showed that the relative humidity ranged from a low of 46% to a high of 100%. Throughout the evening and the following morning, when most of the data were recorded, it is estimated that the relative humidity was probably higher than 85%, since the temperature stayed close to its low of about 60°F.

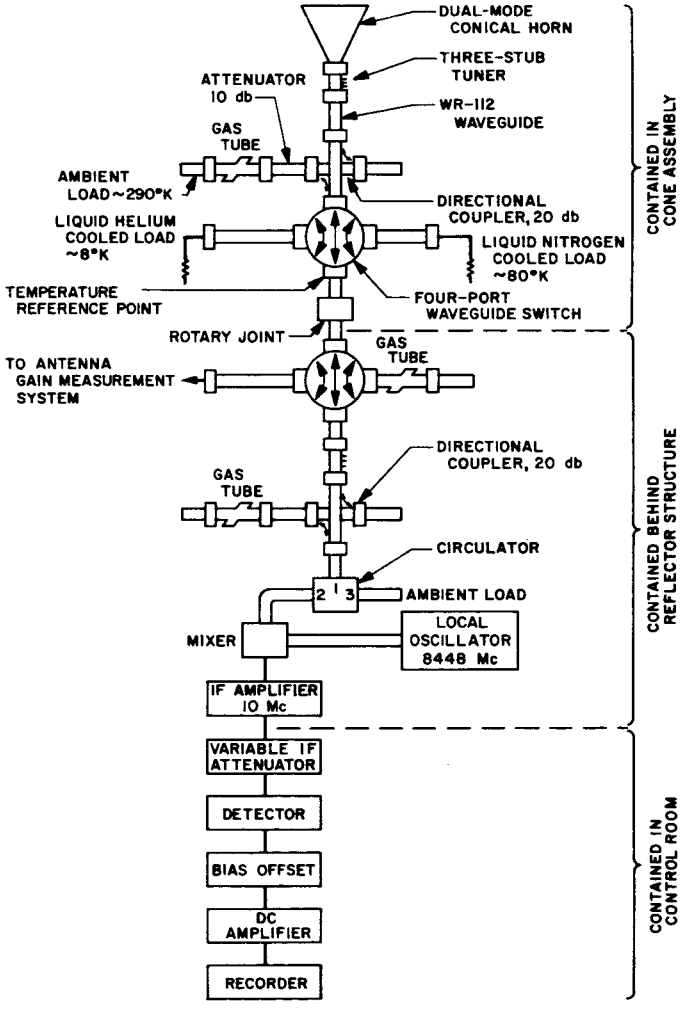

Fig. 7. Block diagram of calibration system and radiometer

All data was taken with a recorder time constant of 1 sec. This resulted in a peak-to-peak jitter of 1°K and a gain instability of about 2°K. The performance of the radiometer was poorer than reported in *SPS 37-23*, Vol. III, due to increased input mixer noise temperature ($F = 5.5$ db, corresponding to a radiometer noise temperature of 740°K), and slightly poorer gain stability. The radiometer noise temperature reported in *SPS 37-23*, Vol. III, was incorrect and should have read 390 ± 80°K. Fig. 8 shows one data record cycle in which the radiometer is switched between a helium load, a nitrogen load, the antenna, and the antenna plus a gas tube contribution. Table 2 shows the measured and calculated parameters regarding the waveguide system and calibrated loads.

When referring all temperatures to the output of the upper four-port waveguide switch (Fig. 7), we must consider the attenuation between the source and the reference point, and also the contribution of the lossy elements between the two points. We may write:

$$T_e = \left(\frac{1}{L}\right) T_g + \left(1 - \frac{1}{L}\right) T_p + (Mismatch)$$

where

T_e = effective temperature at the reference point.

T_p = physical temperature of lossy transmission line.

T_g = apparent temperature of the source.

L = insertion loss of the transmission line

$$L(db) = 10 \log\left(\frac{P_{in}}{P_{out}}\right).$$

Mismatch = effective temperature reflected back to the radiometer from a source impedance mismatch—source sees the radiometer as an ambient load.

In the case of the antenna line (Table 2), the 0.156-db total insertion loss in the transmission line introduces an attenuation of 3.6% corresponding to the $[1 - (1/L)]$ term. The transmission factor $(1/L)$ is thus 96.4%. Any experimental determinations of the antenna temperature at the horn output must take this missing 3.6% into account.

The final experimental result for the minimum zenith antenna temperature on September 20 to 21 is, considering all contributions, 18.5°K ± 2.7°K, including an excess atmospheric humidity contribution for which we

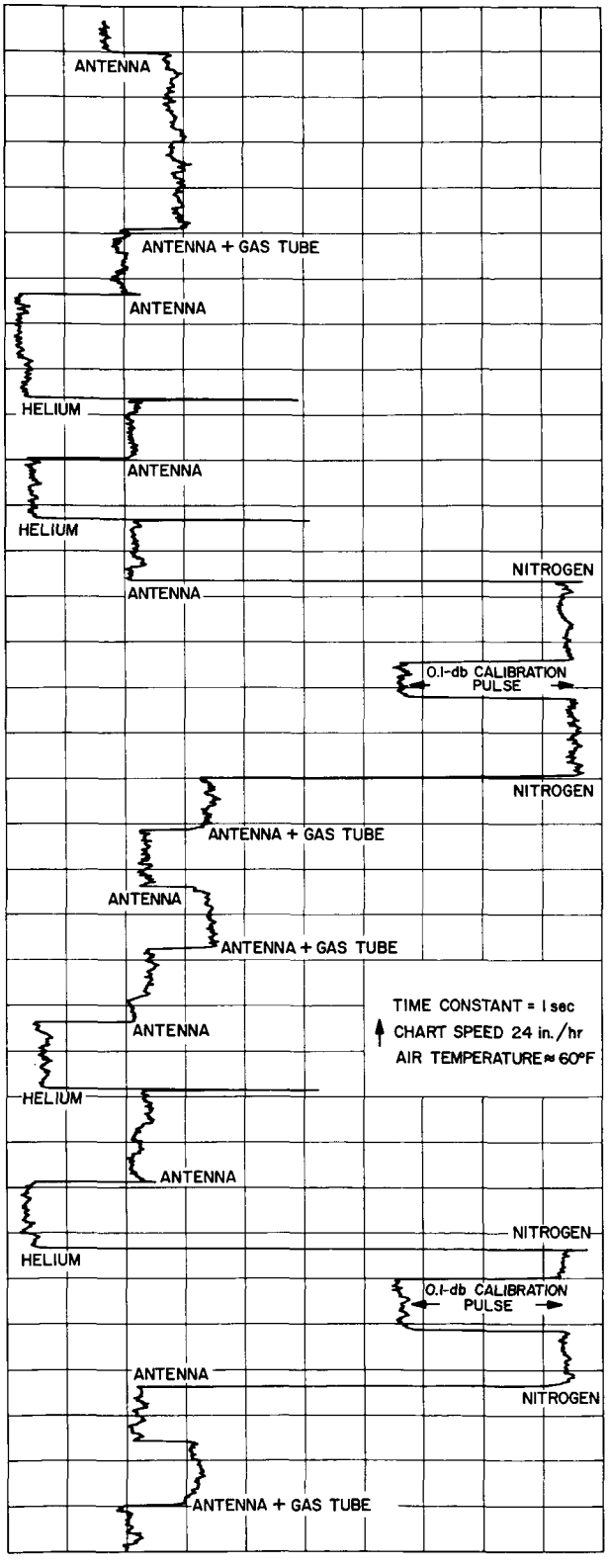

Fig. 8. X-band radiometer recording for antenna temperature calibration

Table 2. Parameters of antenna temperature measurement

Helium load	
Reference temperature at load output	8.2 ± 0.7°K
Insertion loss of transmission line from load output to four-port switch input	0.071 ± 0.003db
Insertion loss of switch port	0.031 ± 0.003db
Reference temperature at four-port switch output	8.0 ± 0.7°K
Net temperature contribution from transmission line loss at 290°K	6.7 ± 0.3°K
Mismatch contribution from ambient load on circulator	<0.01°K
Net effective helium load reference temperature	14.7 ± 0.8°K
Antenna line	
Reference temperature at load output	79 ± 2°K
Insertion loss of transmission line from load output to four-port switch input	0.071 ± 0.003db
Insertion loss of switch port	0.031 ± 0.003db
Reference temperature at four-port switch output	77 ± 2°K
Net temperature contribution from transmission line loss at 290°K	6.7 ± 0.3°K
Mismatch contribution from ambient load on circulator	0.2 ± 0.2°K
Net effective nitrogen load reference temperature	83.9 ± 2°K
Nitrogen load	
Antenna temperature at output of dual-mode horn	T_a
Insertion loss of transmission line from horn output to four-port switch input	0.124 ± 0.003db
Insertion loss of switch port	0.032 ± 0.003db
Net temperature contribution from transmission line loss at 290°K	10.4 ± 0.3°K
Mismatch contribution from ambient load on circulator	0.3 ± 0.2°K
Net effective antenna temperature as measured at output of four-port waveguide switch	T_a (0.964) + 10.7 ± 0.4°K
Final antenna temperature at output of dual-mode horn (including excess humidity)	18.5 ± 2.7°K
Final antenna temperature at output of dual-mode horn (corrected for normal Goldstone day)	18.4 ± 2.7°K

Notes:
(1) All tolerances as stated are rms.
(2) Transmission line insertion loss values are dependent on possible waveguide corrosion subsequent to initial measurements.

must account. The calibration of the gas tube contribution resulted in $T_{gt} = 7.5°K \pm 1.4°K$. The purpose of calibrating the gas tube is to enable one to compare an equivalent temperature pulse of known magnitude to a radio source contribution of unknown magnitude. We can thereby determine the equivalent noise temperature of the radio source. It would appear from the spread of the data that the gas tube amplitude is not repeatable from cycle to cycle and would not give us a reliable standard with which to compare unknowns in source temperature determinations.

We can consider the effect of humidity on the antenna temperature by utilizing Fig. 9 and Refs. 1 and 2. Calculations show that a humid day (85% relative humidity) at Goldstone's elevation corresponds to a normal day (57%

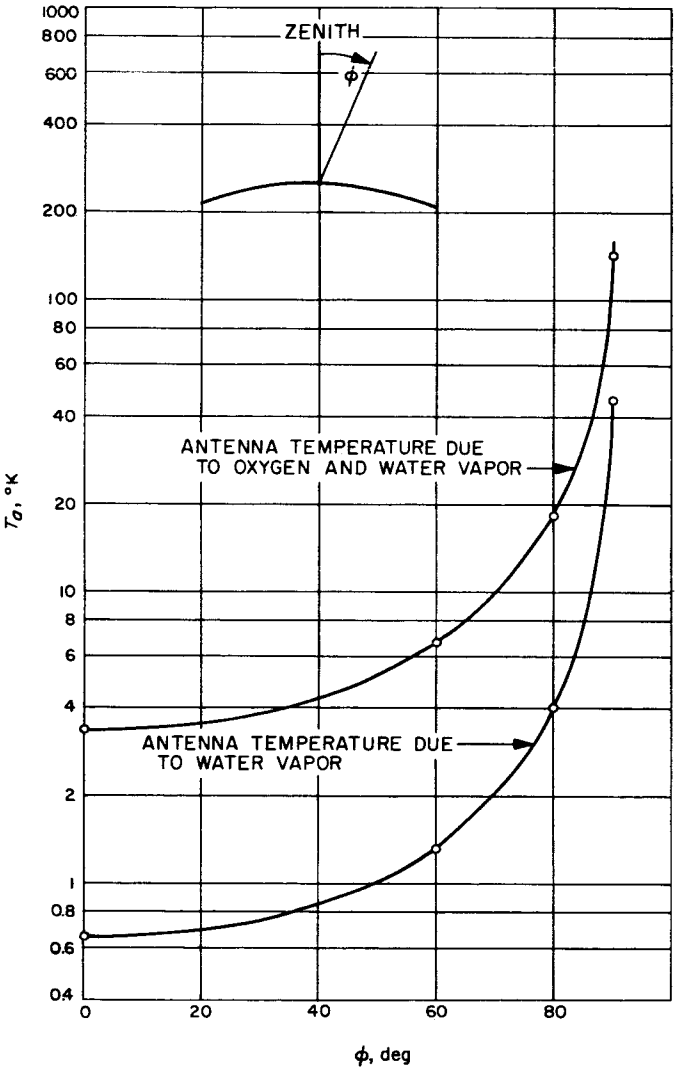

Fig. 9. Atmospheric contributions to effective antenna temperatures at 8448 Mc (Ref. 1)

relative humidity) at sea level as far as absolute water vapor content of the air is concerned. However, since a normal summer day at Goldstone has a relative humidity of 50%, we may reduce the water vapor contribution from 0.65°K to 0.57°K (Fig. 9). Fig. 9 also predicts that the total atmospheric contribution to the antenna temperature at 8448 Mc is about 3.3°K in the zenith-look position. The correct minimum antenna temperature for a normal Goldstone day is 18.4°K ± 2.7°K.

a. Boresight calibrations for DSIF antennas.

Summary. We have been working on development of practical techniques for using radio star sources to boresight the DSIF ground antennas. In *SPS 37-23*, Vol. III, results from the use of a drift curve method for obtaining boresight errors were given. The method used digital recording and digital computer processing of the drift curve data. Recently, boresight measurements on radio sources have been made using a different operational technique. The measurements were made on the 85-ft Az-El antenna at the Venus site. The radio source was continuously tracked using an ephemeris angle drive tape to slave the antenna to the precise computed angular location of the source. If the drive tape did not steer the antenna exactly on the source, angular offsets were inserted until it did. The offsets required determine the boresight error. Results of the radio source and some optical source measurements are reported; on the basis of these data, the antenna was realigned and a few additional verifying tracks were made.

Recent work. A series of radio source tracks has been made with the 85-ft Az-El antenna at the Venus site to obtain azimuth and elevation boresight errors as a function of antenna orientation. The tracks were made using precomputed ephemeris angle drive tapes for the radio sources. The ephemeris angle drive tape mechanization is described in *SPS 37-18*, Vol. III, pp. 40–42. The angle drive tape was prepared on the IBM 1620 computer by taking a known source position in terms of sidereal hour angle and declination and converting this to azimuth and elevation versus time; a refractive index correction is then

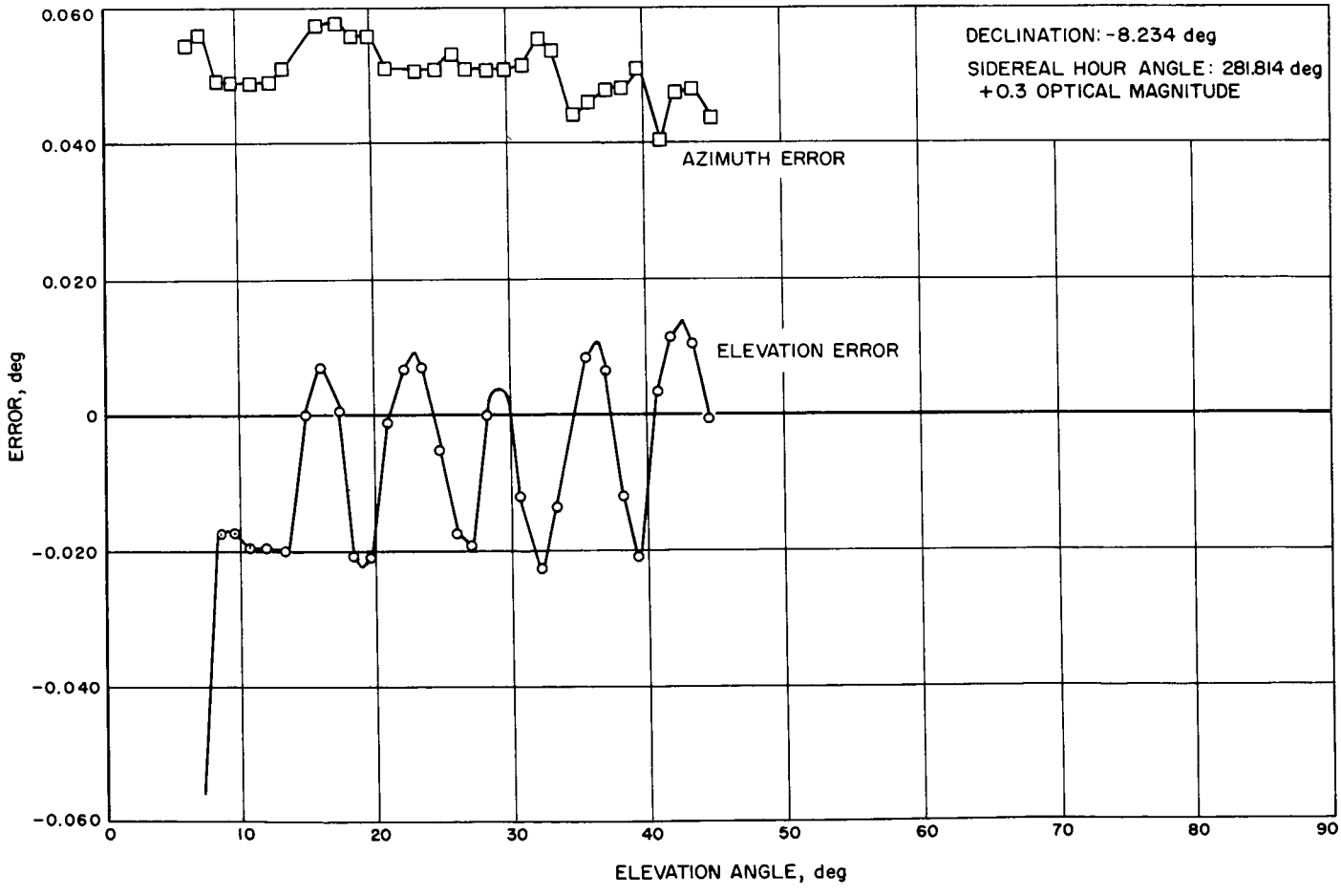

Fig. 10. Optical star track boresight errors for Rigel, September 23, 1963

applied to the elevation. From this, a punched tape is prepared which has an azimuth and elevation command every 64 sec. The tape reader and processor then interpolates between the 64-sec commands to give smooth continuous angle position commands which are compared with the antenna axes positions to generate error voltages for the drive servos. For a perfect ephemeris, the antenna is pointed continuously at the position of the source, provided the antenna angular calibration is perfect. To determine the indicated position of the radio source, the beam is "scanned" over the source using an angle offset control mechanism as described in *SPS 37-19*, Vol. III, pp. 18–20. The actual operating procedure for the radio star tests is as follows:

(1) The antenna is steered to the nominal position of the source using the angle drive tape.

(2) A positive angular offset is made in one coordinate so that the apparent antenna temperature decreases between 3 and 10 db below the maximum with the beam on the source.

(3) After a temperature level is set at a given positive angular offset, a negative angular offset is inserted, and by trial and error and interpolation an angular negative offset is found which gives the same apparent antenna temperature as the positive angular offset.

(4) The positive and negative offsets in one coordinate system which gave the same temperature are used to compute the midpoint which indicates the offset of the beam center. This sequence is then repeated for the other coordinate. One data point consisting of an Az and an El boresight offset takes about 4 min to obtain.

A very similar procedure was used to obtain azimuth and elevation error for optical sources. Similar drive tapes were prepared, but instead of using the RF system for determining position, the boresight television camera was employed. The servo operator keeps the optical source in the cross hairs of the television presentation by means of the offset control panel. The angular offsets to keep the target centered are read periodically and plotted.

Figs. 10, 11, and 12 show azimuth and elevation errors as a function of elevation angle for the optical stars Rigel,

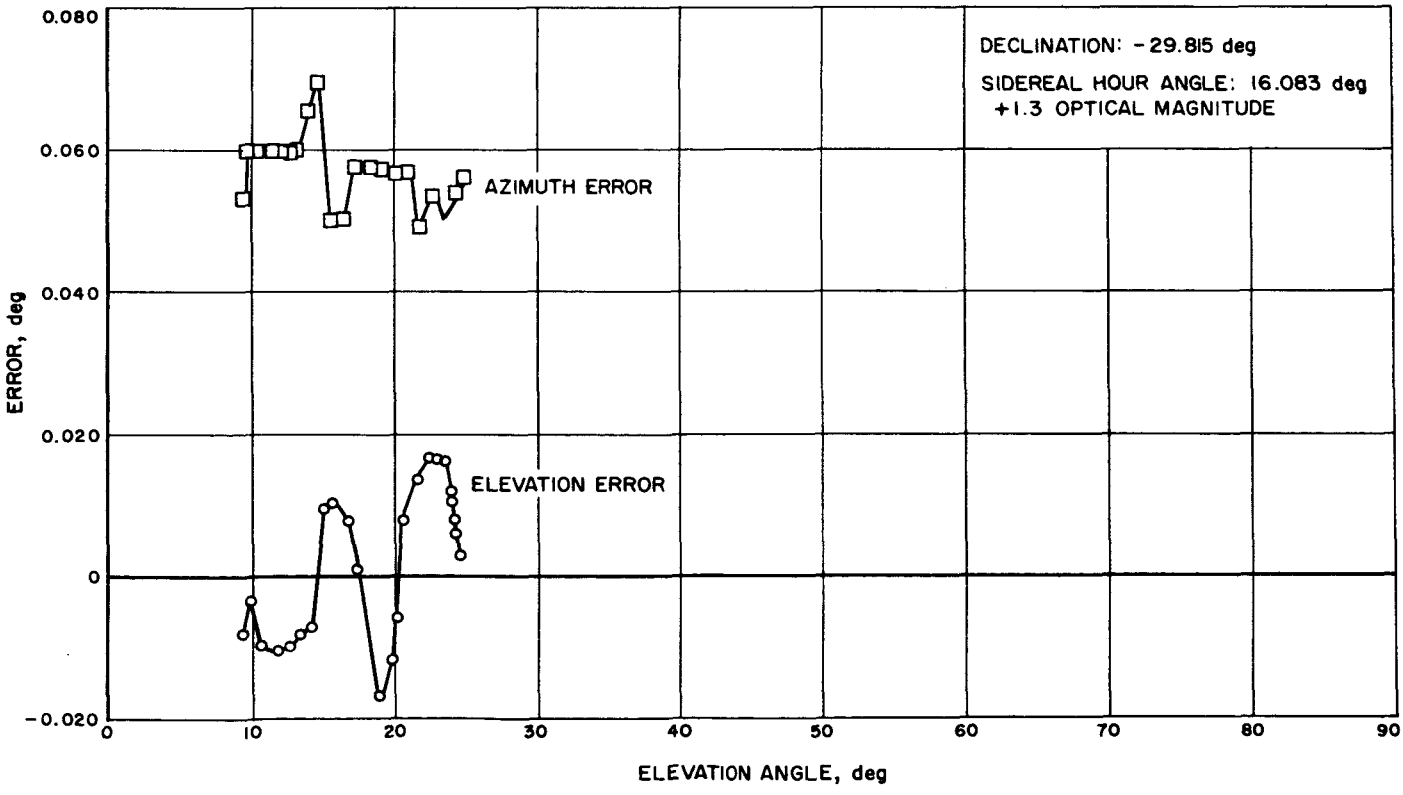

Fig. 11. Optical star track boresight errors for Fomalhaut, September 23, 1963

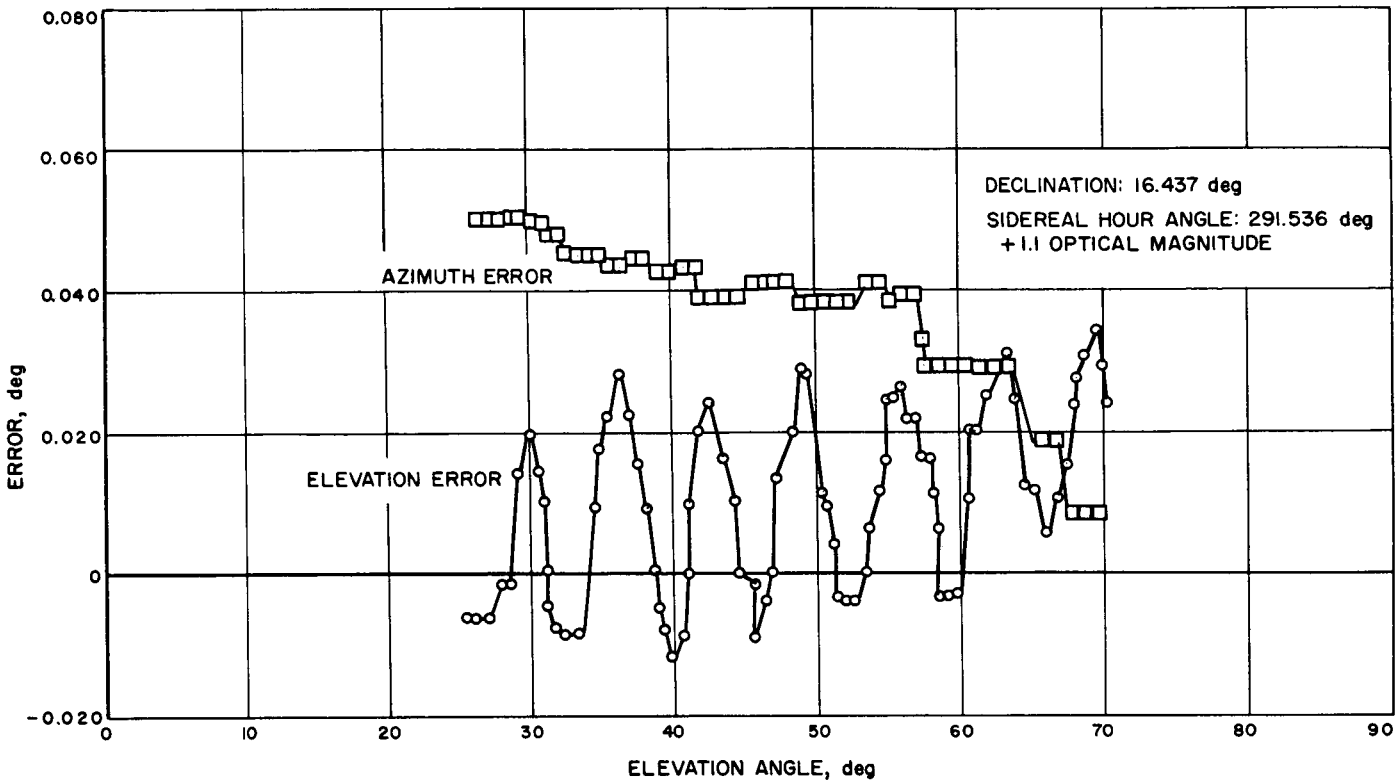

Fig. 12. Optical star track boresight errors for Aldebaran, September 25, 1963

Fomalhaut, and Aldebaran. The signal of the error is such that apparent angular coordinates plus the error give two coordinates of a source. The cyclic errors in elevation are due to a systematic error in the elevation readout system.

Figs. 13, 14, and 15 give azimuth and elevation errors versus elevation obtained by observations of the radio source Cygnus A on the nights of September 20, 26, and 27. The agreement between the three graphs is good. Approximately the same phase and amplitude elevation error is observed in both the optical and radio star track data. Fig. 16 shows the azimuth and elevation errors from observations of the radio source Cassiopeia A; Figs. 17 and 18 give the boresight for the Crab Nebula observations on the nights of September 19 and September 27, respectively.

After these optical and radio star tracks were obtained, the boresight of the antenna was changed by repositioning the shaft angle encoders on the antenna. A correction of -0.061 deg was made in the azimuth readout and a correction of $+0.021$ deg was made in the elevation readout. Since the encoders were adjusted, a few more observations of radio and optical sources have been made. Fig. 19 shows the error curves obtained for Cygnus A after the adjustment of the encoder. A comparison of Figs. 15 and 19 shows that elevation correction appears good (ignoring the sinusoidal encoder problem) but that the azimuth error is approximately $+0.020$ deg. Fig. 20 was obtained from the Crab Nebula after adjustment of the encoders; it shows a mean elevation error of about 0.015 deg and a mean azimuth error of about 0.007 deg at low elevation angles.

After resetting the shaft encoders, the cross hair alignment of the television boresight optics was also readjusted. The old coordinates of the target at the base of the collimation tower were azimuth 260.452 deg, elevation 6.594 deg; after encoder and television optics readjustment, the azimuth was 260.418 deg and the elevation was 6.560. Fig. 21 shows the errors for the optical source Aldebaran after the adjustment of the encoders and the television camera. The elevation errors appear the same as shown in Fig. 12. The mean azimuth error at low elevation angles is -0.02 deg. The increase of azimuth error at high elevation angles is due to orthogonality errors in the

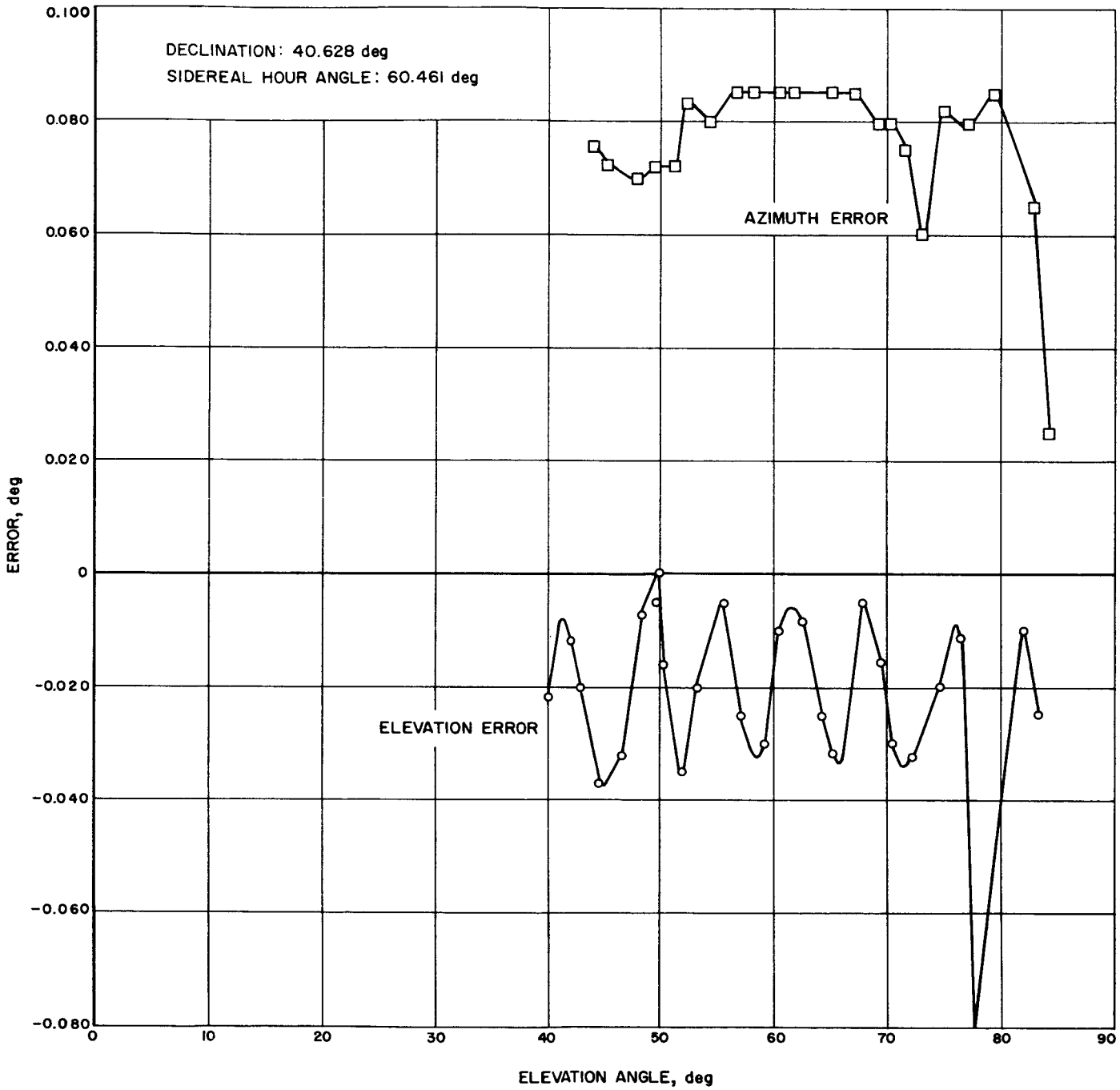

Fig. 13. Radio star track boresight errors for Cygnus A, September 20, 1963

antenna. This increase in error is not reflected in "source coordinates" but only in antenna coordinates as the source approaches the antenna mount gimbal lock position.

3. Antenna Instrumentation

a. Summary. A transportable instrumentation system is being built for use in research and development testing of the structural and mechanical properties of large ground antennas. It will be used initially on the 30- and 85-ft antennas and, later, on the 210-ft-diameter Advanced Antenna System. There is a detailed description of the instrumentation system in *SPS 37-20*, Vol. III and progress reports in *SPS 37-21*, Vol. III and *SPS 37-22*, Vol. III. The system was first used for structural and thermal testing conducted as part of the 85-ft Az-El antenna resurfacing

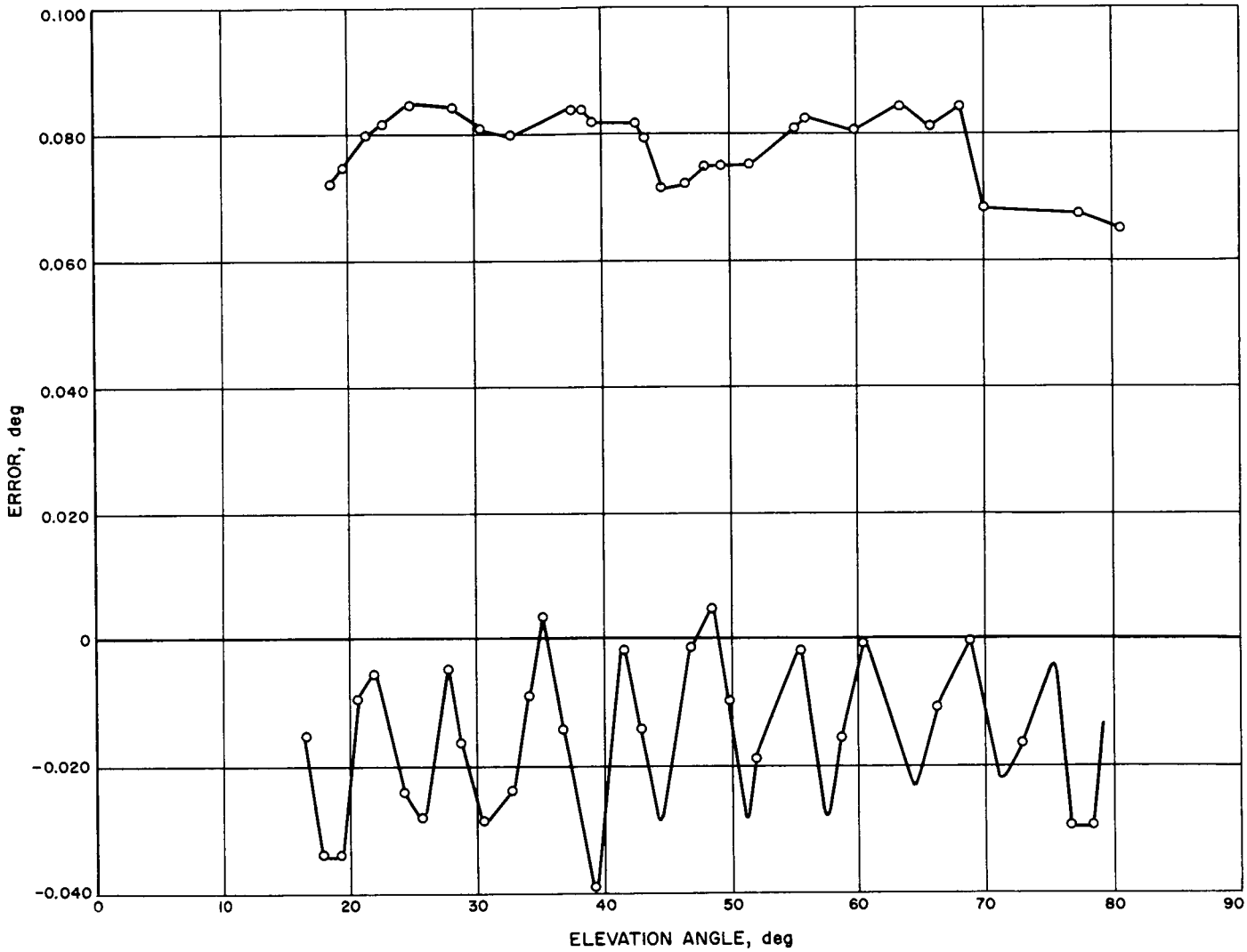

Fig. 14. Radio star track boresight errors for Cygnus A, September 26, 1963

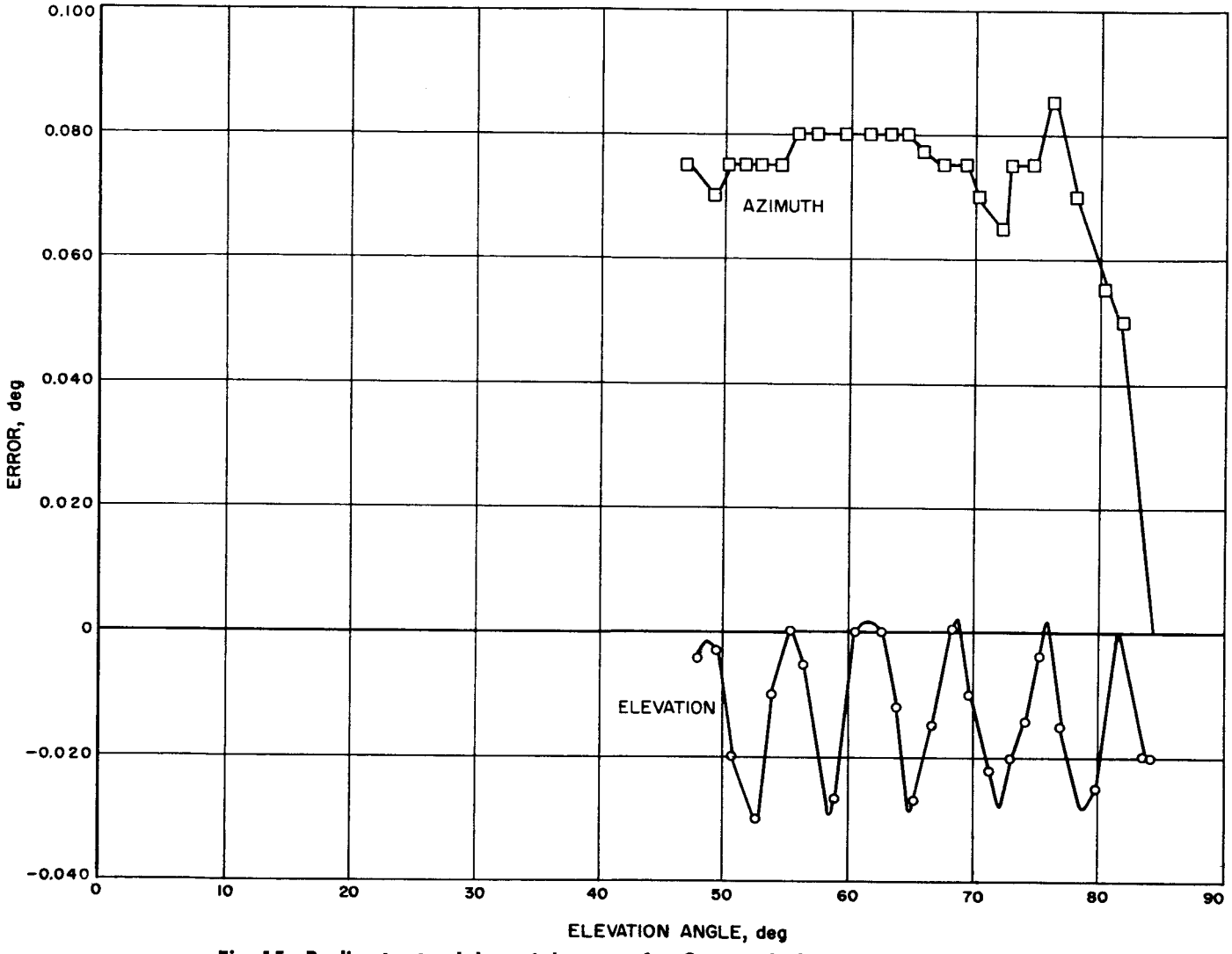

Fig. 15. Radio star track boresight errors for Cygnus A, September 27, 1963

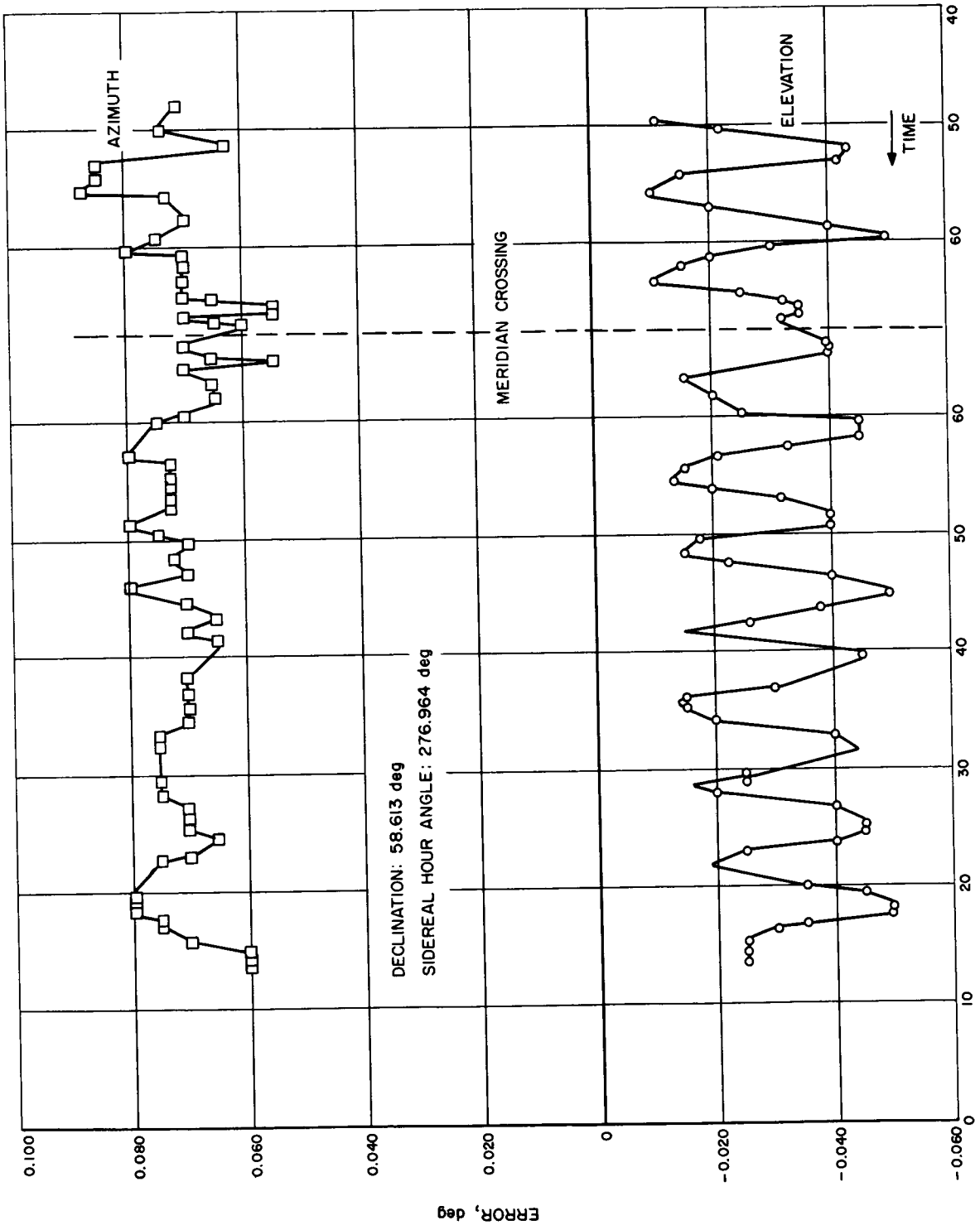

Fig. 16. Radio star track boresight errors for Cassiopeia A, September 19, 1963

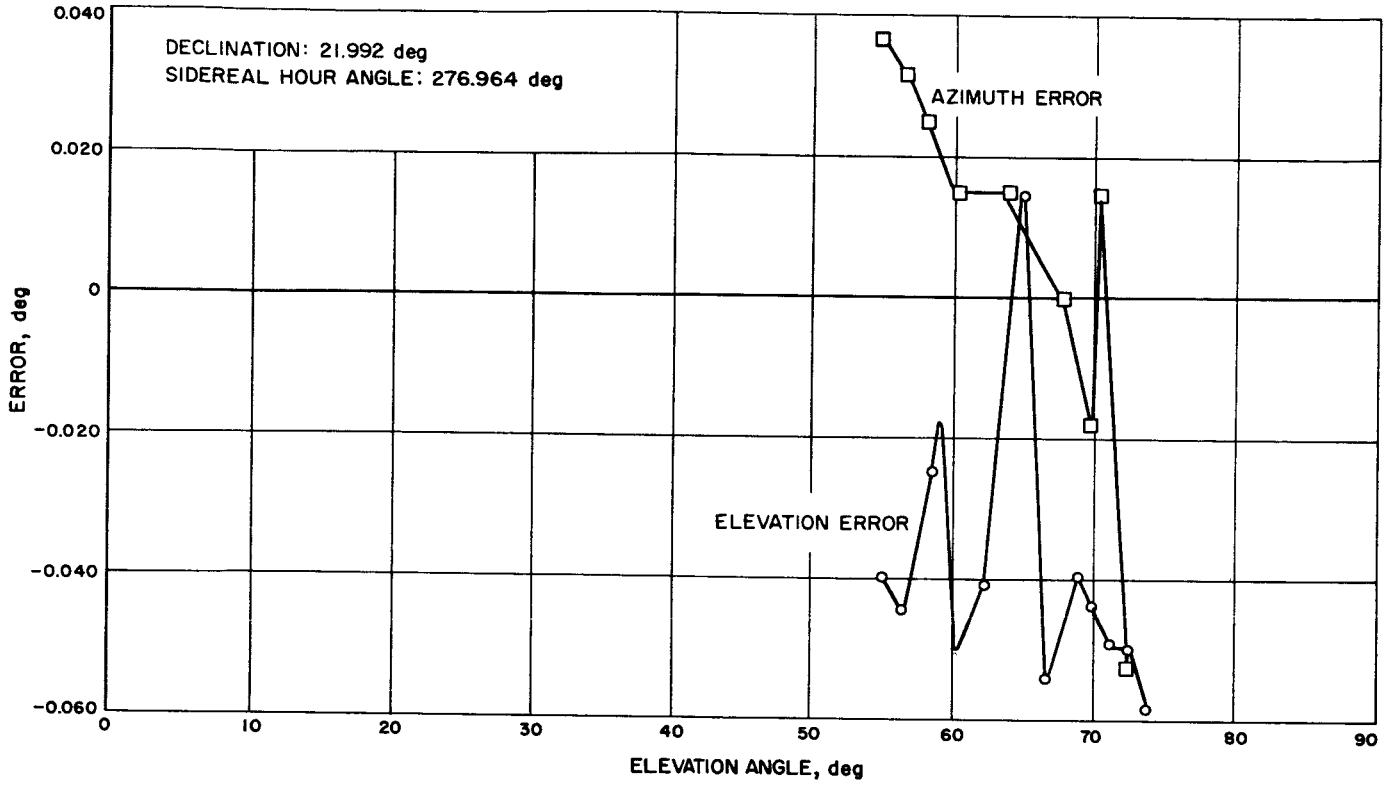

Fig. 17. Radio star track boresight errors for Crab Nebula, September 20, 1963

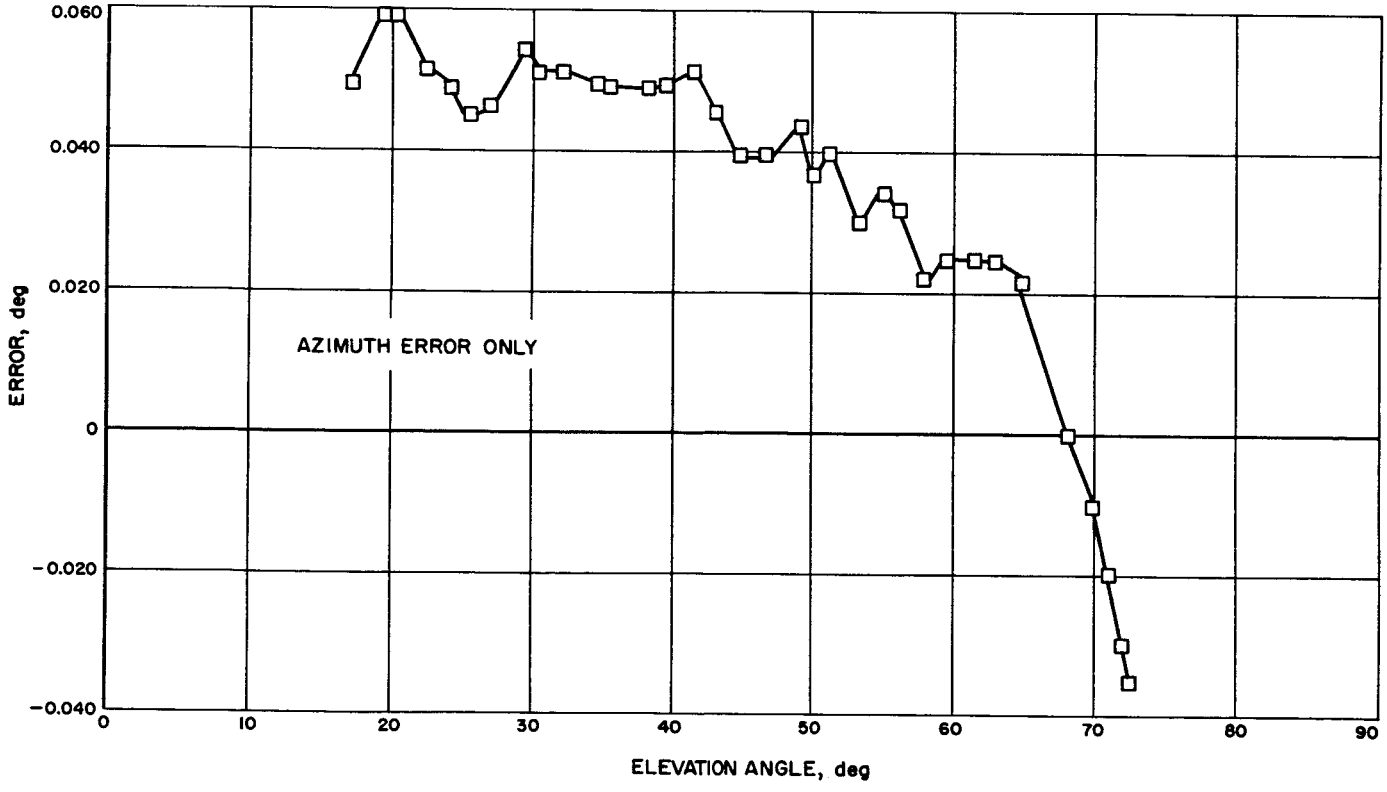

Fig. 18. Radio star track boresight errors for Crab Nebula, September 27, 1963

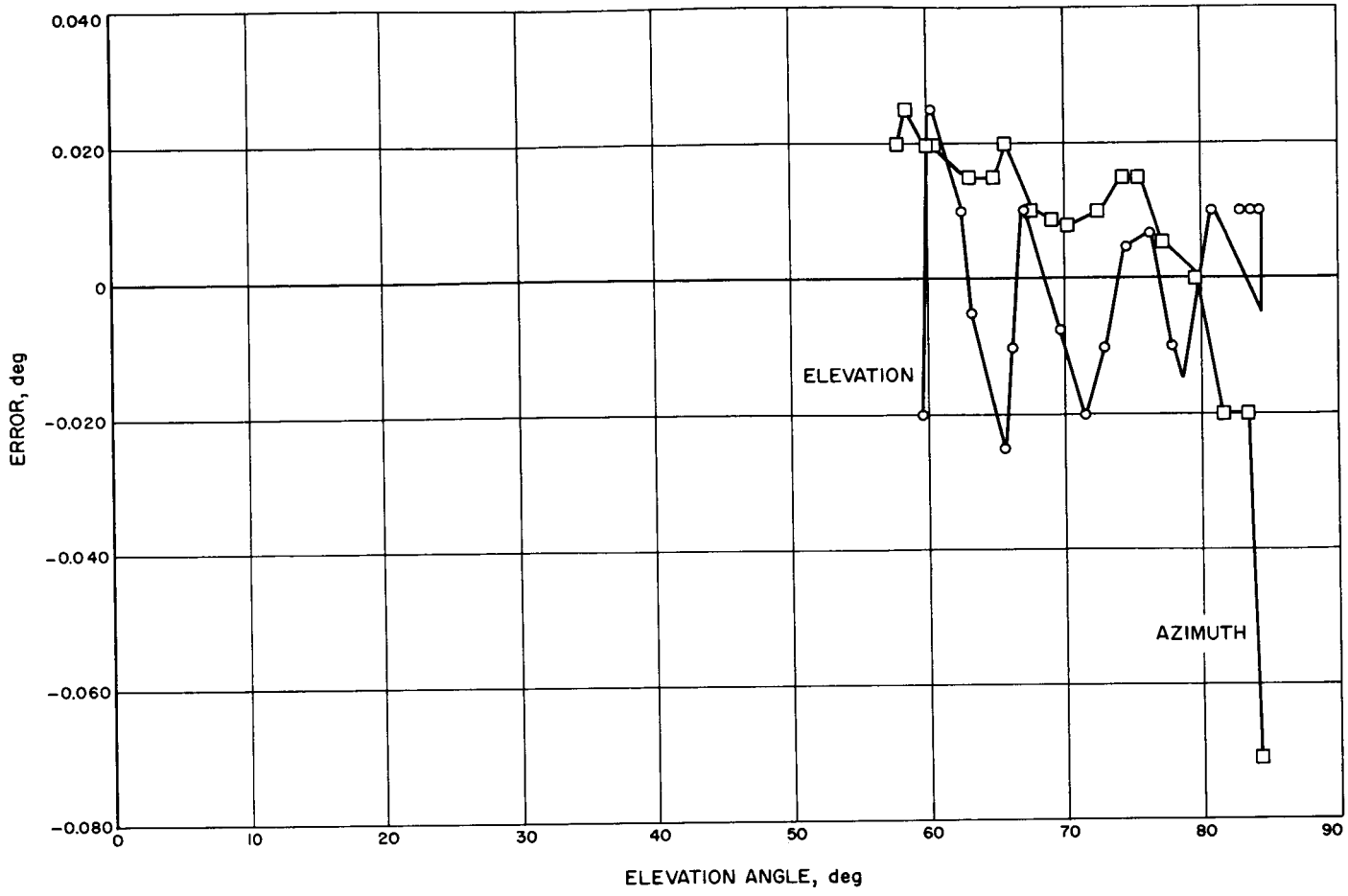

Fig. 19. Radio star track boresight errors (after corrections) for Cygnus A, October 9, 1963

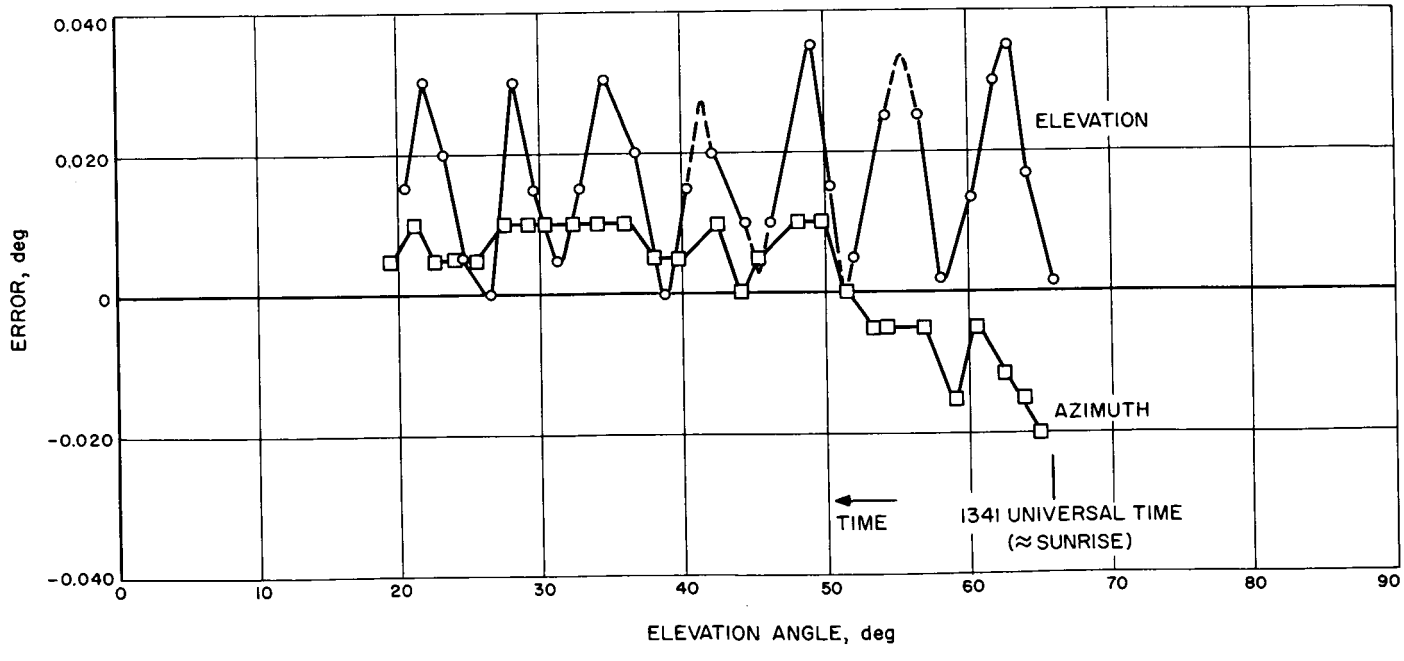

Fig. 20. Radio star track boresight errors (after corrections) for Crab Nebula, October 9, 1963

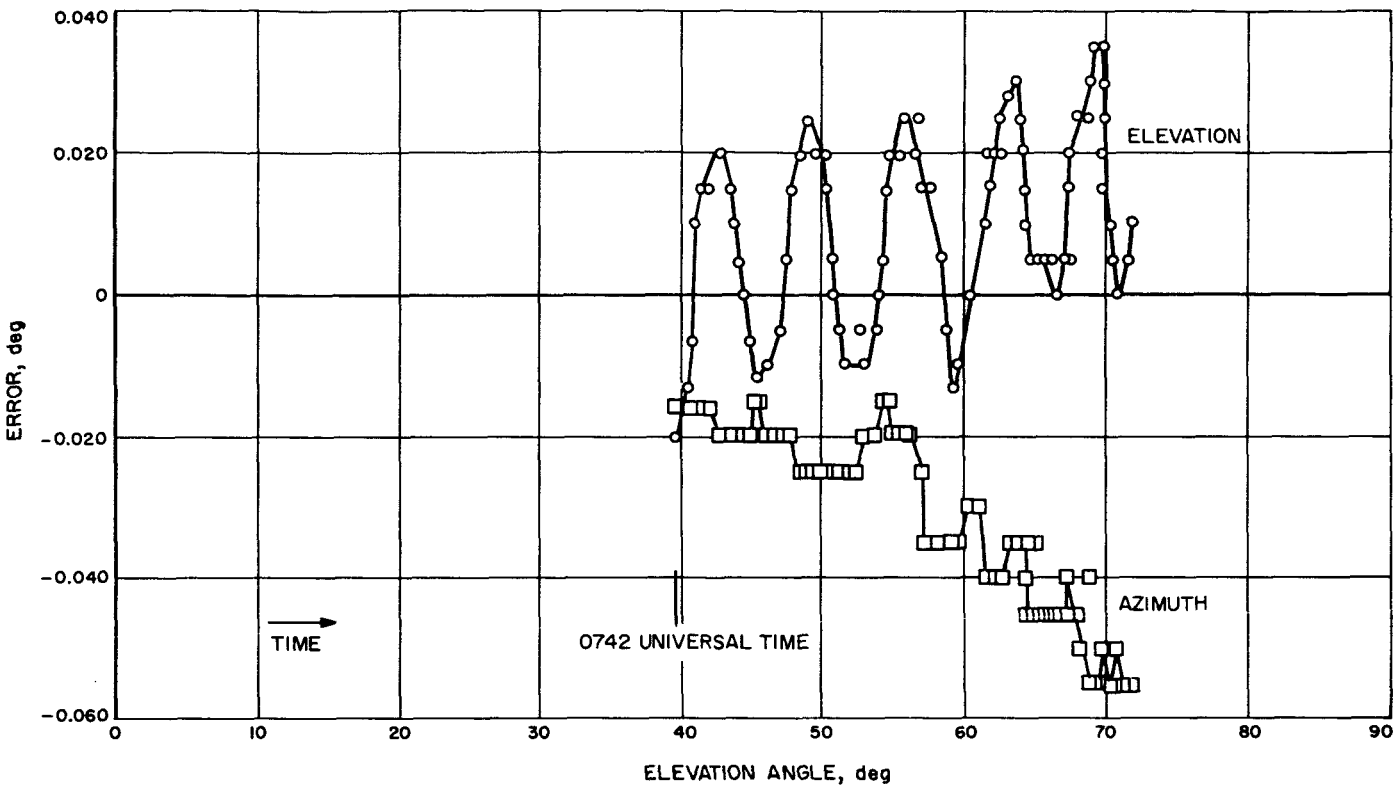

Fig. 21. Optical star track boresight errors (after corrections) for Aldebaran, October 9, 1963

work during July and August 1963. Results of extensometer tests on the Az–El antenna are presented.

b. Recent work.

Instrumentation setup for 85-ft Az–El tests. For the structural deformation measurements ten extensometers were used in the configuration of Test Nos. 1 and 2 as shown in Fig. 22 (reproduced from *SPS 37-22*, Vol. III, p. 16). An ambient temperature reading was taken at the completion of each scan of the extensometers. Also, wind velocity and vertical and horizontal directional components were measured continuously and typed on the data sheets.

Data were recorded on an electric typewriter for quick-look and paper-tape punch for reproduction.

Temperature recording of 24 thermocouples placed across one entire rib structure from North to South and one measuring ambient air temperature were interposed with the extensometer scans. The temperature samples were made at the beginning and end of each extensometer run.

Test procedure. Simplified diagrams of the two test setups used are shown in Fig. 23 and noted as setup 1 and setup 2, corresponding to Test No. 1 and Test No. 2 of Fig. 22. With the instrumentation zeroed at 90-deg elevation the antenna was rotated at 15-deg increments to 0-deg elevation and returned to 90-deg elevation; that constituted a run. Three runs were made for both setups. At each position, each extensometer output was read to determine the distance from the zeroed position. Resolution of the instrumentation on the extensometers was equivalent to 0.0001 in. This is a much greater accuracy than can be expected from the extensometer itself at the present stage of refinement.

Although data for the thermal expansion compensation of the tungsten wire spans were taken, it was subsequently discovered that an equipment malfunction lost the data. Throughout the tests, wind velocities up to 25 mph, with occasional gusts to 40 mph, were observed.

The extensometer readings were reduced to changes in distances between the anchor points. A positive (+) sign indicates an increase in distance between the anchor points.

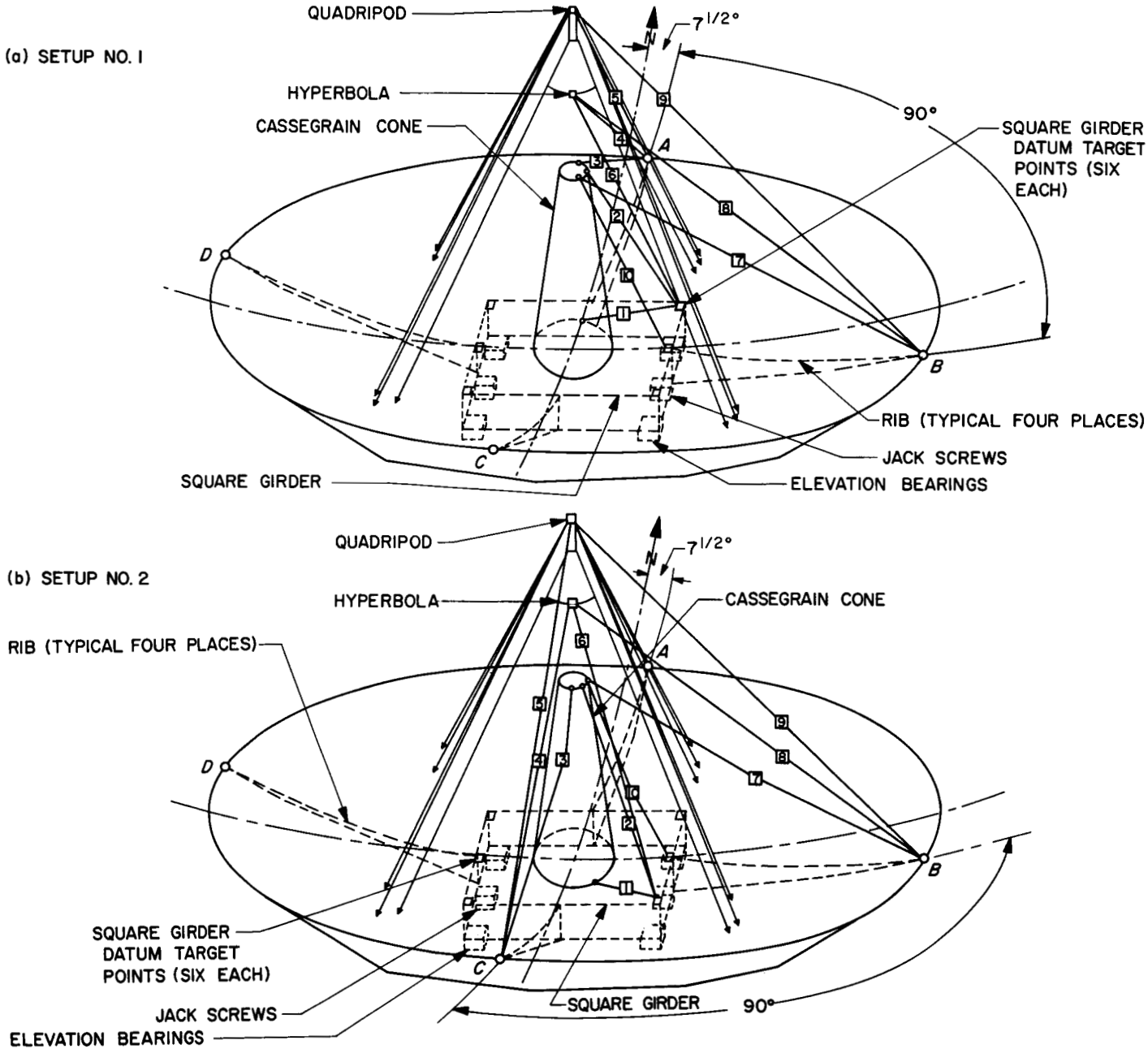

Fig. 22. Extensometer locations for 85-ft Az–El antenna tests

Fig. 24 shows the data from extensometer No. 5 (Fig. 23 for identification) for setups 1 and 2. As the antenna moves from 90-deg elevation angle to 0 deg, the upper dish edge shortens its distance to the tip of the quadripod while the lower edge moves away from the quadripod tip. The algebraic sum at the extreme positions of the dish edges with respect to the quadripod tip of 0.02 in. shows that very little change occurred in the vertical aperture diameter. Also, it can be concluded that the quadripod tip moves toward the upper edge of the dish, relative to the dish.

The motion of the subreflector with respect to the top and bottom edges of the dish is shown in Fig. 25. Relative to the quadripod tip, the subreflector drops about 0.08 in. at 0-deg elevation.

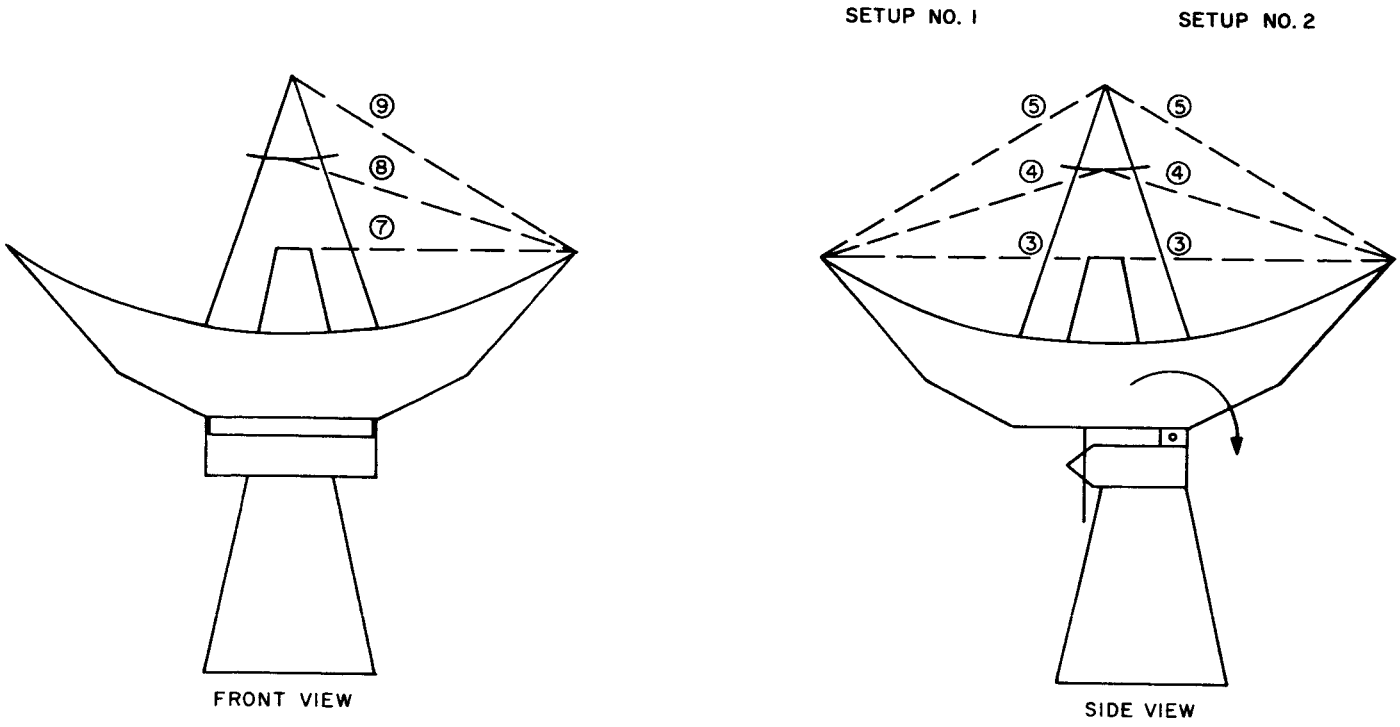

Fig. 23. Extensometer setup on 85-ft antenna

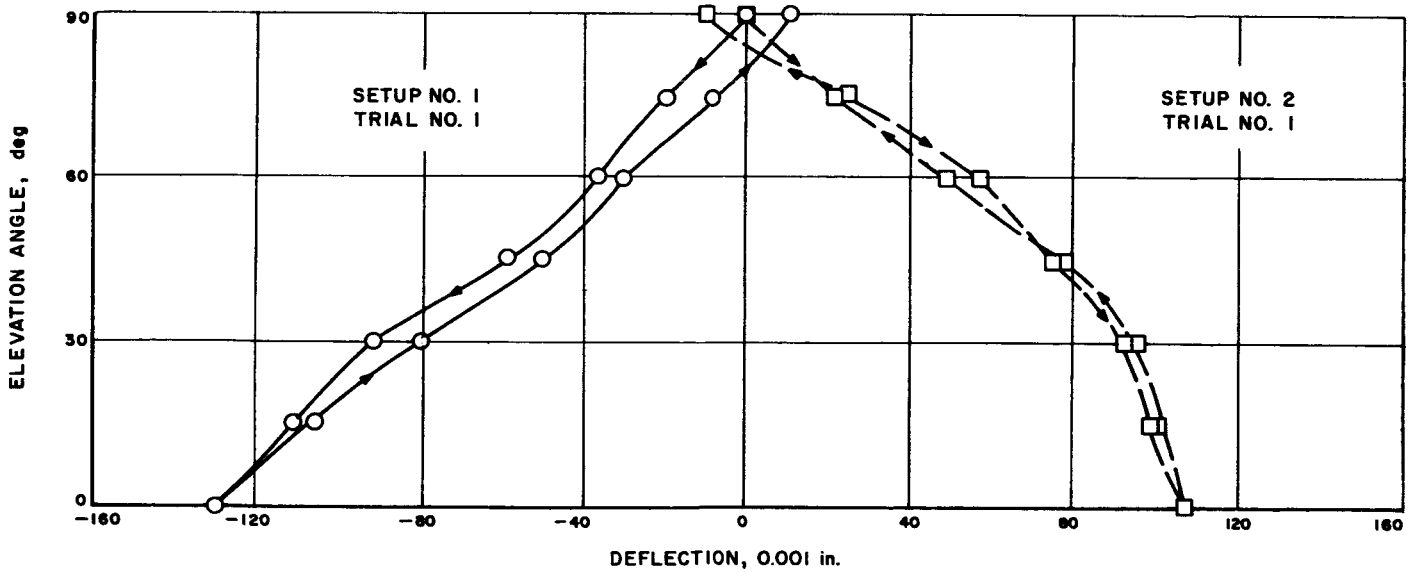

Fig. 24. Deflection curve—extensometer No. 5

The data from the extensometers connected to the feed cone are shown in Fig. 26. The feed cone apparently drops more than the subreflector, about 0.12 in. below the quadripod tip at 0-deg elevation.

The data from extensometer Nos. 8 and 9 are presented in Figs. 27 and 28; there is a direct correlation between the outputs of the two extensometers. Since one end of both extensometers was connected to the same dish edge

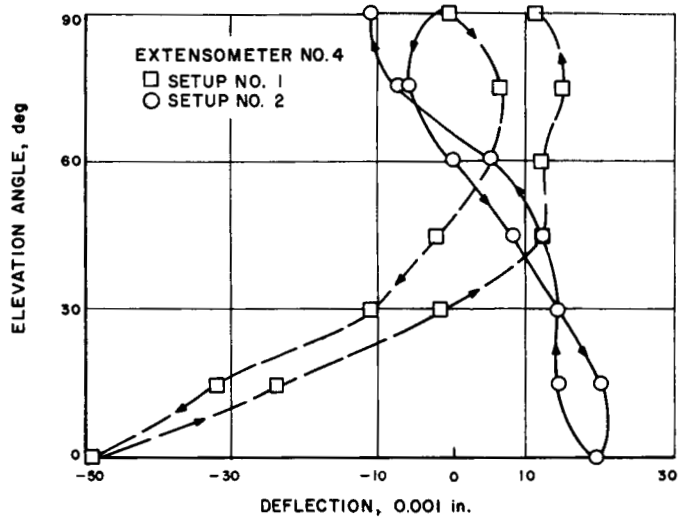

Fig. 25. Deflection curve—extensometer No. 4

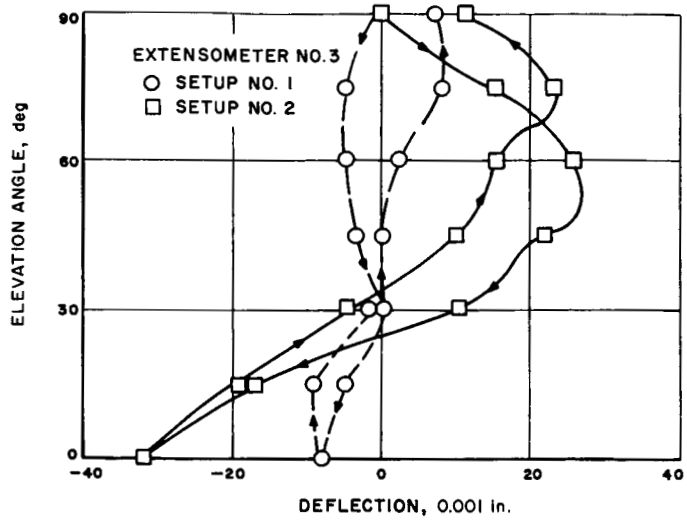

Fig. 26. Deflection curve—extensometer No. 3

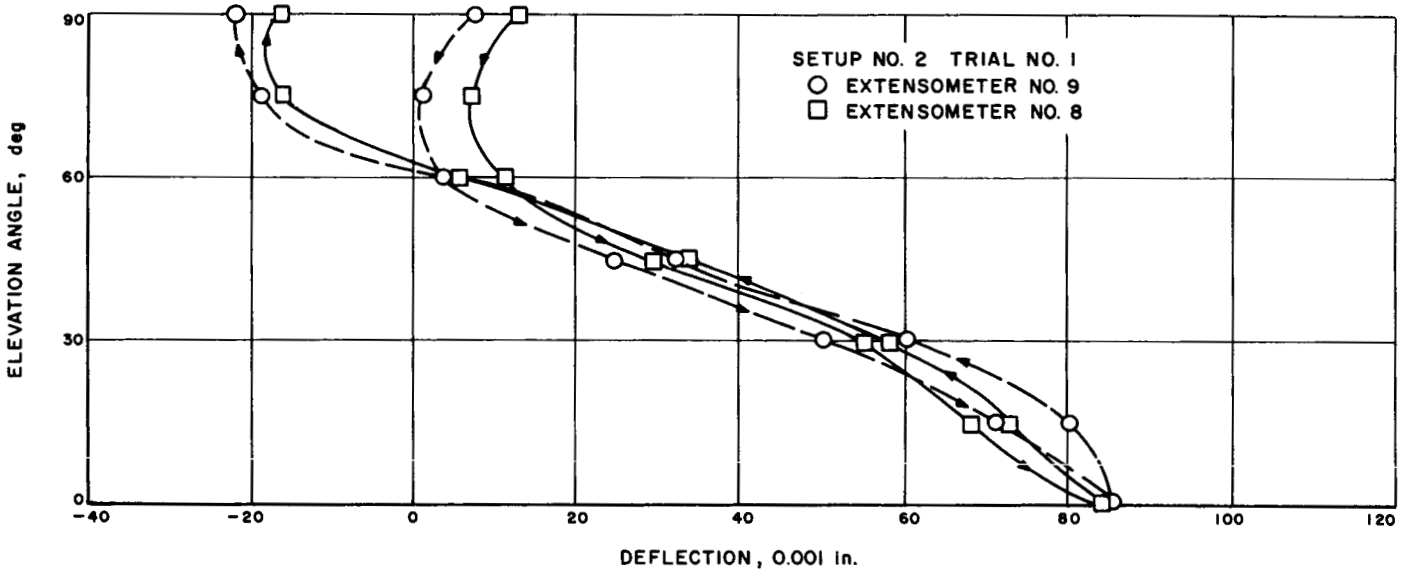

Fig. 27. Deflection curve—extensometer Nos. 8 and 9

and the other ends were connected to the center of a symmetrical structure, effectively the two extensometers were measuring the deformation of two same anchor points. It follows that if the deflection curves are similar, stiction inside the extensometers cannot be blamed for the hysteresis loops. Either the structure itself is deforming to cause these loops or there is an exactly similar effect occurring in the extensometer from a possible voltage change or from a similar thermal change. Based on presently available facts, we have concluded that the structure is deforming to cause these hysteresis loops. During the next series of tests, we expect to make more checks on this conclusion. Laboratory tests are now underway to determine the effects of stiction, temperature, and winds on the extensometer-wire system.

From the structural viewpoint, the data from extensometer Nos. 8 and 9 is interesting as it shows that the connected dish edges are deflecting upward about 0.11 in. for the dish in zenith-look position (90-deg elevation) when gravity is "turned on" from the "gravity off" condition.

The structural deformations measured during the tests were smaller than expected; additional tests are planned

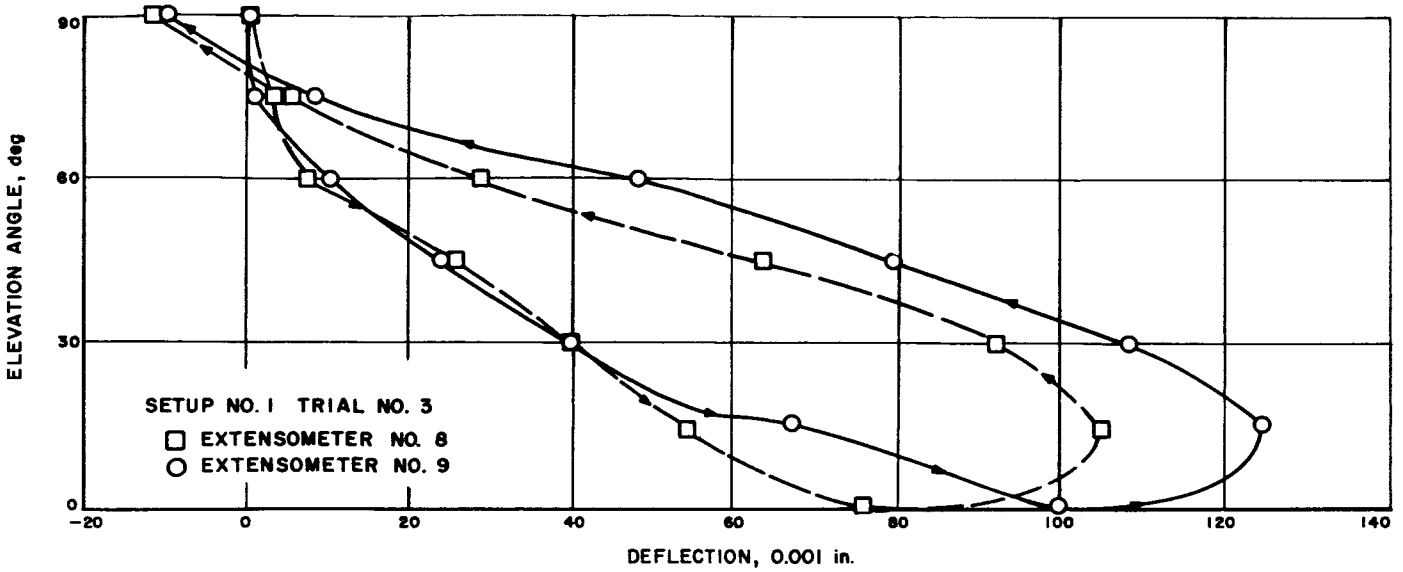

Fig. 28. Deflection curve—extensometer Nos. 8 and 9

to verify and extend the results. Also, reflector structure reflections will be computed using the STAIR computer program to obtain comparative data.

B. Planetary Radar Project

1. Water Rotary Joint for Az–El Antenna

a. Summary. A high-capacity rotary joint is being developed to carry cooling water for the 100-kw transmitter across the azimuth axis of the 85-ft Az–El antenna. In *SPS 37-23*, Vol. III, p. 49, the testing and installation phases were discussed. This report covers the final phase of installation and subsequent testing and operational use of the antenna.

b. Recent work. Installation of the rotary joint and its auxiliary piping has been completed. Previous to availability of the joint, the transmission of klystron cooling water between the ground and the elevation axis was accomplished by a pair of high-pressure rated 2.5-in.-diameter fire hoses. These hoses were intended to be an interim installation during development of the rotary joint. However, it was decided to retain a capability for quick and convenient reinstallation of the fire hoses in case of failure or required maintenance down time of the rotary joint. Fig. 29 shows the selector valves that were installed as a portion of the back-up installation. These three-way plug valves are located next to the antenna base skin in the southern direction, a location which allows normal sidereal tracking in the southern hemisphere with the fire hoses in place. Fig. 30 shows the upper end of this back-up installation and the translation from the antenna alidade to the elevation axis. Bypass of the rotary joint including the fire hose installation can be accomplished in about 10 min and with an inconsequential loss of water.

Carrying the water lines from the alidade across the elevation axis to the tipping parts presented a difficult problem. Standard type rotary joints could not be located on the axis of rotation; however, standard rotary joints were incorporated in a manifold assembly providing a transition from rigid copper pipe to flexible hoses (Fig. 30). In this design concept about one-half of the required motion is provided by the rotary joint and the balance from the flexible hose. The design concept has proved to be satisfactory.

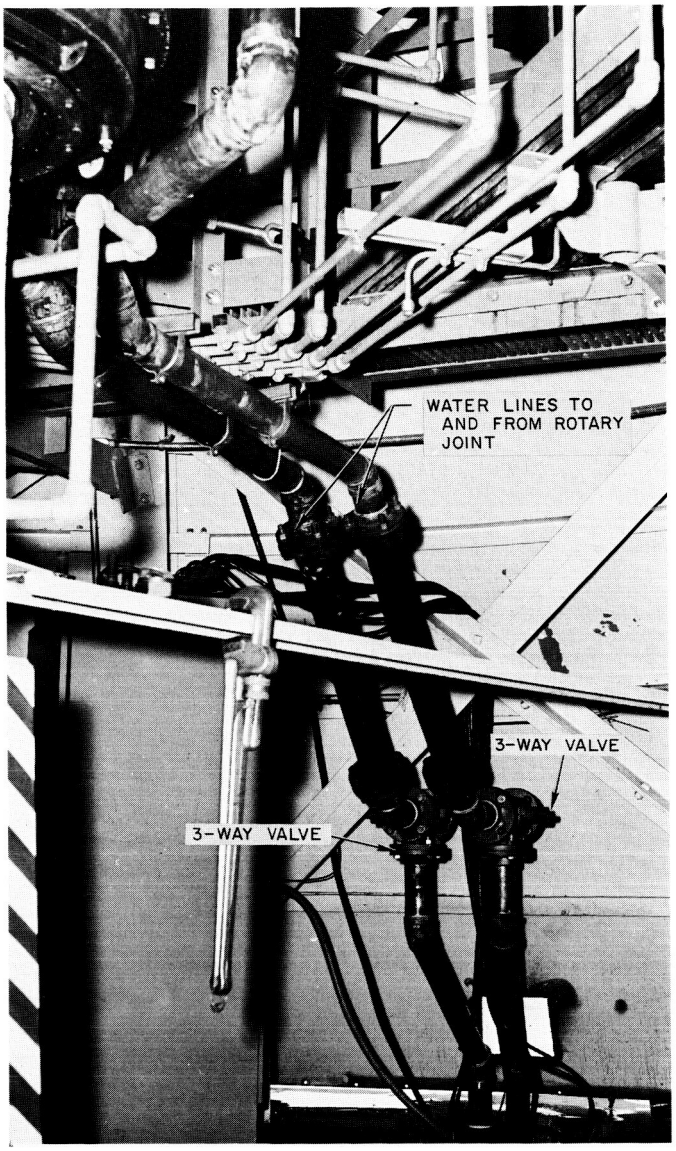

Fig. 29. Rotary joint bypass

Fig. 31 shows the final installation of the large rotary joint on the azimuth axis. From dynamic testing at JPL the torque values for the restraint arms were established (*SPS 37-23*, Vol. III, p. 50). The torque was resisted by a coupled force taken out with 1-in.-diameter steel rods (Fig. 31). This restraint was fully adjustable through turnbuckles. This semi-rigid type of restraint had a steadying influence on the (existing) azimuth axis hydraulic rotary joint located directly below the water joint. The restraint reduced the nutation of the joint by a factor of 3. This reduction also resulted in a more accurate alignment of the magic tee that is used to drive the azimuth readout package.

Complete flow and pressure tests were conducted after the system was installed on the antenna. With a system pressure of 150 psi and a flow of 300 gal/min, the pressure drop across the joint was measured; it was 5 psi in both supply and return lines. This was precisely the design goal.

When the rotary joint was first used in service, there appeared to be little or no leakage. After a few days of operation at various temperatures and pressures, a steady drip appeared in the high-pressure section. This leakage was collected and measured to be approximately ½ gal/hr; daily records of leakage have since been kept. The rotary joint has now been in operation for about 2 mo and the leakage rate has reduced to less than 1 gal/day. This indicates the seals are wearing in. However, measurements of the joint leakage will be continued to make certain that is the case.

2. 100-kw S-Band Transmitter

a. Introduction. In this reporting period, maintenance, design improvements, and documentation were performed on the 100-kw S-band transmitter at the Venus site followed by a short period of data acquisition on the planets Venus and Mercury. A klystron was damaged by an external arc in the filament supply and is being rebuilt. Preliminary reliability studies of silicon rectifiers in megawatt power supply service were made.

b. Documentation. The 100-kw transmitter contract was cancelled before completion, and JPL received only very incomplete documentation. Complete documentation is required for maintenance and for possible additional procurements of similar transmitters. Therefore, a program of documentation for the 100-kw transmitter is in operation. Sixteen contractor-furnished schematic diagrams are being redrawn to the JPL format. Thirteen new drawings are also being prepared. The transmitter cable assignments have been recorded with each conductor identified and point of origin and destination specified. A maintenance and record book has been completed indicating every terminal, terminal location, signal name, and related terminations in the transmitter, exclusive of individual chassis. The connections internal to the chassis are covered by their individual schematics.

c. Design improvements. Several chassis in the transmitter are being redesigned and new units constructed. The crowbar auxiliary power supply has been completed.

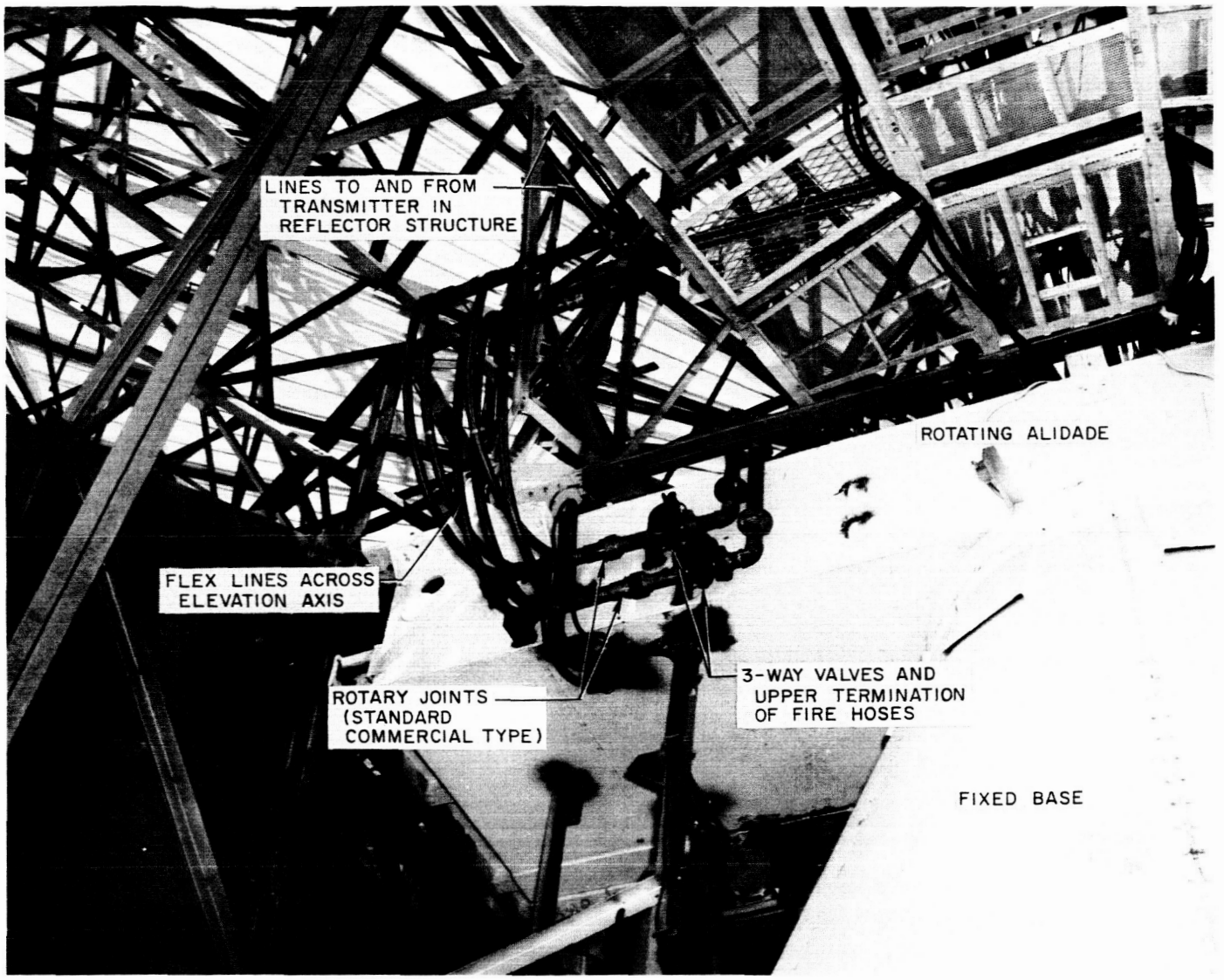

Fig. 30. Alidade-elevation translation

The crowbar trigger unit and the crowbar positioning unit are in the process of being built. The present units will serve as emergency spares.

A new crowbar logic chassis (*SPS 37-23*, Vol. III, p. 40) has been installed and tested. It has eliminated the false crowbar operation due to spurious switching transients occurring from operation of the transmitter controls. Crowbaring is an automatic, emergency shut-down of the transmitter and power system and is intended to protect the klystron from destruction in the event of an internal arc in the tube or by loss of the focus magnet current. False crowbaring results in unnecessary and intermittent shut-down of the system. Following the installation of the new chassis, satisfactory crowbar operation was demonstrated when a newly installed klystron out-gassed and internal body arcing occurred during the initial operation of the tube.

d. Klystron failure. The VA-858 Klystron, Serial No. 3, which had been in service throughout most of the operating life of the 100-kw transmitter, was damaged by an external arc occurring in the filament supply and was replaced by Tube No. 1. The malfunction was of such a nature that the crowbar could not protect the tube. The filament and cathode operate at −32,000 v with respect to ground, and the dc filament power supply is floating at this potential. Immediately following an arc-to-ground from the corona shield of the filament

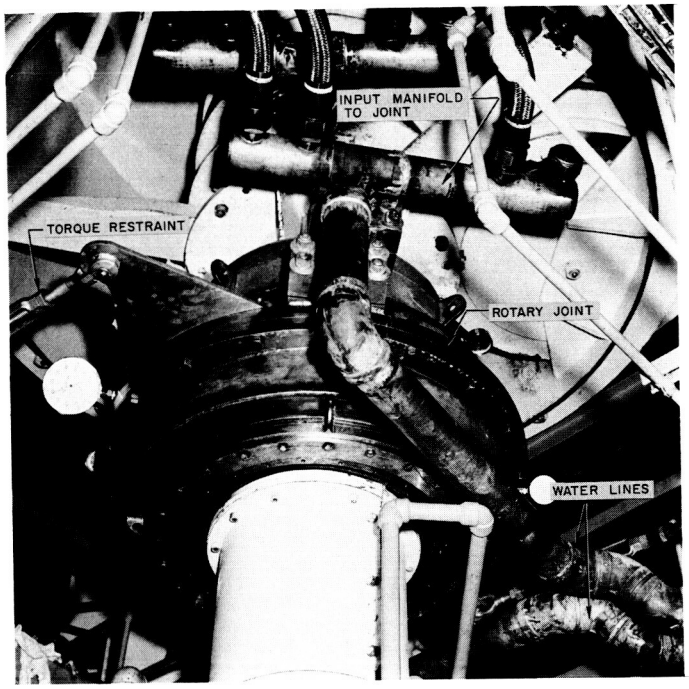

Fig. 31. Rotary joint final installation

reactor, the klystron was observed to have a partially shorted filament. It is thought that the arc placed the 32 kv across the filament, vaporizing some of the heater wire at a weak spot in the ceramic insulation and creating a partial short; dissection of the tube at the manufacturer's facility substantiates this theory. Adjacent turns in the filament are spaced about 0.0025 to 0.005 in. apart. While the crowbar is capable of limiting the current so a body arc does no serious damage to the interior of a tube, the residual energy was probably sufficient to damage the filament when it was concentrated across the small gap between filament turns. At the time of failure the tube had a total of a 1,092.5-hr filament operating time and a 785.0-hr beam operating time. This tube was a prototype and was guaranteed for only 250 hr. It was approaching the end of its service life. The collector exhibits some evidence of localized stress cracking of the internal surface which is attributed to utilization of the tube in keyed or pulse service. Production versions of this klystron have a more rugged cathode structure and larger coolant entry ports in the collector. The collector should run cooler with less localized heating and cracking, although all high power klystrons exhibit this defect and ultimately fail from eroded and cracked drift tubes and collectors. The damaged tube will be refurbished and fitted with the new versions of cathode and collector.

A new dc filament supply is being procured to replace the existing one. It is designed to withstand higher voltages and should prevent a recurrence of the type of arcing described here. Until this new supply is delivered, the replacement tube is being operated with ac on the filaments.

f. Silicon rectifier reliability. The reliability of silicon rectifiers in megawatt power supply service will be further studied in the near future. In the early phases of this investigation, the existing 46,500-v, 400-cps, three-phase transformer will be connected to a full wave silicon bridge rectifier contained in a separate oil-filled tank, the silicon rectifier temporarily replacing the vacuum rectifier tubes. This arrangement will be subjected to operational duty cycles in the planetary and lunar radar programs as well as to R&D type testing. A specification has been prepared to describe the new unit and procurement is in process. Briefly, the device will deliver 0 to 33 kv at 30 amp dc and 33 to 55 kv at 1 Mw. It will withstand fault currents of 160 amp per leg, will be forced oil cooled, and will be designed to operate over the temperature range of -25 to $\pm 135°$F.

3. Mod IV Ranging Equipment

A previous article (*SPS 37-21*, Vol. III, pp. 43–47) described the functions which the Mod IV ranging equipment performs as a digital subsystem of the Mod II planetary radar system. Specifically, these functions consist of:

(1) Providing ephemeris programmed signals for use in spectrum analysis, radiometer analysis, and multiple range-gate analysis of radar echos from planets.

(2) Implementation of a closed-loop range measuring system.

(3) Providing transmit–receive keying signals to control the alternate connection of transmitter and receiver to a single antenna.

This article contains a general description of the structure of the Mod IV ranging equipment, and a functional description of the internal organization of the Mod IV during operation.

a. Structure. A basic block diagram of the Mod IV is shown in Fig. 32. The Mod IV, as is apparent from

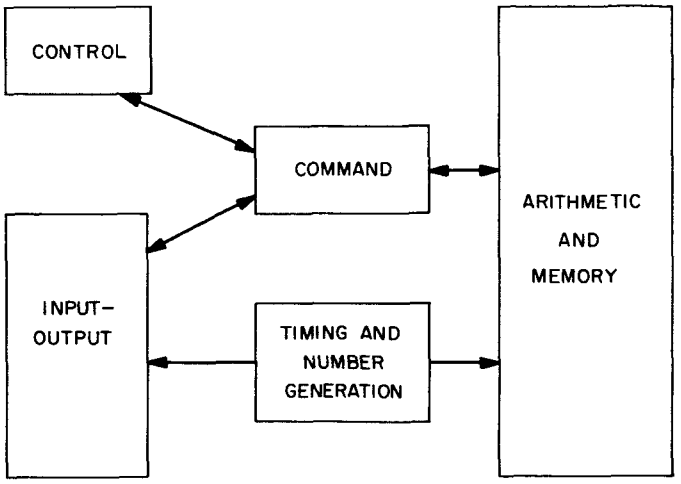

Fig. 32. Mod IV block diagram

this block diagram, consists essentially of a special purpose digital computer with associated input–output equipment.

The special purpose computer within the Mod IV is a wired program machine. That is to say, the several programs for the machine exist in permanently wired form within the equipment. The particular program desired is selected by means of a pushbutton located on the control panel. Once a program has been selected, the execution of that program is under the control of internal timing signals. The machine will continue to operate in the program mode selected until such time as a different program is selected, again by means of a control panel pushbutton. Each wired program controls all of the input–output equipment which is necessary in the execution of that program. It should be noted that the wired program feature of this machine is a result of the fact that the system requirements on the Mod IV are limited and are not expected to expand.

The control unit in Fig. 32 consists of the control panel mentioned previously and a number of static flip-flops. An operator controls the Mod IV by means of the control panel pushbuttons. These pushbuttons, in turn, set or reset static flip-flops which provide control signals for use within the equipment. Thus, for example, selection of a particular program sets certain of the control flip-flops which, in turn, cause the machine to enter and execute the particular program selected.

The command unit controls the operation of the special purpose computer during program execution. Under commands from the command unit, numbers are read in and out of memory, are added, subtracted, or compared with other numbers in the arithmetic unit, and input or output lines are sampled or activated. The command unit, then, contains all of the commands, in wired form, which are necessary to implement each of the several programs. Which commands are executed during a particular program is determined by the status of the control unit, and the order of execution of commands is determined by the status of the control unit, the command unit, and internal time ticks from the timing and number generation unit.

The special purpose computer in the Mod IV utilizes a word length of 50 μsec with each microsecond representing 1 binary digit (bit). The machine is serial, so that words appear sequentially in time. The timing and number generation unit generates a 50-μsec clock which is used throughout the machine as a word timing signal, for example, to gate and retime words during arithmetic operations. In addition, this 50-μsec clock is counted to produce 1-sec and 8-sec time ticks which are used as timing signals.

The timing and number generation unit also generates numbers (in binary form) which are required during the execution of the several programs for comparison purposes in the arithmetic unit or to provide initial loading conditions in the memory unit. These numbers are available in serial form every 50 μsec whether they are needed or not. A particular number is gated out of the timing and number generation unit by a command from the command unit.

The arithmetic unit is capable of addition, subtraction, and comparison of 50-bit numbers. All arithmetic operations are performed on integral numbers.

The memory unit consists of eight serial memory lines which provide eight 50-bit words of storage. Each serial memory line consists of a magneto-strictive delay line with associated logic to provide read-in, read-out, erase, and recirculate capability.

The input–output unit contains equipment which performs the following functions:

(1) Processes input data or signals.

(2) Generates output signals.

(3) Records data.

An example of equipment in the input–output unit which processes input data is the paper tape reader with

associated tape read logic which reads data from the range ephemeris tape into the Mod IV. The code generators provide an example of equipment which generates output signals. The transmitter coder generates a signal which is used to modulate the RF carrier, and the local coder generates a delayed replica of the transmitted code for use in correlation detection. Finally, examples of data recording equipment are a paper tape punch and a printer.

b. Programs. The Mod IV has six programs, five of which are available for selection by an operator via control panel pushbuttons. These six programs are listed and briefly described in this section. The program descriptions are given in terms of the system functions which the Mod IV performs.

(1) *Ephemeris-track program.* Mod IV provides ephemeris programmed signals. In this mode, the local coder and range tally are slaved to the range ephemeris.

(2) *Range-track program.* Mod IV performs a closed-loop range measuring experiment. In this mode, the local coder and range tally track the target during receive cycles and the ephemeris range rate during transmit cycles.

(3) *Range-track-and-calibrate program.* Mod IV performs a closed-loop range measuring experiment as above with the following addition. During transmit cycles, a second range measuring experiment, employing a second local coder and range tally (called the calibrate coder and calibrate tally), is performed on a closed loop which consists of the transmitter, receiver, and Mod IV, only. The range measurement from this calibration experiment provides a measure of the signal delay through the range measuring system itself.

(4) *Calibrate program.* Mod IV performs only the closed-loop calibration portion of (3) continuously.

(5) *Transmit–receive program.* Mod IV provides transmit–receive keying signals to control the alternate connection of transmitter and receiver to a single antenna. This program is not manually selected by means of a control panel pushbutton. Rather, the machine executes this program continuously and concomitantly with a selected program as long as ephemeris range information from an ephemeris tape is available.

(6) *Tape-load program.* Mod IV synchronizes the ephemeris tape with station time by comparing station time with tape time, and then either advancing or retarding the tape until the comparison shows that tape time and station time agree.

c. Functional organization. The functional organization of the Mod IV during execution of the several programs listed in Sec. *b* is shown in Fig. 33. Since Fig. 33 is a functional block diagram, a particular block in Fig. 33 does not necessarily correspond to a particular piece of equipment or to a particular location within the Mod IV.

The symbol shown in the key to Fig. 33 is similar to a logical *OR* symbol and is used to indicate that an input (or output) may be selected from one of several alternative functions. Which particular function is selected is determined by the status of the control input (y). The choice is exclusive, that is, a only or b only or c only, etc., but several alternatives may be selected by ordering them sequentially in time. Control inputs labeled "control and command" in Fig. 33 indicate joint control by the control unit and the command unit; control inputs labeled "control panel" indicate control by the control unit alone.

The ephemeris-track, range-track, range-track-and-calibrate, and calibrate programs, hereafter referred to collectively as the Tracking Programs, are similar in that they consist essentially of a number controlled oscillator (NCO) controlling a local coder and tally. The Tracking Programs differ primarily in the method by which the error number input to the NCO is generated. (See *SPS 37-21*, Vol. III, pp. 43–47, for details concerning the generation of NCO error numbers and NCO operation.) Thus, one NCO, which suffices for all of the Tracking Programs, is shown in Fig. 33.

The NCO error number, $N(t)$, is shown in Fig. 33 as being generated in the block which drives the NCO. The computations which are performed in generating error numbers and the initial conditions, $N(0)$, are listed for each of the Tracking Programs. An initial condition for a particular program is that error number generated when the machine first enters that program.

The input functions required in generating the error number for a particular Tracking Program are selected jointly by the control unit and the command unit. These inputs are each in the form of a binary number with sign. The inputs E_{T+s} and E_T are range numbers from the range ephemeris tape, and the input Δ is an error input from the range channel. In the case of the ephemeris track program, $\Delta = 0$ always.

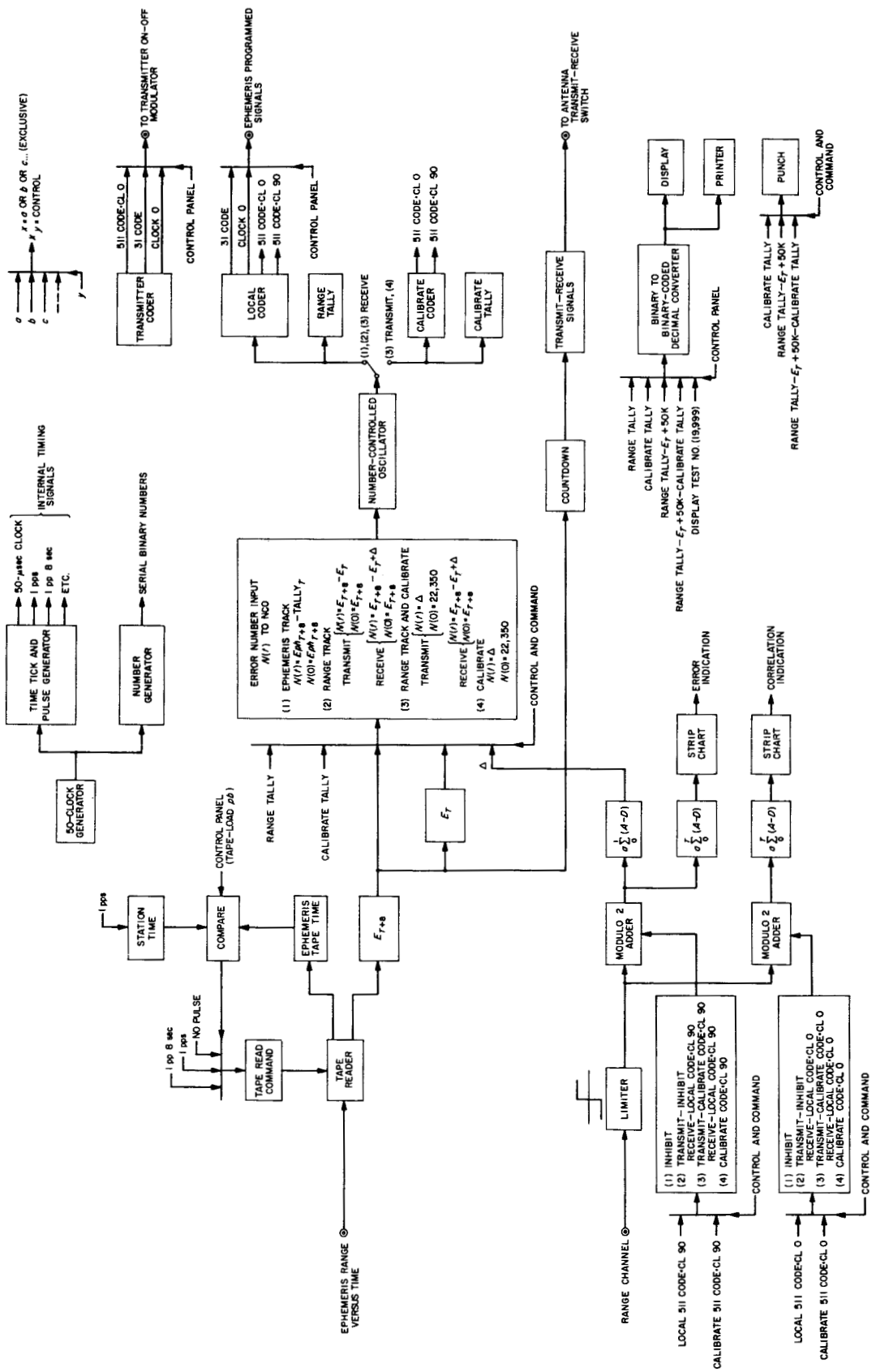

Fig. 33. Mod IV functional block diagram

The NCO output drives either the local coder and range tally or the calibrate coder and calibrate tally. Switching between these two alternatives is under the joint control of the control unit and the command unit. Note that during execution of the ephemeris-track and range-track programs the NCO drives the local coder and range tally only, while during execution of the calibrate program the NCO drives the calibrate coder and calibrate tally only. During execution of the range-track-and-calibrate program, however, the NCO drives the local coder and range tally during receive cycles and the calibrate coder and tally during transmit cycles.

The transmit–receive program is represented in Fig. 33 by the two blocks labeled COUNTDOWN and TRANSMIT–RECEIVE SIGNALS. The method by which transmit–receive keying signals are generated is discussed in detail in *SPS 37-21*, Vol. III, pp. 43–47.

The tape-load program is represented in Fig. 33 by the block labeled COMPARE. During execution of the tape-load program, a comparison is made between station time and tape time. The result of this comparison determines the interval between successive reads of the tape. Normally, a tape read occurs coincident with each 8-sec time tick. If the comparison indicates that tape time is behind station time, the tape is advanced by reading the tape on every 1-sec time tick. If the comparison indicates that tape time is ahead of station time, the tape is delayed by inhibiting a tape read command until station time "catches up" to tape time. Once synchronization has been established, the 8-sec tape read interval is resumed.

4. Radar Observations of Mercury

Radar observations of Mercury were made during its recent conjunction in May. The series of measurements was made at the Venus site of the Goldstone DSIF Station. Mercury was illuminated with the 100-kw S-band transmitter working into the 85-ft paraboloidal antenna. Essentially the same low-noise, ephemeris-tuned receiver was used for Mercury as was used for the Venus experiments of the Fall of 1962.

Three different types of signal processing were used, yielding three different kinds of information about Mercury. The same techniques were used with Venus as the target during the 1962 conjunction, so the two sets of data may be compared directly.

The simplest processing method used the receiver in the configuration of a Dicke radiometer (except that the transmitter was keyed instead of the receiver), and measured the total power of the echo. Typically, 4 hr of signal were integrated, producing about an 11-σ detection from a signal power of only 5×10^{-22} w. The radar cross-section of Mercury was measured as 5% of its geometric cross-section. This compares with 10% for Venus and 3% for Mars.

A second type of data processing analyzed the echo into its frequency components, using the autocorrelation function approach. A spectrally pure wave was transmitted to Mercury, but the echo was both shifted and broadened in frequency by the doppler effect. The shift is caused by the relative orbital velocity between Mercury and the radar station; while the broadening is caused by the apparent rotation, which imparts differing line of sight velocities to different parts of the surface.

Fig. 34 is a sample spectrogram, taken with over 4 hr of signal integration. The lines marked on the abscissa show the calculated position of echos reflected from the limbs of Mercury. As can be seen, echos are detected almost to the limbs. This corroborates our conclusions of a slow retrograde rotation for Venus, for such a conclusion requires that Venus echos (which are much stronger) be detectable near the limbs.

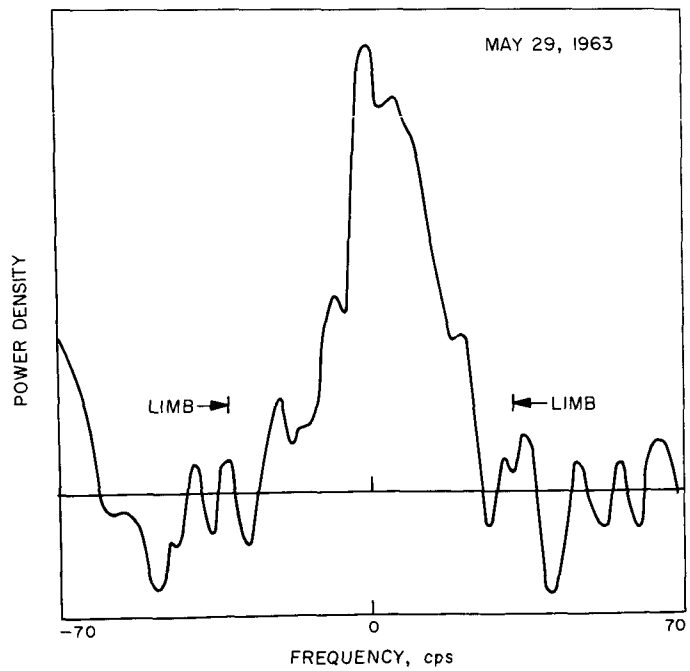

Fig. 34. Mercury spectrogram

The width of the spectrograms, in relation to the size and rotation of Mercury, is a measure of the roughness of its surface. In this sense Mercury is much rougher than Mars and perhaps twice as rough as Venus.

The doppler shift of the signal was removed by an ephemeris-tuned receiver; hence, the center frequencies of the spectrograms give directly the velocity errors of the ephemeris. Table 3 is a list of these residuals.

Table 3. Residuals

Date	Velocity, cm/sec	Range, m
May 15, 1963	−28	
May 16, 1963	−20	
May 21, 1963	−49	
May 23, 1963	−44	
May 24, 1963		$+1.1 \times 10^5$
May 25, 1963	−38	
May 26, 1963	−25	
May 28, 1963	−22	$+1.7 \times 10^5$
May 29, 1963	−22	

A third method of signal processing combines a range-gate with the spectrometer. In this mode, the transmitter was modulated with a wide-band waveform. The range-gate was set to accept echos from a specified 178-km slice of Mercury, and to reject all other echos. The selected signal was then analyzed for its frequency content. A typical range-gated spectrogram is shown in Fig. 35.

Since these echos originate from known areas on Mercury, its speed of rotation may be inferred. Of course, it has long been known that the period of Mercury's rotation is 88 days; but the measurement, which was in excellent agreement, serves as a powerful check on one of the techniques we used to measure Venus' rotation.

Spectrograms of this type were also used to measure the round-trip time-of-flight, and hence the range to Mercury. The internal consistency of this method was good to within 15 km. Since the orbital velocity of Mercury carries it through one range zone in only 12 sec, it is necessary to control the range-gate with an ephemeris also. Thus, the range-gated spectrograms give the range error of the ephemeris. These residuals are also presented in Table 3.

The trends seen in this data are essentially eliminated by adjusting the argument of the ephemeris by only 6 sec, and the astronomical unit (AU) by only 10^5 m.

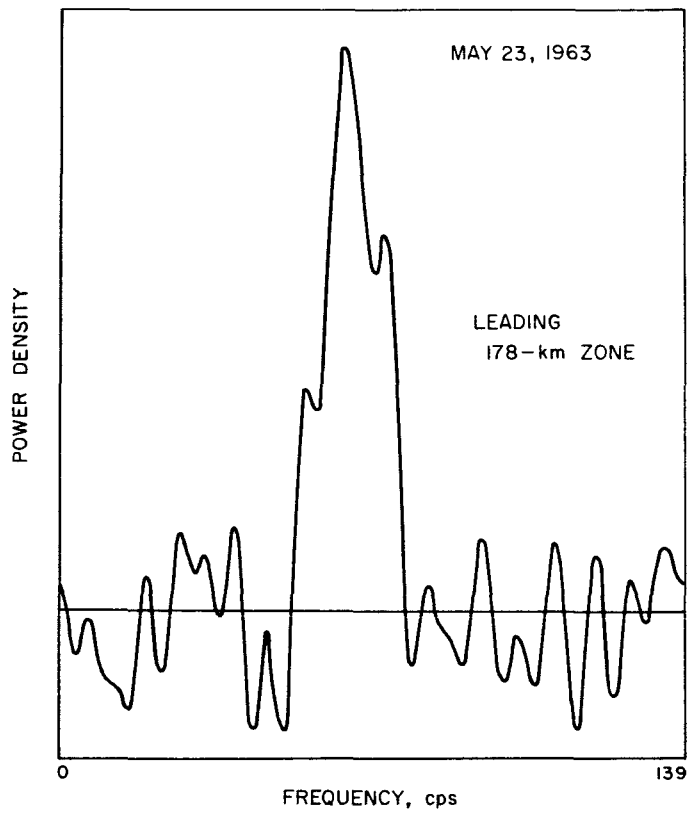

Fig. 35. Range-gated spectrogram

This data provides a striking configuration of the AU reported by Muhleman and based on radar observations of Venus during the conjunctions of 1961 and 1962.

C. Lunar Radar Project

1. Mod III Transmitting System, 2388 Mc, 100 kw

a. Klystron noise power. The klystron noise power is one of the major parameters in designing a monostatic radar for lunar use. The effect of the klystron noise was analyzed in *SPS 37-23*, Vol. III, pp. 52–55. This analysis was based on limited data since, at the time the klystron noise was measured (*SPS 37-22*, Vol. III, p. 17), false crowbar actions limited the tuning of the klystron. For this reason, and because the klystron has been changed from Serial No. 3 to Serial No. 1, a more extensive test was conducted during this reporting period.

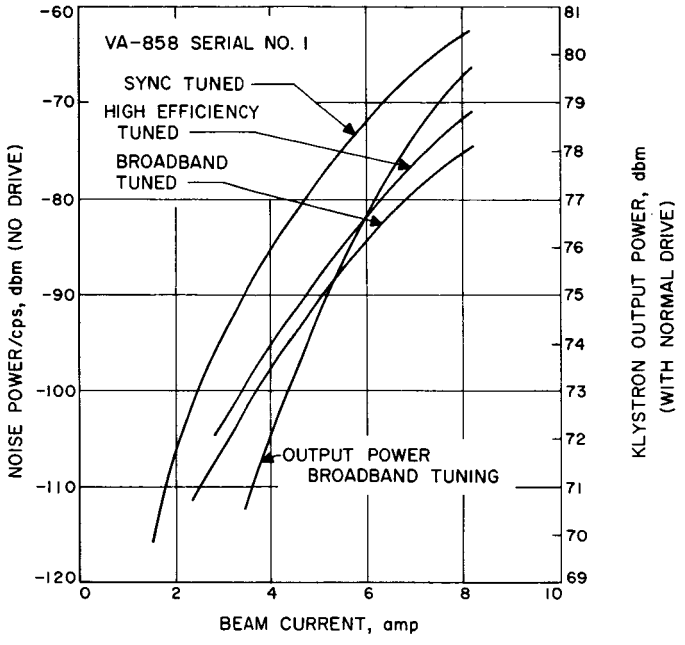

Fig. 36. Output power and noise power versus klystron beam current

Fig. 36 is a plot of noise power versus beam current for three different klystron bandwidths. The curves indicate that the noise power per cycle decreases as the klystron bandwidth increases. For reference the output power versus beam current (with normal drive) is also plotted on this figure. As an aid to lunar system analysis, the information in Fig. 36 was transposed to a plot of klystron noise power versus output power in Fig. 37.

During this test the noise power was measured at the input to the maser monitor receiver having a 3-db bandwidth of 14 Mc, at the input to the preamplifier of the Mod IV receiver with a 3-db bandwidth of 1.7 Mc, and at the 455-kc IF of the Mod IV receiver having a 3-db bandwidth of 12 kc. The results are plotted in Figs. 38, 39, and 40 for three different klystron tunings.

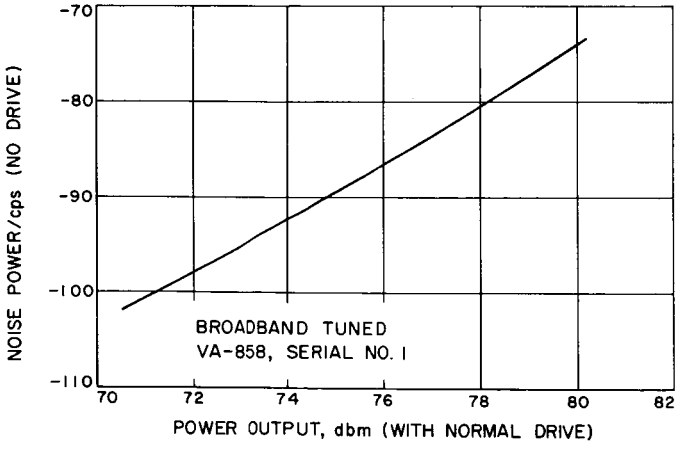

Fig. 37. Klystron noise power versus output power

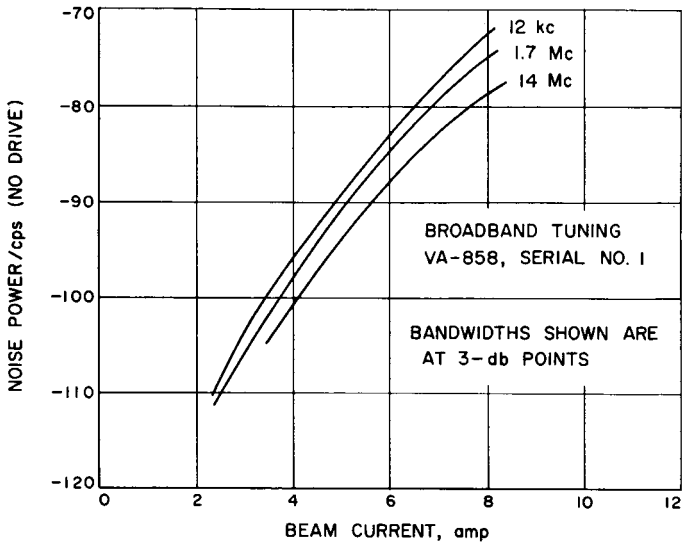

Fig. 38. Noise power versus klystron beam current—broadband tuning

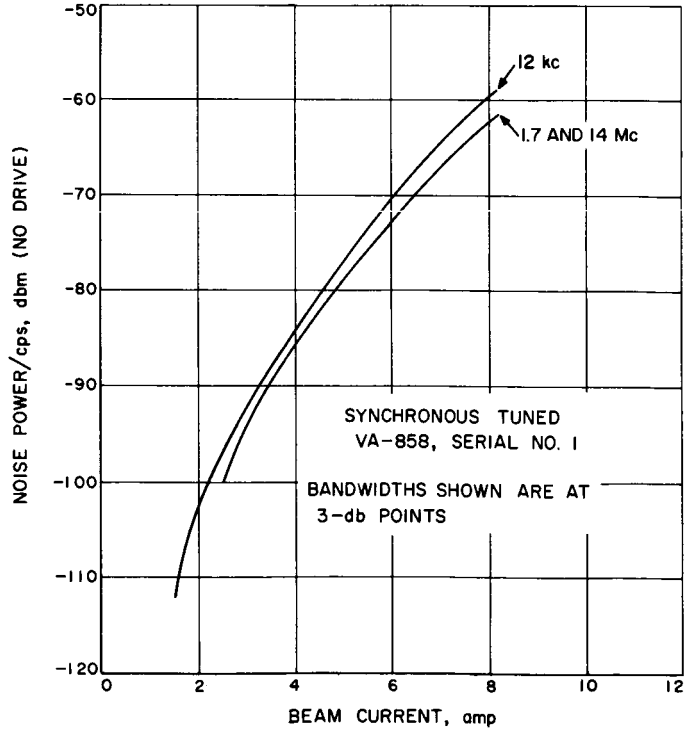

Fig. 39. Noise power versus klystron beam current—synchronous tuning

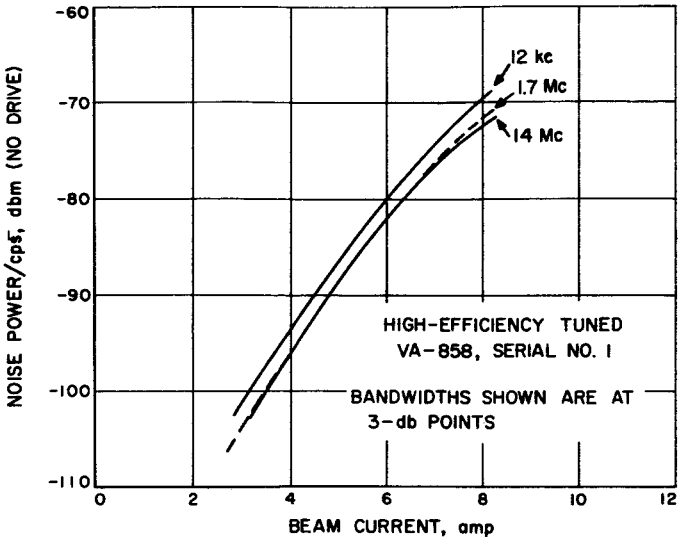

Fig. 40. Noise power versus klystron beam current—high efficiency tuning

In Fig. 38, with broadband tuning, the noise power per cycle decreases as the bandwidth of the detector increases. This indicates that 3-db noise bandwidth for this tuning is about 2 Mc.

With high efficiency tuning, Fig. 39 shows that the noise power per cycle decreases only slightly when the bandwidth of the detector is increased from 1.7 to 14 Mc. This indicates that, for this particular tuning, the noise power is nearly uniform over at least a 14-Mc bandwidth.

For the measurements plotted in Fig. 40, the klystron was tuned to the minimum bandwidth possible for this particular klystron. As indicated in the plot, and within the accuracy possible in these measurements, there is no difference between the noise power per cycle as the detector bandwidth is increased from 1.7 to 14 Mc. This indicates that, for this tuning, the noise power is nearly uniform over at least a 14-Mc bandwidth.

2. Microwave Configuration for Lunar System

a. Summary. The microwave configuration of a lunar mode adaptation of the Venus site planetary radar is presented.

b. Recent work. A general description of the Lunar Radar Project was given in *SPS 37-23*, Vol. III, pp. 51–55. A decision has been made to mechanize for reception on a 6-ft-diameter antenna and transmission on the normal planetary radar feed system. This approach is necessitated by the short round-trip time for lunar radar and the comparatively long time for the waveguide switching used in the planetary radar mode.

The microwave system block diagram is shown in Fig. 41. Installation of this system was completed in September 1963. The entire system is pressurized with dry nitrogen; the waveguide run used the new JPL flanges described in *SPS 37-23*, Vol. IV.

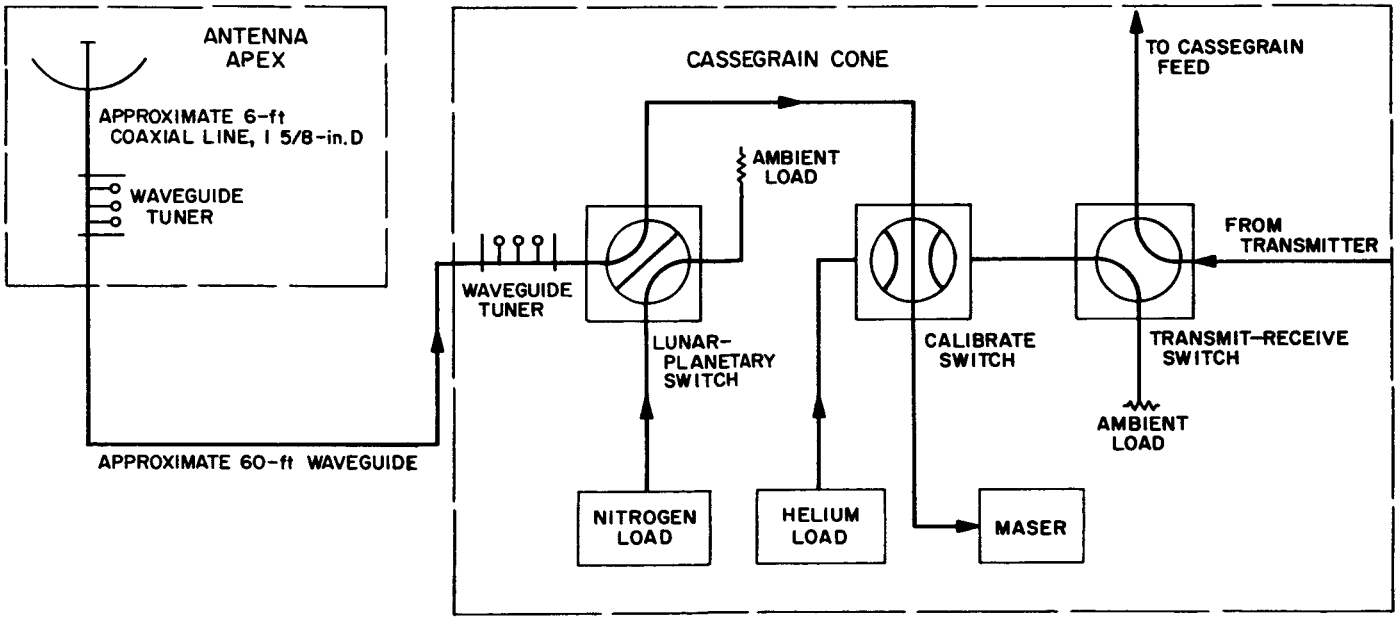

Fig. 41. Lunar radar microwave circuitry

The most critical microwave performance requirement for the lunar radar system is that of isolation between the two antenna systems; the system sensitivity may be limited by klystron beam noise if the isolation is not sufficiently great. Based on previous work (*SPS 37-20*, Vol. IV, pp. 142–145) the tunneled 6-ft dish was expected to yield roughly 90-db isolation at high elevation angles. The tunnel length was, however, increased from 12 to 20 in., since previous pattern data indicated that the antenna back radiation was minimized for this tunnel length. Time has not yet permitted the measurement of isolation directly. An indirect measurement is described in the following article.

3. Lunar Radar System Noise Temperature Measurements

a. Summary. In *SPS 37-23*, Vol. III, pp. 51–55, a discussion of a proposed adaptation of the Venus site planetary radar for lunar measurements was given. In the preceding article of this report, a block diagram was presented of the microwave system of the radar. The lunar radar system employs an 85-ft diameter antenna for transmission and a 6-ft paraboloidal antenna, mounted on the 85-ft antenna quadripod structure, for reception. The results of measurements are presented here of system temperature as a function of elevation angle, and system noise temperature as a function of klystron beam voltage. A figure of merit is defined as the power that would be transmitted with the klystron beam voltage on and RF excitation applied, divided by the system temperature measured with this beam voltage alone applied. The figure of merit is presented as a function of the power which would be transmitted if RF excitation were applied.

b. Recent work. On October 3 and 4, 1963, a series of measurements of antenna temperature was made at the Goldstone Venus site. Fig. 42 presents the measured system temperature using a left-hand circularly polarized (LCP) feed on the 6-ft receiving antenna and a right-hand circularly polarized (RCP) feed on the 85-ft transmitting antenna. This is the normal radar matched mode of operation where RCP incident on a target is reflected as LCP. The two curves in Fig. 42 are for 0 and 25 kv applied to the klystron beam; 25 kv is equivalent to an excited transmitter output power of 47 kw. These curves were run with the beam voltage applied but no RF excitation so that the klystron was acting as a noise diode. Fig. 43 shows an expanded curve of system temperature as a function of elevation angle with no beam current.

In Sec. IV-C-1 of this report, measurements are discussed of the noise power from the klystron acting as a noise diode. This noise data, with high efficiency tuning, has been used to obtain transmission loss between the transmitter tube and the receiver input. The high efficiency tuning for the klystron at 25-kv beam voltage produced a noise spectral density of −82 dbm per cycle. The effective path loss from klystron to receiver input for the matched polarization case illustrated in Fig. 42 is, therefore, approximately 94 db.

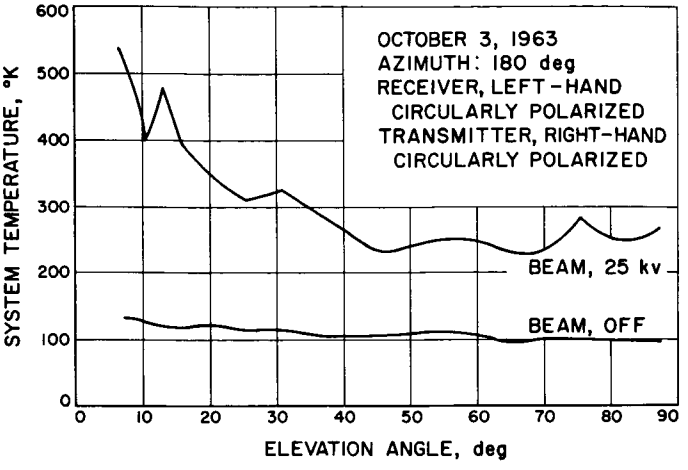

Fig. 42. Lunar radar receiver system temperature versus elevation angle, October 3, 1963

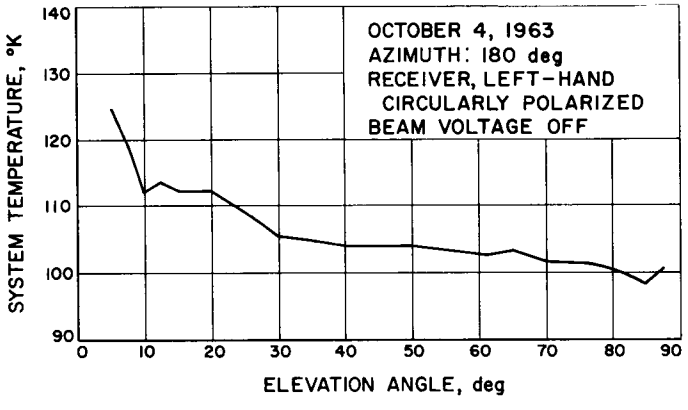

Fig. 43. Lunar radar receiver system temperature versus elevation angle (expanded), October 4, 1963

Fig. 44 is a plot of system temperature versus elevation angle using an LCP transmitted signal and accepting an LCP received signal. The system temperature is much higher in this case than it was for the case of RCP to LCP. This can be interpreted as an effective ellipticity of the back lobe of the 6-ft antenna. This has been computed for high elevation angles by first calculating the transmission path loss from transmitter tube to receiver input of the mismatched case; the loss is 87 db as compared to

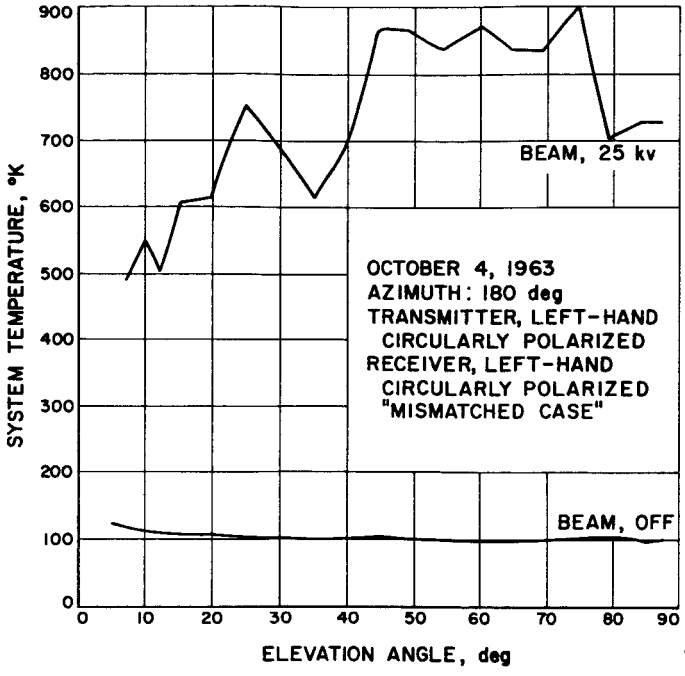

Fig. 44. Lunar radar receiver system temperature versus elevation angle, October 4, 1963

94 db for the matched case. A difference of 7 db for circular modes results in an ellipticity of approximately 8 db. The absolute accuracy of the path loss is approximately ±4 db, but the accuracy of the mean difference is ±1 db.

For the matched case the system temperature increases with decreasing elevation angle (Fig. 42). The noise signal on reflection has its sense of polarization reversed so that the reflected signal is picked up through the side lobes by the receiving antenna. In the LCP transmit, LCP receive case, the effective system temperature decreases with elevation angle (Fig. 44). One would not expect to receive as much backscattered energy through the side lobes as elevation angle decreased with this polarization configuration; however, the actual decrease with elevation angle is unexpected and, as yet, unexplained.

For the matched polarization case it was found that, at low elevation angles, the system temperature is strongly a function of the horizon mask. At an azimuth of 180 deg at which the data for Figs. 42, 43, and 44 were taken, the horizon mask is approximately 4 deg. Fig. 45 shows the system temperature as a function of elevation angle for an azimuth of 90 deg where the horizon mask is also approximately 4 deg. Fig. 46 shows the system temperature as a function of elevation angle for an azimuth of 260 deg where the horizon mask is 7 deg. The system

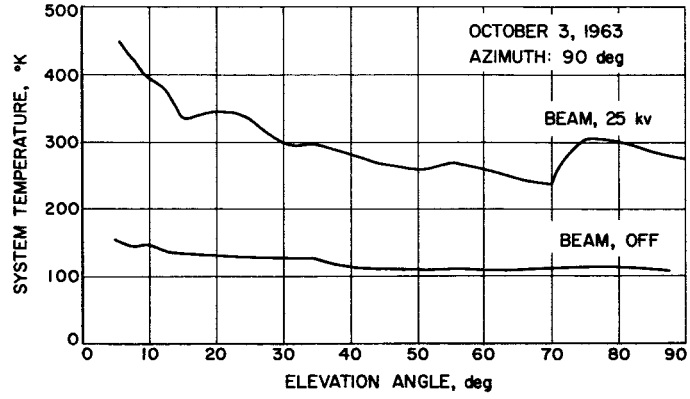

Fig. 45. Lunar radar receiver system temperature versus elevation angle (Azimuth = 90 deg), October 3, 1963

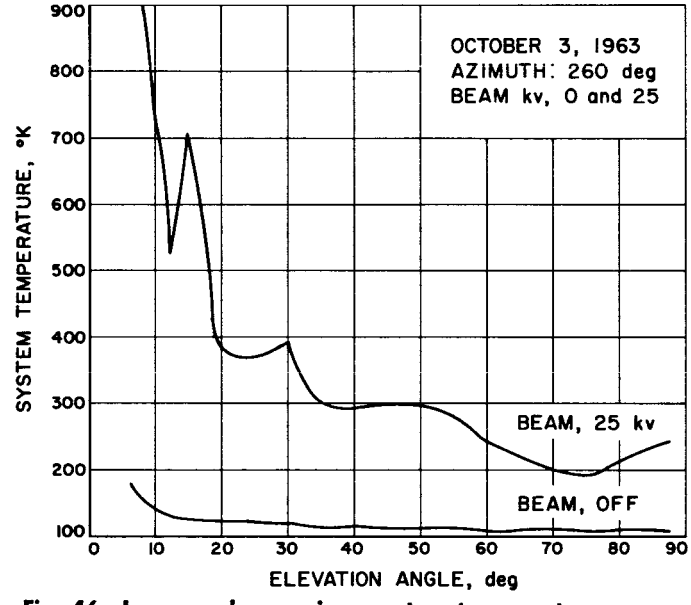

Fig. 46. Lunar radar receiver system temperature versus elevation angle (Azimuth = 260 deg), October 3, 1963

temperature at low elevation angles is much greater in this case than for the 4-deg horizon mask azimuths. At 7-deg elevation the temperature could not be measured but was in excess of 1000°K. A Y-factor method of system temperature measurement with a gas pulse tube of 56 deg was employed in the tests; an increase of 56 deg in the total temperature was not sufficiently great to be measured accurately. The accuracy of calibration of the gas tube pulse, which was used in all temperature measurements, is approximately ±6°K.

To determine an optimum transmitter power level, a figure of merit is defined as the power which would be transmitted at the beam voltage level used if RF excita-

tion were applied, divided by the system temperature which is measured when the same beam voltage is applied, but with no RF excitation. An analysis of this optimization problem was presented in *SPS 37-23*, Vol. III, pp. 52–55. In Fig. 47, this figure of merit is plotted against the transmitter power which would be transmitted with RF excitation applied for a given beam voltage. There are two curves in Fig. 47: one for the case of RCP transmitted and one for the case of LCP transmitted. The receiving antenna in both cases is LCP. For the RCP transmitter case it can be seen that there is a broad maximum extending from approximately 32 kw to approximately 48 kw. For the case of LCP transmitted the maximum occurs roughly at 25 kw and drops off rapidly as the beam voltage is increased. Figs. 48 and 49 show the same data taken at elevation angles of 65 and 87 deg, respectively. The data for Figs. 47, 48, and 49 were taken at an azimuth of 180 deg.

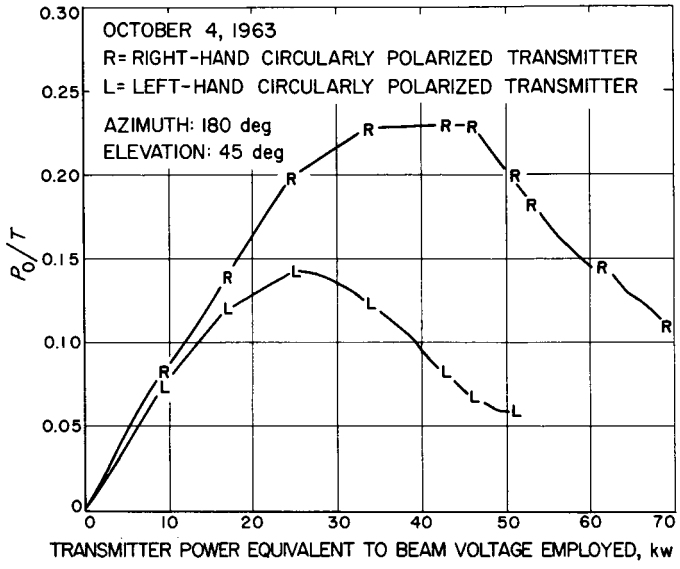

Fig. 47. Lunar radar system figure of merit versus transmitter power (Elevation = 45 deg), October 4, 1963

In the lunar and planetary radar system the return signal power is normally computed by measuring the signal-to-noise ratio. The power of the return signal, therefore, cannot be known any more accurately than the system temperature. This places a requirement on the stability of the system noise temperature. The stability of the system temperature was measured for a variety of conditions. Fig. 50 shows a stability recording of the detected receiver output at a klystron beam voltage of 25 kv. The large "transients" in all these recordings are caused by the gas tube being used in Y-factor measurements. The Y-factors measured, as well as the corresponding system temperatures, are indicated on the recordings. Very small changes in measured Y-factor produce large changes in calculated system temperature when the temperature being measured is large compared to the gas tube pulse. The transmitting and receiving antennas for

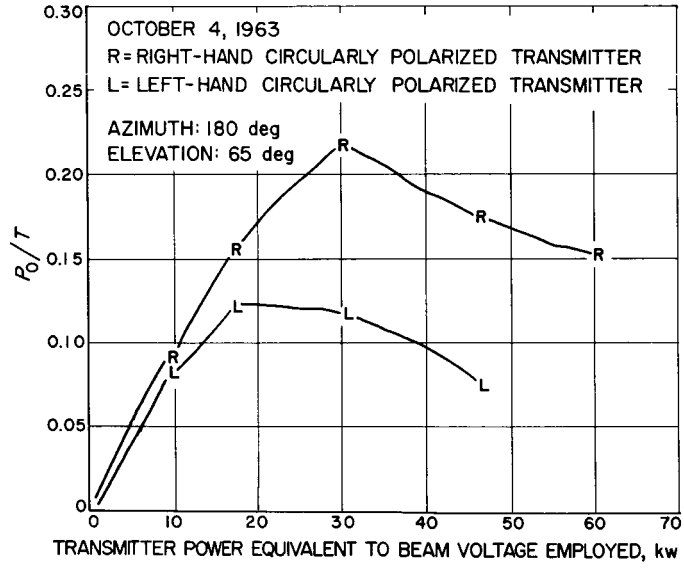

Fig. 48. Lunar radar system figure of merit versus transmitter power (Elevation = 65 deg), October 4, 1963

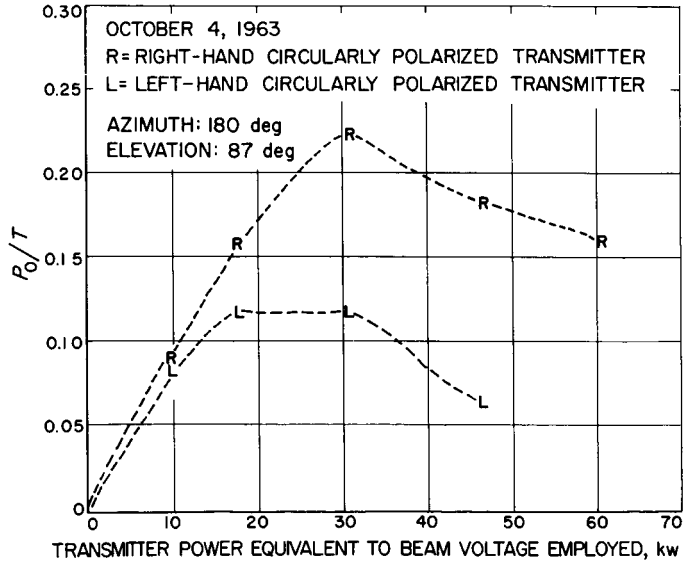

Fig. 49. Lunar radar system figure of merit versus transmitter power (Elevation = 87 deg), October 4, 1963

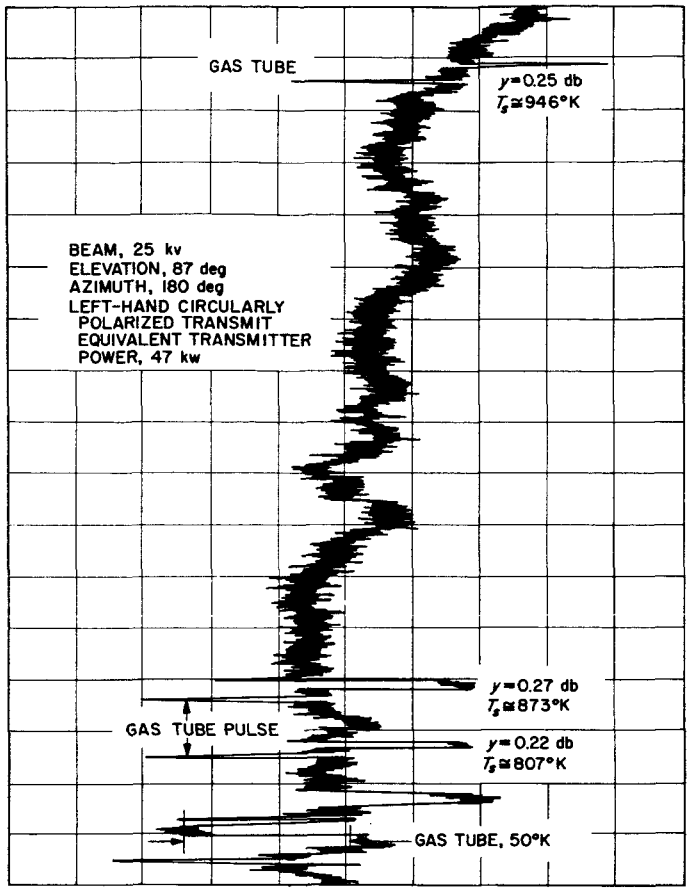

Fig. 50. System temperature stability run

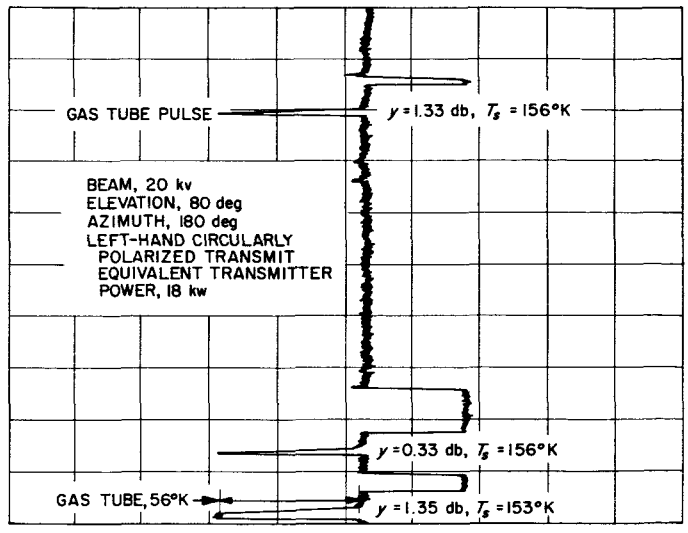

Fig. 51. System temperature stability run

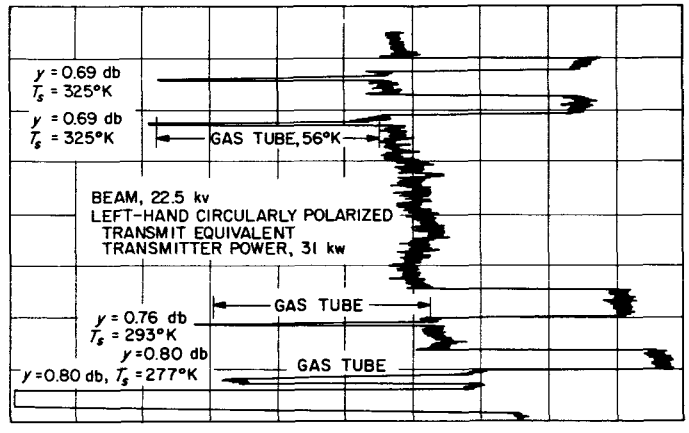

Fig. 52. System temperature stability run

the data of Fig. 50 were LCP; a noise pulse of 56°K is indicated. The effective system temperature during the period of this recording varied between 873°K and 1076°K as measured by the Y-factor method. The peak-to-peak jitter was about 14°K. In 10 min it can be seen that the system drift in excess of 60°K occurred. The chart recorder speed is 1 min per division in this recording; the time constant used in all stability runs was approximately 1 sec.

In Fig. 51 the same parameters were used; however, the klystron beam voltage was reduced from 25 to 20 kv. The system temperature is much reduced as is the peak-to-peak jitter (≈3.5°K) and the long-term drift. Fig. 52 shows the beam voltage at the 22.5 kv; the gain setting on the recording has been increased by 2 db from the data of Fig. 51. The peak-to-peak jitter is about 8.5°K.

Noise stability runs were also taken for the matched case of RCP transmitted and LCP received. The path loss between the transmitter output and the receiver input is greater for the matched case than the mismatched case, and, therefore, the temperature for any given beam voltage level is less. Fig. 53 shows the case with the beam voltage off. Peak-to-peak jitter is approximately 1.7°K. On all the matched case stability recordings, the speed of the chart recorder was 32 divisions per hour.

Fig. 54 shows the case of 17.2-kv beam voltage or an equivalent transmitted power of 10 kw, the peak-to-peak jitter of 2.5°K. Fig. 55 shows a beam voltage of 19.5 kv or an equivalent transmitter power of 15 kw; the peak-to-peak jitter is about 5°K and the long-term stability is excellent. Fig. 56 shows a beam voltage of 23 kv or an equivalent transmitted power of 33 kw; the long-term stability is starting to deteriorate and the peak-to-peak jitter is approximately 6°K. Fig. 57 shows a beam voltage of 25 kv or an equivalent transmitter power of 47 kw;

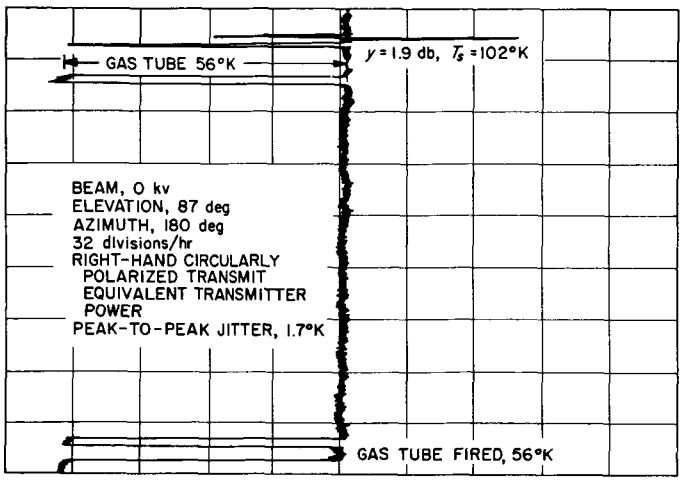

Fig. 53. System temperature stability run

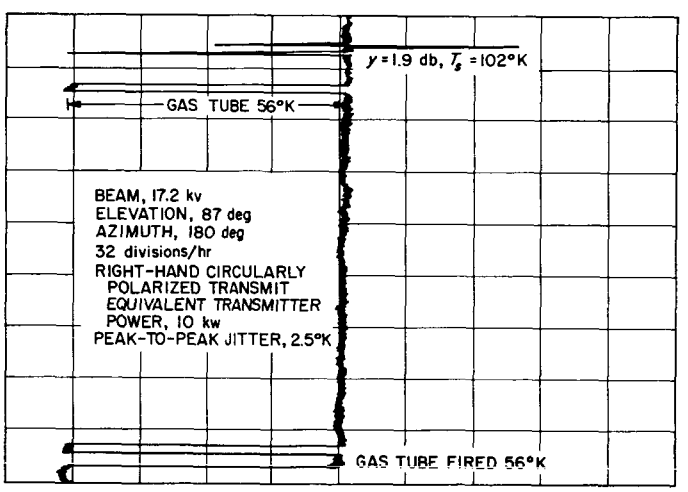

Fig. 54. System temperature stability run

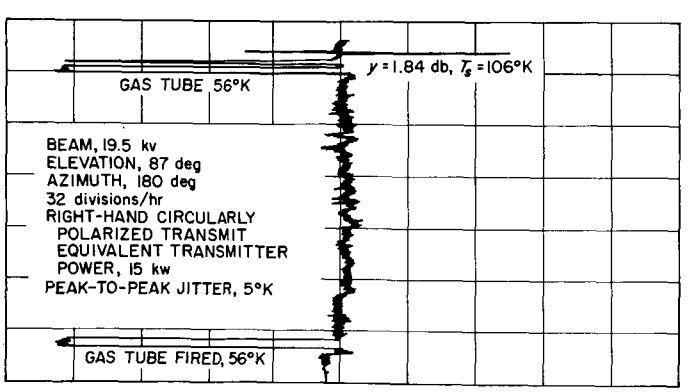

Fig. 55. System temperature stability run

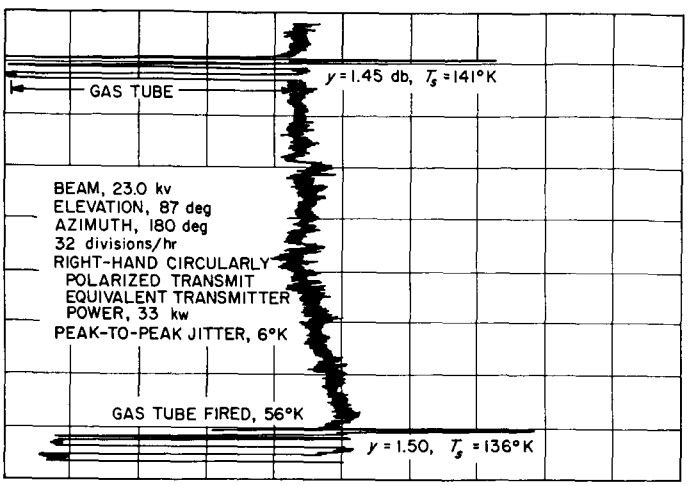

Fig. 56. System temperature stability run

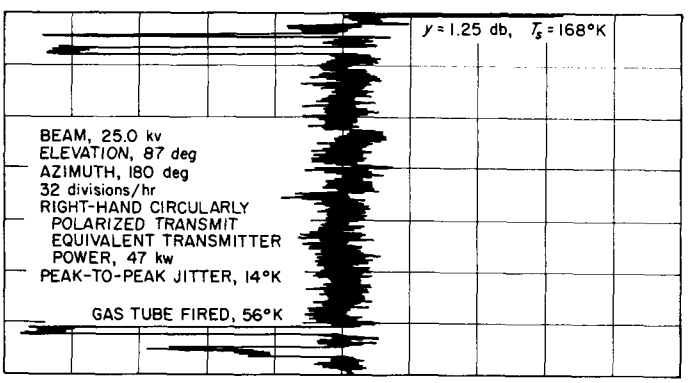

Fig. 57. System temperature stability run

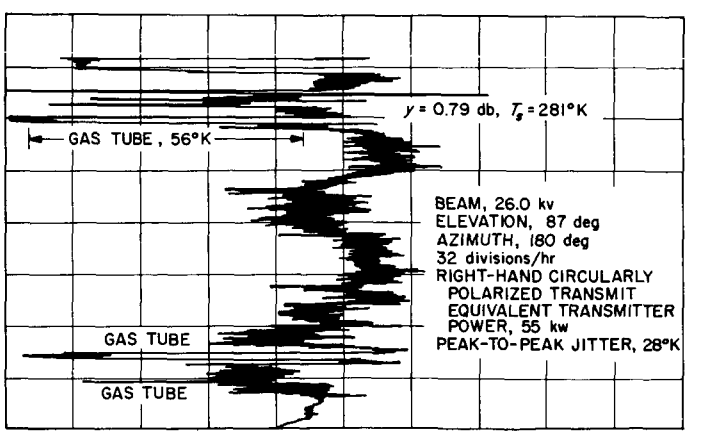

Fig. 58. System temperature stability run

peak-to-peak jitter has increased to 14°K. Fig. 58 shows the beam voltage at 26 kv for an equivalent transmitted power of 55 kw. The peak-to-peak jitter is 28°K and the long-term stability is poor.

Figs. 47, 48, and 49 presented the figure of merit for various levels of transmitter power. On the basis of this figure of merit alone, one would take the equivalent power of the maximum of the figure of merit as an optimum power for lunar radar operations. However, on the basis of noise temperature stability, it appears that one should take the minimum power consistent with a reasonable figure of merit. More complete stability data may show that for high accuracy work it might pay to sacrifice a db of figure of merit to improve the stability of the system temperature performance, and therefore the accuracy of the power measurement. Although figure of merit plots have not yet been obtained for elevation angles below 45 deg, it is clear that the matched case will approach the shape of the mismatched case as the elevation angle is decreased.

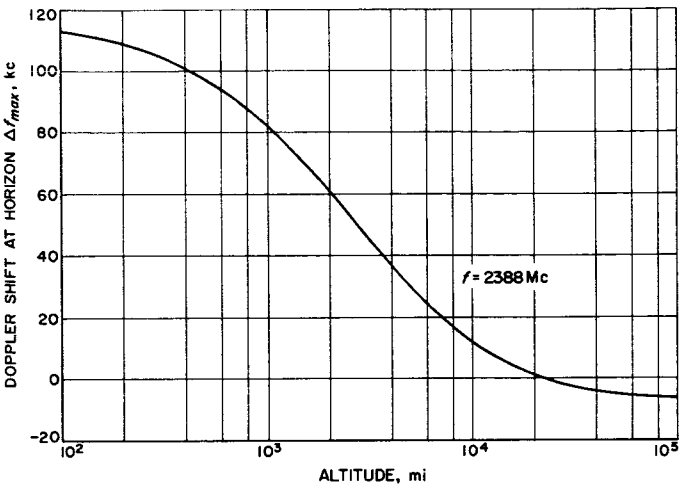

Fig. 59. Maximum doppler shift

D. Ranging and Tracking System Development

1. Monostatic Radar

a. Résumé. In order to establish operating parameters for a feasibility model satellite radar operating at S-band, a preliminary analysis of expected worst case target dynamics has been made. The effects of maximum doppler shift and doppler rate upon receiver parameters, most particularly loop bandwidth, are presented graphically. With a minimum loop bandwidth thus tentatively established, limitations on receiver threshold and system keying rates are investigated.

b. Doppler frequency shift. Although the intended target of the interim system is the *Echo* balloon (assume 800-mi altitude), the data of Fig. 59 was used to establish a worst case doppler tracking requirement of ±120 kc (approx 50 ppm). For a maximum static phase error of 6 deg, it follows that the threshold loop gain must not be less than:

$$\frac{G}{360} = \frac{\Delta f}{\Delta\phi} = \frac{120 \times 10^3}{6} = 20 \times 10^3 \text{ cps/deg.}$$

The required voltage controlled oscillator constant Kv is given by:

$$Kv = \frac{G/360}{75\alpha_0 K_d} = 4330 \text{ cps/v,}$$

where the number 75 represents the receiver frequency multiplier phase gain, α_0 is the threshold limiter suppression factor (assumed 0.088 for this calculation) and K_d is the phase detector constant (0.7 v/deg). Present techniques limit the oscillator constant to approximately 250 cps/v for an oscillator capable of sufficiently linear control over ±50 ppm. Such an oscillator has been evaluated for this purpose. The additional ×20 in dc loop gain was obtained by means of an operational amplifier. Brief tests at $2\beta_L = 20$ cps indicate that both short- and long-term stability, as well as ease of acquisition, will be adequate provided that the amplifier gain is feedback limited to that value actually required to maintain the loop static error within bounds as stated above. The results of further testing of the oscillator (without the dc amplifier in the loop) are given in Fig. 60, identified as "wide-swing" stable oscillator. As was expected, the rms phase error due to the "wide-swing" oscillator is sufficiently greater than the narrow swing or "Hi-Q" standard to dictate the use of a bandwidth $2\beta_L$ greater than 5 cps. Accepting 3 deg rms as a limit, the lowest usable bandwidth is approximately 20 cps for this combination of transmitter and receiver oscillators.

c. Rate of change of doppler frequency shift. For the same simplifying orbital assumptions as taken for Fig. 59, the worst case doppler rate has been computed as a function of altitude (Fig. 61). Superimposed is a plot of bandwidth, $2\beta_{L_0}$, as a function of doppler rate for ¼-rad tracking error, according to the relation:

$$\beta_{L_0} = \left[\frac{\alpha_0}{\alpha}\frac{9\pi}{4}\dot{f}_{max}\right]^{1/2},$$

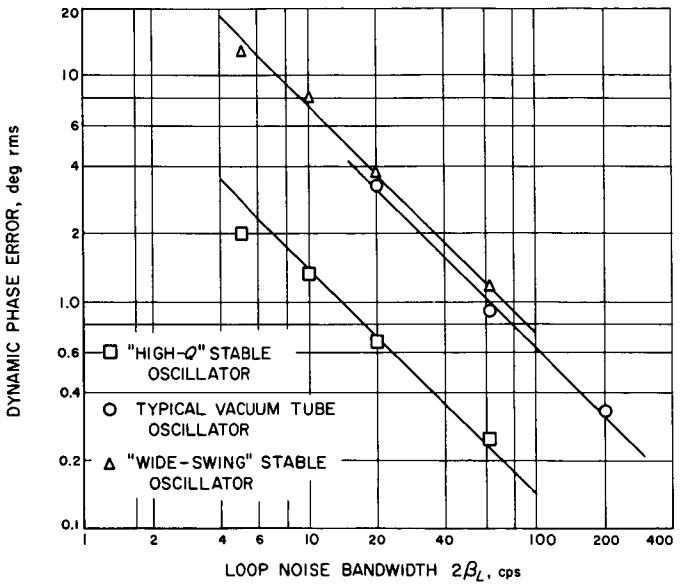

Fig. 60. Comparison of voltage controlled oscillators for short-term stability

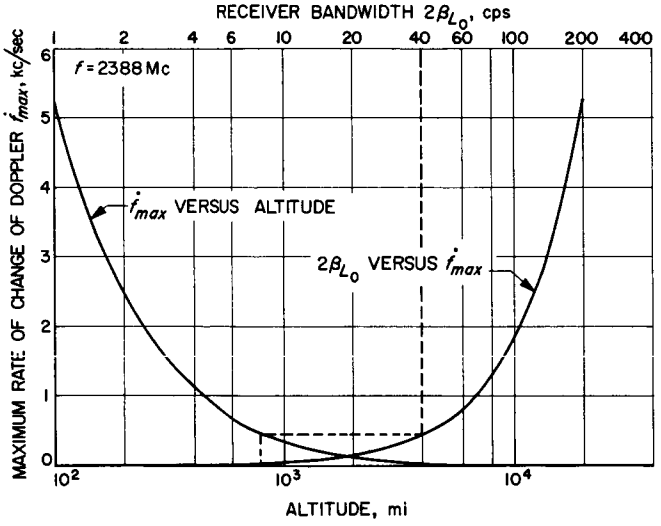

Fig. 61. Receiver bandwidth versus satellite altitude

where, as before, α_0 is the appropriate limiter suppression factor determined by β_{L_0} and the assumed predetection bandwidth of 2000 cps. The value of α is taken as unity throughout, assuming a strong signal condition at zenith.

For unaided tracking of a 250-mi altitude satellite through all passes including zenith, a bandwidth $2\beta_{L_0} = 100$ cps will be required. Since this would result in a 13-db threshold reduction as compared to the goal of $2\beta_{L_0} = 5$ cps, the receiver will require either programmed assistance in frequency (previously discussed for ultimate system) or variable bandwidth (during a satellite pass) in order to achieve full tracking of intended targets near threshold.

For the interim, consider the bandwidth requirement of an 800-mi satellite. According to Fig. 61 (dotted lines), the maximum doppler rate of 450 cps/sec requires a bandwidth $2\beta_{L_0} = 40$ cps.

d. Effect upon system of wider loop bandwidth. The above constraints result in the requirement of operating, at least temporarily, at bandwidths:

$$20 \leq 2\beta_{L_0} \leq 63 \text{ cps.}$$

The specific numbers given above have historically been used for strong signal operation and represent a threshold differential of 5 db.

Referring to a previous threshold analysis (*SPS 37-19*, Vol. III, Fig. 24—note correction: S-band threshold −164 dbm should be −170 dbm), and assuming *Echo I* as a target, the threshold degradation resulting from $2\beta_{L_0} = 63$ cps instead of 5 cps, would still allow a signal-to-noise ratio of 11 to 13 db at maximum range. Obviously, this penalty at either S- or X-band would result in considerable loss of tracking capability for 36-in. satellites.

A more immediate effect of this bandwidth widening will lie in the choice of keying rates required for transmitter and receiver time sharing of the antenna. As previously reported (*SPS 37-23*, Vol. III, p. 56), undesirable effects in poor phase integrity and degradation of the performance of the anti-sideband system now under development result when the keying rate is not high with respect to the loop bandwidth.

Prior to establishing the numerical effect upon keying rate of a given bandwidth, consider Fig. 62. Here the keying rate (and round-trip propagation time) has been plotted as a function of all conceivable target ranges. For a detailed discussion of N and the countdown number, the reader is referred to *SPS 37-15*, Vol. III, p. 42.

A band of keying rates has been defined as "partial tracking of keying sidebands" for a typical $2\beta_{L_0} = 5$ cps. The alternative restrictions:

$$10\beta_{L_0} \leq f_K \leq \frac{\beta_{L_0}}{10}$$

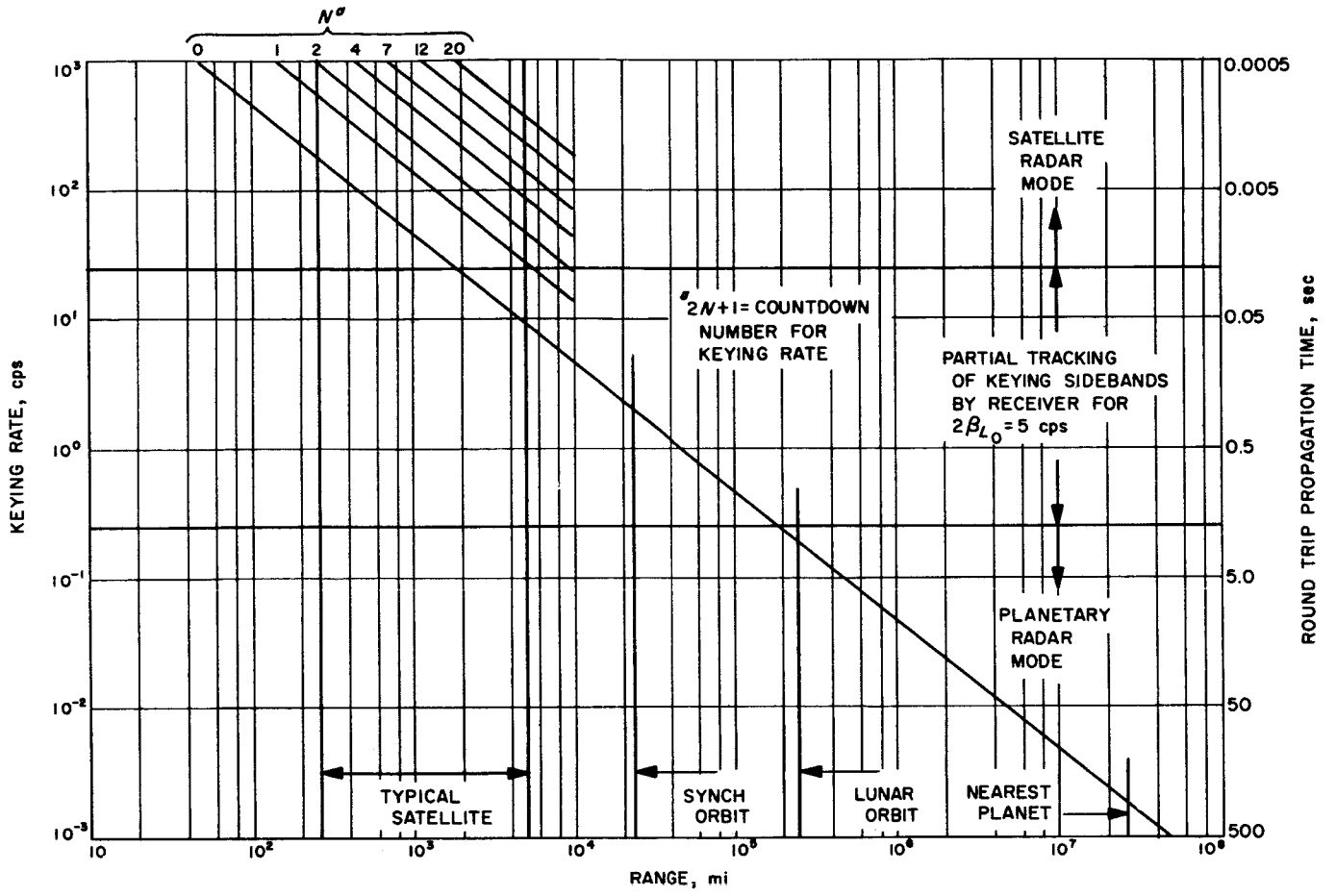

Fig. 62. Keying rates for monostatic radar

determine that the sinusoidal response of the loop (considered at threshold) to the first-order keying sideband is down at least 27 db for high keying rates *or* that the natural frequency of the loop at least equals the third-order keying sideband frequency for low keying rates. The spectrum of keying rates has thus been divided into a planetary radar mode (in which the loop must relock to each returning pulse interval), a transitional range of poor phase integrity and, finally, the satellite radar mode (in which the loop remains continuously locked to the carrier).

In passing, it is interesting to note that while the Moon may be conveniently treated in the planetary mode, particularly with slightly wider bandwidths, it may also be signaled by maintaining $2\beta_{L_0} = 5$ cps or *less* and utilizing a keying countdown rate of approximately 141 (corresponding to $N = 70$).

Returning to the problem of increased bandwidth in the case of the satellite radar, the use of $2\beta_{L_0} = 63$ cps (or even 20 cps) would have the effect of raising the "partial tracking" band of keying rates. In the worst case, values of N would range from 1 or 2 through approximately 20 for the "typical satellite," rather than the 0 to 3 previously envisioned (*SPS 37-15*, Vol. III, p. 42). Stated more simply, it appears that keying rates in the range of 300 to 900 cps may be required for satellites at ranges of 250 to 5000 mi rather than 50 to 150 cps (48 to 168 cps) previously reported. Current consideration of Mt. Clark (approx 70-mi range) as a full system ranging calibration target location would then lead to a unique application (for this configuration) of $N = 0$, but resulting in a "typical" keying rate of 670 cps for the system.

2. Monostatic Radar System Description

a. Introduction. The monostatic keyed radar program is intended to provide a model for a DSIF S-band tracking system for use during the initial passes of a spacecraft. In the course of development a number of

problems have been encountered. The solutions to these problems have influenced the system design and have been the subjects of recent reports. This article presents a detailed description of the system as it has evolved. Frequent references are made to other, usually more detailed, publications. The system discussed, with primary emphasis on ranging, is the first step toward a full tracking radar. Ultimately, the capability will be extended to include the tracking of doppler, range, and angles which are necessary for advanced development in the areas of acquisition and system control.

b. General description. The purpose of the monostatic interrupted CW radar program is to develop a precision ranging system capable of tracking passive satellites within the range of 110 km to approximately 8000 km. Resolution of the distance is better than 1.25 m. This system differs from previous models in its use of a single antenna for both transmission and reception (Refs. 3, 4). Necessarily, the transmitter and receiver must be keyed alternately so that only one is operating at a given time.

Fig. 63 illustrates the basic principle of operation. When a transmitted signal strikes an object in space, a fraction of that signal is reflected and returns to its point of origin as an echo. Since the propagation velocity of radio waves is well known, the distance to the satellite can be determined by measuring the elapsed time between transmission and reception. Unfortunately, delays within the equipment are an integral part of this elapsed time and must be discounted before an accurate range can be established (Fig. 64). The calibration of the ranging system is an important part of the project and will be the subject of a future article.

Referring to Fig. 63, the ranging system operates in the following manner. The transmitter, modulated by a ranging code, is activated for a specified amount of time. At the conclusion of the transmit period, the transmitter is turned off and the receiver "listens" for an equal time interval. The time, T, of each transmit or receive period is given by the expression:

$$T = \frac{2R}{Nc} \tag{1}$$

where

R = range to satellite in meters.

c = velocity of light in meters/sec.

N = a constant, constrained to odd integers (i.e., 1, 3, 5, $\cdots$, N).

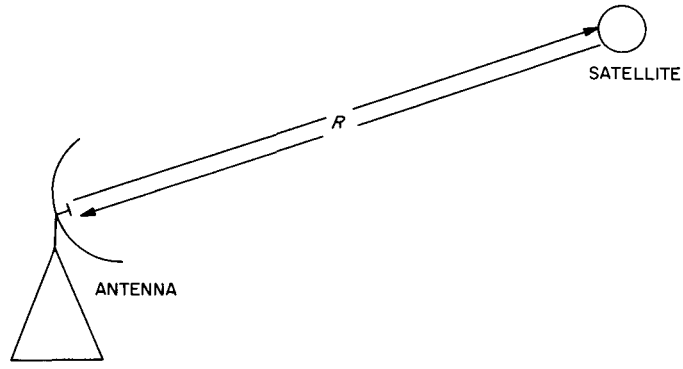

Fig. 63. Method of operation

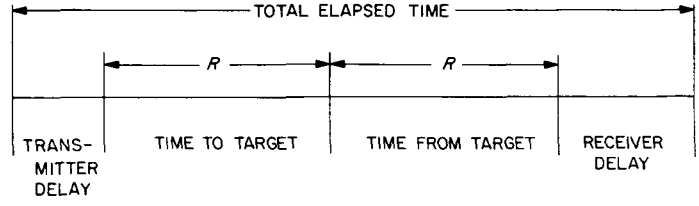

Fig. 64. Propagation delays

Conformance to the previous equation assures that there will be no overlap in the transmit and receive cycles. Restated, the system will not begin a new cycle before all of the information from the previous cycle has been received. Thus, the space separating the antenna and target will always be filled with an odd number of transmit and receive cycles. For a further discussion of keying rates and their dependency upon satellite range, refer to a description of the Mod I-D ranging system (Ref. 5). Having discussed the basic principles of operation, the remainder of this article will be devoted to the specific equipment comprising the present monostatic radar system.

A simplified block diagram of the system is shown in Fig. 65. The system is divided into four main sections: the transmitter, the antenna, the receiver, and the digital control equipment. In addition, the receiver is further subdivided into the RF loop, a ranging channel, and an anti-sideband discriminator.

Fig. 66 is a more complete block diagram which includes all of the important functions. The following discussion, which considers the detailed operation of each subsystem, is made with reference to this figure.

c. Transmitter. At the heart of the system is a rubidium vapor frequency standard and the frequency synthesizer

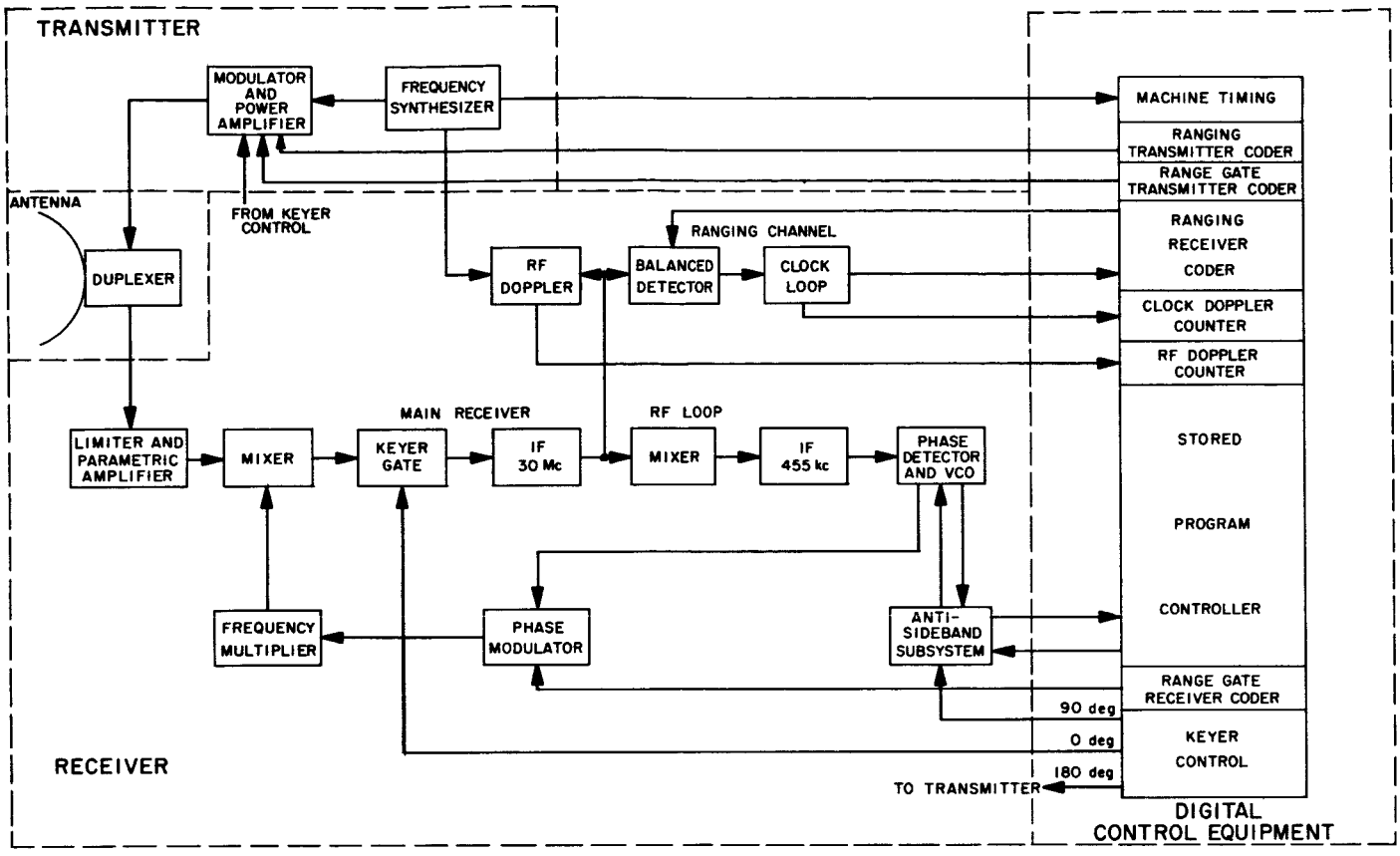

Fig. 65. Simplified block diagram of monostatic radar system

(Refs. 6, 7). The rubidium standard (or station clock) is a highly stable 1-Mc frequency source which serves as a common reference for all subsystems. By a judicious combination of the standard's harmonics, the frequency synthesizer generates all reference signals required by the transmitter and receiver.

One of the outputs from the frequency synthesizer is used to excite the transmitter. After an initial frequency multiplication, this RF signal is phase modulated by the ranging code. The ranging code, generated by the range coder, is a pseudorandom time-series of ones and zeros. The code has the interesting property of possessing a two-level autocorrelation function whose value at any displacement, τ, is given by (Refs. 8, 9)

$$C(x, x+\tau) = \frac{A-D}{A+D} \qquad (2)$$

where

C = value of the correlation at displacement τ.

A = number of agreements.

D = number of disagreements.

For clarity's sake, the range coder is shown as a part of the transmitter; however, the coder is physically located within the digital equipment (Ref. 10).

The transmitter is unconventional in that a second phase modulator has been added. This second modulator, together with its associated coder, forms a portion of the range-gating subsystem. An identical coder and phase modulator are found in the main RF loop of the receiver. Designed to be used during system calibration or for mapping large targets, the range-gate allows only that information returning within a specified time interval to be processed. For proper operation, the range-gate code must produce a phase shift in the transmitted signal of ± 90 deg, while the shift produced by the ranging code is on the order of ± 30 deg. Because of the frequency multiplication involved, the two modulators are only required to produce phase shifts of ± 6 and ± 2 deg, respectively.

The remainder of the transmitter is virtually identical to the unit used in the 1962 Venus radar experiments (Refs. 11, 12). The power amplifier employed is capable of delivering a minimum of 10 kw at S-band frequency.

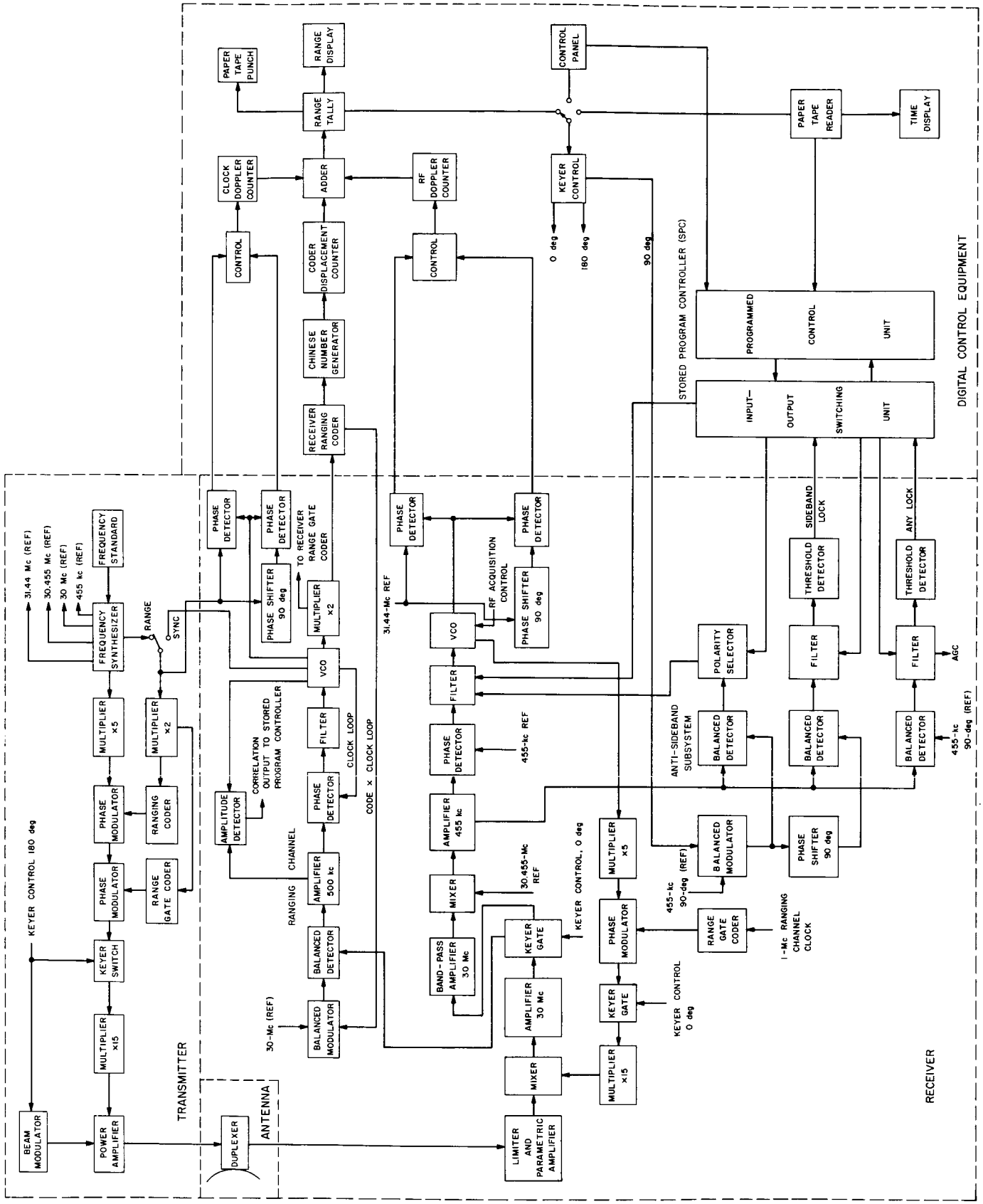

Fig. 66. Monostatic radar system block diagram

During the receive portion of the cycle, the drive to the second frequency multiplier will be interrupted by the keyer switch. Additional noise reduction can be achieved by disabling the klystron's beam modulator. Under these conditions, the transmitter-to-receiver leakage is expected to be at least 20 db below the receiver threshold.

d. Antenna. A medium size (30-ft-diameter) antenna has been installed at the Venus site of the Goldstone Tracking Station and will be used with this monostatic radar project (Ref. 13). The antenna is a fully steerable Az–El type, capable of efficient operation at either S- or X-band frequencies. Its structure is currently undergoing a series of mechanical and electrical tests which are expected to be completed by midyear 1964.

Available with the 30-ft antenna is a circularly polarized apex tracking feed (Ref. 14). Although originally designed to operate at 2115/2295 Mc, test data indicates that operation at 2388 Mc results in only a slight degradation in performance. Initial system feasibility studies call for optical positioning of the antenna; during this time the feed will function only as a duplexer. Tests suggest that receiver–transmitter isolation is in excess of 30 db. As an alternative to the apex tracking feed, a Cassegrain feed could be used. The final selection will depend upon the availability of the Cassegrain hardware.

e. Receiver.

RF section. The receiver being developed for the monostatic radar program is of the conventional double conversion, phase-locked type. Use of a low-noise parametric amplifier and post-detection filtering results in a receiver threshold of −170 dbm for S-band and −167 dbm for X-band. Following the parametric amplifier, the signal is mixed with another from the local oscillator; the resulting difference frequency of 30 Mc is amplified in the first IF amplifier. The high keying rate, possibly 1 kc in the calibration mode, requires that the IF amplifiers have a fast amplitude rise time to minimize distortion of the received signal. A keyer gate follows the first IF amplifier to prevent the integration of noise during the transmit cycle. By keying the receiver in opposition to the transmitter, an additional 3-db improvement in the signal-to-noise ratio can be realized.

Mixing the 30-Mc signal with a local reference, generated by the frequency synthesizer, results in the second IF frequency of 455 kc. Following suitable amplification, phase detection is performed using a coherent 455-kc reference. Under phase-locked conditions, the voltage appearing at the output of the phase detector represents the loop dynamic phase error and can be expressed as

$$V = K\cos\left[N\omega_k t + \theta(N) + \varepsilon\right] \tag{3}$$

where

K = a constant.

N = number of sideband to which system is locked (i.e., $\pm1, \pm3, \pm5, \cdots, \pm(2N-1)$).

ω_k = angular frequency of keying signal.

$\theta(N)$ = phase angle between VCO output and phase detector input.

ε = phase error.

For the desired carrier lock the preceding equation reduces to

$$v = K\cos\varepsilon. \tag{4}$$

After filtering, the voltage represented by the above equation serves to control the voltage controlled oscillator (VCO). Frequency multiplication of the VCO output provides a signal which can be used as a local oscillator (LO). Thus, the loop is closed, enabling the receiver to operate as a phase-locked system. Should the incoming frequency change due to a doppler shift, the loop reacts, adjusting the VCO frequency until the output from the first mixer is again 30 Mc.

Because the VCO tracks doppler frequency shifts, it must be a relatively wide-band device. Design of a wide-band VCO involves compromises in the noise performance. As a result, a programmed local oscillator is normally inserted between the VCO output and the multiplier chain. Using a precomputed ephemeris, the programmed LO adjusts its output frequency to compensate for the doppler shift. Then, since the VCO need only track second-order frequency errors, its design can be optimized. A programmed LO is a rather complete device; therefore, this subsystem has been eliminated from the initial feasibility tests. It is intended that a programmed local oscillator be included in the final system.

Range-gate. Following the first multiplier in the local oscillator is a phase modulator used for range-gate decoding. When the range-gate is desired, the local oscillator signal is phase modulated by a coder identical to the one used in the transmitter. As for the transmitter, a modulation index of ±90 deg is required. Mixing the

received signal with the local oscillator results in an IF carrier described by the relationship:

$$v = (4pn - 2n - 2p + 1) A \cos [\omega_c t + (2k - 1) \phi_m] \quad (5)$$

where

n = possible states of transmitted range-gate coder (i.e., 0 or 1).

p = possible states of receiver range-gate coder (i.e., 0 or 1).

A = maximum amplitude of IF carrier.

ω_c = angular frequency of IF carrier.

k = possible states of ranging code $\oplus$ clock (i.e., 0 or 1).

ϕ_m = modulation index of ranging code.

Note that there are four possible combinations of n and p which determine the phase of the IF carrier. A list of the possible states will be found in Table 4.

Table 4. Effect of code correlation upon IF carrier phase

Case number	Transmitted code n	Range gate receiver coder p	IF carrier phase
1	0	0	+
2	0	1	−
3	1	0	−
4	1	1	+

When the receiver coder is not correlated with the incoming signal, any of the four states can occur with equal probability. Conversely, correlation imposes the constraint that n and p be equal at all times; hence, only the first and fourth combinations are possible. Under these circumstances, the ranging channel functions as it would for a single target.

Sideband lock detector. One of the most important problems confronting the system designers resulted from the sidebands generated by the keying frequency. Significant power is present not only at the carrier frequency but also at the sideband frequencies. Difficulty often arises in locking the receiver to the carrier. If the power contained in the sidebands is sufficient, the result may be a sideband lock rather than the desired carrier lock. A sideband lock results in completely erroneous data and, hence, must be avoided.

A subsystem has been designed for the detection and rejection of sideband locks (Refs. 15, 16, 17). The unit, which is used in conjunction with the main receiver loop, consists of an "anti-sideband" circuit, a "sideband lock" detector, and an "any lock" detector. These two lock detectors are required to determine the system's status and are used in conjunction with the digital processing equipment. Operation of the anti-sideband circuit is based upon an analysis of the loop's dynamic phase error given by Eq. (3). As previously noted in Eq. (4), the expression for the phase error reduces to a dc voltage for the carrier-locked condition. Conversely, a sideband lock results in the presence of an odd keying harmonic in the loop phase error. Proper detection and inversion of this error signal in the anti-sideband circuit results in a cancellation voltage for all but the desired carrier lock. Thus, a sideband lock is broken immediately with no loss in search time.

Ranging channel. Received ranging information is extracted from the main receiver loop following the keyer gate in the first IF amplifier. Consider the modulation phasors to be found at the output of the IF amplifier. In a ranging operation these represent the modulo 2 sum of the ranging code and the clock. For a single target with optimum phasing, the two possible states are defined by

$$v = A \cos [\omega_c t + (2k - 1) \phi_m]. \quad (6)$$

The above equation can be represented by the phasor diagram in Fig. 67(a). To recover the clock frequency it is necessary to remove the code component from the composite signal. This can be done by a modulo 2 addition of the composite signal and the correlated code component. In order to accomplish the required carrier demodulation, as well as the clock separation, a code modulated reference frequency is required. Thus, a local model of the range code is used to balance modulate the 30-Mc reference. The resultant output from the balanced modulator can be expressed as

$$v = (2x - 1) \cos \omega_R t \quad (7)$$

where

ω_R = angular frequency of the reference = ω_c.

x = possible states of the ranging code (i.e., 0 or 1).

A phasor diagram for the code modulated reference is shown in Fig. 67(b).

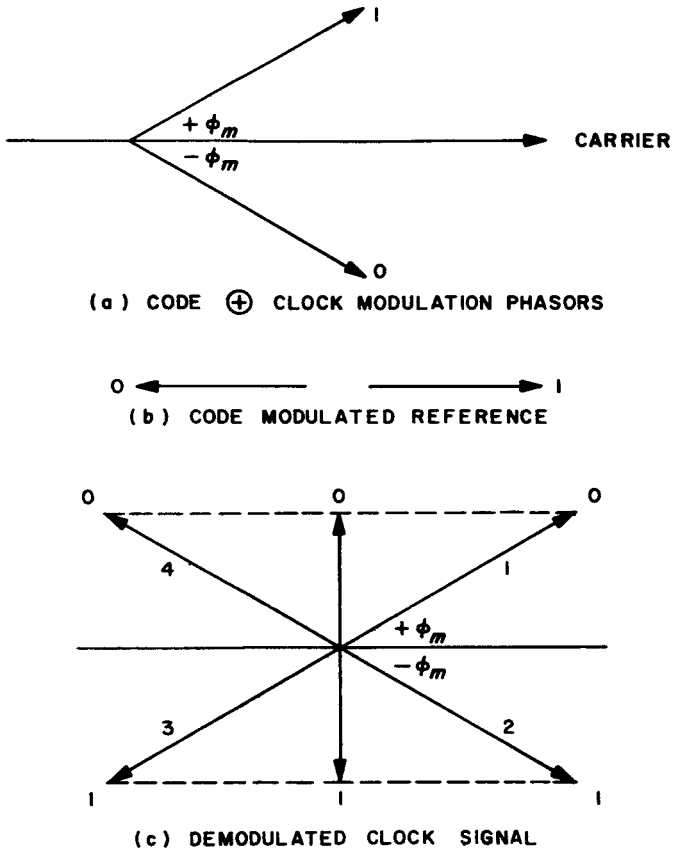

Fig 67. Ranging channel phasor diagram

The balanced detector performs a multiplicative operation with the signals represented by Eqs. (6) and (7). The operation produces both sum and difference terms in the detector. If the receiver coder is correlated with the incoming signal and the sum is removed by filtering, the remaining difference term represents the clock frequency. Thus, the balanced detector's output can be written as:

$$v = (2x - 1)\, A \cos (2k - 1)\, \phi_m. \qquad (8)$$

The phasor diagram corresponding to Eq. (8) is shown in Fig. 67(c). Each state of the clock can be produced by either of two phasors. Table 5 is a truth table identifying each of the clock phasors. The table also demonstrates the interesting property that the mod 2 sum of any two elements forms the third element in the group.

Summarizing, the ranging channel operates as two phase-locked loops. The larger, code-clock loop serves to separate the clock from the received signal, while the smaller, clock loop acts as a narrow-band filter which passes only the clock frequency.

Table 5. Clock truth table

Code ⊕ clock	Code	Clock	Clock phasor
0	0	0	4
0	1	1	2
1	0	1	3
1	1	0	1

f. Digital control equipment.

Operation. To establish the range, it is necessary to determine accurately the amount of time required for the transmitted signal to strike the target and return to the receiver. The measurement of the round-trip time can be effected as follows:

(1) The two coders are initially synchronized by placing the drive switch on the transmitter coder in the SYNC position. By connecting the two coders to a common clock, the bit rates and phases are made equivalent.

(2) Transfer of the bit pattern from one coder to the other results in an identical sequence from each coder. The receiver coder is now in phase with the transmitted signal and, were the round-trip time negligible, it would also be in phase with the received signal. Since the round-trip time is not negligible, the receiver coder must be displaced from the initial reference position to establish synchronization with the received signal.

(3) The transmitter coder drive is shifted to a stable reference by changing the switch from the SYNC position to the RANGE position. Since the two coders are no longer connected to a common clock, they are free to drift apart. The rate at which the coders move, relative to one another, is determined by the doppler frequency of the returning clock signal. A clock doppler counter within the digital control equipment monitors the displacement of the two coders relative to their initial synchronized position.

(4) The final operation is the acquisition of the received ranging code. This is accomplished by stepping the receiver coder until synchronization with the incoming code has been effected (Refs. 18, 19). The displacement between the two coders is recorded in a coder displacement counter and, when summed with the clock doppler counter, provides a measure of the range.

The ranging code is generated by combining several shorter PN sequences according to the rules of a Boolean

function (Refs. 3, 9, 20). Synthesizing the code in this manner provides an advantage in the acquisition phase. Unfortunately, a shift in the phase of one of the components is not simply related to a shift in the phase of the composite code. The ratio of the total code shift to a shift in one of the components is termed the Chinese Number. These numbers can be computed for specific codes using the "Chinese Remainder Theorem" (Ref. 21).

As noted previously, the range is the sum of the numbers accumulated in the coder displacement counter and the clock doppler counter. This result is stored in the range tally and is available to the outside world via several media (e.g., visual display, printed page, punched paper tape, etc.).

Once the code has been acquired, no further changes occur in the coder displacement counter, and increments in the range are assessed entirely by the clock doppler counter. Clock doppler is measured by comparing the received clock frequency with that which was transmitted. The comparison is made in a phase detector whose output is the clock doppler frequency. Two channels with a quadrature phase relationship can be used to improve the accuracy and establish the sense (i.e., whether the doppler is positive or negative, Ref. 4). The control unit decides the correct sense and supplies an appropriate count pulse to the clock doppler counter.

Because the clock doppler provides only a relatively coarse indication of the range, it is desirable to include a vernier to further refine the measurement (Refs. 4, 22). The RF doppler, whose frequency is substantially higher than that of the clock doppler, provides an excellent means for increasing the resolution. RF doppler measurements are made by comparing the receiver's VCO output with a reference generated in the frequency synthesizer. The techniques for measuring RF doppler are the same as those previously described for the measurement of clock doppler, and all earlier comments apply.

When it becomes desirable to tally the RF doppler, the clock doppler counter is disabled and is replaced by the RF doppler counter. The point of transition is extremely important in its effect upon the accuracy of the range measurement. Because of the noise present in the received signal, the changeover point may be ambiguous. A vernier error estimator can be used to provide the ultimate resolution of one quarter of an RF cycle (Ref. 23). This resolution corresponds to a distance of approximately 1.25 m and is the maximum accuracy with which the range can be measured.

Stored program controller. The digital equipment includes a stored program controller (SPC) as the major control element (Ref. 10). The machine resembles a general purpose computer in that commands defining sequential operations can be stored in its memory. The SPC is capable of performing arithmetic operations as well as making logical decisions. Some of the blocks shown for the sake of clarity in Fig. 66 are, in reality, synthesized by the SPC. Examples include the adder and the range tally. These are replaced, respectively, by an addition instruction and a memory cell. The SPC provides other services as well. It can be programmed to search for the target and, once located, can automatically step through the acquisition procedure. During the initial RF acquisition, the SPC controls the anti-sideband locking subsystem and provides the necessary decision making element (Ref. 15). When the antenna pointing and programmed local oscillator subsystems are added, one or more stored program controllers will be required to govern their operation.

Keyer control. A device is also required which will alternately key the transmitter and receiver. The keyer control provides this service (Refs. 5, 24, 25). The input to the keyer control is the range number. This number can be derived from the SPC keyboard or from punched paper tape for open-loop operation. For closed-loop performance, the range number is extracted directly from the range tally. In a typical ranging operation an estimated range is entered from the SPC keyboard. Once the target has been acquired, the measured range, stored in the range tally, can be employed. During a programmed search operation or during the ranging of specific types of targets, a punched paper tape input could be used.

The keyer control is also required as a reference for the operation of the sideband rejection subsystem (Refs. 15, 24). This reference, which is delayed in phase by 90 deg relative to the receiver keying signal, is used to balance modulate the RF in the anti-sideband loop. The existing keyer control provides an additional, adjustable, delay to compensate for the phase shift in the receiver IF amplifier.

The foregoing description reflects the current concept of the monostatic radar system. Greater details concerning specific subsystems, as well as a history of their evo-

lution, are available in the cited references. Work is continuing on all phases with a view toward producing an operating prototype.

3. Digitally Controlled RF Acquisition

a. Introduction. The problem of acquiring an RF carrier in the presence of strong modulation sidebands has been outlined in *SPS 37-21*, Vol. III, p. 80, and in *SPS 37-22*, Vol. III, p. 38. A strong-signal discriminator was used to distinguish the carrier from the neighboring sidebands, keeping the receiver tracking loop disabled until it had been tuned sufficiently close to the carrier to assure a correct lock.

The present article describes an extension of this attack, using the stored program controller (SPC) to generate the VCO control voltages and to perform all necessary switching functions. For brevity, the earlier experiments will be referred to as the "analog system" while the present approach will be called the "digital system."

An additional function was included in the present experiment, that of acquiring the ground-to-transponder (or "up-link") signal, so that two-way RF lock was achieved entirely under computer control. The experiments show that the techniques used will operate sucessfully for down-link signals which are 25 db or more above RF threshold and for up-link signals all the way to transponder RF threshold.

b. Equipment used. The digital experiments were performed with the L-band transmit–receive system used in transponder ranging experiments and described in *SPS 37-18*, Vol. III, p. 53. Fig. 68 shows the components with which we are concerned, primarily the RF tracking loop, the AGC system and the transmitter system.

Components added for the analog experiments include a 455-kc isolation amplifier, a level detector to derive the "Any Lock" signal, an amplitude detector and filter to derive the "No Signal" indication, and the strong-signal discriminator.

An interface adapter panel connects the rest of the system to the stored program controller, providing some signal conditioning and switching facilities. The switching is performed by small relays which are controlled by SPC output signal relays. The 5-digit numbers in Fig. 68 are the SPC addresses which pertain to the related units.

b. Flow diagram. The flow diagram for the RF acquisition program is shown in Fig. 69. The blocks will be described briefly, with a detailed treatment following.

Block A applies a voltage to the receiver VCO and sweeps until "No Signal" indicates that the signal is within the passband of the receiver. It marks an error if it reaches the end of the sweep without finding a signal.

Block B continues the sweep until the discriminator indicates that the receiver is within an assigned null-width of the carrier.

Block C enables the RF tracking loop to pull in, marking an error if the loop does not lock within a specified time.

Block D returns the control voltage to zero and disconnects from receiver VCO.

Block E checks that the down-link is properly locked, marking an error if the discriminator output is larger than a prescribed threshold.

Block F connects the control voltage to the transmitter VCO and sweeps it until a filter program recognizes a ramp voltage on the receiver static phase error.

Block G returns the control voltage to zero and disconnects from the transmitter VCO.

Block H rechecks the down-link as in Block E.

Block I tallies runs, down-link errors, and up-link errors.

Block J tests the run tally to decide whether to output results.

Block K, every N runs, punches out null control number, run count, down-link error rate, and up-link error rate.

Block L adjusts parameters for the next series of runs. Typically, null width is increased progressively until error rate reaches 100% and then recycled to the minimum value.

c. Down-link procedure. At the start of an acquisition, the receiver tracking loop is disabled and the AGC clamp level is set for the anticipated signal level. This setting is not critical; it should provide the receiver with enough gain so the signal will cause the 455-kc isolation amplifier

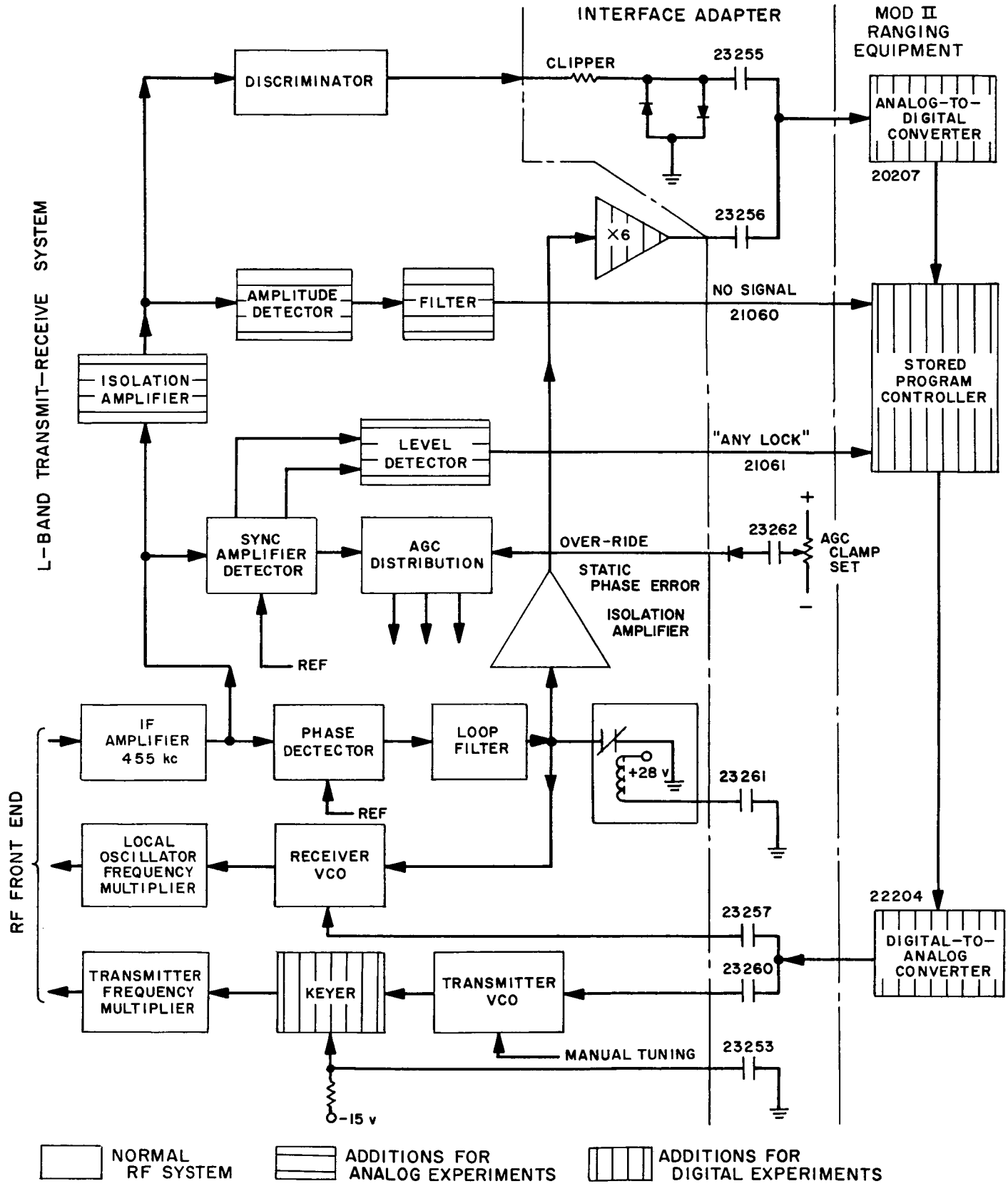

Fig. 68. RF acquisition equipment

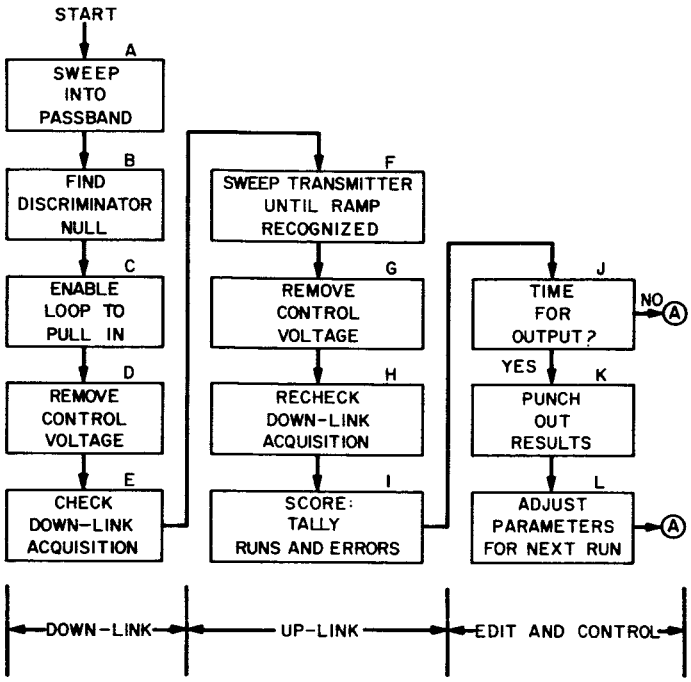

Fig. 69. Flow diagram

to limit, but it must restrict the gain so that the receiver noise will not produce an output from the No Signal detector. It was found that one setting could be used over a dynamic range of 40 to 50 db; so early in the program this was set at a value which works for the weakest signals the system will tolerate.

The digital-to-analog converter (DAC) is connected to the receiver VCO acquisition input via relay 23257, the DAC driven to the start of its range and then swept through the range, with the SPC monitoring "No Signal" for an indication that the signal is within the passband of the 455-kc IF (about 2 kc wide). During this sweep the DAC generates a staircase voltage waveform with rather coarse steps, the primary consideration being that it must not jump over the passband without seeing it. By experiment, this sweep rate was tailored so the signal would be close to the center of the passband by the time the "No Signal" time constant allowed the SPC to recognize the signal.

At this point the analog-to-digital converter (ADC) is connected to the output of the discriminator via a clipping circuit and relay 23255. The discriminator output is about 10 v/kc for a ±1-kc range. The analog experiments increased this sensitivity in the center of the range by means of an additional amplifier; in the digital experiments this was accomplished by using the ADC at its ±1-v range, disregarding (or rather limiting on) signals further than 100 cycles or so from the carrier. The clipper was added primarily to keep from overdriving the *X-Y* plotter used to monitor the operation; the Adage ADC will tolerate considerable overdriving, recovering in a few microseconds when the signal returns to the proper range.

The program now searches for the discriminator null, testing the discriminator output to see if the absolute value is small, and using the sign of the output to point the direction of the null. In the early digital experiments the DAC output was changed by one unit at a time (out of a total of 1023 units) so that the signal gradually "slid" down the discriminator curve toward the zero point. As there is a considerable amount of modulation present on the discriminator output, digital filtering of a simple sort was applied by taking the sum of a number of ADC samples each time a reading is desired. Experiments showed that 128 samples taken at 100-μsec intervals would do an adequate filtering job. Further consideration showed that it would be better to take the samples at larger intervals, on the order of two samples per cycle of modulation, since the aim is to estimate the mean voltage, not to reproduce the waveform.

While the process of stepping the DAC voltage one unit at a time is a sure one, it is somewhat slower than it needs to be, since the discriminator's linear region is on the order of 50 DAC steps wide. So the process was accelerated by stepping the DAC by an amount proportional to the discriminator output. Here again the proportionality constant was determined empirically, a value being found which causes the process to converge in about 6 iterations. The system could not be made to converge much faster without running a risk of excessive hunting and even oscillation.

When the "nulling" program has moved the signal close enough to the center of the discriminator, the sweeping is stopped and the RF loop enabled by relay 23261 which operates the coax relay to remove the ground from the output of the loop filter. The SPC monitors the "Any Lock" signal waiting for it to indicate that the AGC system is operating. When the developed AGC voltage exceeds the clamp level "Any Lock" becomes true. If, for any reason, the system does not lock up, after a reasonable time the SPC program decides that this is an error condition and in an operational situation it would return to the start of the procedure and try

again. The "reasonable time" was determined by slowly moving the DAC voltage toward the center of the passband, waiting at each step to see if the loop would try to pull in when it was enabled. It readily appeared that if it were going to pull in at all, it would do it within a set time, and this measured time with a little added for safety was included in the program as a "statute of limitations."

After the "Any Lock" signal indicates that the loop is locked, the AGC clamp is removed by resetting relay 23262. Additional time is allowed to permit the AGC loop to settle and then the program checks to see if this is a proper carrier lock or not. This is done by looking at the discriminator output with the ADC, again summing 128 samples and then checking the absolute value of that sum. Since the loop would track modulation components within the loop bandwidth, there is a lower limit to the modulation that can be used. With a 64-cps loop bandwidth, this limit would certainly be over 200 cps. So it is fairly certain that, if the receiver is locked to the carrier, the output of the discriminator will be less than, say, 1 v, which is what it would be if it were tuned 100 cps away from the carrier. Therefore, the discriminator absolute value is compared with the number corresponding to a 100-cycle error; if it is less, the acquisition was successful, while if it is more, the receiver is either unlocked or locked to a sideband. Since it has already been established that the receiver is locked, by virtue of the fact that it is developing AGC voltage, the program can identify this condition as a sideband lock and again return to the start for another try.

In this experimental program, each type of error has been tallied along with a count of runs attempted, so as to obtain quantitative information on the reliability of the procedure. In the portion of the program which attempts to drive the discriminator voltage to zero, the program has a threshold which it attempts to satisfy. Whenever the discriminator absolute value is less than this threshold number, the program accepts this as indication of a "null." By making this number progressively larger, the program can be made more easily (and hence more quickly) satisfied, but eventually a null width is reached where the loop has a chance of locking to a sideband, and if the null is made still wider, the loop will not pull in at all. Study of the relation between error rate and null width for various modulation frequencies indicate that this choice, like the AGC clamp setting, is not a critical one, and that the program can achieve a carrier lock with virtually zero error probability.

Typical signals at various points in the system are shown in Fig. 70. The horizontal scale represents frequency (actually it is the VCO control voltage) covering a range of about 7 kc. Modulation was varied from nothing in Fig. 70(a) to 500 cps in Fig. 70(b) to show the response of the discriminator as more of the sideband energy is out of the passband.

The upper trace in each section is the output of the No Signal detector. In Fig. 70(a) it represents the shape of the 455-kc IF amplifier passband.

The second trace is the discriminator output. The notch at the left-hand edge of the passband is a beat note against one of the oscillators in the discriminator. At stronger signals there is a corresponding notch at the other side as well. If the IF passband were more symmetrical and had sharper skirts these notches would disappear. If they were troublesome they could be removed by tuning the local oscillators (in the discriminator) farther away from 455 kc, or by using a sharper IF. In this program they cause no trouble because the initial entry into the passband is made with a fast sweep which skips right over the notch.

As the modulation frequency increases, bumps develop in the sides of the passband, and extra dips appear in the discriminator curve. However, since the ADC monitors the limited output of the discriminator, illustrated by the third line in each section of Fig. 70, the program will not be confused by the dips. It will be noted that the steep, essentially linear portion in the center of the limited discriminator curve covers a range of only a few hundred cycles, and in that region the direct discriminator is quite clean.

d. Up-link problem. The acquisition of the up-link, that is, the ground-to-transponder link, is of a different nature. Here, sideband lock is not a problem, inasmuch as the modulation is under control of the ground station, and can be turned off during the acquisition process. The transmitter frequency can be swept through the region of uncertainty at a rate which is guaranteed to "capture" the transponder RF tracking loop, after which the transmitter frequency is returned to the desired frequency for precision doppler measurements.

The most serious problem in the up-link acquisition is that of knowing that the capture has taken place, particularly in the case of the lunar transponders where the receiver VCO is always controlling the transmitter,

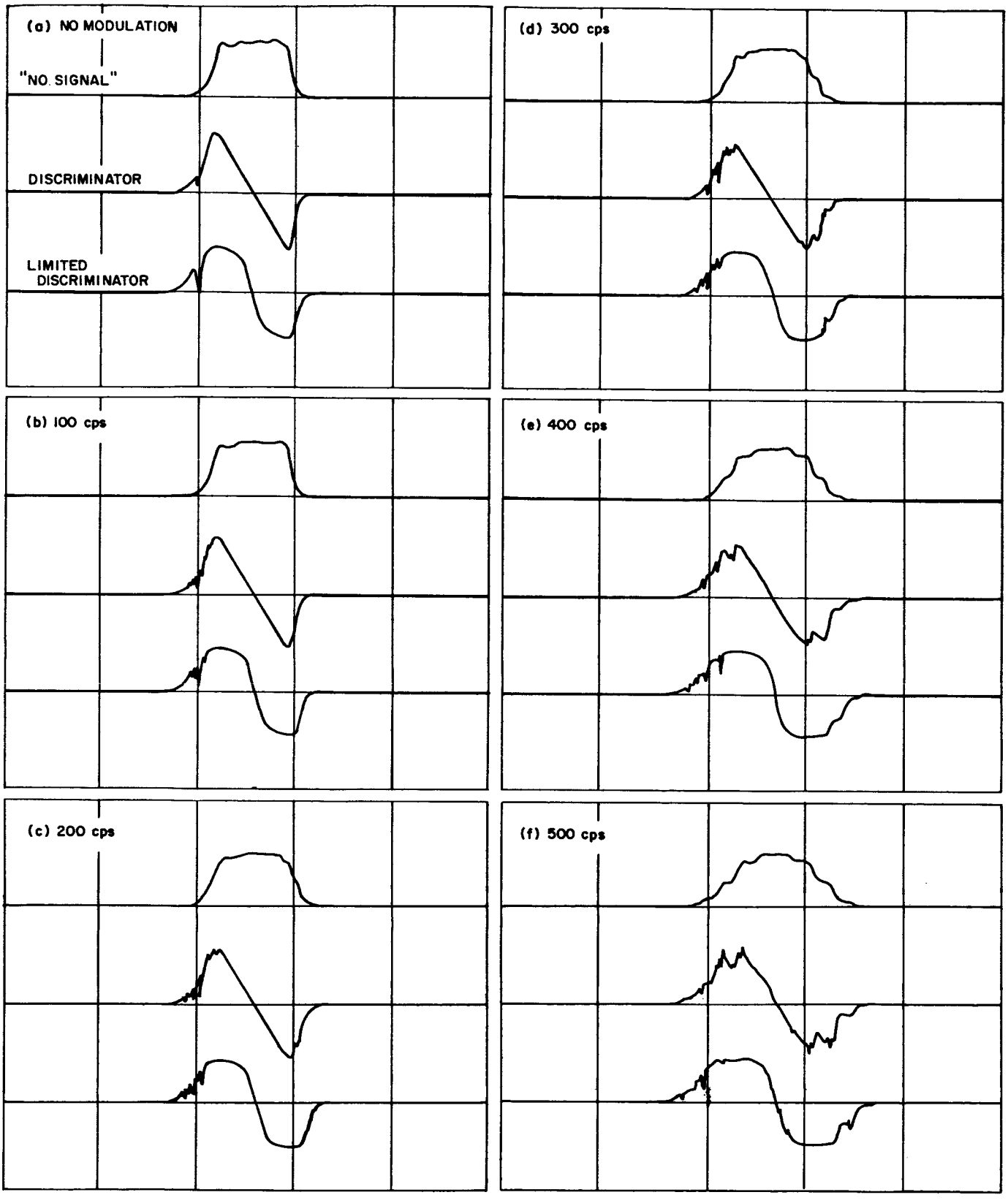

Fig. 70. Typical waveforms

whether the receiver is locked or not. Earlier transponders, which transmitted with a crystal oscillator until the receiver locked up and then switched to the VCO, would indicate the lockup by causing the ground receiver to drop out of lock and have to be reacquired.

One proposed method for transponder lock indication is to modulate the ground transmitter with a sine wave of low enough frequency that the ground receiver can track it, and to watch for the appearance of that modulation on the receiver static phase error output. This method can be programmed, but it was noted that the sweeping of the transmitter is essentially a modulation with a ramp, and it is easy to recognize the appearance of a ramp in the static phase error and use this information to verify the acquisition and terminate the sweep.

e. Up-link procedure. Up-link acquisition adds a few complications to the down-link procedure. Since we have only one DAC, which we have been using to tune the receiver but now need to tune the transmitter, we must be able to disconnect it from one place and connect it to another. Further, before we disconnect it from the receiver VCO, we must sweep it to a point where it is not supplying current to the VCO, and this sweep must be at a rate which the loop can track. Having swept it to zero, we reset relay 23257 and set 23260, connecting the DAC to the transmitter VCO. Now we can set the DAC to the beginning of its range and start to sweep, but we must go to the starting point slowly, since in this L-band system the transmitter VCO is also the master oscillator for the frequency synthesizer, and we must sweep slowly enough that we don't upset any of the reference loops.

Before we start the sweep we reset 23255 and set 23256, connecting the ADC to the output of the static phase error isolation amplifier. Since the down-link is already acquired, this SPE voltage is an indicator or transponder VCO frequency. In the absence of the up-link this will fluctuate in a random manner.

Relay 23253 controls the keyer which turns on the transmitter as the program starts sweeping by the VCO by means of the DAC. At this time the SPC starts sweeping the VCO by means of the DAC. Then the SPC starts a program which simulates a differentiator which eliminates the dc component of the SPE voltage, followed by an RC filter, followed by a threshold detector. The RC time constant rejects the slow fluctuations of the transponder VCO, but builds up to a fixed value when the transponder locks to the transmitter and its frequency starts following a ramp. When the RC output passes the threshold, the program knows that the transponder has acquired the up-link so it can terminate the sweep and return the control voltage to zero. The sweep and return must be made at a rate such that the ground receiver will not lose lock, and there is a possibility that the pull-in rate of the transponder will be too fast for the ground receiver to follow, but this only occurs with extremely strong signals, and can be eliminated either by decreasing transmitter power or by planning for reacquisition of the down-link in case of loss. This would be needed in the case of a transponder that switches oscillators, in any case.

f. Results. The experimental procedure has been to choose a modulation frequency and index (usually 3-db carrier suppression) and a loop bandwidth, and leave the system running overnight, weekends, and during weekdays when other work is not going on. The program makes ten runs with one null test number, records the results and moves to the next number. Any time the error count equals the run count, the presumption is that the maximum usable null width has been reached and the null test number is reset to its starting value. By recording the data from small groups of runs, the systematic errors and drifts in the equipment are distributed over all the null widths.

The output data tape from such a series of runs is processed by a compression routine which assembles the error counts from all runs made at each null test number and punches out a single short tape. After the addition of headings, the output of such a tape can be printed, as in Table 6 and plotted, as in Fig. 71. In these runs, up-link acquisitions were not attempted, but the nonlock errors were tallied separately from the false-lock errors. The peak in nonlock errors at a null number of 000300000 probably represents the situation which holds when the loop is enabled when it is midway between the carrier and the first sideband. It does not lock to either signal, but rather "hangs up" in a quasi-lock condition, with the loop tracking the signal but no AGC being developed. At the dynamic phase error test point, where modulation would normally be recovered, a 200-cps signal can be observed, indicating that the loop is in fact tracking something. This condition, which has been described as a "half-lock," can readily be eliminated by use of a smaller null width.

Table 6. RF acquisition tests: October 10,1963; October 14, 1963; and October 15, 1963

Null test number (octal)	Runs	False lock rate	Nonlock rate
000010000	0560	0.000	0.000
000020000	0560	0.000	0.000
000030000	0580	0.004	0.000
000040000	0580	0.002	0.000
000050000	0580	0.000	0.002
000060000	0580	0.002	0.002
000070000	0580	0.000	0.000
000100000	0580	0.002	0.003
000110000	0580	0.000	0.004
000120000	0580	0.002	0.013
000130000	0580	0.002	0.022
000140000	0560	0.004	0.023
000150000	0560	0.005	0.043
000160000	0560	0.005	0.045
000170000	0560	0.011	0.057
000200000	0560	0.018	0.086
000210000	0560	0.050	0.114
000220000	0560	0.039	0.120
000230000	0560	0.075	0.159
000240000	0560	0.104	0.205
000250000	0560	0.171	0.239
000260000	0560	0.202	0.225
000270000	0560	0.254	0.248
000300000	0560	0.300	0.275
000310000	0560	0.382	0.255
000320000	0560	0.477	0.270
000330000	0560	0.543	0.264
000340000	0560	0.666	0.252
000350000	0560	0.773	0.198
000360000	0560	0.882	0.112
000370000	0540	0.904	0.096

Modulation, 400 cps; loop bandwidth, 64 cps.

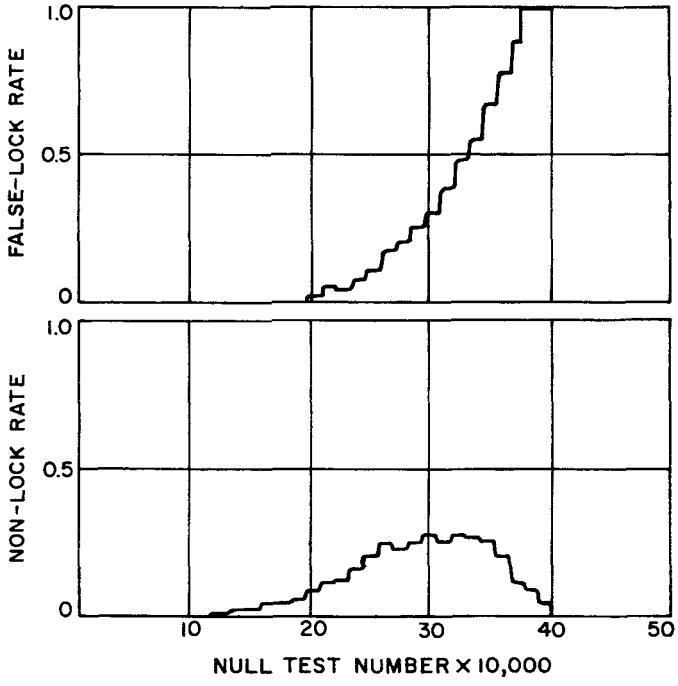

Fig. 71. RF acquisition tests: Modulation = 400 cps, loop bandwidth = 64 cps

The upper curve in Fig. 71, the false-lock rate, shows a shape that is characteristic of the majority of the tests made with this system. As the null width is increased, it becomes more likely that the loop will be enabled at such a place that it can lock to the first or second sidebands. The reason it is so characteristic is that the limited discriminator curve covers such a narrow region. If it were made wider, or if the direct discriminator were used, it would be possible to force sideband locks, and the curve would have a succession of peaks at the various sideband frequencies.

g. Recommendations. The procedure would be somewhat less complicated if two DAC units were provided: one for the receiver VCO and one for the transmitter VCO. This would eliminate the need for removing the control voltage (Blocks D and G, Fig. 69). Similarly, if the ADC is equipped with an addressable multiplexer, then it can be used to monitor the No Signal input as well as the discriminator and static phase error test points, eliminating some relay operations. A third DAC can be used to set the AGC clamp level, as it might be desirable to vary it during an operation, starting with minimum gain and systematically increasing it until a signal is acquired.

The DAC's used for tuning the receiver and transmitter should have high resolution, probably 13 binary digits. The SPC uses a 10-bit DAC, and while this would be sufficient to sweep through the frequency and doppler uncertainty ranges, it could not handle the gross doppler excursions that would be encountered in a low-flying Earth satellite, and still retain sufficient resolution to adequately acquire the carrier and reject sidebands.

A faster computer, such as the unit under study for antenna control, would permit finer control of sweep rates, a feature which is of interest when trying to reduce acquisition time to the absolute minimum. The SPC changes rates by varying the time per step of DAC voltage. This time can easily be changed in increments of

800 μsec; other increments are much more difficult to program. A core-memory computer with an 8- to 10-μsec memory cycle would have a 50-to-100-fold advantage over the SPC in this respect. However, it should be pointed out that the SPC requires less than 5 sec to acquire a signal with a 3.5-kc uncertainty, so that for many applications it might not be necessary to use the faster machine.

In summary, then, it is felt that these tests have shown that the computer which controls the pointing of an antenna can also perform the two-way RF acquisition for strong signals, with the addition of a small amount of RF equipment and signal conditioning for the computer.

E. S-Band Implementation for DSIF

1. TWM for DSIF

a. Summary. We plan to equip the DSIF with traveling wave masers (TWM's) in closed cycle refrigerators (CCR's) as part of the S-band implementation program. Six TWM systems are required; subsystem construction is being done by commercial engineering firms; system integration will be done at JPL. Past work on the TWM's has been reported in previous issues of this summary. Satisfactory progress is being made in all areas of the program. The experimental prototype TWM/CCR system was installed in the planetary radar receiver at the Venus site on September 5 and has been operating satisfactorily since then; the use of the TWM has reduced the radar receiver total system temperature to a minimum of 25°K. The field usage of the prototype will provide important operational data applicable to the DSIF installation.

b. Recent work.

System technical problems. The block diagram for the TWM subassembly is shown in Fig. 72; it may be broken into three main categories as shown by the dashed lines. The portion at the top provides for various test signals to be injected into the TWM as necessitated by the various missions. The section on the left comprises the essential parts of the TWM; the TWM monitoring network is shown on the lower right. We expect that the objective of providing a very-low-noise preamplifier subsystem with adequate means for calibrating and evaluating its performance can be met with the configuration shown.

Closed cycle refrigerator (CCR). Preliminary tests on the first CCR system indicate satisfactory performance, and A. D. Little, Inc. expects to ship this unit to JPL in October. Units 2 and 3 are expected at JPL in November and December, respectively. Difficulties in production will make it impractical to use the direct induction motor drive for the crosshead as proposed in the previous report. However, A. D. Little has recently perfected applicable heat-treating techniques, and is confident that the gear drive system in the crosshead will not be a problem.

In order to begin our training program in maintenance and operation of the CCR as soon as practical, a spare crosshead assembly will be obtained from the contractor.

TWM structure. A contract is being negotiated with a commercial engineering firm for four TWM structures. These units are basically the type originally designed at Bell Telephone Laboratories and differ from the experimental prototype JPL versions only in minor mechanical detail.

The maser will use 9 in. (two 4½-in. sections) of active structure with round fingers. Contact to the ruby for cooling is accomplished by bolting the structure together so that the flat copper surface presses against one entire surface of each ruby. The assembled maser is bolted to a flange, which in turn is bolted to the 4.3°K heat station of the refrigerator. Indium gaskets of 0.005-in. thickness will provide adequate heat transfer across these joints. The cross-sectional area of the maser structure will exceed 1 in.^{2} which will provide sufficient conduction for cooling.

Coupling adjustments, and changes in the "hat" type loading, to determine center frequency, gain, and bandpass, are made by disassembling the maser. Because the structure is bolted together this is possible.

Microwave heads. Fig. 73 shows the microwave head ready for installation in a CCR. These units will be supplied to A. D. Little for installation prior to delivery of the CCR's.

Magnet assembly. A purchase order has been written to Airborne Instruments Laboratory for four magnet assemblies. An important specification for these assemblies is that the field due to the "trim-coils" shall initially be

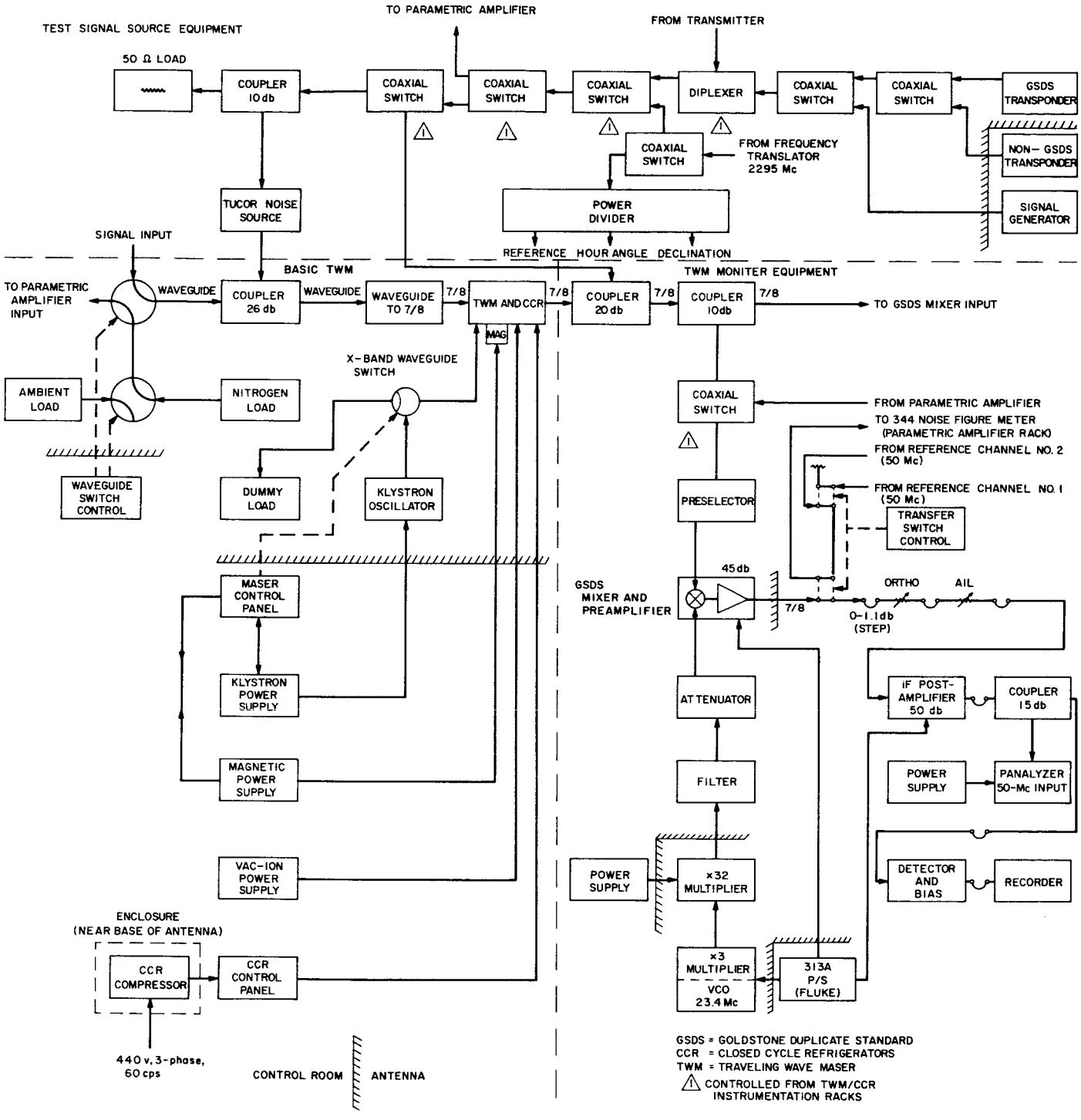

Fig. 72. Block diagram for the TWM subassembly

opposed to the permanent magnet field. (That is, the permanent magnet field will be on the high side.) This will help to ensure adequate field strength during the life of the system.

Pump assembly. A block diagram of the klystron pump package for the TWM is shown in Fig. 74. A prototype of this package is now in operation at the Venus site, and its performance is very satisfactory.

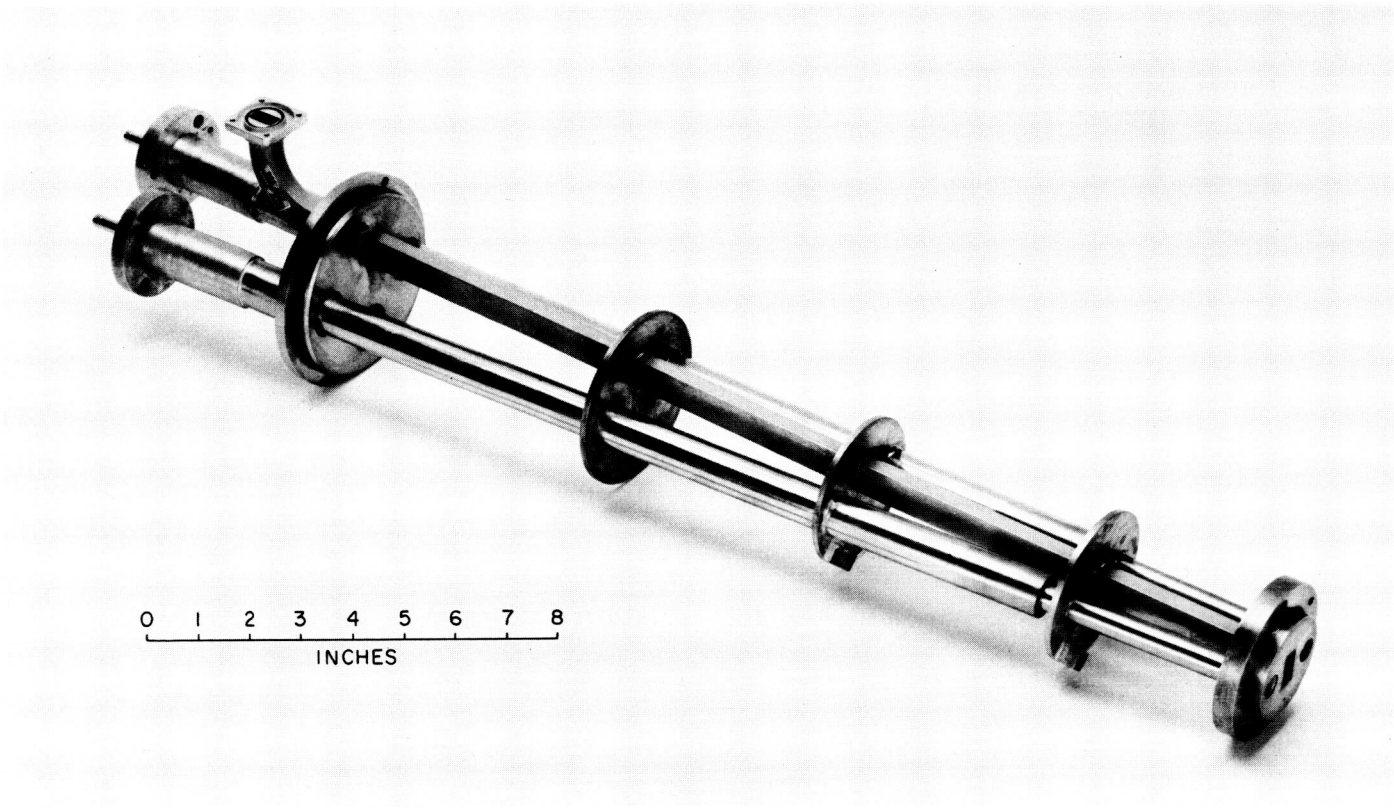

Fig. 73. Microwave head ready for installation in a CCR

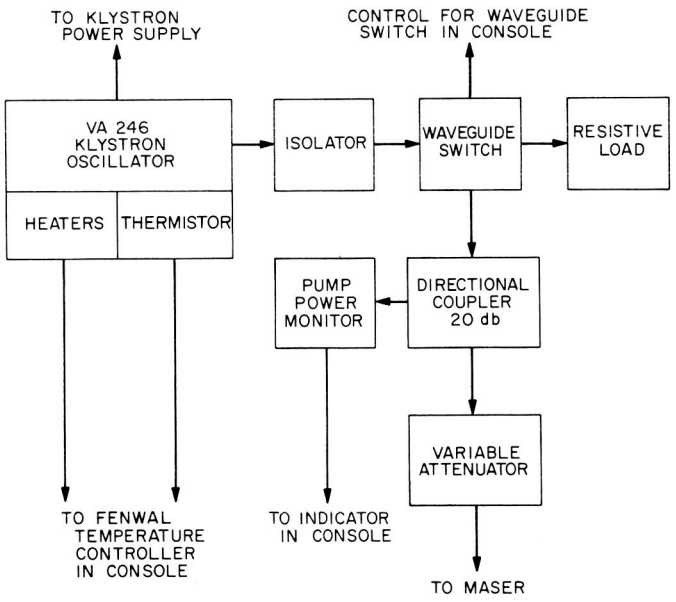

Fig. 74. Block diagram of pump assembly

Monitor receiver. Four solid-state modules will be used in the monitor receiver chain (Fig. 72); two will be identical to DSIF S-band receiver modules, and two will be modified versions of DSIF modules. These modules will be built by the engineering firm which is building the rest of the DSIF S-band receiver (Motorola, Inc.).

The modules which are identical to the DSIF units are the mixer and preamplifier and the $\times 32$ frequency multiplier; pilot models of these units are near completion. The modules which are to be modified are the oscillator–$\times 3$ combination and the 50-Mc IF amplifier. Pilot model design and construction will begin soon; these pilot models are scheduled to be available before January 1964.

For TWM subsystem testing and evaluation which is scheduled before these modules will be available, an interim monitor receiver has been assembled which uses on-hand spacecraft and commercial hardware.

The 50-Mc amplifiers, which are sensitive to power supply fluctuations and drift, will be powered by the new John Fluke 313A calibrated dc power supply. The supply was chosen because of its high stability. Preliminary evaluation has shown that the supply has a stability (relative to a second identical supply) of < 100 μv/8 hr

with a 1.5-amp load on each. Assuming a typical gain versus voltage sensitivity, for the amplifier, drift introduced by the power supply will be less than 0.001 db in 8 hr which is satisfactory.

Control rack and monitor rack. The wiring of all six sets of racks is nearly complete; the first operational set of racks will be ready for checkout in November. A few (about 5%) of the components for the racks have not been received.

Figs. 75 and 76 show the CCR control panel and the TWM control panel, respectively. These two panels are the heart of the control rack; the various control and indication functions are shown in the figures.

TWM package. Preliminary drawings have been completed and two packages are now being fabricated. The over-all dimensions of the maser package are 20 × 22 × 47.5 in.; it contains the maser and CCR, the klystron pump, and the noise source package.

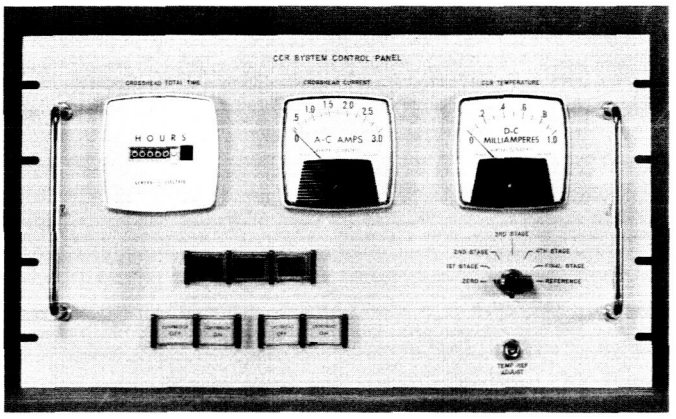

Fig. 75. CCR control panel

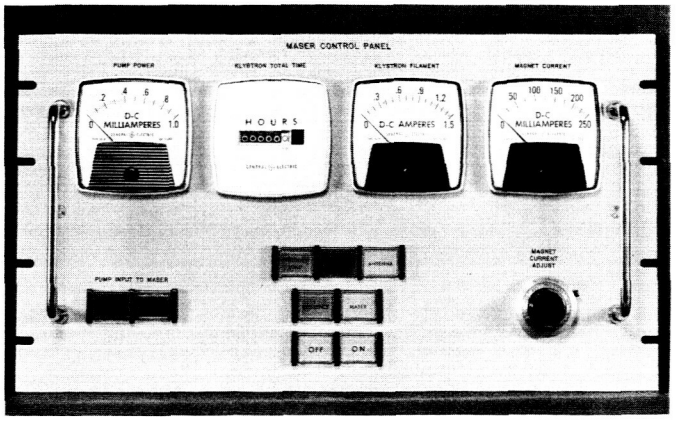

Fig. 76. TWM control panel

Prototype system field testing. The prototype TWM CCR at the Venus site accumulated 600 hr of operation in September when there were indications of malfunction in the CCR. The difficulty was diagnosed as a clogged J-T circuit due to condensation of impurities in the low-temperature gas supply line. To correct the problem the machine was shut down and the helium circuit pumped out with a vacuum pump. In addition, a charcoal trap was reactivated before restarting the machine. This is classed as a failure resulting from improper maintenance procedures. Operation is now back to normal. It is estimated that three such stops and restarts can be made per cylinder of gaseous helium; thus, this sort of occurrence would cause no serious difficulties at the overseas DSIF Stations where supply of helium is limited.

The performance data for the Venus site TWM is as follows:

Net gain, 40 db.

Bandwidth, 12 Mc.

Noise temperature, 9°K.

CCR temperature, 4.4°K.

2. Acquisition Aid for DSIF

a. Summary. An acquisition aid is being developed for the DSIF 85-ft antennas at S-band. The basic design has been completed, and all major components are on order for the prototype system.

b. Recent work. As described in *SPS 37-23*, Vol. III, pp. 60–61, an S-band acquisition aid (SAA) is being developed for the DSIF. This system is basically similar to the existing L-band system (*SPS 37-23*, Vol. III, pp. 8–11), but with certain changes to improve performance. Fig. 77 shows the SAA subsystem block diagram; the associated angle offset system is shown in Fig. 78. As can be seen in these two figures, the SAA and the 85-ft antenna have essentially independent receiver and angle tracking systems. The offset bias adjustments shown in Fig. 78 allow the operator to bring the average SAA tracking into alignment with the 85-ft antenna main beam, thereby partially eliminating the problem of the relative boresight alignment of the SAA and main antenna (SCM) systems.

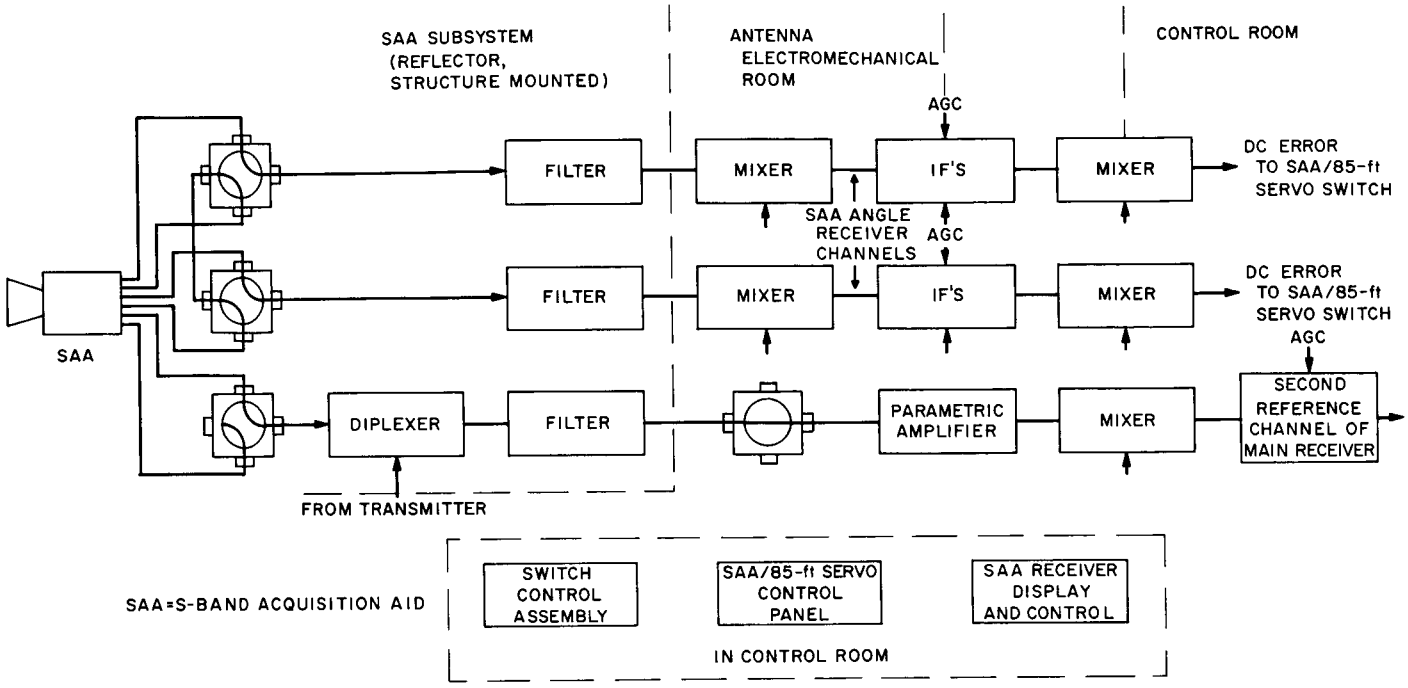

Fig. 77. SAA subsystem block diagram

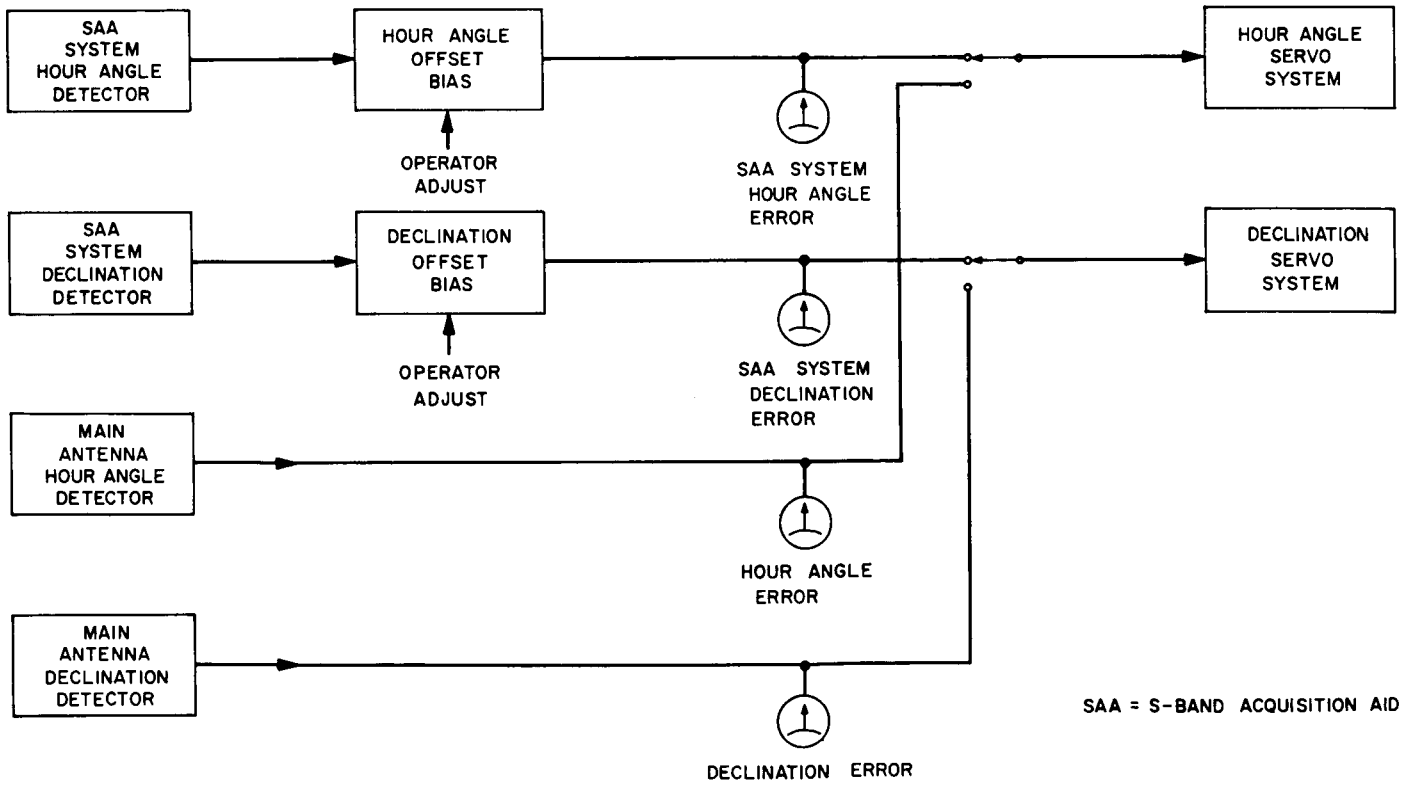

Fig. 78. Angle offset system

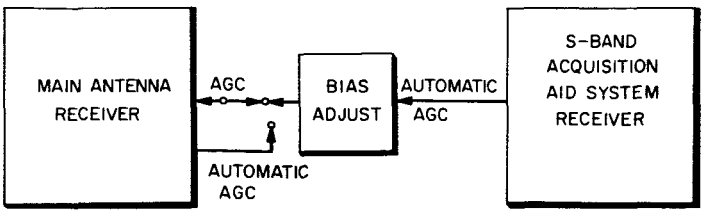

Fig. 79. AGC modification

Fig. 79 shows the system which will be utilized to prevent SCM tracking on the SCM sidelobe structure. As shown, the SAA receiver controls the AGC voltage on the SCM (main antenna) receiver until successful antenna switchover occurs. Since the *relative* received signal strength for the two antenna systems is known accurately ahead of time, the AGC bias can be set such that SCM receiver responds only when the 85-ft antenna is tracking in the main beam.

The SAA antenna is identical to the SCM feedhorn, and consists of a multimode, suppressed sidelobe, single horn monopulse unit. A contract has been awarded to the Hughes Aircraft Company, Fullerton, California, for the design, development, and construction of two units together with the antenna mounting and alignment devices. These two SAA antennas, scheduled for delivery in January 1964, will be tested with helicopter flights early in 1964 and, if proved satisfactory, will become the Johannesburg and Woomera DSIF Station operational units.

F. Telemetry System Development

1. Error Probability of Biorthogonal Telemetry System

A large number of trial runs has been performed on the biorthogonal telemetry system described in *SPS 37-18*, Vol. III, pp. 68–71. The agreement between these experimental results and the theoretical prediction for the error probability of such a system (Ref. 26) is amazingly close at all signal-to-noise ratios. In fact, the signal-to-noise ratio necessary, experimentally, to obtain a particular error probability was within 0.3 db of that predicted theoretically for all signal-to-noise ratios; in some cases the noise power was more than fifteen times as great as that of the signal.

A block diagram of the experimental system is illustrated in Fig. 80. The code-modulated subcarrier is a 4-kc square wave. It is sampled every 125 μsec, producing 8000 samples per second at the output of the analog-to-digital converter. Before sampling, a bandpass filter (BPF) with a bandwidth of 5.4 kc centered about 4 kc is used rather than a matched filter. Since the signal is centered about 4 kc (*SPS 37-18*, Vol. III), the parameter ST/N_0 is not appreciably changed by the relatively narrow BPF followed by the sampler. This is because of the well-known fact that the maximum amplitude of the fundamental frequency of a square wave is equal to the amplitude of the square wave. The samples are taken both at positive and negative maximum values of the 4-kc sinusoidal wave. It is therefore legitimate to use a BPF, and its inclusion is justified by the excellent experimental results. The filter is an electronic BPF consisting of two sections: a fourth-order Butterworth HPF and a fourth-order Butterworth LPF. They are cascaded together to make a BPF with nominal insertion loss of about 9 db.

The analog-to-digital converter, after sampling the filtered signal, every 125 μsec, converts each sample into digital form consisting of one sign and ten data digits. The maximum input level of the converter is ± 10 v. For such a high noise-to-signal ratio, it is necessary to cut off some noise power which is far from the region about which the frequency is concentrated—hence, the insertion of the BPF.

The noise channel (*SPS 37-22*, Vol. III, pp. 43–47) generates Gaussian noise which is flat over a 10-kc bandwidth. The signal and noise are added, and the noise corrupted signal is available for decoding after proper amplification. After sampling 55 times each symbol, the 55 eleven-bit data words are accumulated digitally. The correlation is performed digitally and is followed by a decision device to give the most probable 5-bit code word.

It is worthwhile noting that the data pertaining to each symbol is accumulated digitally. The digital accumulation will not itself further degradate the sampled signal. It is true, as shown in Fig. 81, that the discrete summation will not represent the exact area under the curve unless an analog integration is made along the smooth curve. However, the area under the staircase curve, as shown in Fig. 82, will be the exact area whether digital summation or analog integration is used:

$$\text{area} = \sum_{i=1}^{n} y_i \, \Delta x = \int_{x_0}^{x_n} y \, dx.$$

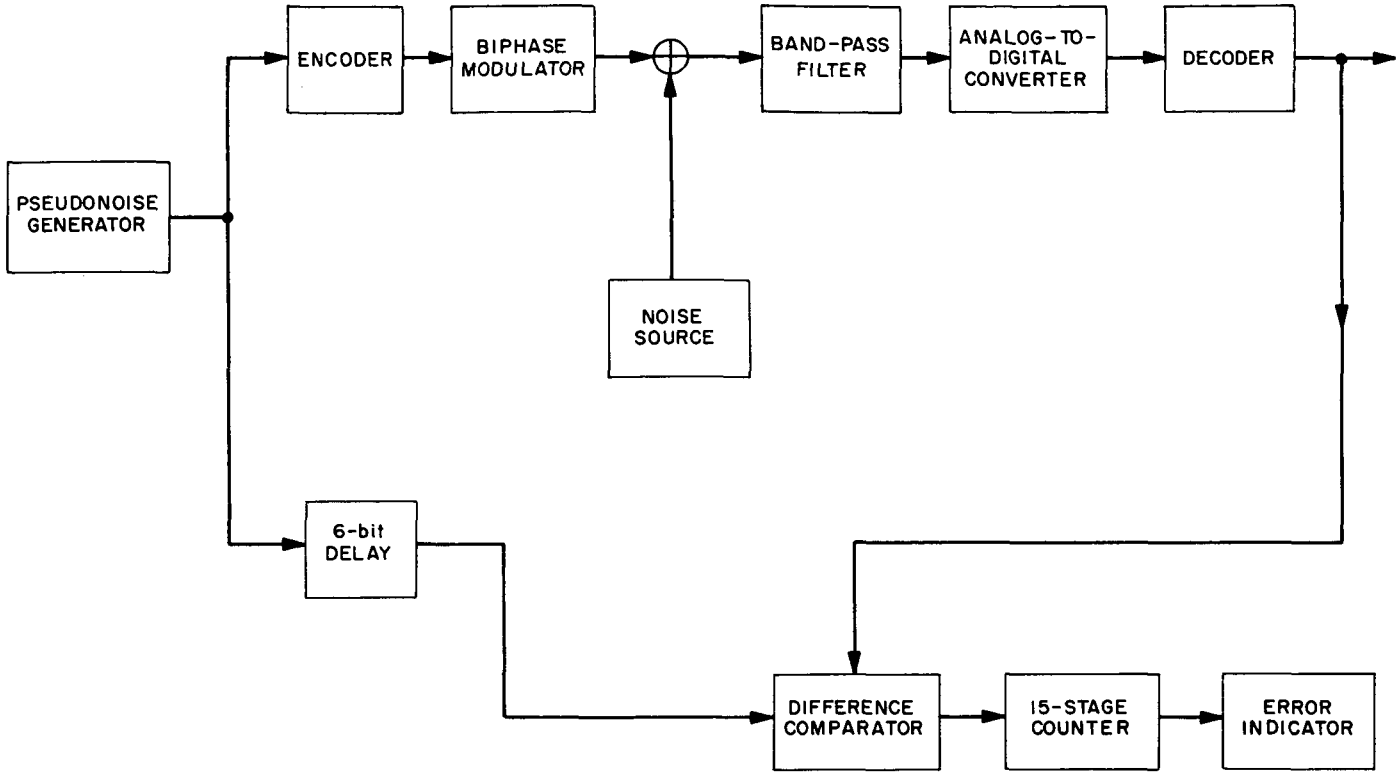

Fig. 80. Error probability measurement setup

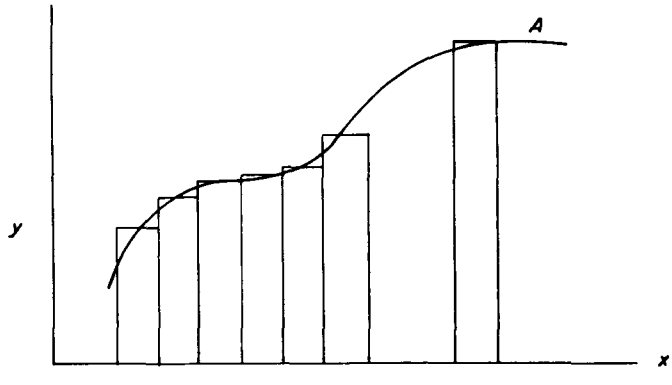

Fig. 81. Area under smooth curve

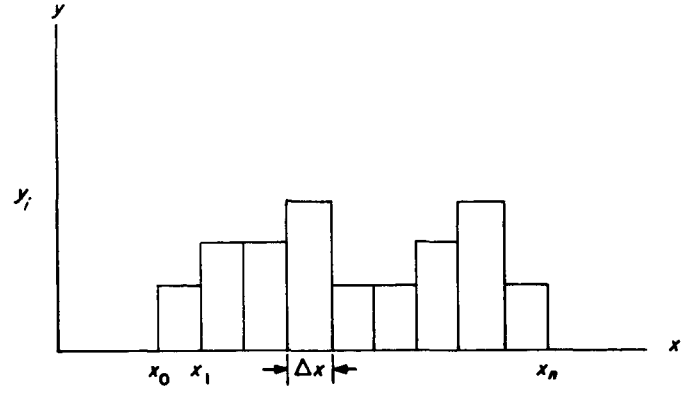

Fig. 82. Area under staircase curve

A telemetry testing unit (*RS 36-7*, Vol. I, pp. 67–69) was used to generate a length 131,071 pseudorandom (PN) sequence of about 48-min duration. Every 110,000 μsec 5 consecutive bits from this sequence are fed into the encoder in parallel, and a 16-symbol code word is generated from them. The 4-kc square wave is then biphase modulated by the code words. The symbol period is 6875 μsec, the bit time is 22,000 μsec, and the word period is 110,000 μsec.

The decoder output is bit-by-bit with a 6-bit time delay. A word-by-word output is also available. The PN sequence with 6-bit time delay is compared bit-by-bit with the decoded information in the difference compar-

ator. The disagreements are counted by a 15-stage binary counter. The total number of errors after a complete 48-min run are shown in binary form by neon indicators.

The results are summarized in Figs. 83 through 88, and the average of these results is shown in Fig. 89. Each point in Fig. 89 is the average of more than 1,000,000 bit comparisons. For the most interesting portion of the error probability region (from $P_e = 10^{-1}$ to $P_e = 10^{-5}$), the experimental results agree to within 0.3 db of the theoretical curve.

2. Development of Digital Circuit Modules

a. Summary. This report is the first in a series of reports on the development of a set of highly reliable digital circuit modules. The report reviews the historic background of such modules as used in the Communications Systems Research Section. It discusses the:

(1) Need for a change to a set of more advanced circuit modules.

(2) Criteria for their specifications.

(3) Market search.

(4) Selection and acquisition of such modules.

The parts of the digital circuit modules development project and activities which will be reported in follow-on reports are the:

(1) Dynamic evaluation of the acquired modules.

(2) Specification of auxiliary circuit modules.

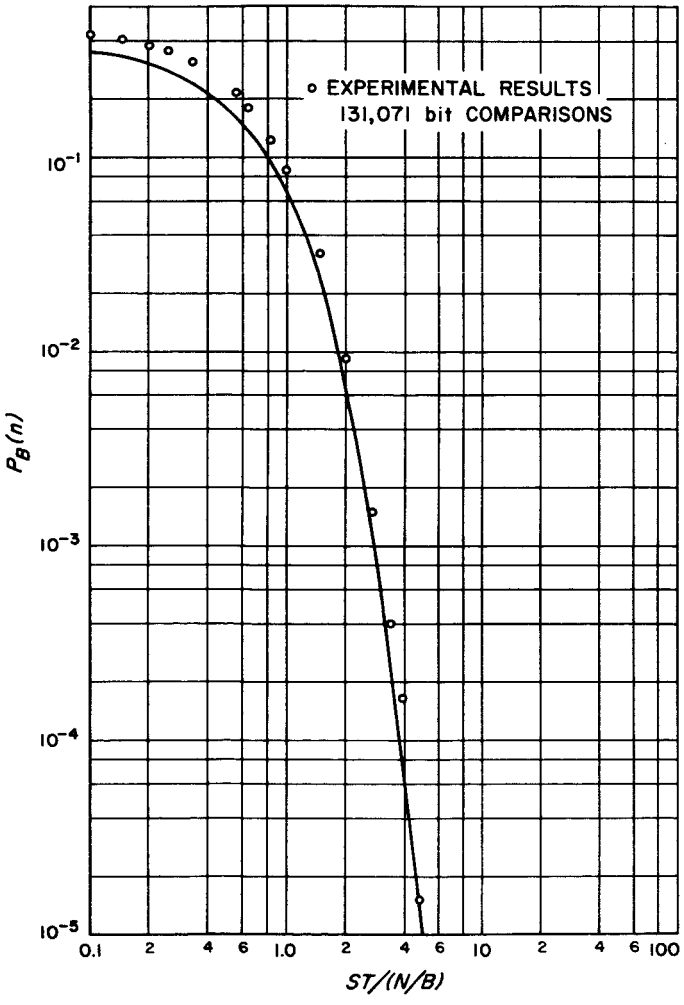

Fig. 83. Bit error probabilities — biorthogonal codes

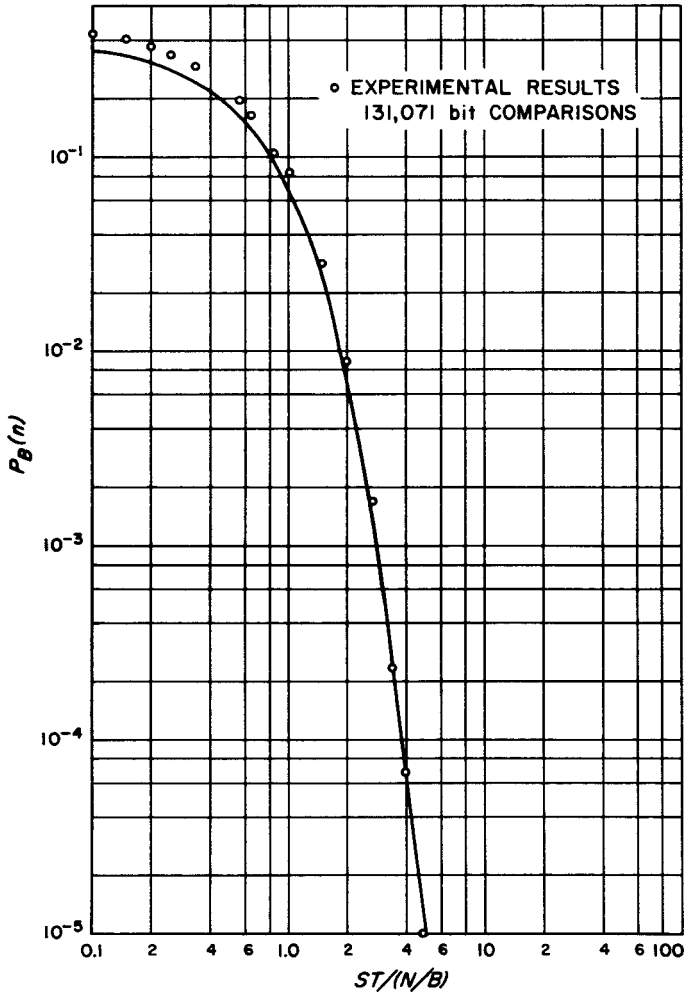

Fig. 84. Bit error probabilities — biorthogonal codes

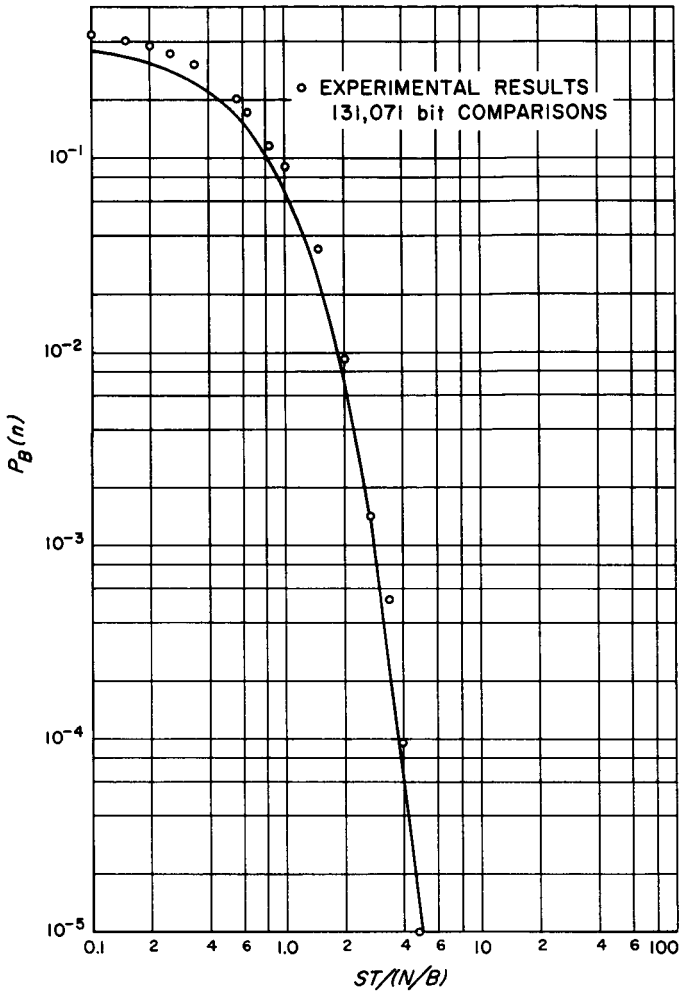

Fig. 85. Bit error probabilities — biorthogonal codes

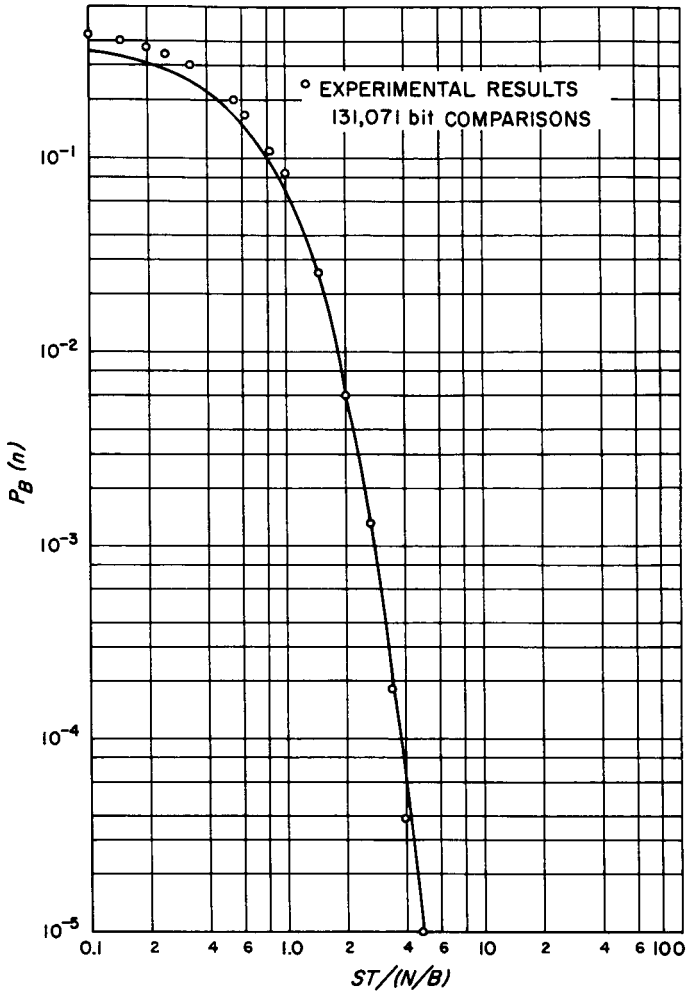

Fig. 86. Bit error probabilities — biorthogonal codes

(3) Development of design techniques using these modules.

(4) Development of a special connector.

(5) Packaging of systems using a large number of these modules.

b. Historic background. Supplementary to theoretical work in areas of digital communication such as encoding, decoding, synchronization, ranging, and information processing, the Communications Systems Research Section has for several years engaged in the design and construction of experimental systems. These systems, which for the main part have been used in ranging experiments, show, in both their design and construction, great similarities with digital computer systems.

At the start of these activities, a thorough market search and evaluation was conducted of the digital circuit building modules available for laboratory use at that time. As a result of that evaluation the Computer Control Company's T-PAC line of modules was selected. The selection was mainly based on its specific adaptability for code sequencing applications. The T-PAC line utilizes the dynamic type of logic, with recirculating delay lines used as information memories. The circuitry is then tuned to a certain frequency. Another consideration favoring the selection of the T-PAC series at that time was its unusual adaptability in the implementation of circuitry directly based on mathematical expressions. A shorthand method of documentation was developed for the T-PAC modules. The method may be described as the compiling of all information pertinent to system and logic functions, as well as to the detailed wiring, into one centralized form. The method facilitates easy documentation of changes and/or additions. Again to facilitate easy changes in an experimental system, the wiring was performed using taper pins. The systems that

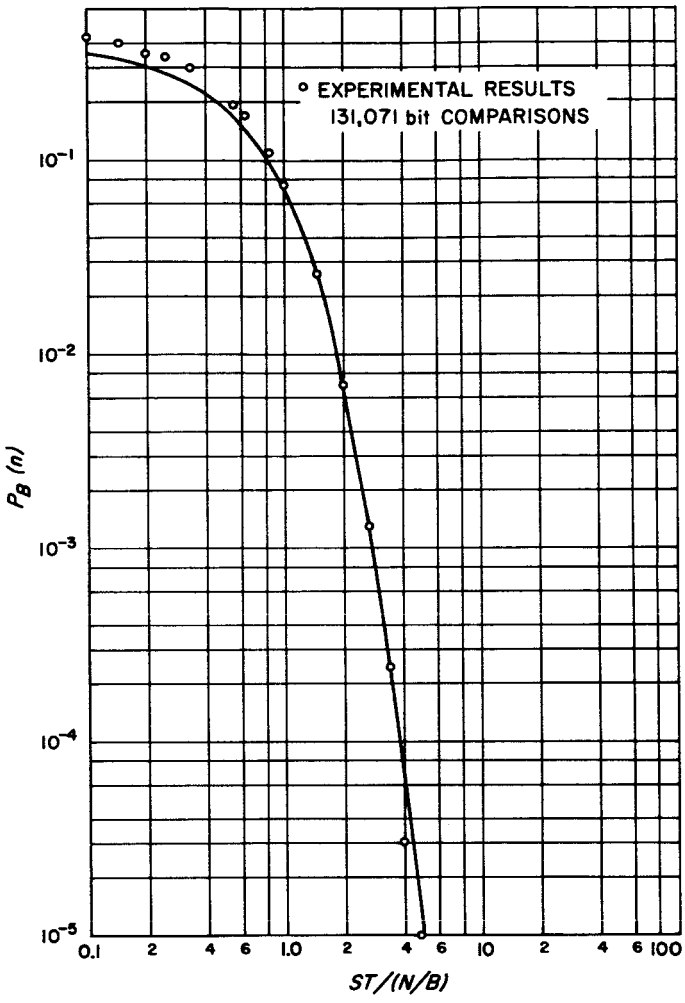

Fig. 87. Bit error probabilities — biorthogonal codes

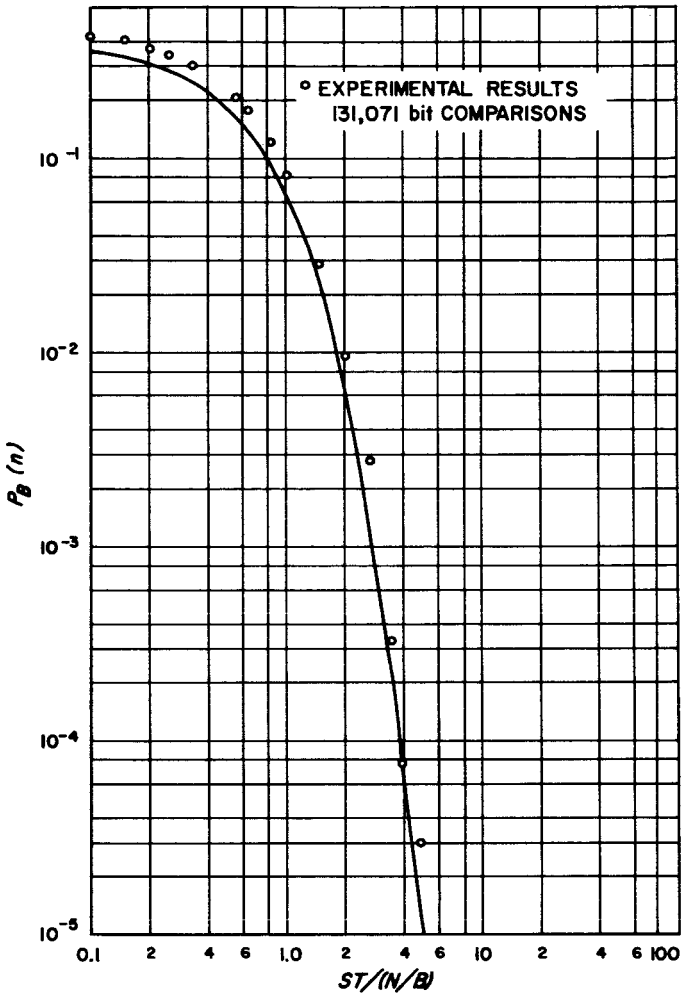

Fig. 88. Bit error probabilities — biorthogonal codes

have been built by the Section are thus truly modular in regard to electrical design, physical packaging, and documentation. They are true experimental systems and lend themselves well for rearrangement and/or expansion. Standardization of modules proved to greatly enhance the procurement of the modules. Standardization also afforded a high degree of familiarity with the circuits and their operation. It further minimized all phases of record keeping involved. It decreased the need for spare parts and tended to keep the total inventory to a minimum.

c. Reasons for initiating a change of standard digital circuit modules. The rapid development in the semiconductor field which has taken place in recent years, resulting primarily in higher speed and higher reliability components coupled with more advanced design techniques, was perhaps the most salient reason for initiating the change of modules. Other reasons for making the change of standard modules imminent were:

(1) In connecting a dynamically operated system to input–output equipments (which by their nature operate in a static mode), special and often costly measures must be taken.

(2) With a clock frequency of 1 Mc, serial operations (necessitated by virtue of the dynamic system) often required excessive time; a higher frequency line was not readily available.

(3) A need to be able to vary the clock frequency was often encountered but could not be readily executed in a system using frequency-tuned circuitry.

(4) Asynchronous operation might in some cases be preferable. In a system using tuned circuitry, the mode of operation is inherently synchronous.

(5) The single-source supplier excluded further competitive development, to the disadvantage of the Laboratory.

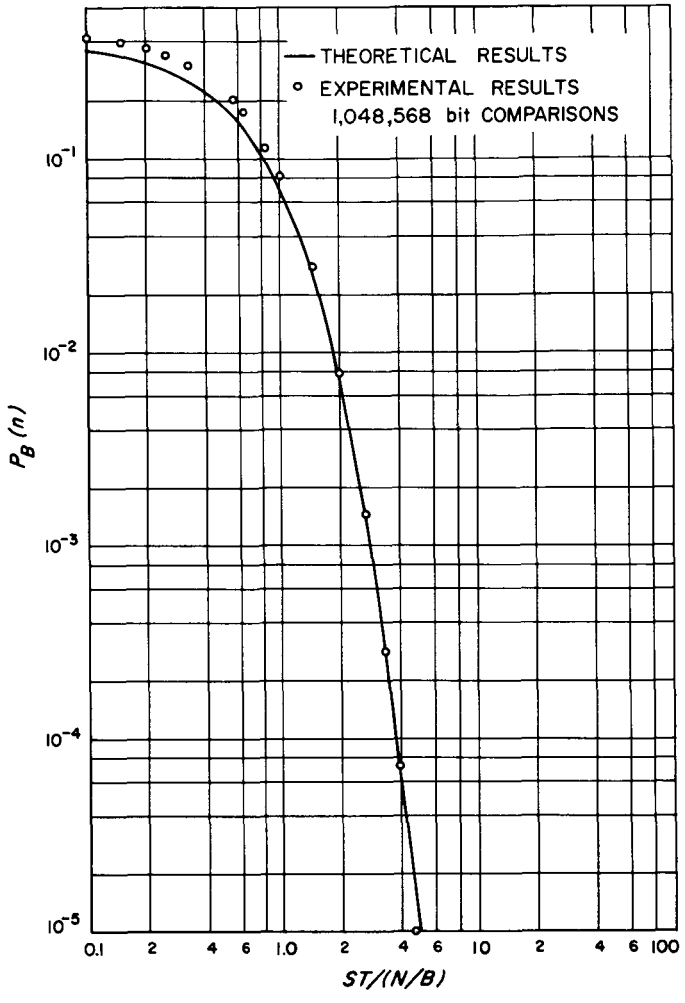

Fig. 89. Bit error probabilities — biorthogonal codes

(6) Presumably the result of diminishing demand, due to the fact that the general trend in digital circuitry and design techniques followed a different path, the modules used were more or less being discontinued by their originators.

Resulting from the viewpoints related above the desire grew to investigate presently available digital circuit modules. A study was conducted of possible alternatives to the present line of modules. The study included a thorough market search.

d. Evaluation of digital circuit modules presently offered by manufacturers. Catalogs, brochures, specification sheets, application notes, and other descriptive literature from some 80 different manufacturers of digital circuit modules were collected and studied. Furthermore, most manufacturers offered several standard lines of modules. The different lines reflected the advancement of the state-of-the-art, mainly in the speed of operation. Some manufacturers offered complementary lines in PNP germanium circuits and NPN silicon circuits. Available information was normalized on form sheets for convenient reference.

Personal visits to about ten plants in the Los Angeles area were conducted; in each case these visits included lengthy discussions with the chief engineers and circuit designers. About ten additional visits by representatives and, in some cases circuit designers, from outside the Los Angeles area were made to the Laboratory.

In summarizing the results of the survey, no standard line of tuned circuits adapted to the dynamic type of logic operation was encountered. There appeared to be little or no price difference between germanium and silicon circuits. Besides the silicon semiconductors' ability to withstand higher temperatures, the general increase in reliability displayed by the silicon semiconductors was expressed by the majority of circuit designers. This increase in reliability can be summarized as follows:

Planar-diffused silicon semiconductors. For device uniformity, producibility, and resulting low cost, the diffusion manufacturing technique is an improvement over any of the alloy processes, particularly when high speeds (narrow base widths) are anticipated. Diffused transistors also have a flat-bed collector mounting, which makes shock resistance two or three orders of magnitude higher than a post-mounted alloy transistor. The desirability of a planar diffusion technique, as opposed to a mesa construction, has been proven on *Minuteman* contracts and has received industry-wide acceptance. The planar construction insures that all junction surfaces are completely covered by silicon oxide, virtually eliminating surface leakage and junction contamination. Since junction contamination and excessive heating account for virtually all transistor failures, the use of planar passivated silicon increases reliability manyfold.

In addition to the physical reliability improvement, device performance is improved with the planar process, since the rate of surface recombinations is held constant. This constant rate provides constant Beta over the collector current range, and also reduces variations in other parameters, such as speed.

Epitaxial silicon semiconductors. In choosing a transistor for low leakage, low saturation voltages, high speed, and high breakdown voltage, conflicting requirements

are encountered. Doping to increase speed, for example, reduces breakdown voltage.

Introduction of the epitaxial process allows the collector body resistance to be made high in a thin layer near the collector-base junction, giving high breakdown voltage. Behind the thin layer is a highly doped layer which reduces effective collector resistance without reducing breakdown voltage. As a result, epitaxial silicon transistors have an order-of-magnitude less stored base charge at a given current. High speeds of operation are then possible, even in saturated logic circuits.

Finally, saturation voltages of epitaxial transistors are approximately one-fifth that of similar nonepitaxials at logic current levels, allowing better logic level discrimination and lower noise levels.

The presently concentrated development effort in the fields of silicon, as opposed to germanium, semiconductors is well known. Of special interest is that the "micrologic" elements and, of late, the "integrated circuits" mostly use the silicon planar epitaxial process.

e. Logic circuits evaluation. As to the basic type of logic operation and the type of logic circuits, the prevailing opinion gained from the survey may be expressed as follows:

A large number of techniques have been explored and are available to the digital system designer. To mention but a few opposing basic types of operations:

(1) A static type of logic may be used, as opposed to a dynamic type.

(2) A synchronous type of operation may be used, as opposed to an asynchronous type of operation.

(3) The voltage mode of circuit operation may be used, as opposed to the current mode.

In a *dynamic* system, opposed to a *static* system, the circuits are usually tuned to a fixed frequency, while a static system is operated at any frequency to the limit of the individual circuit switching times. In a dynamic system special measures must often be taken in connecting input–output equipment which are usually static by nature. The delay line memory, which is a special feature of the dynamic system is, however, easily transferable to the static system.

In *synchronous* logic all switching operations are performed in synchronism with a clock pulse. The clock pulse frequency thus determines the speed of operation. In *asynchronous* logic, no clock pulse is used to control the sequencing of operations. Therefore, the logic must be so designed that no operation can begin until all prerequisite operations have been completed. Appropriate interlocks must be built into the logic. In particular, each operation must produce a pulse at its completion to be used to trigger the following operation. The advantage of the asynchronous approach is that the speed of operation is limited only by electronic delays. The advantage of the synchronous approach is that the logic is usually simpler and easier to design, since no system interlocks are required.

The mode of operation known as *current* mode is well suited for long transmission lines, and also for very high switching speeds. The *voltage* mode of operation is more common, which is a consideration when merging with auxiliary equipment. The voltage mode produces more easily identifiable logic levels for added convenience in checkout.

The type of circuit and logic operation selected and discussed in further detail in this report is the *voltage* mode of operation of switching circuits for use in *synchronous static* systems. Occasionally, some operations may be shown to be best performed in an asynchronous mode. Also, dynamic components such as delay line memories can be employed.

In keeping with a rigorous standardization, the benefit of which is expressed in the *historical background* discussion, the selection of modules not only included circuits and their logic operation, but also the minimum number of basic types that best make up a complete set. The following four circuits were selected to constitute the basic set of modules:

(1) Decision element module.

(2) Memory element module.

(3) Logic amplifier module.

(4) Input expansion module.

The following is a detailed discussion of the design of each of these modules:

f. Decision element. Typical decision elements or gates are designed using either *diodes, or resistor–transistors,* or *diode–transistors.*

Gates using strictly diodes (and a return resistor) are inexpensive as separate units, but have a number of

practical shortcomings when used in system design. Applying a flexible variation of diode logic, the calculation of resistor values and the arrangement of buffers is a time-consuming operation. Whenever, during system checkout or system modification, a logic change is necessary, the logic arrangement has to be re-evaluated and the resistors changed. Drawings, parts lists, and all other delineations have to be revised. Attempts have been made to standardize diode gate combinations, but with little success. In fact, severe restrictions are thereby included in the combination rules. These combination rules often include insertion of a second type circuit, such as a driver and/or a level-restoring circuit.

With the recent decline in transistor prices, gates designed of either transistors only, or resistor–transistors, or diode–transistors, have become more popular. The diode gate followed by transistor emitter follower provides current buffering, but not level restoring or pulse shaping. Also, this circuit is prone to accidental damage. Gates using voltage-weighing resistors followed by a transistor switch, often referred to as a resistor *nor*-gate, are sometimes used. The resistor input provides little isolation between the inputs of a gate and the outputs of the gates driving it.

The requisites for an efficient gate in a standardized set of logic circuits are then as follows:

Besides performing a gate function, the circuit shall provide amplification, and thus normalize the output drive capability for all gates in the system. The gate shall further normalize the logic levels. That is, if any of the inputs is deteriorated as to its voltage level, the output levels shall always be those standardized for the system. Furthermore, the gate shall improve (shorten) deteriorated rise-and-fall times. The gate shall not be prone to accidental damage by, for example, shorting of any input–output terms to ground or to other signal terms.

A simple diode gate followed by a grounded-emitter saturated transistor switch constitutes an arrangement meeting the above requirements. Depending on the direction of the diodes in the diode gate, complementary logic functions can be realized. With the diode anodes common (as input to the base of an NPN silicon transistor switch), a dual-level logic function is offered by connecting two or more collectors in parallel.

The complementary circuit is that with the diodes reversed and no other gate return resistor except the transistor bias resistor. This circuit does not offer the dual-level logic feature with paralleled outputs. Though logically desirable, the occasional use of such a circuit does not warrant the addition of a second-type decision element to the system. It would, in general, complicate the combination rules, and limit higher speed operation.

The circuit selected, the schematic of which is shown in Fig. 90, produces the complement of the logic *and*-function for high-level input variables. By paralleling outputs, a second level logic function, such as the exclusive *or*-function, and the identity functions, can be obtained.

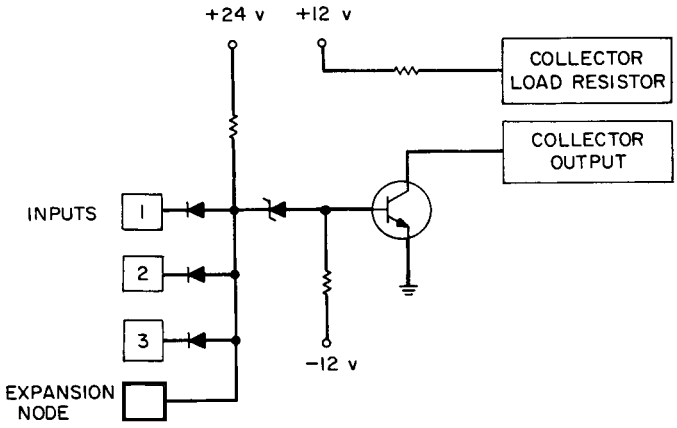

Fig. 90. Decision element (typical schematic)

As a good compromise three inputs have been provided for the standardized decision element. The diode gate node is accessible on the connector for input term expansion. The collector resistor is also accessible on the connector, so that, in parallel output combinations, the resistor[1] can be excluded. However, in single and series gate structures the resistor will be connected. In particular, the resistor will be associated with the gate in the case of "cross-connection" of two such gate elements to form a simple dc memory element.

g. Memory element. A number of different memory elements may be employed in a set of digital logic circuits. The difference often lies in the type of triggering and in the type of logic function that is performed

[1]Occasionally, unconnected resistors may be used for other purposes, such as the use of "pull up" resistors for long floating lines connecting decision elements with mechanical switches.

between the triggering gates and the basic binary element as well as in the element's drive capability.

In a highly standardized set of logic circuit modules, only one basic type of memory element need be included. Thus, the confusion of choice may be eliminated. Special types of operation may be achieved by connecting the decision elements to the basic memory element. Added drive capability may be realized by adding buffers as needed. Reset may be realized either by input gating or by adding a reset driver (a regular decision element) as required.

A common and very useful memory element is one that is equipped with one set and one reset input, each of which contains one enable term and one trigger term. The trigger term includes the capacitive storage that is required in synchronous shift register and ripple-counter applications.

By introducing a diode–resistor–capacitor network at the inputs to two cross-coupled decision elements, a general-purpose storage element of the type indicated above may be realized. Fig. 91 shows a typical schematic of such an element. The set and reset input each consists of a two-term gate function. One term is the enable or control level input and the other term is the trigger, or clock pulse input. Provided the control level is low, the memory element will set or reset, respectively, upon the occurrence of a negative level transition at the trigger input. The memory element is also capable of dc set and reset through its collectors.

h. Logic amplifier. In accordance with the philosophy of simplicity of circuits, the outputs from the decision elements and the memory elements have a moderate drive capability so as not to waste power and circuitry when not needed. When increased drive capability is required (for example, in driving clock lines and large gate matrices), decision elements may be paralleled and used as drivers, or else special logic amplifiers may be used. Such a special logic amplifier may be designed as a higher-power decision element (whose inputs then would represent more than one unit load), or else as a regular decision element followed by a second transistor-switch amplifier.

In order to maintain the unit load input and yet use relatively simple circuitry, the last-mentioned circuit has been selected. A typical schematic is shown in Fig. 92. A complementary emitter-follower output stage provides both positive and negative drive for capacitive loads. A current-limiting resistor permits grounding of the output. The logic function of the logic amplifier when using the node input is a "straight through" function. But the drive capability is then multiplied by six.

In regard to the output, the input terms to the logic amplifier provide for a logical *and*-function for high level variables (i.e., with all inputs high the output is high), or an *or*-function for low levels (with any one input low, the output will be low).

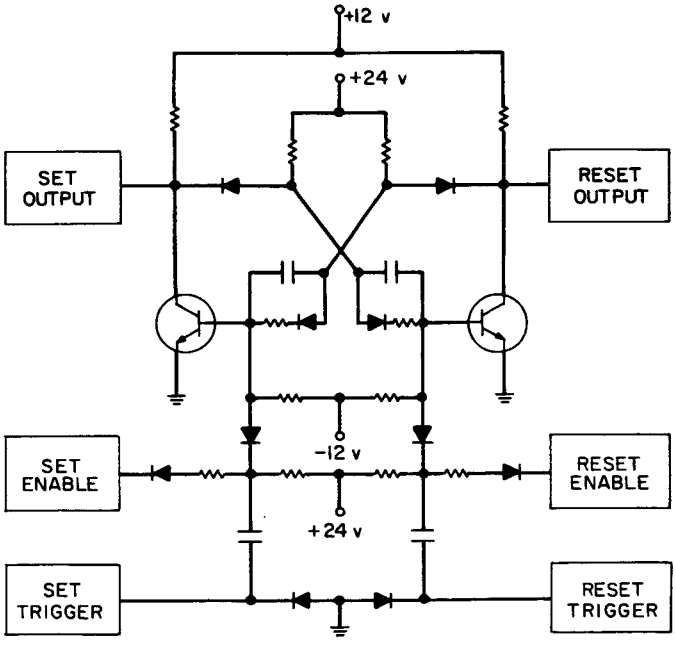

Fig. 91. Memory element (typical schematic)

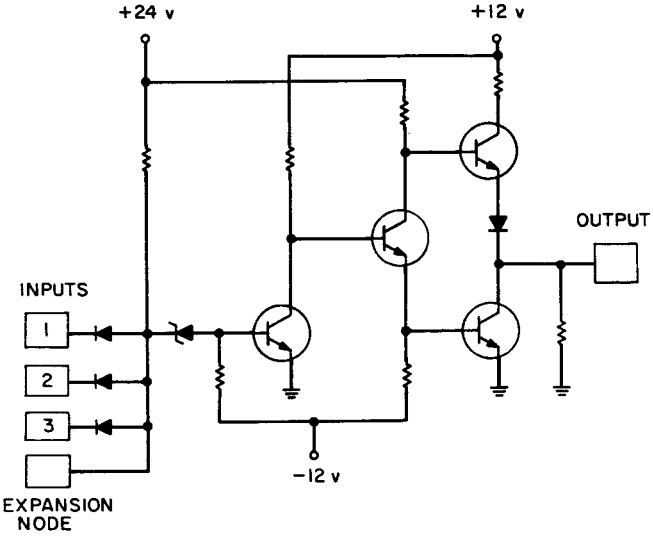

Fig. 92. Logic amplifier (typical schematic)

i. Input expansion module. In keeping with the module philosophy that all circuits on all modules shall, to the greatest possible extent, be used all the time, only three inputs have been provided to both the decision element and the logic amplifier. In considering general purpose data processing systems, if more inputs were provided, it is believed that too many circuit components would be unused. And, if a smaller number of inputs were provided, then, too often, expansions by outside connections to other units would be required. Studies of a number of general purpose data processing systems to determine the distribution of the number of inputs to the decision elements have been made. Distribution curves show peaks between three and three and one-half.

The outside circuit for expansion may, in its simplest form, consist only of diodes, either separate with both terminals available, or in clusters with either the anodes or the cathodes common.

Based on the above discussion, and also for consistency, three-input-term diode arrays, with the common anode available for connection to other input nodes, have been chosen (Fig. 93).

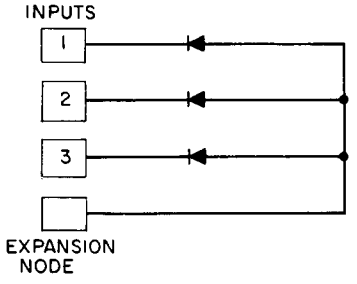

Fig. 93. Expansion element (typical schematic)

j. Power supply levels. In using the kind of circuitry that has been discussed above (the voltage mode of operation of diode gates followed by switching transistors with unclamped output), the limits within which the main power supply level may be chosen can be defined as follows: The choice of the high level is limited by:

(1) Transistor breakdown voltage.

(2) Undue power dissipation.

(3) High-speed requirement.

Since in an unclamped system, one logic level approaches the supply voltage, the choice of the lower level is to a high degree based on the circuit sensitivity to system noise. The general popularity of standard voltages being a multiple of 6 v is well recognized.

+12 v was selected as the main supply. For symmetry, the bias voltage was chosen to be −12 v. A symmetrical system will favor a mixed circuit operation: PNP germanium versus NPN silicon. A symmetrical system also favors the use of a simple ac primary-regulated power supply.

In a clamped system a clamp buss is normally required. In the present unclamped system a third voltage (+24) has instead been introduced as resistor return voltage for the diode gate. This arrangement allows a constant-current mode of operation of the gates. A considerable increase in fan in-fan out ratio for *each* element is thereby achieved.

k. Logic levels. The voltage swing should be small to allow high-speed operation and to keep the dissipation to a minimum. On the other hand, it should not be so small that power supply fluctuations, switching noise, etc., interfere with the transistor switching levels. The use of the most generally accepted logic levels will be of great advantage when mating a custom system to input–output equipment, or to subsystems from various manufacturers.

For germanium circuits, −6 v to ground appears to be the most popular logic swing. For silicon circuits, +8 to ground appears to be the most widely used and has thus been selected. The difference may be accounted for by the higher threshold voltage of the silicon semiconductors.

l. Card size and cabinet packaging. The size of the individual card is a function of the cabinet dimensions, but the exact size of the card is at best a compromise between the following two contradicting requirements:

(1) The board shall be as small as possible. An individual card for each circuit can be used. This approach provides the best "adaptation" of the hardware to the logical design. Each circuit is used in exactly the area where it is needed. The wiring becomes as short as possible; no circuits are wasted. Standard hole patterns can be provided, resulting in minimum tooling to pierce the cards. Maximum production rate of each card type can be achieved, resulting in lower unit cost. Unit cost for rejection is then also low. Conversely, the ratio between circuit cost and the cost of connector and other

mounting hardware and wiring is unfavorable due to higher system labor costs.

(2) The board shall be as large as possible. This approach may provide simpler packaging, allowing more circuits per card. The number of power supply connections per circuit is reduced, and the number of signal interconnections between modules is smaller. The ratio between circuit cost and cost of connector and other mounting hardware and wiring is more favorable, resulting in lower system labor cost. Conversely, poor "adaptation" of the hardware to the logical design exists, since a certain percentage of circuits available on the large card will not be needed. Unit cost for rejects is higher. A definite disadvantage is the resulting distant location of needed circuits. Long wire connections result in reliability and performance risks. In seeking high system package density, a larger card poses severe limitation.

Therefore, in trying to reach a compromise between these contradicting requirements, the adaptation of circuits to the logic design and the ratio between circuit cost and the cost of the connector and other mounting hardware and wiring are chosen as the deciding parameters.

In regard to instrument packages or large systems, it is desirable that the circuit cards, including mounting frame and connector, fit into the RETMA standard 5¼-in. front panel height. This should be possible in either orientation of the card (horizontal or vertical insertion) to allow high packaging density in the system.

Rather than locating many circuits on a single card, in which arrangement some lead lengths may be very long or circuits wasted, a few circuits are placed on each card. This arrangement yields shorter and more equal lead lengths.

In regard to the number of circuit elements per card, the best compromise between adaptation, circuit/connector ratio, production cost, and reject or spare-part cost appeared to be as follows: four decision elements per module, four simple memory elements per module, and four logic amplifiers per module.

Rather than a deep and narrow card, a wide and shallow card where the circuits are close (and all identical circuits *equally* close) to the connector has been chosen. Only like circuits are packaged on any single card.

In using standard components and open circuit mounting (for possible replacement down to the component level) a card size of 4.75 by 3.18 in. has been chosen.

It may be interesting to note that an exhaustive study and investigation of the optimum card size conducted by the Lawrence Radiation Laboratory, University of California (Ref. 27) resulted in a card size 4.25 by 4 in. Other card sizes adopted by manufacturers of circuit modules are: 4.3 by 3.8 in., 4.5 by 4 in., 5.2 by 4.3 in., 5.5 by 2.75 in.

m. Connector. Though the early transistors in most cases were connected through plug-in sockets, transistors are now soldered as are any other components. This results in increased reliability. Printed circuit cards have usually been plug-in units. However, with the simplicity of circuitry and with the high reliability components used in the selected digital modules, there appears to be little need to unplug modules, once installed. In system checkout and in trouble-shooting, it is our experience that the plug-in feature generates more malfunctions than the feature can locate and cure. Examples of these malfunctions are: the wrong insertion of a card, the insertion of a wrong card, soiled contact area, bent pins or springs, etc.

Circuits on one card often are wired to operate in the same general functions of a system. Trouble-shooting by disconnecting cards, therefore, often eliminates circuits necessary for continued operation and further trouble-shooting. The disconnection of a *single* term, however, has been found an efficient method in trouble-shooting. From long experience in system checkout using circuitry similar to those proposed, it was found that the circuits very seldom or never failed.

Based on the above discussion, a *semi-permanent* mounting technique for the modules is being considered. It is to consist of a right-angle printed circuit connector block permanently secured to the module. Connections between modules are to be performed by point-to-point taper pin wiring.

If in the proposed system a single circuit failure *should* occur, the entire card would not be replaced; the faulty circuit will instead be rewired into a spare circuit available on a card in close proximity. In general, it may be commented that in checkout and trouble-shooting, logical reasoning is more powerful than the brute force method of unplugging cards.

Should it in some instances be necessary to make a modification to a standard card, the particular card would, by its semi-permanent mounting, be less likely to be mixed up with the unmodified cards. The quick loan of cards from operating systems without notification is also well known. The proposed semi-permanent mounting of cards would lessen these annoying incidents.

Although little evidence can be filed against the reliability of modern printed circuit connectors, the proposed method of eliminating the connector will no doubt increase the over-all system reliability. In fact, the most reliable weapons system in the country today (the *Minuteman* system) was a technique very similar to that proposed in its ground support and control systems.

n. Number of pins. 95% of all desirable circuit configurations on the suggested standard card size require between 20 and 30 contacts for power and signal connections. A smaller number of pins presents a limitation for most circuit packages. A larger number of pins, however, presents reliability and production problems because the distance between contacts becomes too small. Such smaller distances require higher production tolerances. The failure rate due to contact interconnections increases, and damages occur due to contact shorting in system checkout. The circuitry to be mounted on the adopted cards requires a 24 input–output connection and four power connections.

It may be interesting to note that a thorough study of the optimum size of printed circuit connectors conducted by an industrial concern (Ref. 28) resulted in 31 pins being chosen for ground environment data-processing equipment. But this study concerned plug-in connectors. An integrated connector block should have as *small* a number of connections as commensurate with the circuitry, which in turn has been chosen for its simplicity and the small number of input-output per circuit.

The order in which the input–output terms are terminated on the connector is, in view of system documentation, of the utmost importance. Selected terminations are shown in Figs. 94 through 97.

o. System grounding practices relative to the circuit modules. System noise due to ground loops is only too well known by the experienced system designer. Often the ground loops or their effect on noise defy theoretical analysis. Handling of the system grounding, therefore,

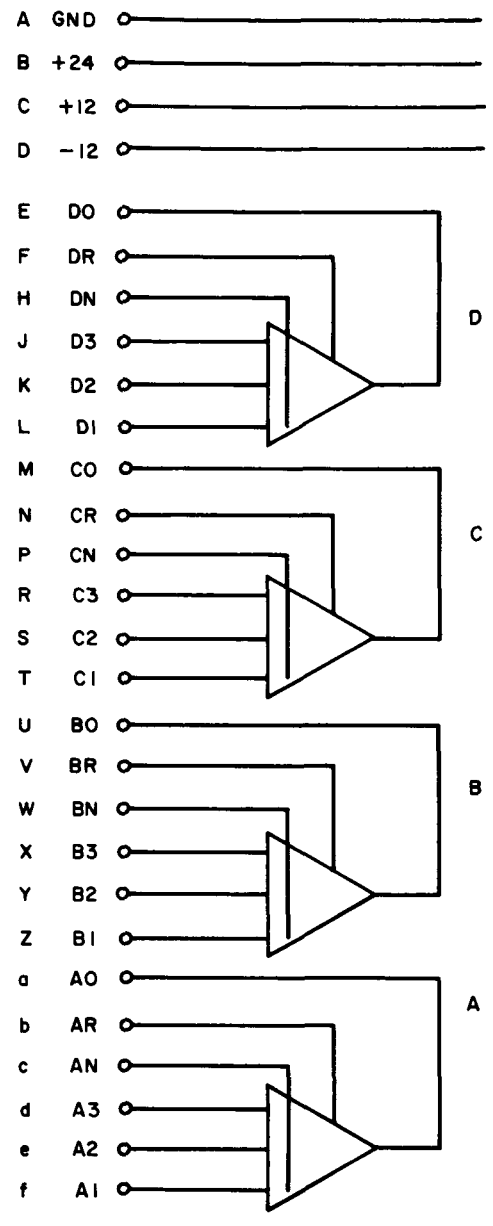

Fig. 94. Connector terminations for the decision element module (symbolic diagram)

becomes subject to each individual's experience. For this reason, the detail circuit modules afford the following variation in grounding technique:

A maximum ground of copper plating has been left on each card. Since pin No. 1 is the ground connection, the ground plate in many cases forms an outer frame terminating in the area of the last pin. Two inserts, one in each end of the connector, will be used to secure the terminal block to the card, and to relieve the strain on the connector pin-to-card connection. These inserts are also used

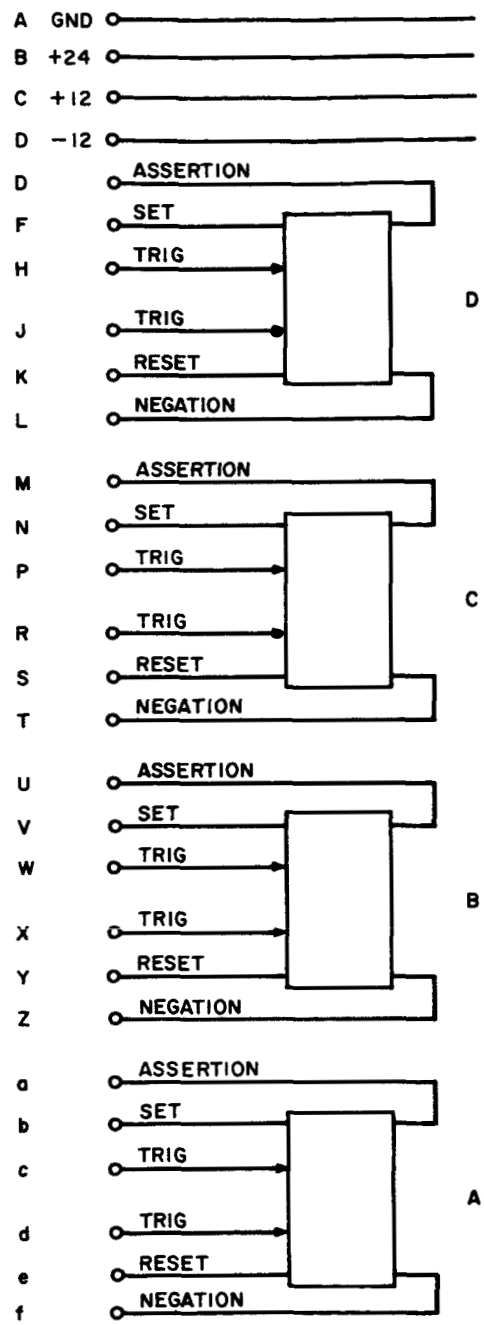

Fig. 95. Connector terminations for the memory element module (symbolic diagram)

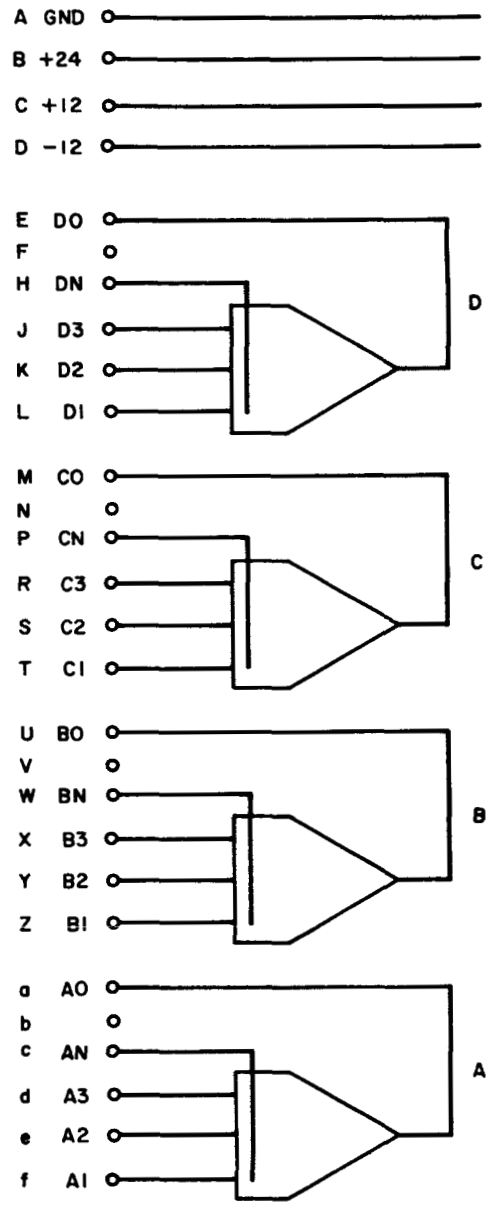

Fig. 96. Connector terminations for the logic amplifier module (symbolic diagram)

to secure the card terminal block assembly to the system rack. And the inserts are also connected to pads on the cards. These pads are located in close proximity to the enlarged ground plate, and can be connected to this plate by jumpers.

With the described arrangement on the card, ground may be handled as an isolated term. Cards can, in respect to their grounding, be arranged in suitable groups, or the ground of all cards can be connected to the system frame or part thereof. The card ground can be connected to the frame via one or both inserts.

p. Acquiring of selected modules. Digital circuit modules having all the properties described above were not directly available from any manufacturer. For example, the semiconductor components, the logic functions, power supply levels, and logic levels required were available from several manufacturers, but not in the combination

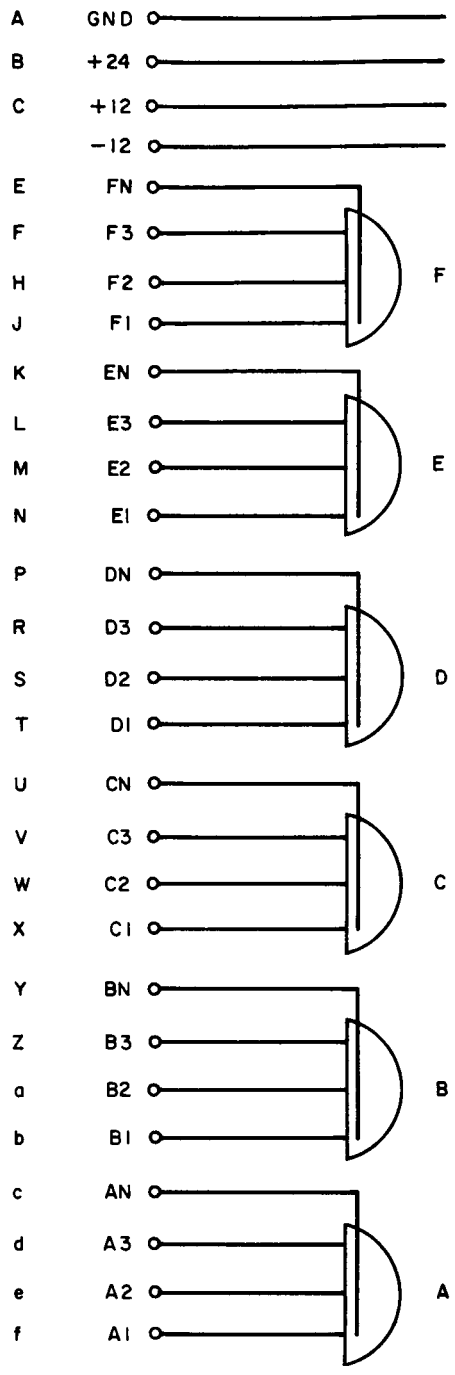

Fig. 97. Connector terminations for the input expansion module (symbolic diagram)

described. The circuit study, the market survey, and especially the plant visits further suggested that the experience and capabilities in digital design presently available in the Communications Systems Research Section were in many cases equal to, and in some cases surpassed that of, the companies visited. Also the quantity of digital circuit modules needed within the Section could well exceed the total production of many of the companies visited. Based on these considerations, it seemed more appropriate that specifications be formulated within the Section, and that request for proposal be initiated. Therefore, envelope specifications[2] reflecting the features above were written. Circuit modules displaying this combination of features is to be considered a significant advance, not only in the circuitry itself, but also in the fact that the availability of such circuit modules will provide an advancement in the system design technique. In regard to the specifications, the detailed circuit design was not provided; however, the design was indicated. The supply voltages, the logic swing, and the load unit were specified, in addition to the mechanical configuration.

It was felt that by initiating envelope specifications that reflected advanced design techniques, demanding the use of silicon semiconductors components packaged in a specified configuration, and by requesting bids from the most experienced manufacturers, nearly identical modules would then be obtainable from several sources. Eight companies were invited to submit technical and cost proposals for the design and development of a basic set of digital circuit modules in accordance with the above mentioned specifications. In order to verify the performance data stated by the manufacturers, a detailed static circuit analysis was conducted by a consultant on contract with the Laboratory.

In order to avoid a future single-source situation, two suppliers were selected. One supplier who was selected absorbed the development cost. The other supplier was reimbursed for the development cost, thus placing the rights to the design with JPL.

Pilot orders, including ten decision elements, ten memory elements, five logic amplifiers, and two input expanders, were awarded to Decisional Control, Costa Mesa, California, and Control Logic, Natick, Massachusetts.

Because the development of the desired connector block has lagged behind the development of the modules, the pilot order modules were obtained as conventional plug-in cards. It is intended that production modules would use the integral connector block being developed. The pilot orders have been received. Figs. 98 through 101

[2]*"Specifications for the Design and Development of Digital Circuit Modules for Use in General Purpose Data Processing Systems,"* JPL Specification GM2-15053-DSN-B, August 2, 1963.

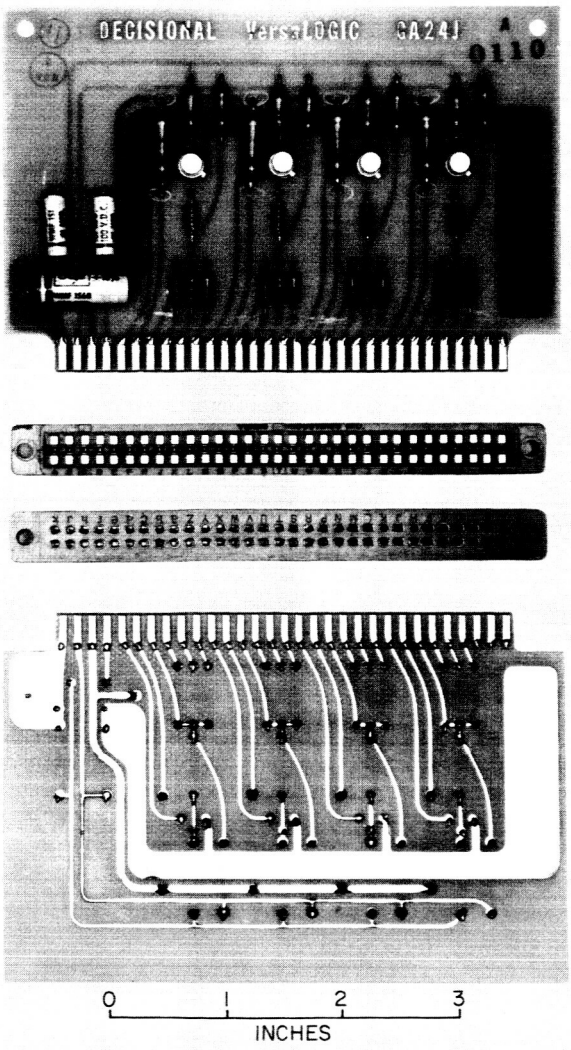

Fig. 98. Decision element module

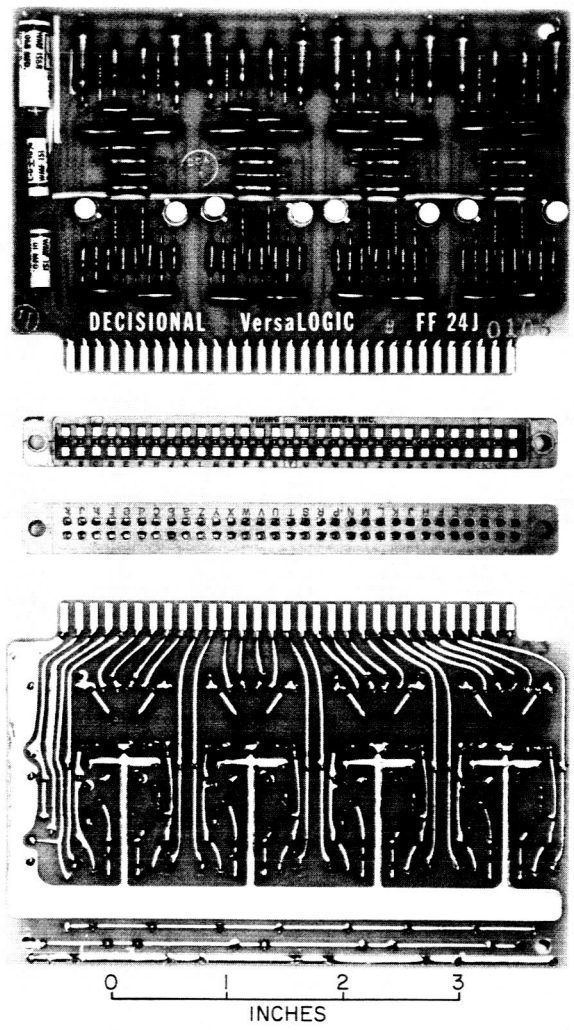

Fig. 99. Memory element module

show the physical appearance of the prototype modules. The modules are presently being evaluated and dynamically analyzed.

G. RF Signal Generation and Control

1. PN Generator Frequency Synthesizer

Several receiver and transmitter systems used by JPL require that the frequency of either the local oscillator or the transmitter be variable, usually in small steps over a large range. The programmed local oscillator (PLO) used in the planetary radar system incorporates a system for accomplishing this.[1] In order that the required number of different frequencies be available, a VCO is used which can be adjusted manually to each necessary frequency once or twice each day. This VCO is one of the two free-running oscillators in the system and contributes one-half of the frequency instability observed in the PLO. Any method of generating the required frequencies that would lock the generated frequencies to the site frequency standard (a Rubidium Vapor Frequency Stand-

[1]Venus Radar Report, Sec. III, Part G, 1962.

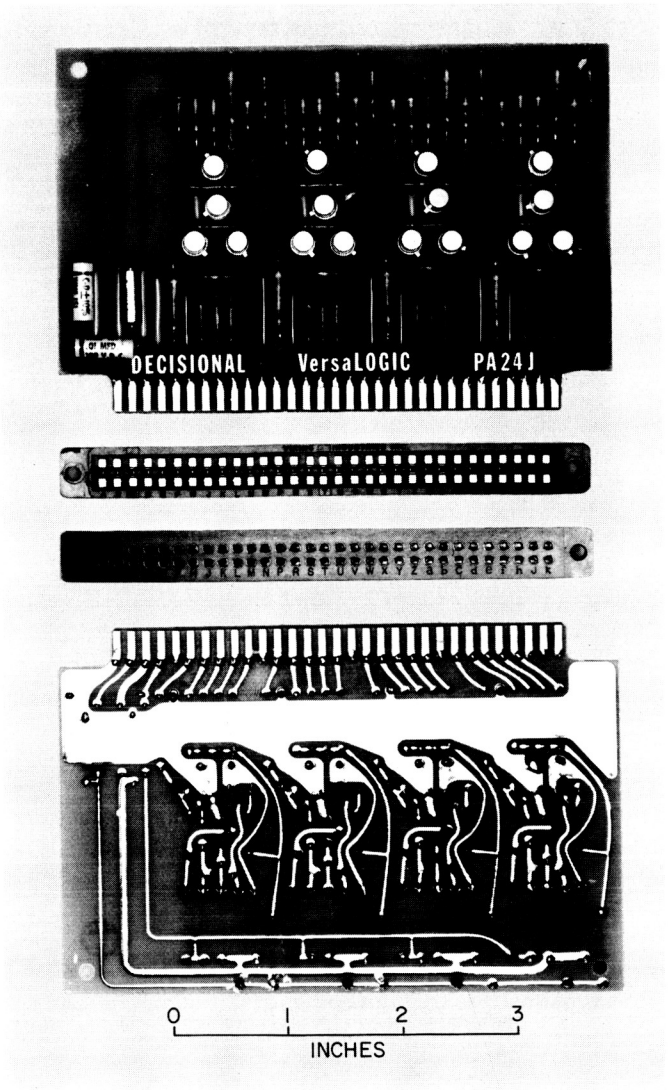

Fig. 100. Logic amplifier module

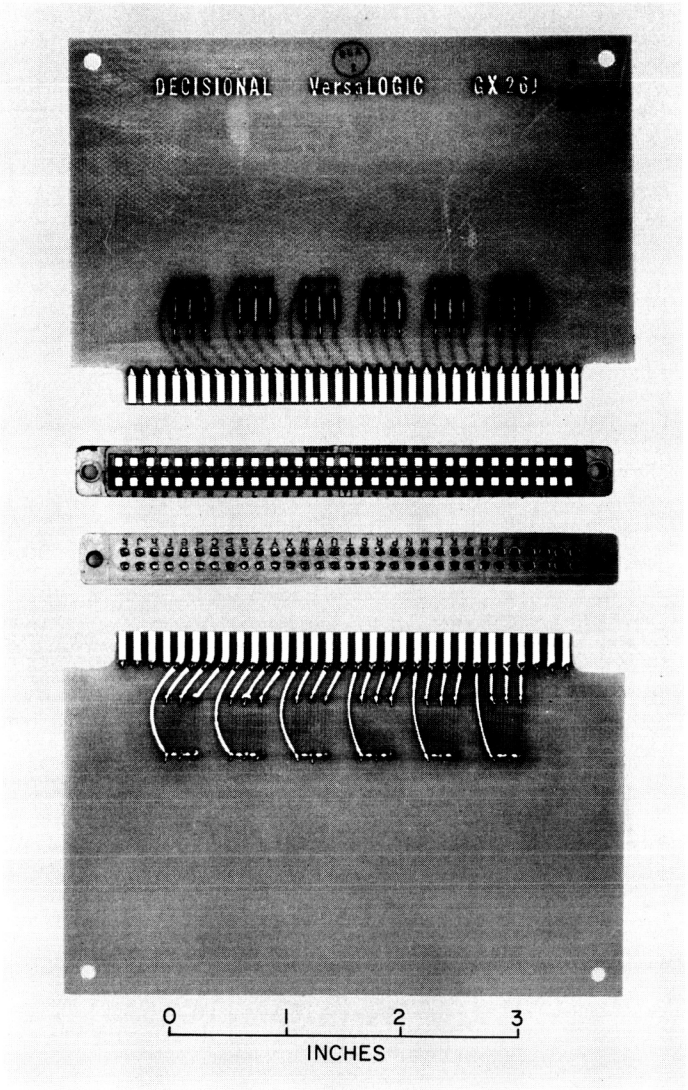

Fig. 101. Expansion element module

ard) would improve the performance of the system by a factor of approximately two.

One method of producing the required frequencies is shown in the block diagram of Fig. 102. The period of the PN code and the clock frequency would be chosen so as to produce the desired line spacing and total available spectrum width.

An experimental set-up using the block diagram of Fig. 103 was used to measure the contribution to the phase noise of the first 30-Mc VCO by the PN sequence generator. The second loop was used to measure the phase noise on the first VCO. The digit period in the PN generator was 6 μsec. The period of the PN sequence was $2^7 - 1 = 127$ bits or 127×6 μsec $= 762$ μsec. The line spacing is then $1/p = 1312.336 \cdots$ cps, and the first null in the spectrum is at 166⅔ kc.

The results of the phase noise measurements are:

30,000,656 cps, 0.35 deg ± 30%
30,000,000 cps, 0.35 deg ± 30%
29,999,344 cps, 0.25 deg ± 30%

While the results are only preliminary since the present experimental set-up could not be used to look at any of

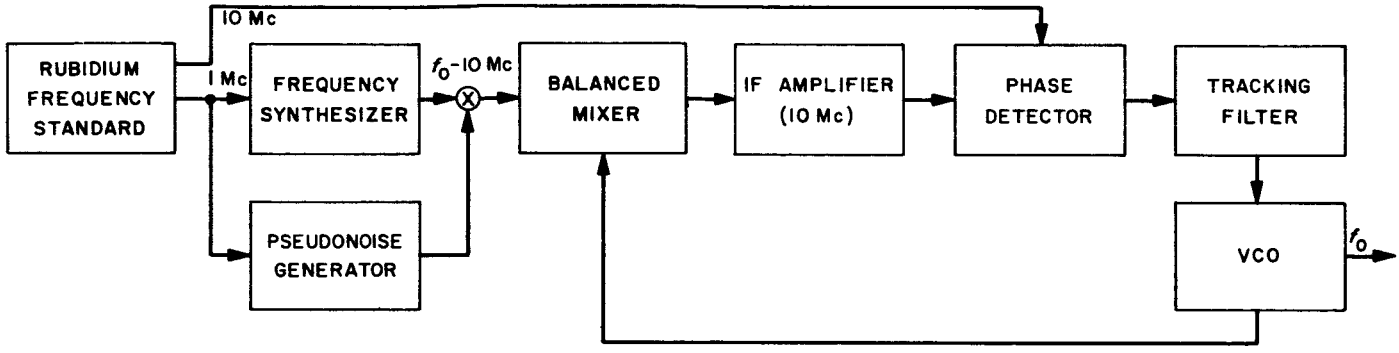

Fig. 102. A frequency synthesizer using a PN generator

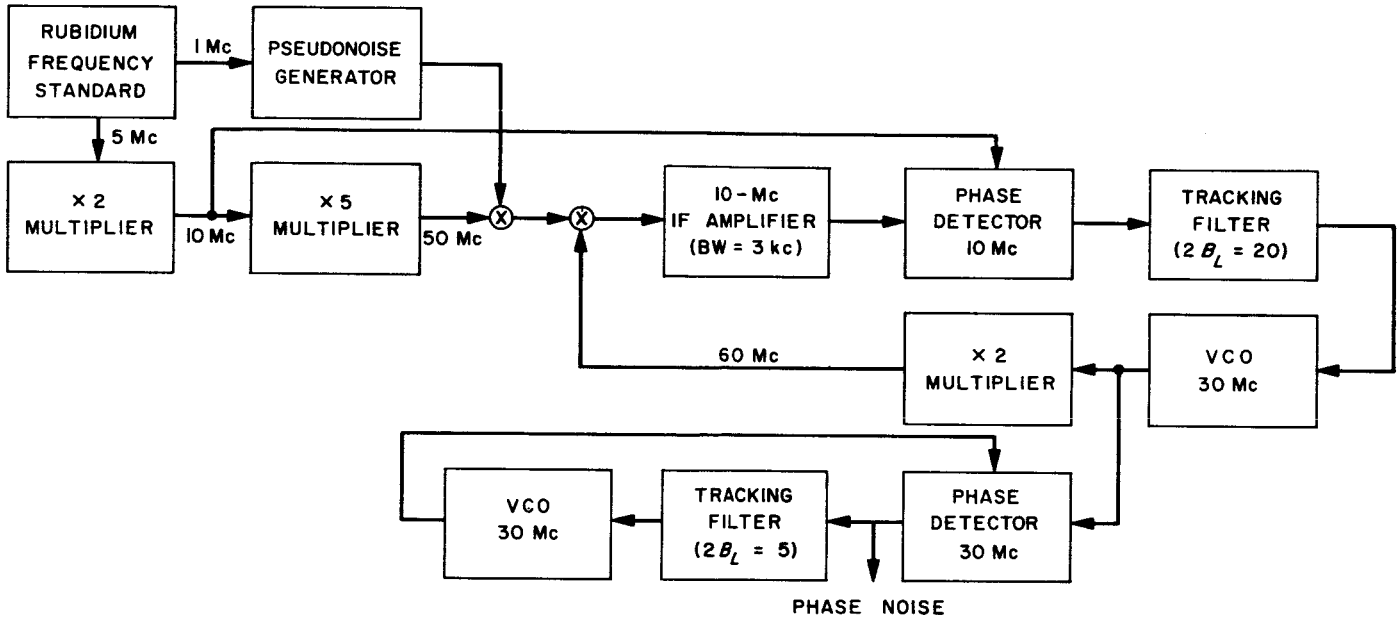

Fig. 103. Experimental PN frequency synthesizer

the lines far displaced from the center frequency, the results indicate virtually no degradation of the phase noise due to the PN sequence modulation, within the accuracy of the measurements.

H. Mesa Antenna Range

a. Summary. The Mesa Antenna Range (Fig. 104) is a facility used for all JPL in-house research and development on ground and spacecraft antennas. Two additions to the range are being made: an anechoic chamber building and a new ¾-mi range for full-scale S-band spacecraft antenna measurements. The plans and progress on these additions are described. The anechoic chamber is in the architect and engineer design phase; the new range is nearly complete.

b. Recent work. The buildings and grounds and technical equipment comprising the Mesa Antenna Range have been described in *SPS 37-10*, Vol. I, pp. 82–87, and *37-12*, Vol. I, p. 86. The following is a discussion of two new additions to the range.

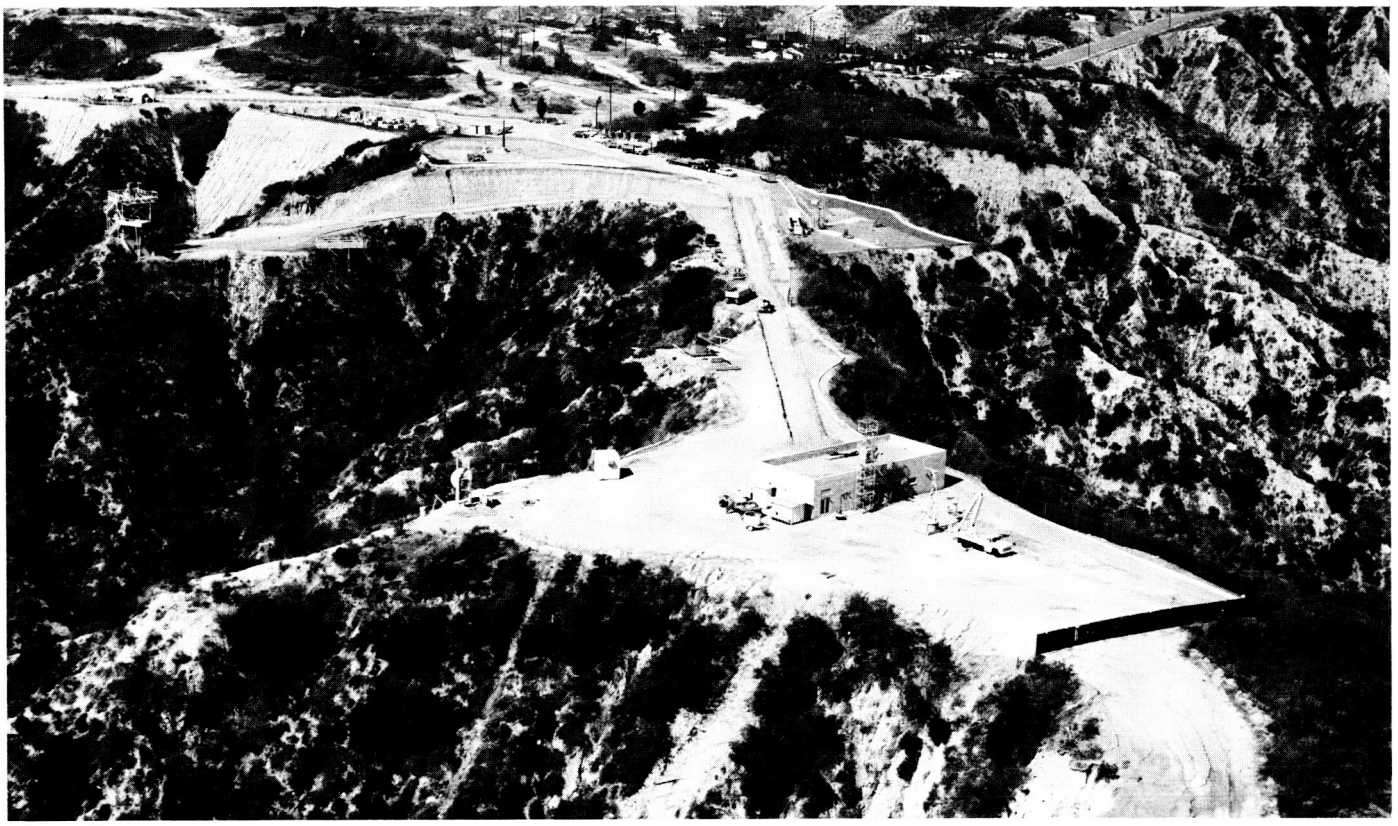

Fig. 104. Mesa Antenna Range

Anechoic chamber building. Studies were made for JPL by Emerson and Cuming, Inc. of Canton, Mass., and by Lockheed Missiles and Space Division, Sunnyvale, California, covering the performance of anechoic chambers (*SPS 37-14*). Upon evaluation of these studies the chamber design concept was changed from that summarized in *SPS 37-15*. Specifically, we now plan the chamber to provide accurate pattern measurement capability at X- and K-band frequencies. Approximate patterns and impedance measurements can be made at lower frequencies.

A contract for the design of the anechoic chamber building has been awarded to the architect and engineer firm of Austin, Field and Fry. According to present schedules, ground will be broken for construction of the building by Spring 1964.

The anechoic chamber building will contain two microwave darkrooms (anechoic chambers), both 20 ft wide and 20 ft high, prior to the installation of the absorber lining. One of these darkrooms, the X-band chamber, will be 60 ft long, the other, the K-band chamber, will be 40 ft long. Each chamber will provide a relatively interference-

Fig. 105. Remote transmitter site — "East Mesa"

free, weatherproof environment. By means of the RF-absorbing characteristics of the chamber lining free space will be artificially simulated. Both chambers will have an operating frequency range from 8 to 40 Gc. At any frequency in that range there will be a cylindrical "quiet zone" in the chambers. This "quiet zone" will be 6 ft in diameter and will be 50 ft long in the larger chamber, 30 ft long in the smaller one. It is expected that within this "quiet zone" the level of reflected energy will be −40 to −50 db. With this quality, the dark rooms will permit measurements of antenna characteristics to be carried out to a very high degree of accuracy. Measurements to be performed in the anechoic chambers include: amplitude and phase of antenna radiation patterns, impedance and VSWR measurements on radiating devices.

¾-mi range. The remote transmitter site—called the "East Mesa"—is about 60% complete; it will provide an illuminating source for a range which is several times longer than any available on the Mesa proper. The rotator for the receiving end will be located on the Mesa. (See *SPS 37-19*, Vol. III, for discussion of design and program use of this range.) An instrument building to house the transmitting equipment has been built, and a short paved road, leading from the paved area around the instrument building to the transmitter pole, has been completed (Fig. 105). The item needed to complete the site is a structure for the support of the illuminating antennas. A metal structure has been designed and we expect that it will be erected at the East Mesa by early 1964.

References

1. Hogg, D. C., "Effective Antenna Temperatures Due to Oxygen and Water Vapor in the Atmosphere," *Journal of Applied Physics*, Vol. 30, No. 9, p. 1417 ff, September 1959.
2. "Density of Pure Water Vapor at Saturation over Water," *Smithsonian Meteorological Tables*, p. 382, Sixth Revised Edition, Smithsonian Institution, Washington, D.C., 1958.
3. "Deep Space Range Measurement, The Role of Ranging Experiments in the Space Exploration Program," *RS 36-1*, Vol. I, p. 39, Jet Propulsion Laboratory, Pasadena, California.
4. "Deep Space Range Measurement, Ranging Subsystem," *RS 36-2*, Vol. I, Part I, p. 31, Jet Propulsion Laboratory, Pasadena, California.
5. "Ranging Systems, Mod 1-D Ranging System," *SPS 37-15*, Vol. III, p. 40, Jet Propulsion Laboratory, Pasadena, California.
6. "Planetary Radar, Transmitter and Receiver Oscillators," *SPS 37-18*, Vol. III, p. 36, Jet Propulsion Laboratory, Pasadena, California.
7. "Ranging Systems, Evaluation of Atomic Oscillator Performance," *SPS 37-17*, Vol. III, p. 30, Jet Propulsion Laboratory, Pasadena, California.
8. Baumert, Leonard, et al., *Coding Theory and Its Applications to Communications Systems*, Technical Report No. 32-67, Jet Propulsion Laboratory, Pasadena, California, March 31, 1961.
9. Titsworth, R. C., *Optimal Ranging Codes*, Technical Report No. 32-411, Jet Propulsion Laboratory, Pasadena, California, April 15, 1963.

References (Cont'd)

10. Baugh, H. W., *Mod II Ranging Equipment,* Technical Report No. 32-337, Jet Propulsion Laboratory, Pasadena, California, September 16, 1962.

11. "Planetary Radar, Mod II Exciter and Transmitter," *SPS 37-16,* Vol. III, p. 45, Jet Propulsion Laboratory, Pasadena, California.

12. "Ranging Systems, Mod II Exciter and Transmitter, 2388 Mc, 10 Kw," *SPS 37-17,* Vol. III, p. 30, Jet Propulsion Laboratory, Pasadena, California.

13. "Ground Antennas, 30-Foot Diameter Azimuth–Elevation Antenna," *SPS 37-19,* Vol. III, p. 32, Jet Propulsion Laboratory, Pasadena, California.

14. "Ranging Systems, Monostatic Radar," *SPS 37-19,* Vol. III, p. 31, Jet Propulsion Laboratory, Pasadena, California.

15. "Ranging System Development, A Phase-Locked Loop with Sideband Rejecting Properties," *SPS 37-21,* Vol. III, p. 76, Jet Propulsion Laboratory, Pasadena, California.

16. "Ranging System Development, Sideband Lock Investigation," *SPS 37-21,* Vol. III, p. 80, Jet Propulsion Laboratory, Pasadena, California.

17. "Ranging System Development, Monostatic Radar," *SPS 37-23,* Vol. III, p. 55, Jet Propulsion Laboratory, Pasadena, California.

18. "Deep Space Range Measurement, Acquirable Ranging Codes and Noise," *RS 36-2,* Vol. I, Part 1, p. 26, Jet Propulsion Laboratory, Pasadena, California.

19. "Ranging Subsystem," *RS 36-5,* Vol. I, p. 46, Jet Propulsion Laboratory, Pasadena, California.

20. "Ranging Subsystem, Ranging Coders," *RS 36-6,* Vol. I, p. 43, Jet Propulsion Laboratory, Pasadena, California.

21. Stewart, B. M., *Theory of Numbers,* The MacMillan Co., New York, 1952.

22. "Ranging Subsystem, Receiver Coder," *RS 36-3,* Vol. I, Part 1, p. 46, Jet Propulsion Laboratory, Pasadena, California.

23. "Ranging Subsystems, Vernier for Error Estimation," *RS 36-4,* Vol. I, p. 36, Jet Propulsion Laboratory, Pasadena, California.

24. "Ranging System Development, Keyer Control for Monostatic Radar," *SPS 37-23,* Vol. III, p. 36, Jet Propulsion Laboratory, Pasadena, California.

25. "Ranging System Development, Monostatic Radar," *SPS 37-23,* Vol. III, p. 53, Jet Propulsion Laboratory, Pasadena, California.

26. Viterbi, A. J., "On Coded Phase-Coherent Communications," *IRE Transactions on Space Electronics and Telemetry,* SET-7, March 1961.

27. Tossic, T., "Optimum Card Size for Printed Circuit Cards," Lawrence Radiation Laboratories, University of California, Berkeley, 1959.

28. Levy, R., "Printed Circuit Card Connector Study to Determine the Optimum Number of Pins," Philco Corp., Palo Alto, California, date unknown.

V. Advanced Antenna System

A. Synopsis

The Advanced Antenna System (AAS) will be a 210-ft diameter, fully steerable paraboloid. It is being designed for operational use at the DSIF Stations at the DSIF S-band frequencies (2.1 to 2.3 Gc).

The principal element of the first AAS, which we term the Contractor Furnished System (CFS), includes the reflector, alidade, pedestal, foundation, and drive system. It has been under contract to the Rohr Corporation since mid-June of this year. JPL Project effort in the past 2 mo has concentrated on engineering design liaison and review with Rohr; in-house supporting studies were temporarily reduced during this phase of work with the CFS contractor.

The Master Summary Schedule of the CFS has been received from the Rohr Corporation and has been approved by JPL; initial operation of the AAS at Goldstone will be in early 1966.

Preliminary design and engineering analysis for the CFS are generally on schedule. The major engineering emphasis during September was on studies that directly related to the detailed design of the underground utility installations and to the pedestal design so that excavations and other site preparations could proceed as scheduled. The system integration studies and dynamic analysis work to date indicate that the pedestal configuration is appropriate and that no untractable design and construction difficulties should be encountered.

The air conditioning system for the equipment, laboratory, and operations areas within the pedestal and the alidade rooms and the feed cone has been extensively investigated. A chilled water air conditioning system is planned, which will be two industrial reciprocating compressors each capable of 60% capacity. The cooling tower will be a closed system, double unit.

A 12,000-gal horizontal water storage tank and distribution system has been designed to provide water for all

domestic requirements. It will be necessary to haul water from Fort Irwin.

On-site preparations at the Mars site, Goldstone, began October 14, 1963; site clearing, construction survey, and access road construction are underway. The progress to date at the site is shown in Figs. 1 and 2.

Planning for the erection of the antenna has been done and Rohr has worked out a scheduled erection sequence.

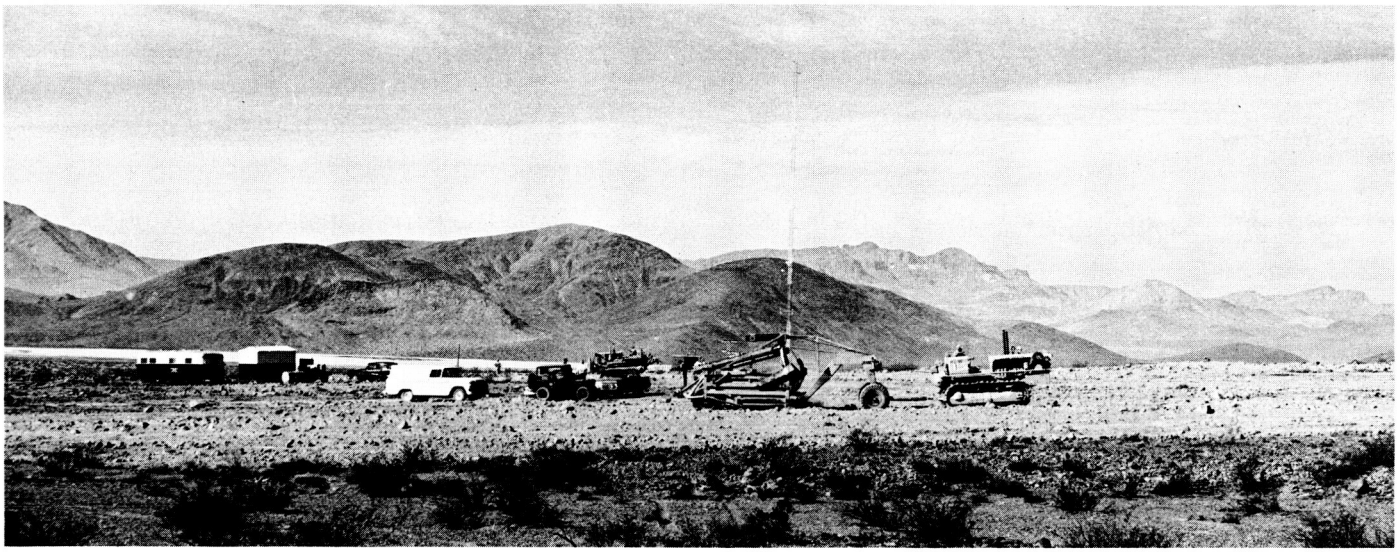

Fig. 1. Site preparation begins at the Mars site, Goldstone

Fig. 2. Access road construction begins

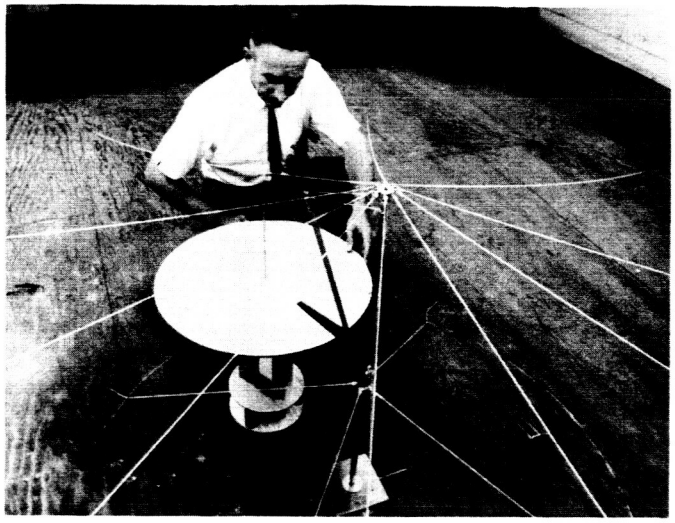

Fig. 3. Model of guy derrick in relation to the antenna structure

Also, Rohr Corporation has obtained a 200-ton 180-ft tall guy derrick mounted on a tower 135 ft high for erection of the antenna and pouring the foundation and pedestal concrete. This unit was previously used to set entire refineries including bubble columns and catalytic cracking units from one derrick location. A model of the derrick, together with a model of the antenna, has been set up to aid Rohr in working out the erection details (Fig. 3).

During this reporting period the contractor has been doing design and analysis work in the following areas:

(1) The relative merits of the double ring truss supported reflector versus a rectangular truss support. It was recently concluded that the rectangular truss support was the preferred configuration for economic reasons.

(2) The quadripod apex structure which integrates the Cassegrain system subreflector support structure and support mechanism.

(3) The effect of quadripod leg design on radio frequency blockage (i.e., effect on aperture efficiency).

(4) The Cassegrain system feed cone configuration including consideration of the transportation problems of this large unit.

(5) Provisions for measuring the reflector surface at all reflector attitudes.

(6) The massive weldment sections of the alidade at the bearing support points and the many interfaces with the mechanical equipment and the alidade building.

(7) An azimuth thrust bearing model for experimental study of alignment techniques and validation of detailed analysis methods, including preparation of test stand activators and measuring equipment necessary to carry out tests.

(8) The deflection of the hydrostatic bearing runner, as mounted on the pedestal.

(9) Definition of drive torques as a function of time for use in long-term wear and reliability calculations on the gears and elevation bearings.

(10) Thermal effects on preload of the radial bearing. Preliminary design of the azimuth radial bearing has been completed through configuration and preliminary layout drawings.

(11) Thirty-five wind loading conditions have been applied to the alidade structure to determine conditions that give critical member stress. Based upon the latest wind tunnel data, the basic wind torque loads for each antenna axis have been determined.

(12) Error analysis of the analog data system from data box input to readout has been completed, indicating performance well within anticipated errors.

As a necessary adjunct to the design of the servo system, a method of developing transfer functions has been formulated by JPL. Experimentation is being conducted to determine the feasibility of the method by applying it to simple dynamic models.

Related JPL in-house supporting studies are reported in Sec. IV-A-1, 2, 3 of this report.